Control over Assembly and Interpenetration of Pd-based Coordination Cages

Dissertation

zur Erlangung des mathematisch-naturwissenschaftlichen Doktorgrades

"Doctor rerum naturalium"

der Georg-August-Universität Göttingen

im Promotionsprogramm Chemie

der Georg-August University School of Science (GAUSS)

vorgelegt von

Rongmei Zhu

aus Jiangsu, VR China

Göttingen, 2017

Betreuungsausschuss

Prof. Dr. Guido H. Clever (Anorganische Chemie, Technische Universität Dortmund, Otto-Hahn-Str. 6, 44227 Dortmund)

Prof. Dr. Franc Meyer (Institut für Anorganische Chemie, Georg-August-Universität Göttingen, Tammannstr. 4, 37077 Göttingen)

Mitglieder der Prüfungskommission

Referent: Prof. Dr. Guido H. Clever (Anorganische Chemie, Technische Universität Dortmund, Otto-Hahn-Str. 6, 44227 Dortmund)

Korreferent: Prof. Dr. Franc Meyer (Institut für Anorganische Chemie, Georg-August-Universität Göttingen, Tammannstr. 4, 37077 Göttingen)

Weitere Mitglieder der Prüfungskommission

Prof. Dr. Dirk Schwarzer (Institut für Physikalische Chemie, Georg-August-Universität Göttingen, Tammannstr. 6, 37077 Göttingen).

Prof. Dr. Inke Siewert (Institut für Anorganische Chemie, Georg-August-Universität Göttingen, Tammannstr. 4, 37077 Göttingen)

Dr. Michael John (Institut für Organische und Biomolekulare Chemie, Georg-August-Universität Göttingen, Tammannstr. 2, 37077 Göttingen)

PD Dr. Birger Dittrich (Institut für Anorganische Chemie und Strukturchemie, Heinrich-Heine-Universität Düsseldorf, Universitätsstr. 1, 40225 Düsseldorf)

Tag der mündlichen Prüfung: 24.03.2017

Affidavit

Hereby I declare that my doctoral thesis entitled "Control over Assembly and Interpenetration of Pd-based Coordination Cages" was written independently and with no other sources and aids than quoted. I have indicated the parts which were performed by project collaborators.

Rongmei Zhu

Göttingen, March 2017

ACKNOWLEGEMENTS

List of Publications

First-author publications

"Stepwise Halide-triggered Double- and Triple-Catenation of Self-Assembled Coordination Cages", R. Zhu, J. Lübben, B. Dittrich, G. H. Clever, *Angew. Chem. Int. Ed.* **2015,** *54,* 2796.

"Synthesis and properties of new Iridium complexes based on π conjugated ligands with tetrathiafulvalene", R. Zhu, L. Hu, F. Zhu, J. Zuo and X. You, *Chinese Science Bulletin,* **2014,** *59,* 1638.

"Syntheses, crystal structures and properties of dinuclear hydrido-tris(3,5-diphenylpyrazol-1-yl)borate complexes with the SS coupled and dimerized quinoxaline-2,3-dithiolate ligand", R. Zhu, L. Hu, Y. Li, Y. Song and J. Zuo, *Inorg. Chem. Commun.* **2013,** *35,* 79.

Manuscript in preparation

"Side Chain-Directed Assembly of Heteroleptic *trans*-[$Pd_2L_2L'_2$] Coordination Cages with Four Picolyl Donors", R. Zhu, W. Bloch, G. H. Clever.

"Assembly and Interpenetration Coordination Cages Based on Multi-dentate Ligands", R. Zhu, B. Dittrich, J. J. Holstein, G. H. Clever.

CONTENTS

Chapter 1: Introduction

Chapter 2: Stepwise Halide-Triggered Double- and Triple-Catenation of Self-Assembled Coordination Cages[1]

Chapter 3: Side Chain-Directed Assembly of Heteroleptic *trans*-[Pd₂L₂L′₂] Coordination Cages with Four Picolyl Donors... 61

Chapter 4: Self-Assembled Coordination Cages Based on Multi-Dentate Ligands 117

Chapter 1: Introduction

1.1 History and development of supramolecular chemistry

Supramolecular chemistry was defined as the "chemistry of molecular assemblies and of the intermolecular bond" introduced by Jean-Marie Lehn in 1978.[1] Originally, supramolecular chemistry was described as intermolecular non-covalent interactions between two different kinds of molecules, hosts and guests, which differentiated from molecular chemistry (Figure 1.1).[2]
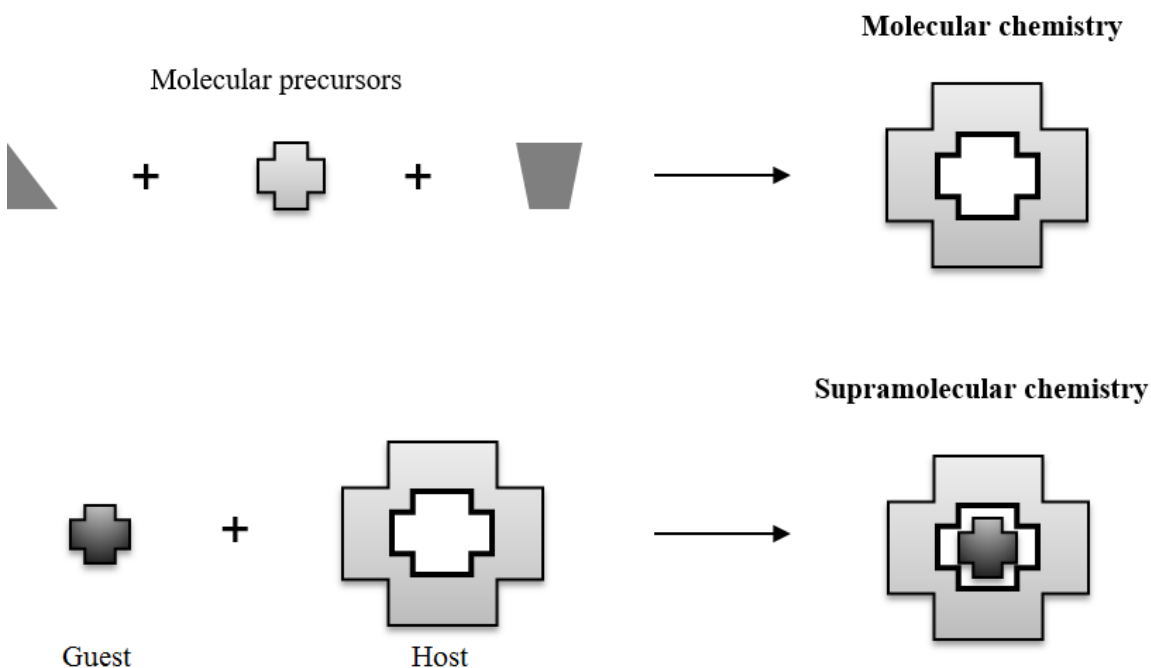
Figure 1.1 Comparison between molecular and supramolecular chemistry. Copyright © WILEY-VCH Verlag GmbH & Co.

The fundaments of supramolecular chemistry can be traced back to the late 19th century, when the first host molecules, cyclodextrins, were discovered by Villiers and Hebd in 1891.[3] Two years later, Alfred Werner proposed the idea of coordination chemistry presenting one central transition metal (Cu, Cr, Pt, etc.) that is surrounded by anionic or neutral ligands.[4] In the following year, Emil Fischer proposed the "lock and key" concept (Figure 1.2a) which established the foundation of molecular recognition in which the substrate has a designated size or shape which is satisfied to the enzyme.[5] Nevertheless, this rigid proposal was replaced by the "induced fit" model (Figure 1.2b) introduced by Daniel E. Koshland in which both the guest and host undertake notable transformations upon binding to each other.[6] In 1906, Paul Ehrlich came up with the concept of receptor by elaborating that any molecule could play a role on the human body unless it is bound.[7]
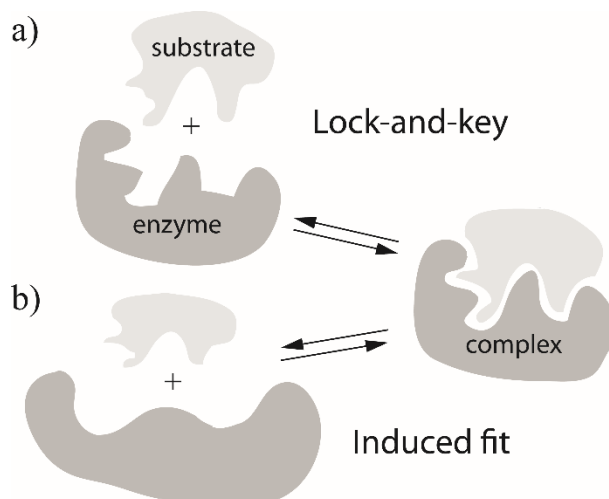
Figure 1.2 a) Lock and key and b) induced fit models of enzyme-substrate binding. Copyright © WILEY-VCH Verlag GmbH & Co.

These concerned theories laid a strong foundation of supramolecular chemistry even though the term supramolecule, "Übermoleküle" in German, first appeared in the literature in the late 1930s, when Karl L. Wolf described the intermolecular interaction in the dimers of carboxylic acids.[8] In 1945, H. M. Powell found the β-quinol molecules linked together through hydrogen bonds forming inclusion compounds which contain methyl alcohol molecules from X-ray crystal structures (Figure 1.3a) and first introduced the term "clathrate" to describe the frameworks consisting of a lattice that can lock molecules in position.[9] In 1967, a new class of cyclic polyethers were published by Charles J. Pederson, which were classified as crown ethers (Figure 1.3b). These compounds are capable of forming stable complexes upon binding alkali and alkaline earth metals.[10] Two years later, Jean-Marie Lehn expanded the two-dimensional crown ethers into three dimensional cryptands (Figure 1.3c) which are much stronger and more selective for the guest ions.[11]
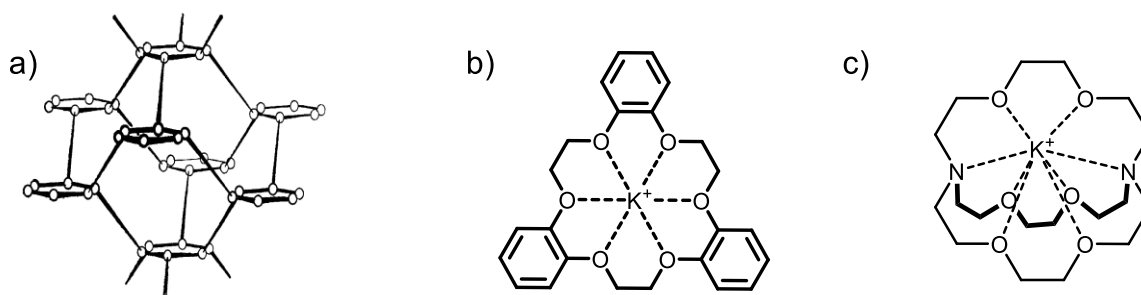
Figure 1.3 a) β-quinol inclusion structure (circles represent oxygen atoms of the hydroxyl groups linked by hydrogen bonds to form approximately plane hexagons, rods represent the quinol molecules connecting hexagons, the benzene rings are omitted for clarity); b) tribenzo-[18]crown-6 complex; c) [2.2.2]cryptand complex.

The year 1987 is regarded as a milestone for supramolecular chemistry in history since Donald J. Cram, Charles J. Pederson and Jean-Marie Lehn were awarded the Nobel Prize in Chemistry for "their development

and use of molecules with structure-specific interactions of high selectivity". It took more than 40 years from the introduction of the term "Übermoleküle" to Lehn's definition of supramolecular chemistry due to limitations of both the perception from scientists and the development of specialized experimental methodology. Since the 1960s, research on supramolecular chemistry has sprung up focusing not only on the aesthetically attractive structures but also on the various promising applications. In 2016, the Nobel Prize in Chemistry was awarded to Jean-Pierre Sauvage (whose related work will be introduced in the following text) Sir J. Fraser Stoddart and Bernard L. Feringa for "the design and synthesis of molecular machines". They have realized the controllable movements between molecules which will be promisingly applied in the development of new materials, sensors and energy storage systems. The concept of molecular machines also gives a brand-new idea in supramolecular chemistry.

1.2 Supramolecular interactions

As mentioned in the first place, supramolecular chemistry relates to non-covalent interactions which include a wide range of attractive and repulsive effects. Non-covalent bonds vary from the relatively strong coordinative bonds up to several hundreds of kJ mol^{-1} to weak van der Waals forces only about several kJ mol^{-1}. They can be divided into several different classes as follows.

Ion-ion interactions are the strongest among these non-covalent interactions ranging in strength ca. $100-350$ kJ mol^{-1} which is comparable to covalent bonds. This interaction depends on the geometric factor coming from two oppositely charged ions, thus there is no strict directional presentation in ion-ion interactions. A typical example of ion-ion interactions in supramolecular chemistry is the interaction between a tricationic host tris(diazabicyclooctane) (**1.1**) and the anion $[Fe(CN)_6]^{3-}$ (Figure 1.4a).[12] Ion-dipole interactions are somehow weaker in the range of ca. $50-200$ kJ mol^{-1} resulting from the bonding of an ion with a polar molecule. This interaction requires a rigid orientation so that the positive and negative parts are next to one another, providing maximum attraction. The interaction of alkali metal cations with crown ethers apparently shows the ion-dipole interactions from supramolecular aspect (Figure 1.3b). Dipole-dipole interactions are electrostatic interactions which are even weaker (ca. $5-50$ kJ mol^{-1}) arising from the alignment of one dipole with another. An example of dipole-dipole interactions can be found in hydrogen chloride (Figure 1.4b).
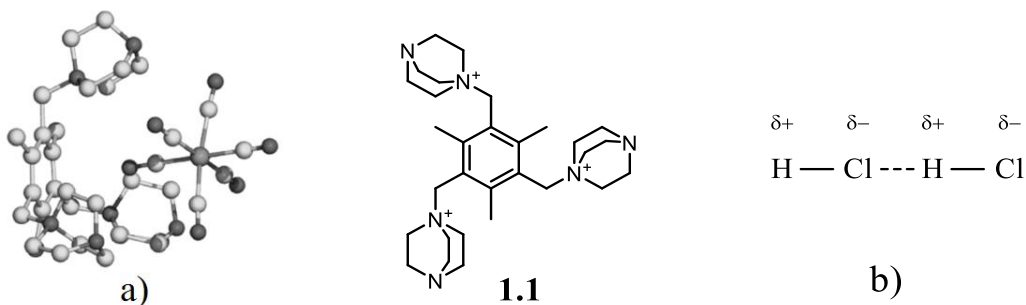
Figure 1.4 a) Supramolecular ion-ion interactions exemplified by the interaction of the organic cation **1.1** with $[Fe(CN)_6]^{3-}$; b) dipole-dipole interaction in HCl.

Hydrogen bonding is regarded as a special class of electrostatic dipole-dipole interactions. It is a strong attraction between a hydrogen atom bound to an electronegative atom and another electronegative atom. The high boiling point of water is just attributed to the intermolecular hydrogen bonding. Hydrogen bonding also plays a quite crucial role in biochemistry such as the double helix formation of DNA. Additionally, the binding strength is determined by the geometry of the hydrogen bond (Figure 1.5).
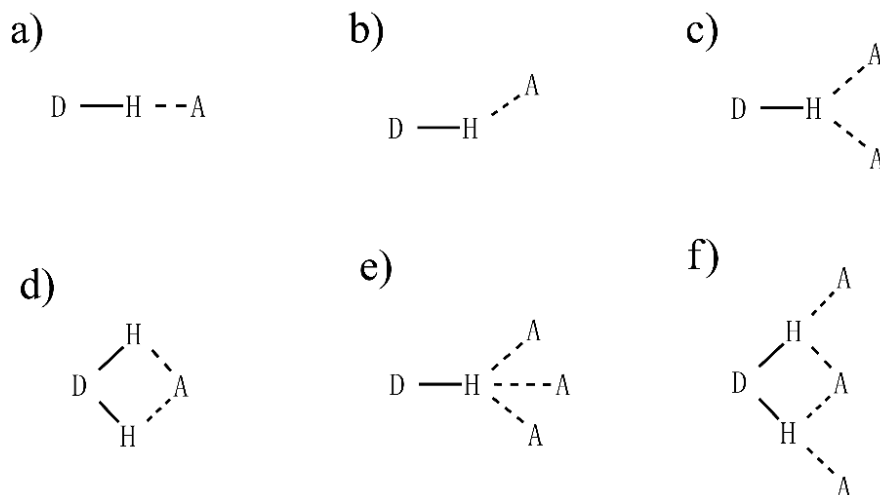
Figure 1.5 Different types of hydrogen bonding geometries.[13]

π-Systems are involved in another type of noncovalent interactions, which include cation-π interaction, anion-π interaction and π-π interactions. Cation-π and anion-π interactions are very similar involving an ion interacting with the electron-rich or electron-poor π-system. π-π Interactions are often associated within aromatic rings, normally engaged in the interaction between an electron-rich unit and a relatively electron-poor one. π-π Stacking is arranged in two major manners: face-to-face and edge-to-face (Figure 1.6). The type of face-to-face stacking is accountable to the slippery sense of touch from graphite and its lubricant properties. The characteristic herringbone pattern in X-ray crystal structures of benzoperylene and γ-SHB is an iconic example of edge-to-face π-stacking interactions.[14]
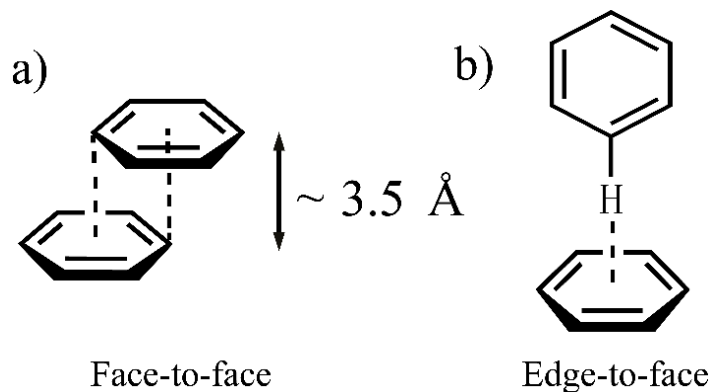
Figure 1.6 Two general types of π-π interactions. Copyright © WILEY-VCH Verlag GmbH & Co.

Among the noncovalent interactions, van der Waals force (< 5 kJ mol^{-1}) is the weakest one which may be strictly divided into London dispersion and exchange-repulsion terms. Van der Waals forces are a subset of poor electrostatic interactions arising from the polarization of an electron cloud by the proximity of an adjacent nucleus. They are pivotal in the formation of inclusion complexes which could incorporate some small organic molecules within molecular cavities in supramolecular system. An example from X-ray crystal structure concretely shows the capture of neutral toluene molecule within the calix shaped *p-tert-*butylcalix[4]arene[15], which is on account of the van der Waals interactions (Figure 1.7).
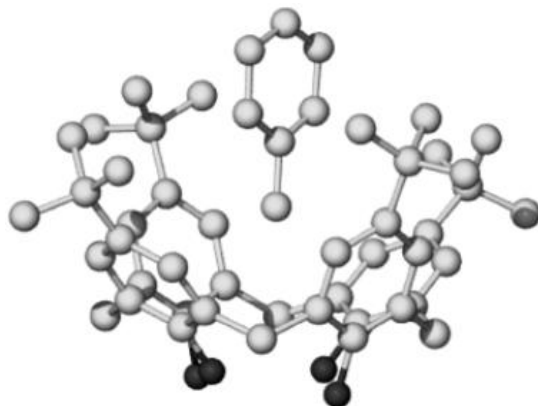
Figure 1.7 X-ray crystal structure of a typical van der Waals inclusion complex *p-tert-*butylcalix[4]arene·toluene. Copyright © 2009 WILEY-VCH Verlag GmbH & Co.

An additional case, which is occasionally mistaken as a force, is hydrophobic effect which is of crucial importance in guest binding and molecular recognition in polar media, demonstrating the influence from the environment. Taking the cyclodextrin as an example, hydrophobic effect could be divided in two energetic parts, enthalpy and entropy. Since the host cavity is hydrophobic, water molecules sitting inside the cavity cannot strongly interact with the host wall. They are expelled from the host's cavity due to the enthalpic effect and replaced by relatively non-polar guests. The formation of complex combining both host and guest leads to a less disturbing system, which also contributes to the increase of entropy (Figure 1.8).
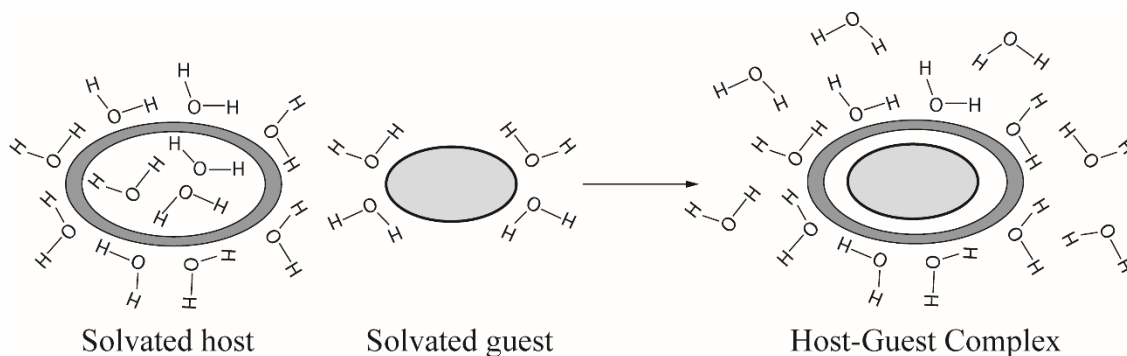
Figure 1.8 Hydrophobic binding of organic guests in aqueous solution. Copyright © WILEY-VCH Verlag GmbH & Co.

There are some more non-covalent interactions in supramolecular systems such as crystal close packing and closed shell interactions. Scientists are continuing to look deep into the nature of supramolecular chemistry.

1.3 Coordination chemistry

Coordination chemistry is the science concerning the interactions of relatively labile metal ions and usually chelating or multi-dentate inorganic ligands. Complex compounds are formed from reactants with formally saturated valences to some extent. Coordination chemistry has sprung up since its modern formulation was proposed by Alfred Werner in compounds composed of cobalt(III) chloride and ammonia (Figure 1.9).[4] In coordination complexes, ligands act as electron pair donors while the metal atoms act as the electron pair acceptors. Therefore, the dative bonds can be considered as Lewis acid-base interactions, which are stronger than intermolecular interactions due to the directional bonds between metal ions and ligands, but weaker than covalent bonds. The characteristics of both metals and ligands are changed upon coordinating with each other.
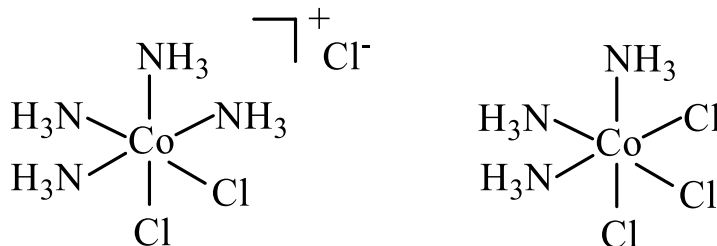
Figure 1.9 Werner formulations of $[Co(NH_3)_4Cl_2]^+(Cl^-)$ and $[Co(NH_3)_3Cl_3]$.

1.4 Self-assembly

1.4.1 Introduction

Self-assembly is defined as "the spontaneous and reversible association of molecules or ions to form larger, more complex supramolecular entities according to the intrinsic information contained in the molecules themselves".[13] It is fundamentally a convergent process in which a disordered system containing multiple components assemble into stable complex architectures, avoiding tedious multistep syntheses often associated with the formation of elaborate structures.

In nature, self-assembly also plays a ubiquitous role and often takes place on hierarchy levels so as to form functional systems.[16] Take proteins as an example, the primary structure, sequence on the linear polypeptide, folds first into secondary structural segments such as α-helices and β-sheets, arranged themselves by hydrogen bonding, stacking interactions and hydrophobic effects in aqueous solution. The tertiary structure is determined by the folding of each polymer chain and finally, from the self-assembly of these individual polymers, the quaternary structure is given as the aggregation of a number of folded protein chains (Figure 1.10).

In general, self-assembly takes place without intervention of external forces, thus the system is thermodynamically preferable with a lower Gibbs free energy. Self-assembly has extended the scope of supramolecular chemistry focusing on mimicking natural processes and synthesizing multi-functional materials.[17]
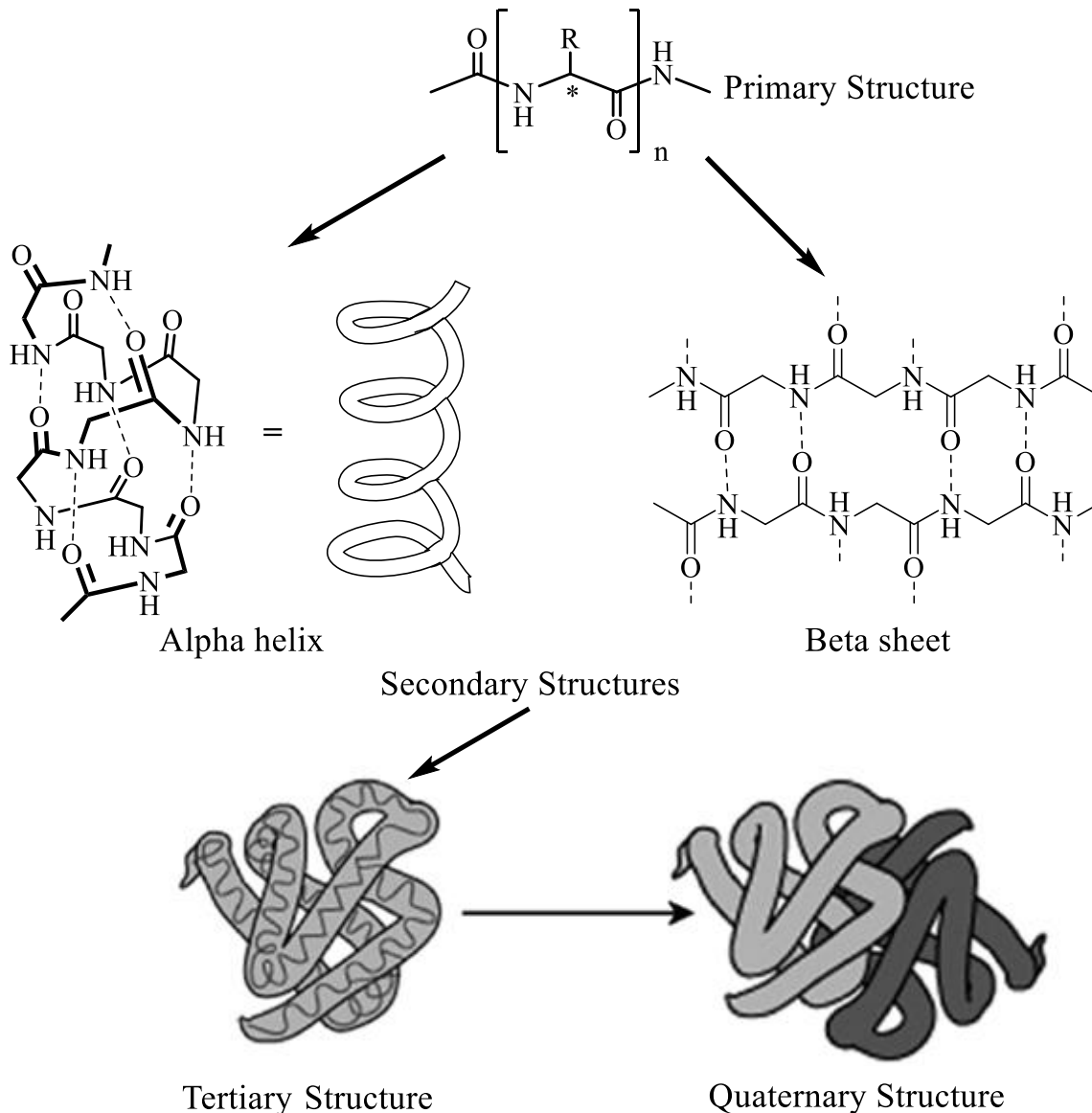
Figure 1.10 The formation of enzyme quaternary structure assembled from its precursory structures. Copyright © 2009 WILEY-VCH Verlag GmbH & Co.

1.4.2 Catenanes

A catenane is a mechanically interlocked structure consisting of two or more macrocycles in which rings cannot be separated without the cleavage of at least one covalent bond (Figure 1.11a). The first synthesis of a [2]catenane (**1.2**) was realized by Wasserman in 1960 (Scheme 1.1) through the statistical approach,[18]

however, this approach is limited by its very low efficiency. The other approach to achieving catenanes which is called as the template-directed synthesis with higher yield relies on the supramolecular self-assembly stabilized by various non-covalent interactions aforementioned. The first crystal structure of a catenane was reported by Sauvage and co-workers in 1985 in which two macrocycles interpenetrate in close proximity and any one fragment can slide freely within its cavity (Figure 1.11b). Sauvage is one of three winners of the Nobel Prize in Chemistry in 2016 due to this catenane structure.[19]
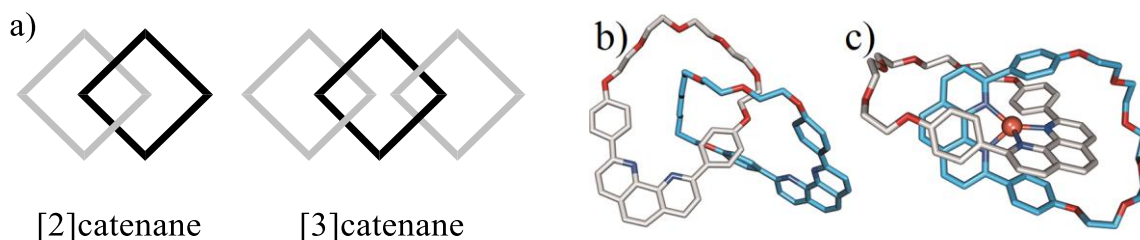
Figure 1.11 a) Two general types of catenanes; b) first crystal structure of a catenane; c) first crystal structure of a metallocatenane. Copyright © 1985 The Royal Society of Chemistry.

Based on the charge-assisted π-π stacking methodology, Stoddart's group synthesized a [2]catenane (**1.5**) in a high yield that contributed to the templating effect from the electronically matched pairs of electron-rich crown ether (**1.4**) and electron-poor paraquat-derived cyclophane (**1.3**) (Scheme 1.2).[20] After the successful synthesis of this typical catenane via self-assembly approach, Stoddart's group were able to successfully synthesize a series of [3]-, [4]-, [5]- and even [7]-catenanes which showed the extreme diversities of catenane structures.[21]
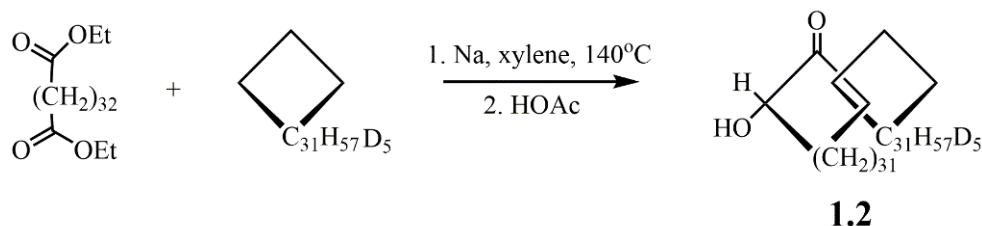
Scheme 1.1 The first catenane (**1.2**) synthesis via the statistical approach.
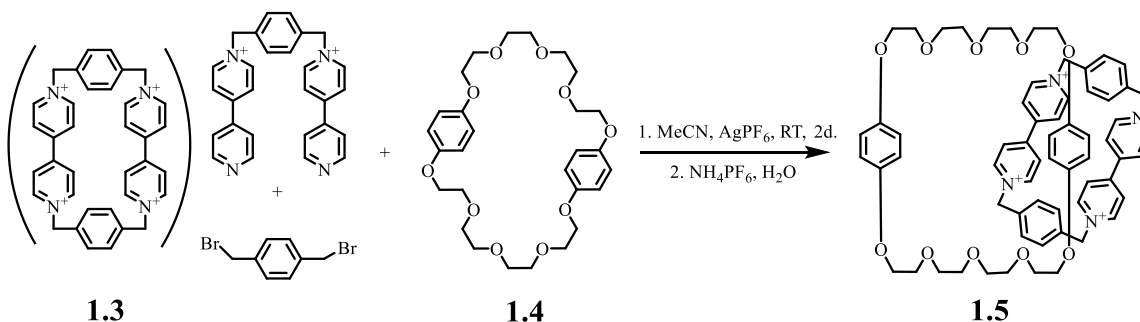
Scheme 1.2 [2]catenane **1.5** synthesis via template-directed synthesis.

The organization of ligands coordinating to transition-metal cations has proven to be a versatile and easily accessible means of an auxiliary linkage for obtaining interlocked complexes. Accompanied with the first crystal structure of a catenane, Sauvage's group has also reported the first crystal structure of metallocatenane (Figure1.11c) in which the bidentate ligands arrange perpendicularly in the presence of a transition metal ion, Cu(I), which possesses a tetrahedral coordination geometry.[19] Beer and co-workers realized metal-templated catenanes by use of the attractive metal-metal interactions in 2001.[22] As shown in Scheme 1.3, the formation of [2]catenane **1.7**-Cu^{II}Cu^{III} is due to the reorganization of the precursor macrocycle **1.6**-Cu^{II} upon its partial oxidation. The driving force for the pre-complex interpenetration can be attributed to charge-transfer interactions between Cu^{II} and Cu^{III} centers in the mixed-valence catenane. Without doubts, other approaches to achieve catenanes can be used such as hydrogen-bond templates,[23] hydrophobic effects,[24] and radical-radical interactions.[25]

1.6-Cu^{II} **1.7**-Cu^{II}Cu^{III}
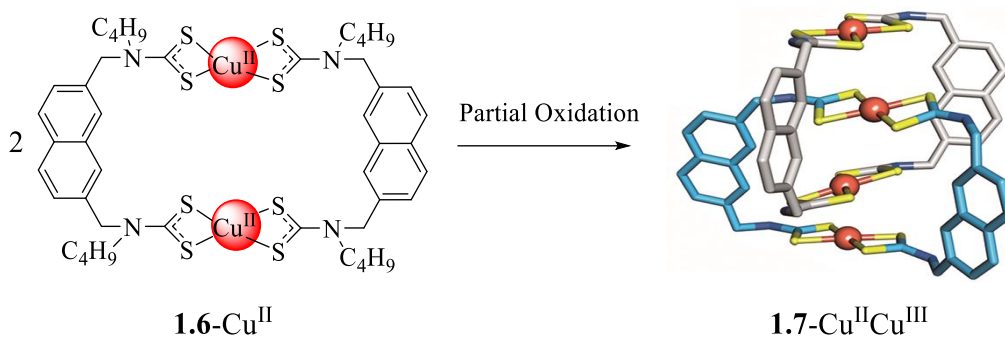
Scheme 1.3 Beer's mixed-valence [2]catenane **1.7**- Cu^{II}Cu^{III} generated from partial oxidation of macrocycle **1.6**-Cu^{II}. Copyright © 2001 WILEY-VCH Verlag GmbH & Co.

1.4.3 Self-assembled coordination cages

Metal-directed self-assembly of 3D architectures has triggered particular interest in the field of supramolecular chemistry. Due to the diversity of available objects in terms of particular size and shape, demands for highly preorganized and multidentate ligands presenting concave properties has raised the research tendency to calixarenes,[26] cavitands[27] and some other architectures as sources of molecular scaffold for the self-assembly of coordination cages.

Through metal-ligand interactions, the self-assembly of a supramolecular calix[4]arene capsule was described by Baldini *et al*.[28] In this case of coordination cages, the metal centers in metalloporphyrins are introduced to the calixarene, resulting a tetra-functionalized structure and the bidentate ligands DABCO serve as the linkers (Scheme 1.4). The dimeric cage **1.9** is not the only complex in this system which manifests the difficulty of driving the self-assembly equilibrium towards a single thermodynamic product. Nevertheless, Cotton and coworkers realized a moderately stable coordination cage assembled by linking two bowl-shaped calixarene scaffolds with four bimetallic units, which was characterized by X-ray crystallography (Figure 1.12a).
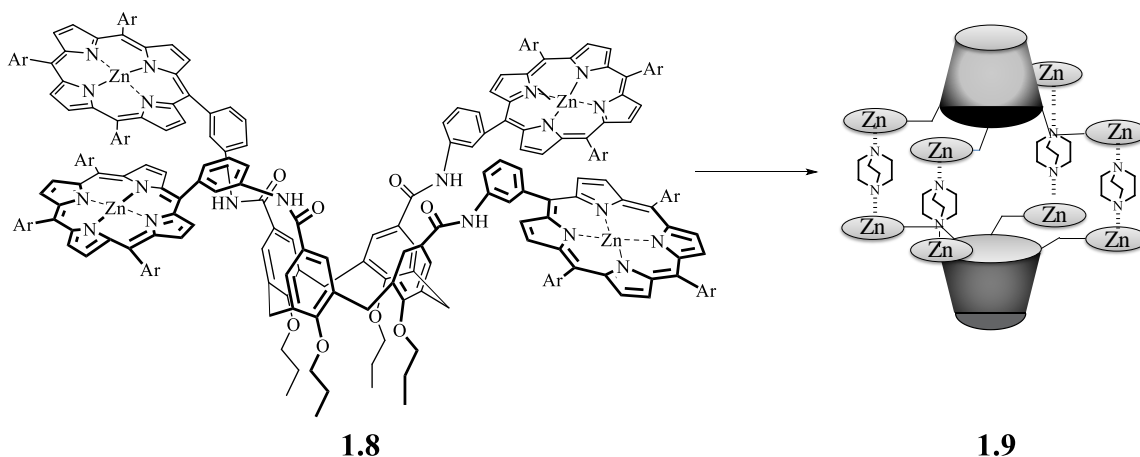
Scheme 1.4 Calix-tetraporphyrin **1.8** and its sandwich complex **1.9** with DABCO. Copyright © 2008 WILEY-VCH Verlag GmbH & Co.
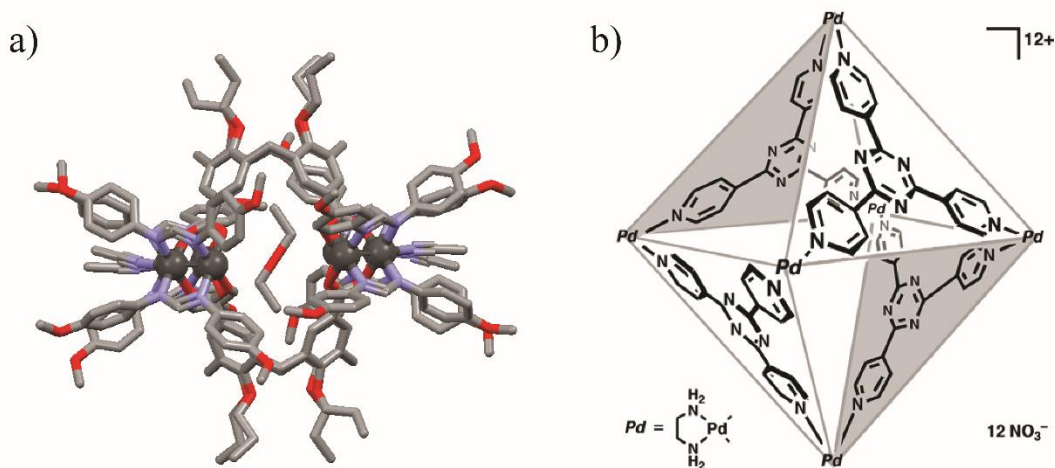
Figure 1.12 a) X-ray crystal structure of a stable cage encapsulating one diethyl ether molecule;[29] b) an octahedral coordination cage with a composition of M_6L_4. Copyright © Nature Publishing, 1995.

Makoto Fujita in Tokyo University has described that complexes obtained from the self-assembly of transition metal-based coordination are controllable and predictable by the nature of the initial building blocks. There are two general types of capsular self-assembly, a ligand as a component consists of convergent binding sites while the metal center possesses divergent binding sites, or the other way around, in consequence, forming a thermodynamically favorable discrete species in an appropriate concentration range (Scheme 1.5).

The formation of a metal-cornered cage was realized by Fujita's group in 1995,[30] in which the six vertices of an octahedron are occupied by *cis*-protected Pd^{II}, whereas the eight triangular faces of the hypothetical octahedron are alternately occupied by four divergent-tridentate ligands (Figure 1.12b), the self-assembly of

polyhedral and polygonal cages and their fascinating properties have subsequently been reported by many groups.[31]
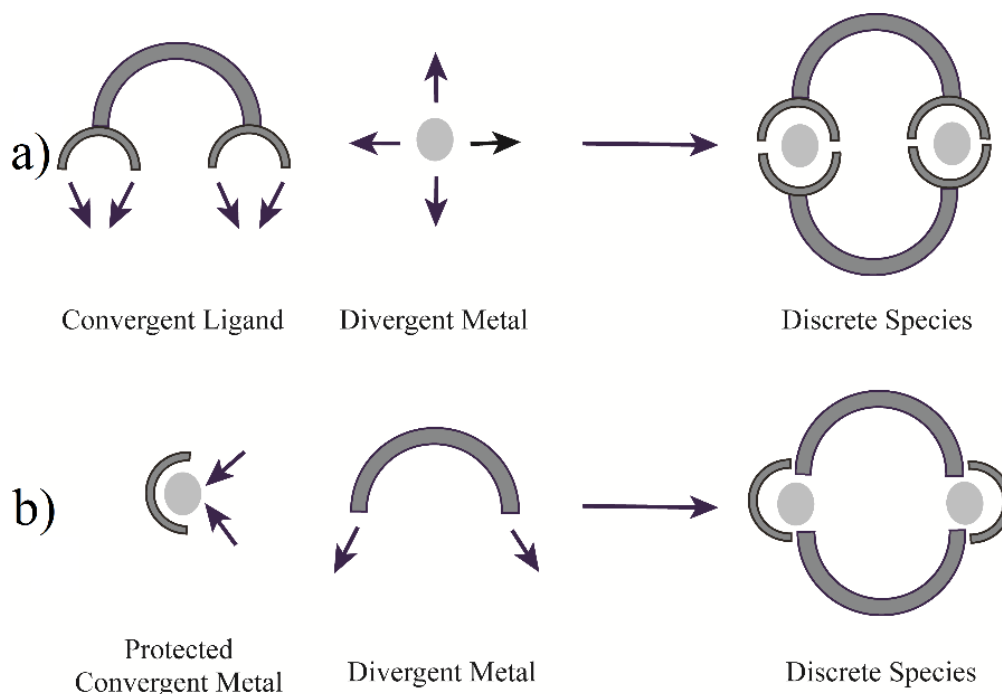
Scheme 1.5 Design of two different capsular self-assembling structures. Copyright © WILEY-VCH Verlag GmbH & Co.

On the basis of principles from self-assembly and their outstanding topologies, a novel class of supramolecular structures termed interpenetrated cages have attracted a lot of attention, in which two discrete components are mechanically interlocked to each other under the support of certain non-covalent interactions. In 2008, Hardie reported a doubly-catenated cage displaying an interlocking motif.[32] In this system, upon the coordination 2,2'-bipyridine moieties with Zn(II) or Co(II), the cyclotriveratrylene-based ligands **1.10** self-assemble discretely to a [2]catenane complex due to two types of weak hydrogen bonding interactions (Scheme 1.6).

Compared with the above example in which the metal ions are located in two parallel planes perpendicular to the axis of highest symmetry (C_3), Kuroda's group reported an interlocked metallohelicate in which the metal ions are located on the C_4 symmetry axis (Figure 1.13). The pattern of interpenetration results in three separate cavities of the cage, which may encapsulate anions or solvent molecules.[33]

The Clever group has worked out a series of structurally related interpenetrated coordination cages and investigated their binding properties and topological transformations in great detail. Firstly, a bis-monodentate pyridyl ligand **1.13** based on a dibenzosuberone backbone was synthesized, reacted with square-planar coordinating Pd^{II} cations forming initially an intermediate monomeric cage and eventually resulting thermodynamically preferable interdigitated cage **1.14** upon heating (Scheme 1.7).

1.10
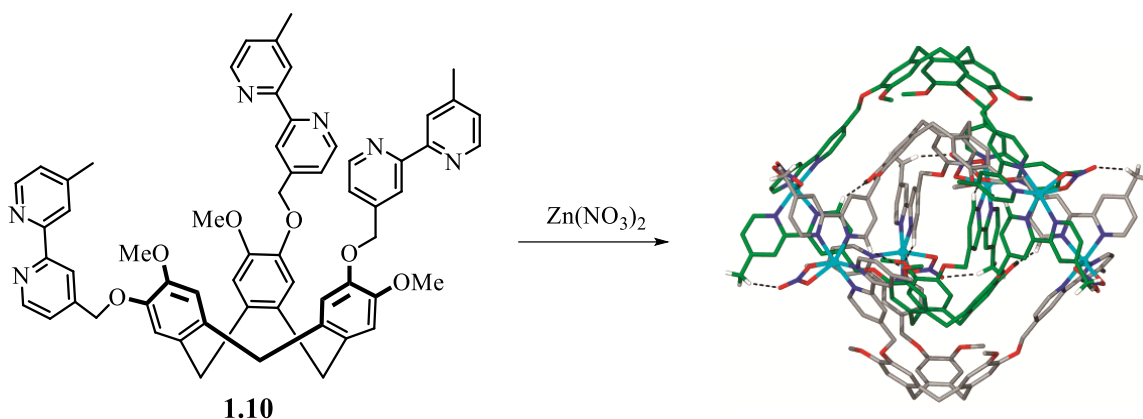
Scheme 1.6 X-ray structure of an interpenetrated cage assembled from cyclotriveratrylene-based ligands coordinating with metal centers. Copyright © 2008 American Chemical Society.

1.11   **1.12**
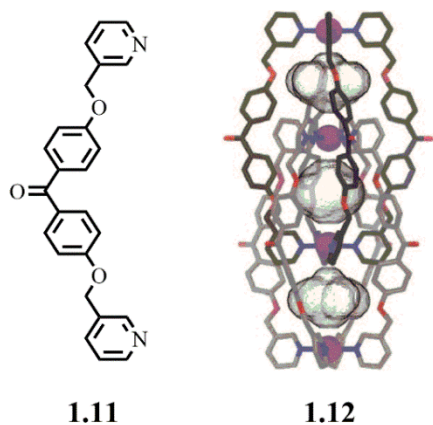
Figure 1.13 X-ray structure of the interlocked metallohelicate **1.12** from the ligand **1.11** coordinating with Pd^{II} cations. Copyright © 2014 The Royal Society of Chemistry.

1.13   **1.14**   **1.15**
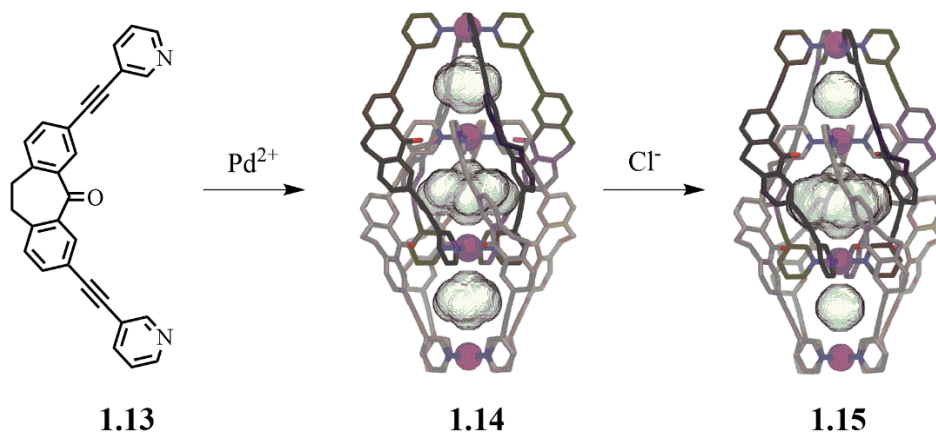
Scheme 1.7 Synthesis and X-ray structure of interpenetrated double cage **1.14** containing three BF_4^- anions in its three pockets and DFT calculated structure of double cage **1.15** after the exchange of BF_4^- from the outer pockets by Cl^- anions (anions not shown). Copyright © 2014 The Royal Society of Chemistry.

Double cage **1.14** is comprised of one central and two outer pockets that encapsulate three BF_4^- anions at first.[34] Upon addition of two equivalents of halide ions per host, two BF_4^- anions occupying the outer two cavities are replaced by two halide ions leading the formation of another interpenetrated cage **1.15** which indicates an allosteric binding mechanism. The halide anion binding causes a considerably structural contraction demonstrated by diffusion-ordered spectroscopy (DOSY) NMR experiments. Furthermore, chloride is bound extremely strong, with a net binding constant of -10^{20} M^{-2} meaning solid AgCl can be dissolved by the cage in solution.[35]

For the purpose of controlling the dimerization process and the guest binding ability of the interpenetrated cage, a bulky aryl substituent was introduced to the carbonyl position of ligand **1.13** producing ligand **1.16**.[36] Because of the steric constraints caused by the attached aryl substituent, a thermodynamically stable monomeric cage is formed in the presence of BF_4^- anions instead of an intercatenated structure. Astonishingly, upon addition of smaller Cl^- anions to the system, interpenetration transformation happened in which chloride occupies in the central pocket as the template. Accompanied with the shrinking of the inner cavity capturing chloride, the other two outer cavities become voluminous enough to encapsulate larger oxyanionic guests, such as ReO_4^- (Scheme 1.8). In consequence, the magnitude of the template inside the central pocket can make a difference of the selectivity of allosteric anion binding in the outer two pockets.

1.16   **1.17**
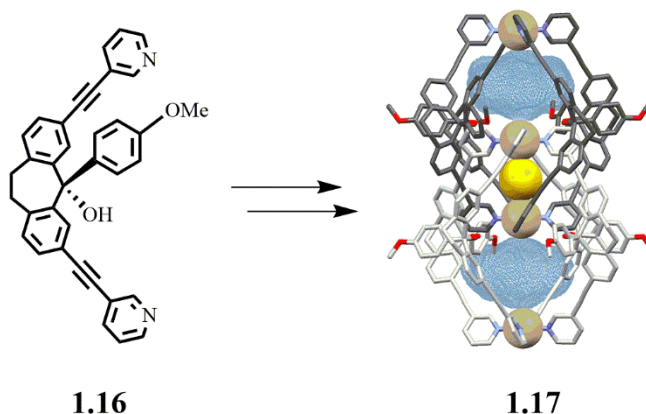
Scheme 1.8 X-ray crystal structure of dimeric cage **1.17** encapsulating one chloride anion within the inner pocket and two ReO_4^- anions within the two out pockets formed from ligand **1.16**. Copyright © 2014 The Royal Society of Chemistry.

One other similar system based on the redox active phenothiazine ligands is discussed by the Clever group.[37] There are three structures in quite close relations which are either without any substituents at the sulfur atom (**1.18a**) or one (**1.18b**) or even two (**1.18c**) oxygen attachments. Upon addition of stoichiometric amounts of $[Pd_2(CH_3CN)_4](BF_4)_2$, the coordination with Pd^{II} leads to the interdigitated complexes **1.19**, **1.20**, **1.21**, respectively. From the X-ray crystal structures (Figure 1.14), the structural differences in these three derivatives can be observed because of the distinct oxidation states of the sulfur atoms. According to a systematic comparison of the halide binding affinities and the structural rearrangements based on NMR

titrations, NOESY experiments and electronic structure calculations, it turns out that the allosteric binding changes along with a structural relay effect and the halide binding affinity decreases while the cavities' size increases in the interpenetrated double-cages.[38]

1.18a: X = S
1.18b: X = S=O
1.18c: X = S=O$_2$

1.19 **1.20** **1.21**
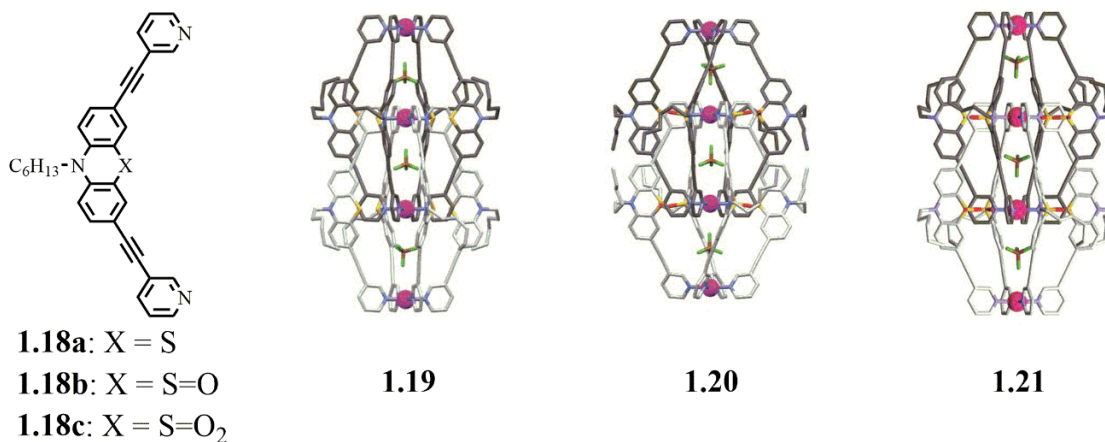
Figure 1.14 X-ray crystal structures of three related dimeric cages based on phenothiazine and its mono- and di-oxygenated derivatives. Copyright © 2014 the Royal Society of Chemistry.

Another noteworthy example that should be mentioned here is that of a self-assembled interpenetrated cage from a bis-monodentate ligand based on the acridone backbone and Pd[II] cations. The resulting double-cage can uptake small neutral guest molecules, which is significantly different from the situation aforementioned.[39] After reacting the ligands with the metal salts in acetonitrile, a similar complex **1.23** is obtained initially showing three BF$_4^-$ anions sitting in the three cavities. Furthermore, a conformational change is triggered by two small halide anions that remarkably endows the inner pocket with the capability to encapsulate a small neutral molecule such as benzene, resulting in the unusual interpenetrated cage **1.24** (Figure 1.15).

1.22 **1.23** **1.24**
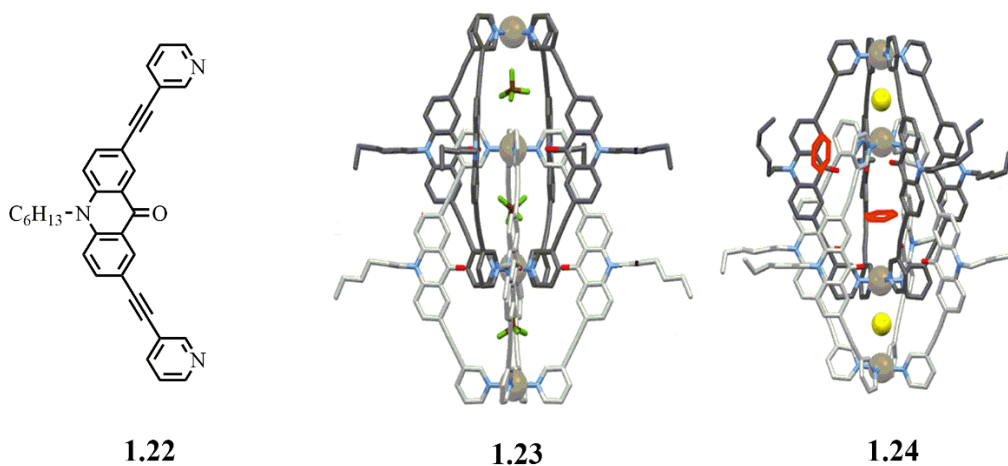
Figure 1.15 X-ray crystal structures of interpenetrated cages **1.23** and **1.24** based on the acridone ligand **1.22**. Copyright © 2015 American Chemical Society.

Light is considered as an ideal external stimulus for molecular switching behavior due to its easy addressability and well-defined regulation, thus molecular photo-switches are applied into supramolecular self-assembly processes such as constructing a photo reversible system.[40] A photochromic coordination cage **1.26** consisting of light-switchable ligands based on the dithienylethene (DTE) chromophore was introduced by Clever and co-workers.[41] As reported, DTE can undergo a reversible transformation induced by different irradiation at wavelengths of light, the ligand **1.25** can interconvert between open- (**1.25a**) and closed- (**1.25b**) ring forms back and forth by irradiation with white light or UV light, respectively (Scheme 1.9). In addition,
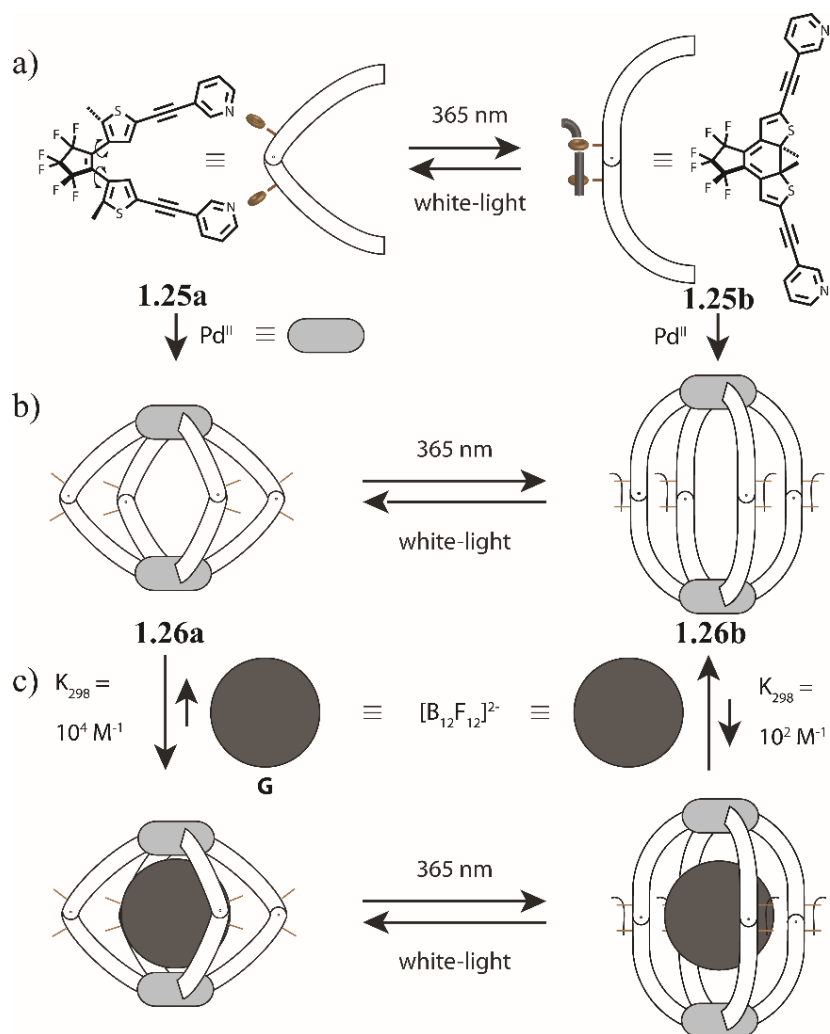
Scheme 1.9 a) Upon irradiation at 365 nm or white light, the conformationally flexible dithienylethenyl pyridyl ligand **1.25a** and the rigid closed-ring isomer **1.25b** can convert fully back and forth; b) Quantitative formation of both cages **1.26a** and **1.26b** upon addition of $[Pd(CH_3CN)_4](BF_4)_2$, the above-mentioned photochemical processes can trigger the interconversion between two cage complexes as well; c) Spherical guest ($[B_{12}F_{12}]^{2-}$) can be encapsulated in both cage isomers but with large different binding constants. Irradiation of the host-guest complexes results in the reversible uptake and release of the guest. Copyright © 2012 WILEY-VCH Verlag GmbH & Co.

the assembled cage **1.26** from the corresponding ligand exhibits the similar photochemical behavior. In case of the reversible interconversion, the size difference between these two cages (**1.26a** and **1.26b**) enables the investigation of anion encapsulation capabilities. According to the host-guest association constants from the titration experiments by non-linear regression method[42] in the presence of dodecafluorododecaborate anion ($[B_{12}F_{12}]^{2-}$) as a guest, cage **1.26a** shows a much stronger affinity ($K_{293} = 3.2 \times 10^4$ M^{-1}) than cage **1.26b** ($K_{293} = 6.7 \times 10^2$ M^{-1}). As can be concluded, the differences in geometry and electronic structures via harnessing the photoactive units play a significant role on taking up and releasing guest molecules.

Based on the same photochromic DTE backbones, another light-switchable ligand **1.27** was synthesized and reacted with square-planar-coordinated Pd^{II} constructing a three ring complex **1.28** at the beginning.[43] Upon light irradiation, a dramatically structural reorganization was triggered resulting a huge rhombicuboctahedral sphere **1.29** (Scheme 1.10). The stimuli-responsive conformational rearrangement involving the fatigue-resistant DTE photo-switch has laid a solid foundation on the manipulation of dynamic supramolecular architectures.
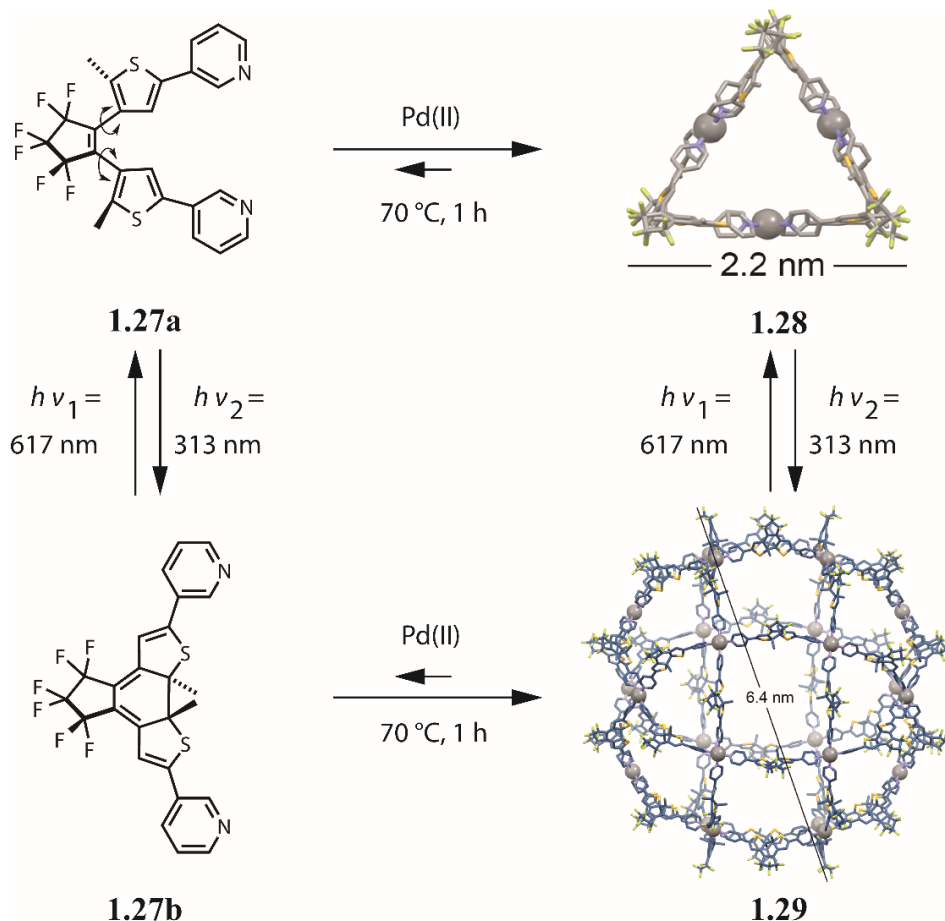
Scheme 1.10 Photoisomerization and self-assembly of the ligand photoisomers **1.27a** and **1.27b** into the triangular ring **1.28** (DFT structure calculation) and the rhombicuboctahedral sphere **1.29** (semiempirical-PM6 geometry-optimized molecular model) separately. Copyright © 2016 WILEY-VCH Verlag GmbH & Co.

1.5 Applications of supramolecular chemistry

Molecular recognition, switchable systems and transport represent the basic functions of supramolecular species. Following the endeavors of supramolecular chemists over the past decades, functions associated with the inner cavities of the supramolecules are achievable and much more promising in applications of molecular sensing, separation, catalysis and biological processes.[44]

1.5.1 Molecular recognition and encapsulation

The synthesis and subsequent characterization of supramolecular architectures are often accompanied with the encapsulation of small species, such as anions, cations or neutral molecules within the cavities inside these supramolecular structures.

The first example of non-covalent anion binding may be traced back to the term "*katapinands*" which means to swallow up or engulf from Greek by C. H. Park and H. E. Simmons in 1968.[45] From then on, a considerable number of anion complexes have been synthesized and realized their distinct encapsulation ability of host molecules.[46,47] Schmidtchen published a series of papers focusing on anion recognition solely by electrostatic interactions.[48] The host employs quaternary ammonium units in a tetrahedral manner forming a cage-shaped receptor in which the anion is bound tightly (Figure 1.16a). Indeed, the selectivity of the hosts for particular halides can be adjusted by changing the length of the alkyl chain between the ammonium centers. The larger host **1.31** is capable to encapsulate large anions such as *p*-nitrophenolate which is too large to be captured within **1.30**. Host **1.30**, in which the cavity possesses an internal diameter of 4.6 Å, provides a better magnitude for smaller iodide anion with 4.12 Å (Figure 1.16b).
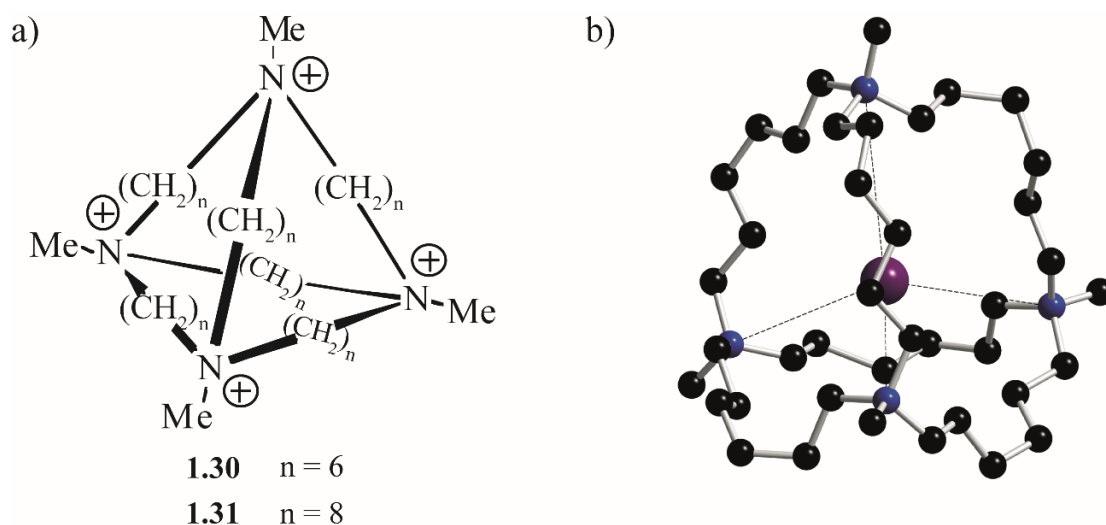

Figure 1.16 a) Tetrahedral hosts **1.30** and **1.31** by Schmidtchen; b) the X-ray crystal structure of the iodide salt of host **1.30**. Only the internally bound iodide (purple) is shown. Copyright © 1984 the Royal Society of Chemistry.

As for metallic and organic cation binding, crown ethers and cryptands are the simplest and most typical hosts in supramolecular chemistry.[49] They have been introduced in the first part of this chapter. And the numerous derivatives followed by spherands and cryptospherands play active roles in the field of molecular recognition in supramolecular chemistry.[50]

The binding and recognition of neutral molecules usually make use of electrostatic, donor-acceptor and particularly of hydrogen bonding interactions.[51] Of special interest is the recognition of enantiomers because of their similar structures. Fujita's group reported a synthetic coordination host which increased the chirality enrichment via bimolecular heterorecognition of enantiomers.[52] The bowl-shaped host **1.32**, which is resulted from the self-assembly of tris(3-pyridyl)triazine ligand and Pd[(en)(NO$_3$)$_2$] (en = ethylenediamine), was introduced to look into the chiral selectivity of 1,1'-bi-2-naphthol (BINOL). The host-guest complex **1.33** formed upon addition of a solution of (*S*)-BINOL in hexane at a 50% enantiomeric excess (*ee*) into the aqueous solution of **1.32** (Scheme 1.11). After separation and extraction with organic solvent, the analysis turned out only 9% *ee* guest encapsulated. As a result, enrichment of chiral compounds increased from 50% to 87% *ee* without adding any external chirality source.
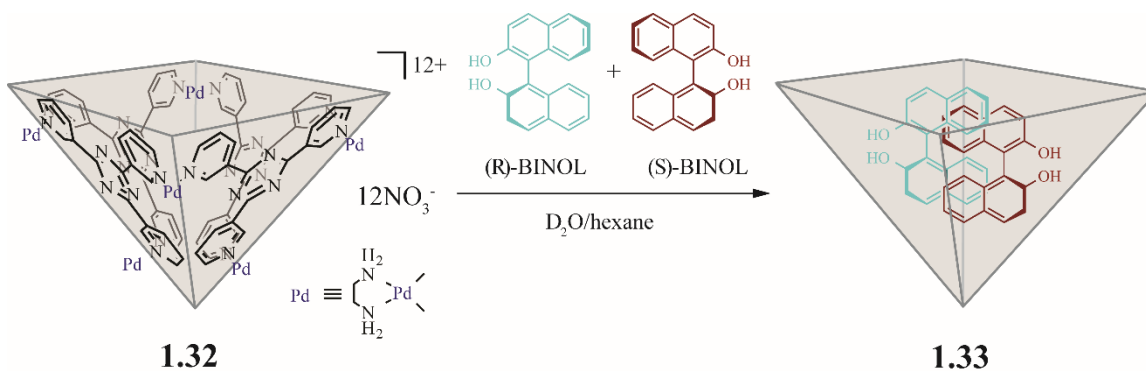
Scheme 1.11 Neutral molecular recognition of enantiomers (*R*)-BINOL and (*S*)-BINOL in host **1.32**. Copyright © 2007 WILEY-VCH Verlag GmbH & Co.

1.5.2 Catalysis and reactions

Supramolecular reactivity and catalysis have attracted much attention of chemists because of the particularly remarkable features displayed in supramolecular processes.[53] The design of highly efficient and selective supramolecular reagents and catalysis could be able to give mechanistic insight into the catalytic principles. It has been demonstrated that supramolecular architectures such as capsules or cages can be used as reaction vessels or catalysts showing excellent selectivity and efficiency.

Self-assembled capsules, which show enclosed cavities formed via noncovalent interactions such as highly directional hydrogen bonding between two or more subcomponents, can be regarded as molecular reaction flasks. In 1998, Rebek and co-workers synthesized a large dimeric cylindrical capsule **1.34** self-assembled from two cavitands stabilized by hydrogen bonding, large enough to encapsulate two different guest

molecules.[54] 1,3-Dipolar cycloaddition between phenyl acetylene and phenyl azide is completely regioselective in the capsule **1.34** and accelerated within a few days, whereas it takes years for this reaction to complete in the absence of **1.34**[55] (Scheme 1.12).

Fujita's group reported a series of self-assembled coordination cages which can be used as catalysts with high regioselectivity in [2+2] photodimerization of olefins.[56] The bowl-shaped cage **1.32** mentioned previously was proved to facilitate the intermolecular [2+2] photochemical reaction of 1,4-naphthoquinones and efficiently control the stereochemistry in stringent geometrical environment.[57] The dimerization of 1,4-naphthoquinones yielded the *syn*-dimer **1.35** in > 98% yield while the same reaction in the absence of **1.32** gave the *anti*-dimer product **1.36** predominantly (Scheme 1.13). In addition, the octahedral coordination cage (Figure 1.12b) aforementioned was thoroughly investigated as an ideal molecular vessel for Diels−Alder reactions with considerably high selectivity and reactivity.[58]
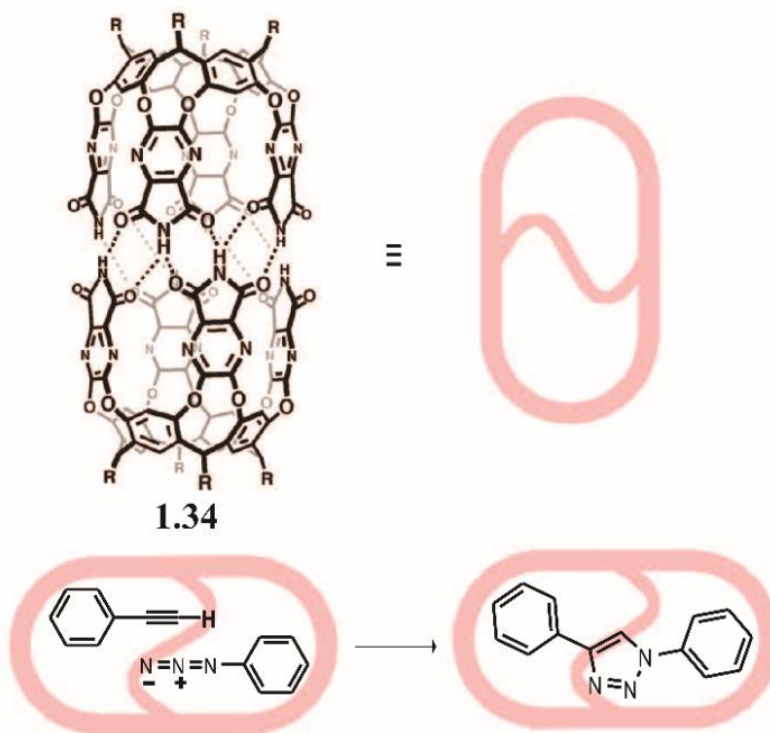
Scheme 1.12 Cylindrical capsule **1.34**, which is self-assembled from two resorcinarene subunits, and the 1,3-dipolar cycloaddition reaction that is accelerated within this capsule. Copyright © 2002 American Chemical Society.

1.5.3 Supramolecular devices

Supramolecular devices are by definition formed from non-covalently linked components, which show structural organizations and functional integrations. Depending on whether the components are photoactive,

electroactive or ionoactive, it can be defined as supramolecular photonics, electronics or ionics, respectively.[2]
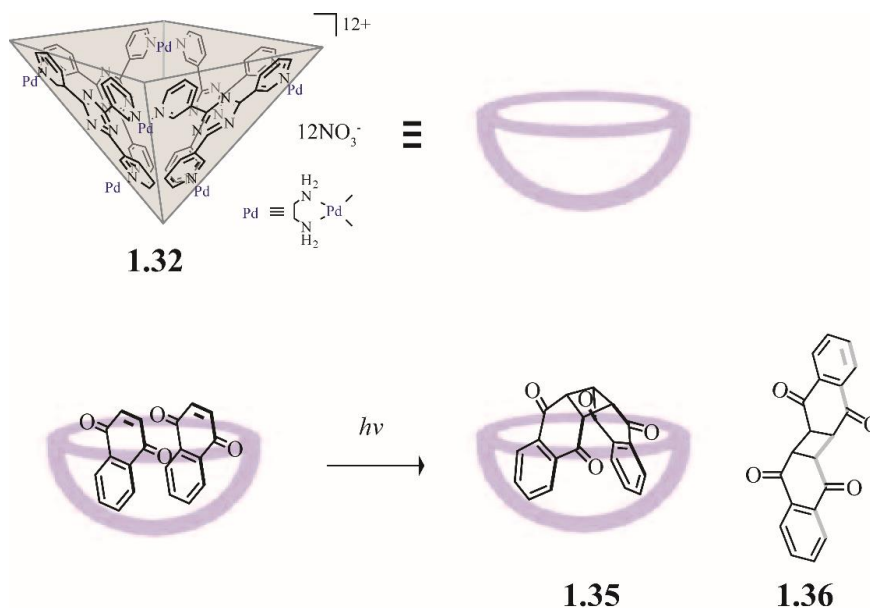
Scheme 1.13 Schematic representation of the photodimerization of 1,4-naphthoquinone by the half open metallocage **1.32**. Copyright © 2006 American Association for the Advancement of Science.

Achieving photo-induced charge separation is of much interest for the transfer of photosignals.[59] Lehn's group has focused on a novel system which can function as an efficient molecular photodiode.[60] In this system, it contains a zinc-porphyrin group as a photosensitive subunit and two lateral [18]-N_2O_4 macrocycles which can bind metal ions[61] forming a multi-substrate cryptate complex. As a result of the complexation of silver ions by the lateral macrocycles, the singlet excited state of Zn-porphyrin center was quenched by an efficient intracomplex electron transfer, from porphyrin to Ag(I), attributing to a charge-separated state and yielding a porphyrinium cation of long life time (Figure 1.17).

Switching devices, triggered by external electrical[62], optical[63], thermal[64] or magnetic stimuli[65], are also of high interest in synthetically supramolecular receptors and carriers due to the multiple molecular and supramolecular features such as binding geometry, strength and selectivity of ions.[66] The formation of photo-, electro- and ion-switching devices is still a promising and encouraging field bringing functional materials in supramolecular chemistry.

1.5.4   Biological and medical applications

In pace with the vigorous growth and interdisciplinary nature of supramolecular chemistry, supramolecular chemists have spent a great deal of efforts in collaborations with theorists, physicists, analysist and especially biologists in attempts to mimic biological processes such as selective transport of metal cations[67] and anions[68], catalytic reactions by enzymes[69] and so on.

Fujita and coworkers found the short peptides **1.38−1.41** adopt special helical conformations within the porphyrin-prism host **1.37** self-assembled from zinc(II) tetrakis(3-pyridyl)porphyrin and [Pd(chxn)(NO₃)₂] [chxn = (S, S)-1,2-diaminocyclohexane] in aqueous solvents.[70] In all cases, these alanine-rich tri- to hexa-peptides take the hybrid β-turn (3_{10})[71]/α-helix (4_{13}) conformations instead of pure α-helix conformations[71] accommodated in the large hydrophobic cavity of the host[72,73] (Figure 1.18).
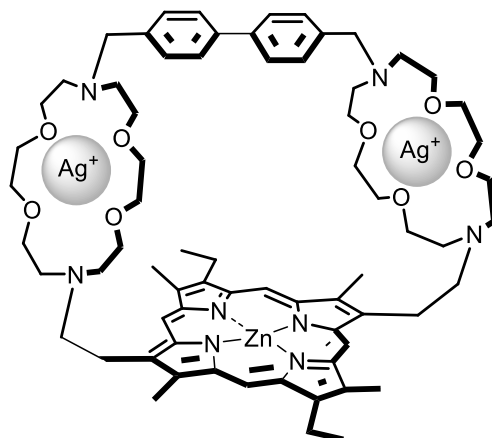
Figure 1.17 Intramolecular electron transfer in the polymetallic cryptate. Copyright © WILEY-VCH Verlag GmbH & Co.

1.38: Ac-Ala¹-Ala²-Ala³-NH₂
1.39: Ac-Gly-Ala¹-Ala²-Ala³-NH₂
1.40: Ac-Gly-Gly-Ala¹-Ala²-Ala³-NH₂
1.41: Ac-Gly-Gly-Ala¹-Ala²-Ala³-Gly-NH₂
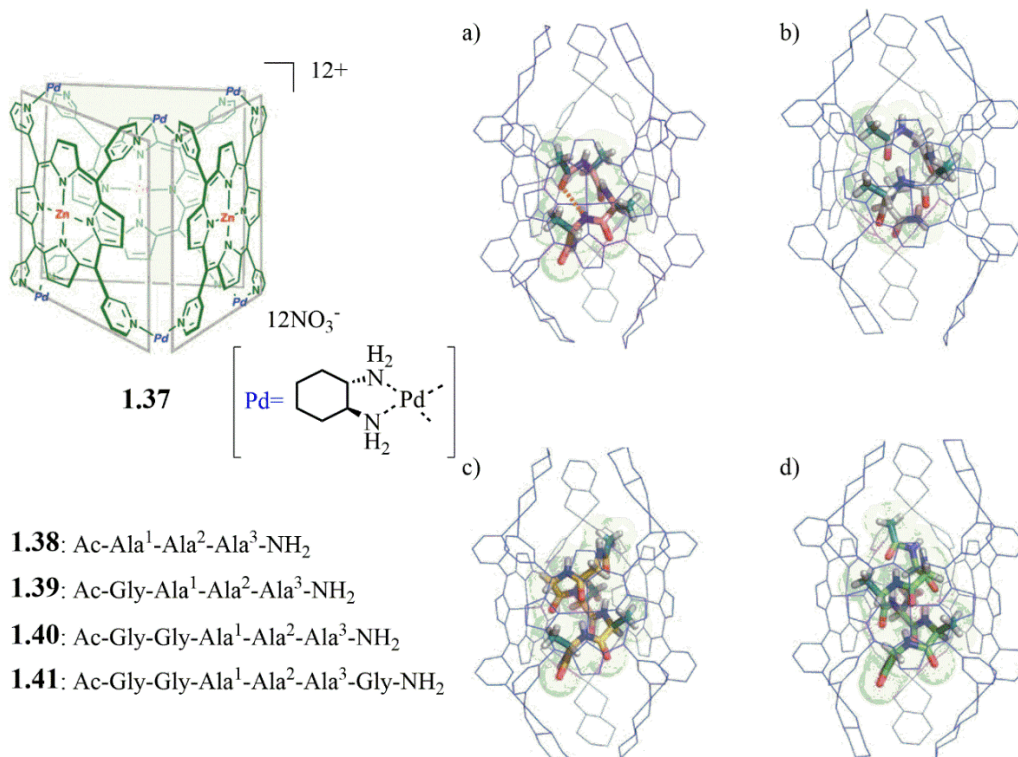
Figure 1.18 Structure of porphyrin-prism host **1.37**; and crystal structures of a) **1.38** in the cavity of **1.37**; b) **1.39** in the cavity of **1.37**; c) **1.40** in the cavity of **1.37**; d) **1.41** in the cavity of **1.37**. Copyright © 2001 WILEY-VCH Verlag GmbH & Co.

The first encapsulation of a protein within a synthetically supramolecular host was also reported by the Fujita group.[74] In their work, a small protein, ubiquitin, which was attached to one bidentate ligand, was encapsulated in a self-assembled $M_{12}L_{24}$ coordination nanocage (Scheme 1.14). Due to the well-defined construction of the host framework, the architecture of the encapsulated protein was able to be distinctly analyzed by X-ray crystallography coupled with maximum-entropy method which clearly shows the electron density of the protein in the coordination cage. This research laid a foundation for the supramolecular chemists on exploring the synthetically capsule-shaped complexes for the conformational and functional control of encapsulated proteins.
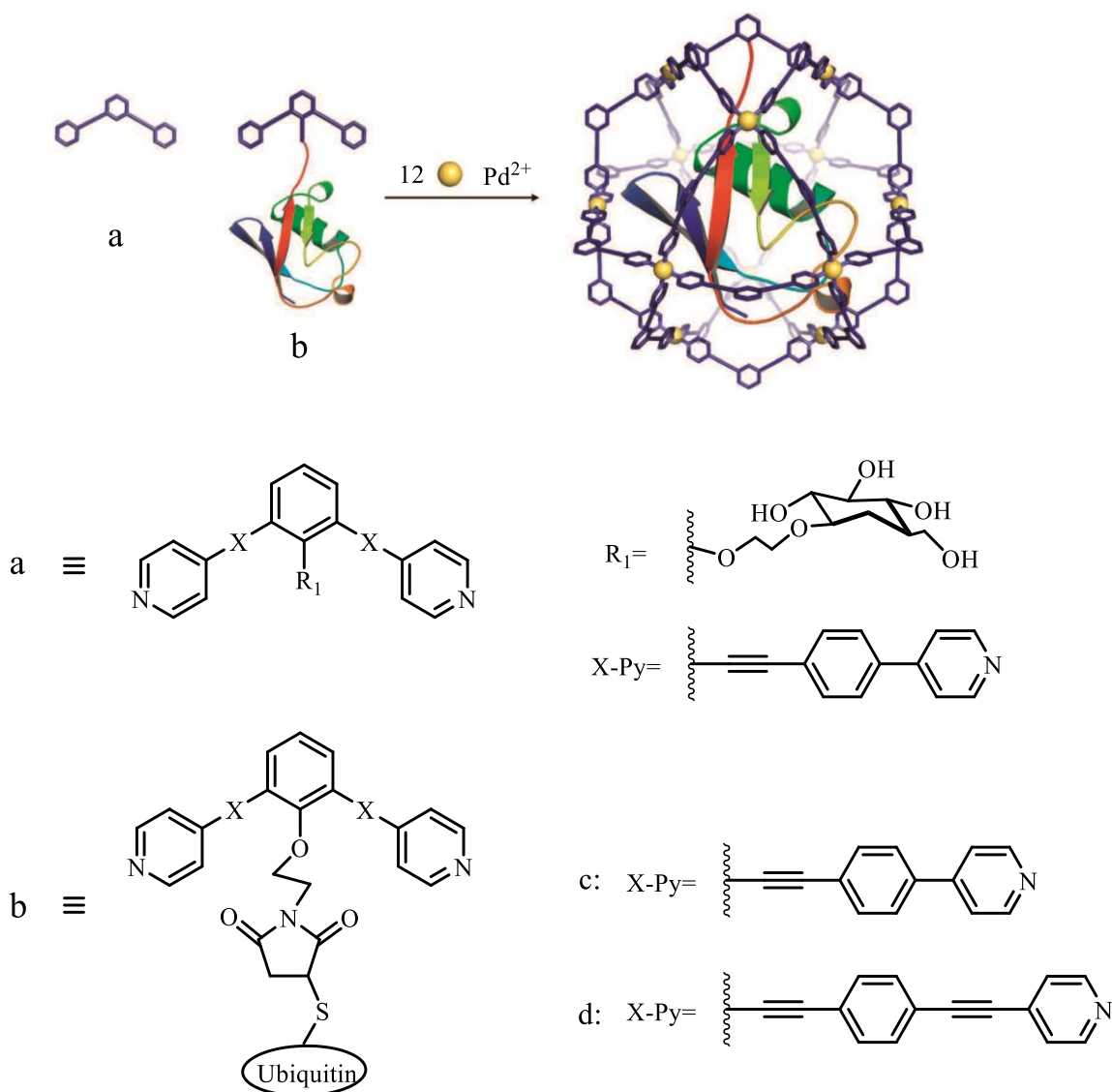
Scheme 1.14 Schematic representation of the encapsulation of ubiquitin. Copyright © Nature Publishing, 2012.

1.6 Supramolecular polymers

Covalent polymers such as polystyrene and polyethylene which are practical and technological materials were interpreted in depth by Staudinger in the early 1920s. When supramolecular chemistry meets polymer science, an extensive area of research, supramolecular polymers, is disclosed rapidly which makes use of non-covalent interactions between bi- or multifunctional monomer units.

In the past two decades, supramolecular polymers have drawn much attention not only because they offer versatile and attractive structures but also because of the self-assembly process from reversible interactions which lead to potentially tunable properties such as recycling, self-healing as well as degradability.[75,76,77] Hydrogen bonding has been widely used in the fabrication of cross-linked materials via self-assembly.[78-82] Lehn's group worked on the two-component assembly **1.44** connecting the hydrogen-bonded groups via imide groups (Figure 1.19). Because of the molecular rigidity, this kind of rigid-rod supramolecular polymers exhibit lyotropic liquid crystalline behavior.[83]

1.42
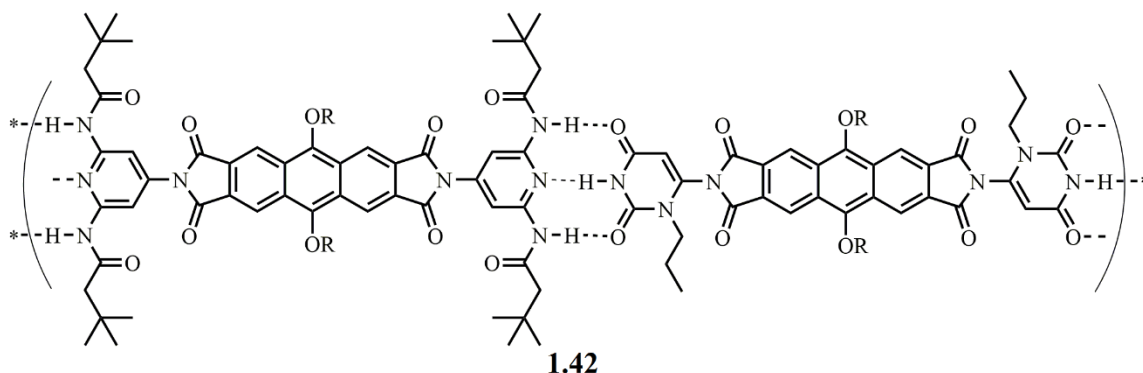
Figure 1.19 Liquid crystalline supramolecular polymers developed by Lehn based on triple hydrogen bonds arrays from rigid monomers.

Owing to the variety of properties in magnetics, electronics and optics of metal ions, embedding metal ions via noncovalent coordination interactions to form metallo-supramolecular polymers has been approached. A typical example of optically healable metallo-supramolecular polymers was reported by Rowan, Weder and coworkers. The polymers are formed by a rubbery amorphous poly(ethylene-co-butylene) ending with 2,6-bis(19-methylbenzimidazolyl)pyridine (Mebip) ligands and metal ions (Figure 1.20). Upon the irradiation of ultraviolet light, the metal-ligand complexes are electronically excited and the absorbed energy is converted into heat, which brings about temporary dissociation of the metal-ligand motifs and a contingent reversible decrease of the polymers' molecular mass and viscosity as the result of quick and efficient defect healing.[84] This innovative approach of light-heat conversion is promisingly applicable in a wide range of supramolecular materials.
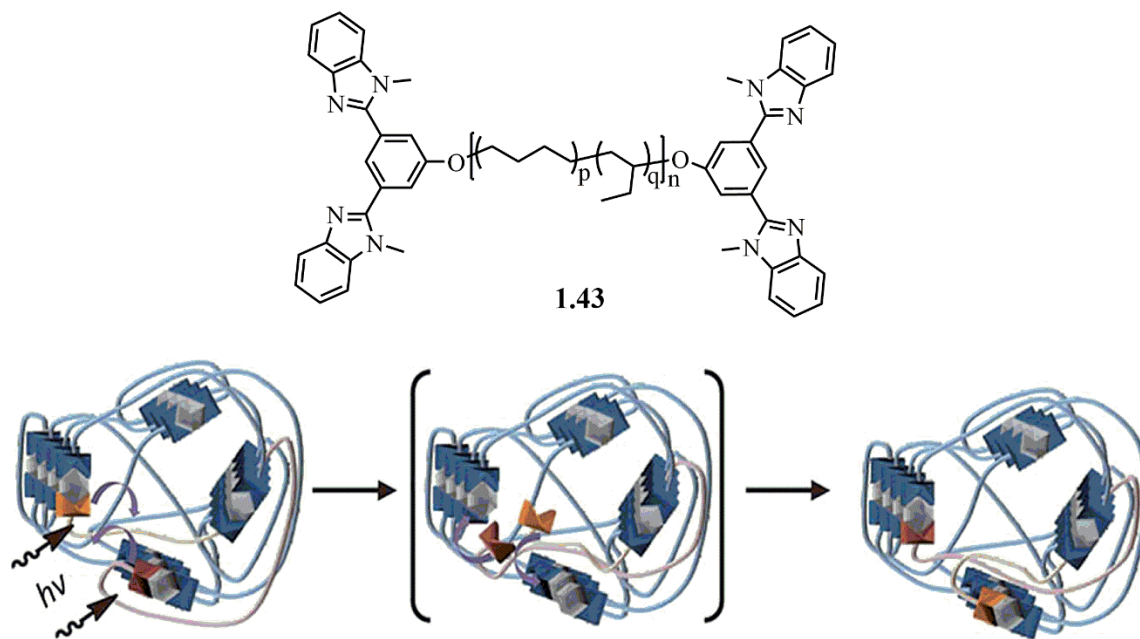
Figure 1.20 Photo-healing mechanism of the metallosupramolecular based on macromonomer **1.43** and Zn(II) ions. Copyright © Nature Publishing, 2011.

In conclusion, the advancement in supramolecular chemistry has accelerated the progress of polymers by assembling small molecules into polymers arrays. On account of the reversible non-covalent bonding in the supramolecular polymers and their thermodynamic nature, the properties can be controlled by external stimuli. Thus, novel tunable polymeric materials are within reach.

1.7 References

[1] J.-M. Lehn, *Angew. Chem. Int. Ed.* **1988**, *27*, 89.

[2] J.-M. Lehn, *Supramolecular Chemistry: Concepts and Perspectives*, 1ˢᵗ ed., Wiley, Weinheim, Germany, **1995**.

[3] a) A. Villiers, C. R. Hebd, *Seances. Acad. Sci.* **1891**, *112*, 435; b) A. Villiers, C. R. Hebd, *Seances. Acad. Sci.* **1891**, *112*, 536.

[4] A. Werner, *Zeitschr. Anorg. Chem.* **1893**, *3*, 267.

[5] E. Fischer, *Ber. Deutsch. Chem. Ges.* **1894**, *27*, 2985.

[6] D. E. Koshland, Jr., *Proc. Natl. Acad. Sci.* USA **1958**, *44*, 98.

[7] P. Ehrlich, *Collected Studies on Immunity*, Wiley, New York **1906**.

[8] K. L. Wolf, H. Frahm, H. Harms, *Z. Phys. Chem. (B)* **1937**, *36*, 237.

[9] D. E. Palin, H. M. Powell, *Nature,* **1945**, *156*, 334.

[10] C. J. Pedersen, *J. Am. Chem. Soc.* **1967**, *89*, 7017.

[11] B. Dietrich, J.-M. Lehn, J.-P. Sauvage, *Tetrahedron Lett.* **1969**, *10,* 2885.

[12] P. J. Garratt, A. J. Ibbett, J. E. Ledbury, R. O'Brien, M. B. Hursthouse, K. M. A. Malik, *Tetrahedron,* **1998**, *54*, 949.

[13] J. L. Atwood, J. W. Steed, *Supramolecular Chemistry*, 2nd ed., Chichester, UK, **2009**.

[14] C. A. Hunter, K. R. Lawson, J. Perkins, C. J. Urch*, J. Chem. Soc., Perkin Trans. 2*, **2001**, 651.

[15] G. D. Andreetti, R. Ungaro, A. Pochini, *J. Chem. Soc., Chem. Commun.* **1979**, *22*, 1005.

[16] T. D. Hamilton, L. R. MacGillivray, *Self-Assembly in Biochemistry in: Encyclopedia of Supramolecular Chemistry*, J. L. Atwood, J. W. Steed (Eds.), Dekker, New York, **2004**, 1257.

[17] L. F. Lindoy, I. Atkinson, *Self-assembly in Supramolecular Systems*. Royal Society of Chemistry, Cambridge, **2000**.

[18] E. Wasserman, *J. Am. Chem. Soc.* **1960**, *82*, 4433.

[19] M. Cesario, C. O. Dietrich-Buchecker, J. Guilhem, C. Pascard, J.-P. Sauvage, *J. Chem. Soc., Chem. Commun.* **1985**, *5*, 244.

[20] P. R. Ashton, T. T. Goodnow, A, E, Kaifer, *et al., Angew. Chem. Int. Ed.* **1989**, *28*, 1396.

[21] a) D. B. Amabilino, J. F. Stoddart, *Chem. Rev.,* **1995**, *95*, 2725; b) D. B. Amabilino, P. R. Ashton, A. S. Reder, N. Spencer, J. F. Stoddart, *Angew. Chem. Int. Ed.* **1994**, *33*, 1286; c) D. B. Amabilino, P. R. Ashton, S. E. Boyd, *et al., Angew. Chem. Int. Ed.* **1997**, *115*, 5286.

[22] M. E. Padilla-Tosta, O. D. Fox, M. G. B. Drew, P. D. Beer, *Angew. Chem. Int. Ed*. **2001**, *40*, 4235.

[23] A. G. Johnston, D. A. Leigh, R. J. Pritchard, M. D. Deegamn, *Angew. Chem. Int. Ed*. **1995**, *34*, 1209.

[24] a) M. Fujita, F. Ibukuro, H. Hagihara, K. Ogura, *Nature,* **1994**, *367*, 720; b) M. Fujita, *Acc. Chem. Res.* **1999**, *32*, 53.

[25] J. C. Barnes, A. C. Fahrenbach, *et al., Science,* **2013**, *339*, 429.

[26] C. D. Gutsche, *Calixarenes*, Royal Society of Chemistry, Cambridge, **1989**.

[27] D. J. Cram, J. M. Cram, *Container Molecules and Their Guests*, Royal Society of Chemistry, London, **1994**.

[28] L. Baldini, P. Ballester, A. Casnati, R. M. Gomila, C. A. Hunter, F. Sansone, R. Ungaro, *J. Am. Chem. Soc.* **2003**, *125*,14181.

[29] F. A. Cotton, P. Lei, C. Lin, *et al*., *J. Am. Chem. Soc.* **2004**, *126*, 1518.

[30] M. Fujita, D. Ogura, M. Miyazawa, H. Oka, K. Yamaguchi, K. Ogura, *Nature,* **1995**, *378*, 469.

[31] a) T. Beissel, R. E. Powers, K. N. Raymomd, *Angew. Chem. Int. Ed*. **1996**, *35*, 1084; b) M. Ziegler, J. L. Brumaghim, K. N. Raymond, *Angew. Chem. Int. Ed*. **2000**, *39*, 4119; c) V. M. Dong, D. Fiedler, B. Carl, R. G. Bergman, K. N. Raymond, *J. Am. Chem. Soc.* **2006**, *128*, 14464.

[32] A. Westcott, J. Fisher, L. P. Harding, P. Rizkallah and M. J. Hardie, *J. Am. Chem. Soc.* **2008**, *130*, 2950.

[33] M. Fukuda, R. Sekiya and R. Kuroda, *Angew. Chem. Int. Ed*. **2008**, *47*, 706.

[34] S. Freye, J. Hey, A. Torras Galan, D. Stalke, R. Herbst Irmer, M. John and G. H. Clever, *Angew. Chem. Int. Ed.* **2012**, *51*, 2191.

[35] S. Freye, D. M. Engelhard, M. John and G. H. Clever, *Chem. Eur. J.* **2013**, 2114.

[36] S. Freye, R. Michel, D. Stalke, M. Pawliczek, H. Frauendorf, G. H. Clever, *J. Am. Chem. Soc.* **2013**, *135*, 8476.

[37] M. Frank, J. Hey, I. Balcioglu, Y. S. Chen, D. Stalke, T. Suenobu, S. Fukuzumi, H. Frauendorf, G. H. Clever, *Angew. Chem. Int. Ed.* **2013**, *52*, 10102.

[38] M. Frank, L. Krause, R. H. Irmer, D. Stalke, G. H. Clever, *Dalton Trans.,* **2013**, *42*, 15906.

[39] S. Löffler, J. Lübben, L. Krause, D. Stalke, B. Dittrich, G. H. Clever, *J. Am. Chem. Soc.* **2015**, *137*, 1060.

[40] T. Murase, S. Sato and M. Fujita, *Angew. Chem. Int. Ed.* **2007**, *46*, 5133.

[41] M. Han, R. Michel, B. He, Y. S. Chen, D. Stalke, M. John, G. H. Clever, *Angew. Chem. Int. Ed.* **2013**, *52*, 1319.

[42] P. Thordarson, *Chem. Soc. Rev.,* **2011**, *40*, 1305.

[43] M. Han, Y. S. Luo, B. Damaschke, *et al*, *Angew. Chem. Int. Ed.* **2016**, *55*, 445.

[44] a) M. Iyoda, J. Yamakawa, M. J. Rahman, *Angew. Chem. Int. Ed.* **2011**, *50*, 10522; b) M. Fujita, S. Y. Yu, T. Kusukawa, H. Funaki, K. Ogura, K. Yamaguchi, *Angew. Chem. Int. Ed.* **1998**, *37*, 2082.

[45] C. H. Park, H. E. Simmons*, J. Am. Chem. Soc.* **1968**, *90*, 2431.

[46] A. Bianchi, K. Bowman-James, E. Garcia-España, *Supramolecular Chemistry of Anions*, Wiley-VCH, New York, **1997**.

[47] J. L. Sessler, P. A. Gale, W. S. Cho, *Anion Receptor Chemistry, in Monographs in Supramolecular Chemistry,* Royal Society of Chemistry, Cambridge, **2006**.

[48] a) F. P. Schmidtchen, *Angew. Chem. Int. Ed.* **1977**, *16*, 720; b) F. P. Schmidtchen, *Chem. Ber.*, **1980**, *113*, 864; c) F. P. Schmidtchen, *Chem. Ber.*, **1981**, *114*, 597; d) F. P. Schmidtchen, G. Muller, *J. Chem. Soc., Chem. Commun.* **1984**, 1115.

[49] G. W. Gokel, *Crown Ether*, Royal Society of Chemistry, Cambridge, **1990**.

[50] a) D. J. Cram, *Angew. Chem. Int. Ed.* **1986**, *25*, 1039; b) D. J. Cram, *Angew. Chem. Int. Ed.* **1988**, *27*, 1009.

[51] a) K. Morokuma, *Acc. Chem. Res.* **1977**, *10*, 294; b) P. A. Kollman, *Acc. Chem. Res.* **1977**, *10*, 365.

[52] M. Yoshizawa, M. Tamura, M. Fujita, *Angew. Chem. Int. Ed.* **2007**, *46*, 3874.

[53] a) S. Zarra, D. M. Wood, D. A. Roberts, J. R. Nitschke, *Chem. Soc. Rev.,* **2015**, *44*, 419; b) J. N. Rebilly, B. Colasson, O. Bistri, D. Over, O. Reinaud, *Chem. Soc. Rev.,* **2015**, *44*, 467.

[54] T. Heinz, D. M. Rudkevich, J. J. Rebek, *Nature,* **1998**, *394*, 764.

[55] J. Chen, J. Jr. Rebek, *Org. Lett.* **2002**, *4*, 327.

[56] M. Yoshizawa, J. K. Klosterman, M. Fujita, *Angew. Chem. Int. Ed.* **2009**, *48*, 3418.

[57] M. Yoshizawa, Y. Takeyama, T. Kusukawa, M. Fujita, *Angew. Chem. Int. Ed.* **2002**, *41*, 1347.

[58] M. Yoshizawa, M. Tamura, M. Fujita, *Science,* **2006**, *312*, 251.

[59] a) M. A. Fox, M. Chanon, *Photoinduced Electron Transfer*, Elsevier, New York, **1988**; b) J. R. Norris, Jr., D. Meisel, *Photochemical Energy Conversion*, Elsevier, New York, **1989**; c) M. R. Wasielewski, *Chem. Rev.,* **1992**, *92*, 435.

[60] M. Gubelmann, A. Harriman, J.-M. Lehn, J. L. Sesslera, *J. Chem. Soc., Chem. Commun.* **1988**, 77.

[61] a) A. D. Hamilton, J.-M. Lehn, and J. L. Sessler, *J. Chem. Soc., Chem. Commun.* **1984**, 311; b) A. D. Hamilton, J.-M. Lehn, and J. L. Sessler, *J. Am. Chem. Soc.* **1986**, *108*, 5158.

[62] A. J. Moore, L. M. Goldenberg, M. R. Bryce, *et al.*, *J. Org. Chem.* **2000**, *65*, 8269.

[63] *Photochromism; Molecules and Systems*, Elsevier, Amsterdam, **1990**.

[64] J. Kröber, E. Codjovi, O. Kahn, F. Grolière, C. Jay, *J. Am. Chem. Soc.* **1993**, *115*, 9810.

[65] O. Kahn, J.-P. Launay, *Chemtronics*, **1988**, *3*, 140.

[66] a) J.-P. Behr, C. J. Burrows, R. J. Heng, J.-M. Lehn, *Tetrahedron Lett.,* **1985**, *26*, 215; b) *Ion Channels 2*, Plenum, New York, **1990**.

[67] J. P. Morth, B. P. Pedersen, M. S. Toustrup-Jensen, *et al., Nature,* **2007**, *450*, 1043.

[68] a) R. Dutzler, E. B. Campbell, M. Cadene, B. T. Chait, R. MacKinnon, *Nature,* **2002**, *415*, 287; b) A. P. Davis, D. N. Sheppard, B. D. Smith, *Chem. Soc. Rev.,* **2007**, *36*, 348.

[69] a) R. Breslow, L. E. Overman, *J. Am. Chem. Soc.* **1970**, *92*, 1075; b) R. Breslow, S. D. Dong, *Chem. Soc. Rev.,* **1998**, *98*, 1997.

[70] N. Fujita, K. Biradha, M. Fujita, S. Sakamoto, K. Yamaguchi, *Angew. Chem. Int. Ed.* **2001**, *40*, 1718.

[71] M. L. Huggins, *Chem. Rev.,* **1943**, *32*, 195.

[72] a) K. A. Bolin, G. L. Millhauser, *Acc. Chem. Res.* **1999**, *32*, 1027; b) I. A. Topol, S. K. Burt, E. Deretey, T. H. Tang, A. Perczel, A. Rashin, I. G. Csizmadia, *J. Am. Chem. Soc.* **2001**, *123*, 6054.

[73] a) M. L. Smythe, S. E. Huston, G. R. Marshall, *J. Am. Chem. Soc.* **1995**, *117*, 5445; b) G. Hungerford, M. Martinez-Insua, D. J. S. Birch, B. D. Moore, *Angew. Chem. Int. Ed.* **1996**, *35*, 326; c) T. S. Yokum, T. J. Gauthier, R. P. Hammer, M. L. McLaughlin, *J. Am. Chem. Soc.* **1997**, *119*, 1167; d) P. Pengo, L. Pasquato, S. Moro, A. Brigo, F. Fogolari, Q. B. Broxterman, B. Kaptein, P. Scrimin, *Angew. Chem. Int. Ed.* **2003**, *42*, 3388; e) M. Crisma, M. Saviano, A. Moretto, Q. B. Broxterman, B. Kaptein, C. Toniolo, *J. Am. Chem. Soc.* **2007**, *129*, 15471.

[74] D. Fujita, K. Suzuki, S. Sato, *et al., Nat. Commun.* **2012**, *3*, 1093.

[75] T. Aida, E. W. Meijer and S. I. Stupp, *Science,* **2012**, *335*, 813.

[76] X. Yan, F. Wang, B. Zhang and F. Huang, *Chem. Soc. Rev.,* **2012**, *41*, 6042.

[77] H. L. Li and L. X. Wu, *Soft Matter*, **2014**, *10*, 9038.

[78] Y. Zhao, G. Yuan, P. Roche, *Polymer* **1999**, *40*, 3025.

[79] T. Kato, H. Kihara, U. Kumar, T. Uryu, J. M. J. Frechet, *Angew. Chem. Int. Ed.* **1994**, *33*, 1644.

[80] L. R. Rieth, R. F. Eaton, G. W. Coates, *Angew. Chem. Int. Ed.* **2001**, *40*, 2153.

[81] R. J. Thibault, T. H. Galow, E. J. Turnberg, M. Gray, P. J. Hotchkiss, V. M. Rotello, *J. Am. Chem. Soc.* **2002**, *124*, 15249.

[82] R. J. Thibault, P. J. Hotchkiss, M. Gray, V. M. Rotello, *J. Am. Chem. Soc.* **2003**, *125*, 11249.

[83] a) M. Kotera, J.-M. Lehn, J.-P. Vigneron, *J. Chem. Soc., Chem. Commun.* **1994**, 197; b) M. Kotera, J.-M. Lehn, J.-P. Vigneron, *Tetrahedron* **1995**, *51*, 1953.

[84] M. Burnworth, L. M. Tang, J. R. Kumpfer, A. J. Duncan, F. L. Beyer, G. L. Fiore, S. J. Rowan and C. Weder, *Nature,* **2011**, *472*, 334.

Chapter 2:

Stepwise Halide-Triggered Double- and Triple-Catenation of Self-Assembled Coordination Cages[1]

This chapter reports the self-assembly of a $[Pd_2L^1_4]$ cage that was observed to dimerize into an interpenetrated double-cage $[3X@Pd_4L^1_8]$ upon addition of 1.5 equivalents of halide anions (X = Cl^-, Br^-). Further structural conversion was carried out by subsequent addition of additional amounts of the same halide, forming a triply catenated link structure. The formation and characterization of all these three different structures are comprehensively explained both in solution and in solid state.

2.1 Introduction

Self-assembly of supramolecules driven by metal coordination has been intensely researched because of its extraordinary characteristics and potential applications.[1] Current research focuses on the implementation of functions such as selective sensing[2] and catalysis.[3] The study of coordination cages in supramolecular chemistry has attracted significant scientific attention since the first interpenetrated molecular topology realized by Fujita and his colleagues.[4] The interlocked-cage complex is realized by self-assembly due to the attractive π–π stacking interaction between two separate cages which constructed from two different tridentate ligands and square-planar metal cations (Pd^{II} or Pt^{II}) (Figure 2.1). In coordination cages, guest molecules of appropriate size and polarity occupy the cavities and bind through specific attractive interactions such as pure electrostatic attractions between anionic species and positively charged metal complexes.[5] Furthermore, the spatial and temporal control of restructuring and encapsulation is of high current interest by
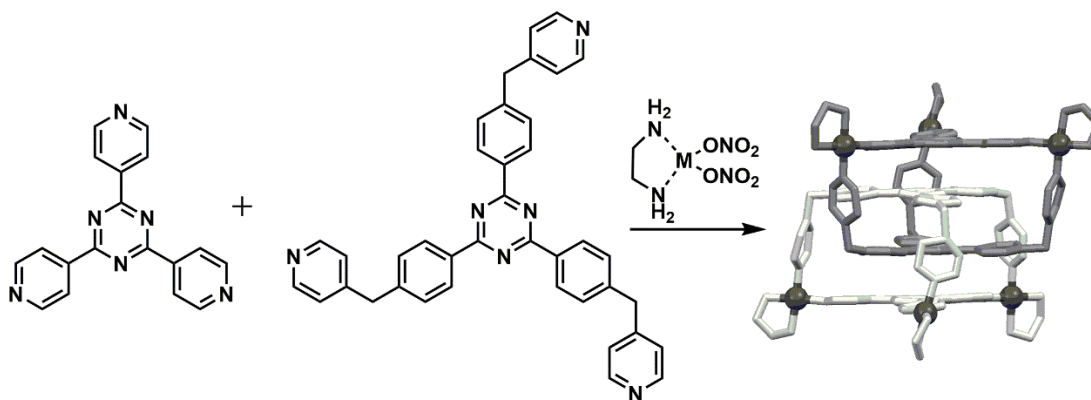

Figure 2.1 An interlocked cage constructed from two different tridentate ligands and *cis*-protected metal complexes. Copyright © Nature Publishing, 1999.

[1] The results presented in this chapter have been published: R. Zhu, J. Lübben, B. Dittrich, G. H. Clever, *Angew. Chem. Int. Ed.* **2015**, *54*, 2796.

the addition of external triggers,[6] the change of pH[7] or electrochemical potential[8] and the irradiation with light.[9]

As mentioned in Chapter 1, anion binding has been widely studied in recent years due to their important roles in chemical[10] and biological[11] processes. Carefully designed anion binders have potential applications in environmental sensors or medical diagnostics.[12] Concentration-dependent changes of structural or mechanistic features in complex molecular systems play a major role in catalysis, pharmacology and many biological regulatory processes. For the purpose of getting a basic understanding of the underlying processes found in such intricate environments, the field of systems chemistry has evolved where networks of interacting molecules can be studied in great details.[13] Such artificial model systems are regularly based on supramolecular self-assembly which utilizes the formation of complex structures from simple building blocks containing a preprogrammed connectivity.[14]

Carbazole and its derivatives show great potential for the application in electro phosphorescent polymers,[15] fluorescent probes,[16-17] and organic field-effect transistors[18] because of their excellent optical and electrical properties such as high luminescence efficiency,[19] the formation of stable radical cations and low oxidation potentials.[20] It makes them desirable host materials in OLEDs[21] and PHOLEDs[22] due to their hole-transporting capability[23] and the high triplet energy levels (2.9 eV) [24] of the carbazole derivatives.

In this chapter, a thermodynamic stable mono-cage is obtained from a bis-pyridyl ligand based on a carbazole backbone with two square-planar-coordinated Pd^{II} cations and two different self-assembled complexes are formed by variation of the concentration of a small anionic additive.

2.2 Ligand design and synthesis

Regarding to self-assembled coordination cages,[25] the Clever group and others have demonstrated first examples of introducing controllable elements such as redox-active[26] or light-switchable[27] functionalities within the last couple of years.

In the previous work of the Clever group, they have achieved the self-assembly of a series of interpenetrated double-cages $[3BF_4@Pd_4L_8]$ based on banana-shaped bis-pyridyl ligands **L** and the tetrafluoroborate salt of square-planar coordinated Pd^{II}.[26a,28,29] In all these cages, three tetrafluoroborate anions occupied the central and two outer pockets while the outer two BF_4^- anions could be substituted by smaller halide anions following an allosteric binding process.[28b–e] By introducing more steric bulk at the center of the ligands, it further showed that the choice of an added anionic template inside the central pocket controls the selectivity of the subsequent binding with further anionic guests in the two outer pockets of these mechanically coupled double-cage systems.[28g]

In this chapter, a structurally related but slightly shorter bis-pyridyl ligand L^1 was designed based on a carbazole backbone and reacted it with the palladium salt $[Pd(CH_3CN)_4](BF_4)_2$ to obtain a stable monomeric cage $[Pd_2L^1_4]$ which shows no tendency to dimerize in the presence of tetrafluoroborate anions (Figure 2.2).
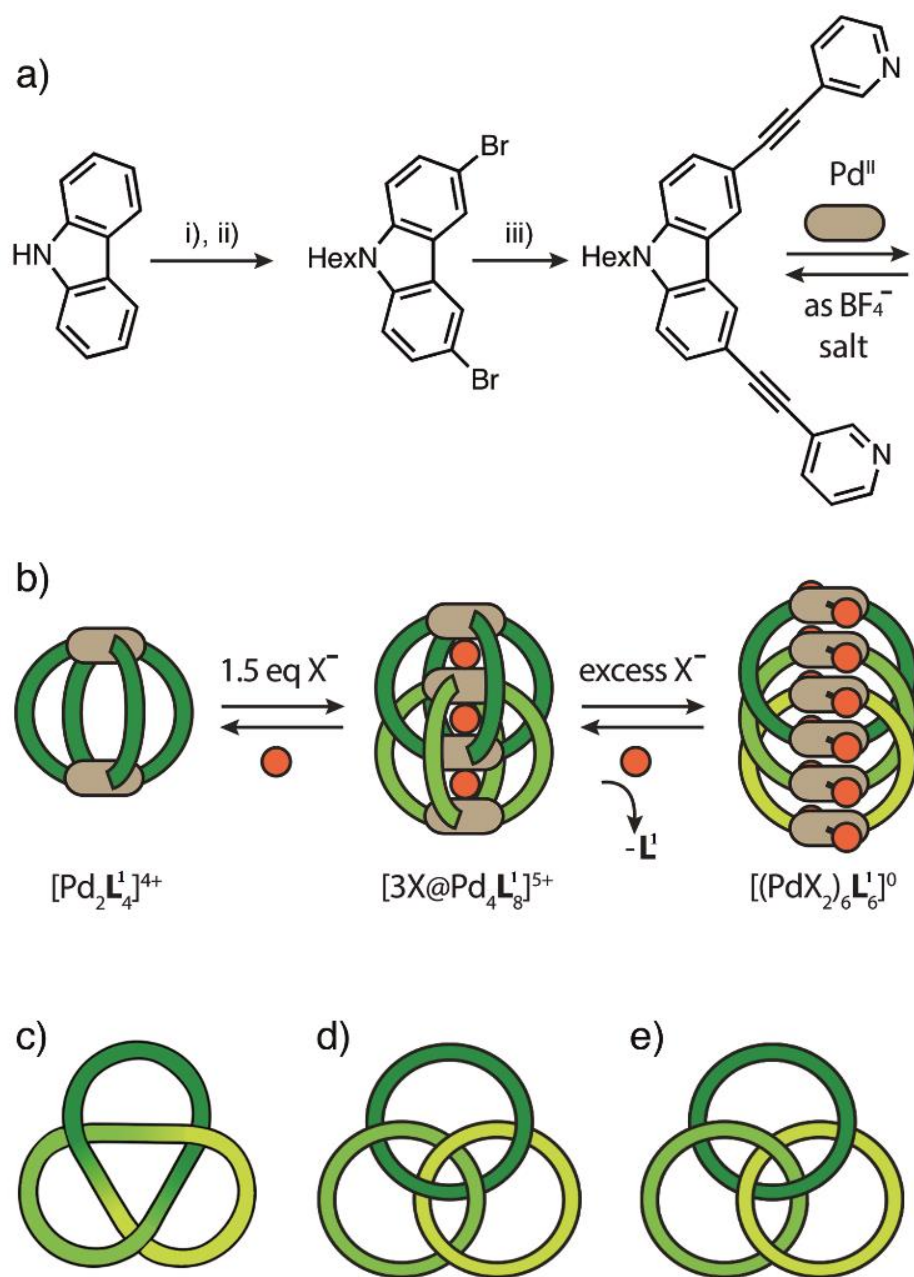
Figure 2.2 a) Synthesis of the ligand: i: NBS, DMF, 0 °C; ii: 1-bromohexane, 50% NaOH, DMSO; iii: 3-ethynylpyridine, CuI, Pd(PPh$_3$)$_2$Cl$_2$, NEt$_3$, 90 °C; b) stepwise assembly of the monomeric cage [Pd$_2$**L$^1_4$**], the halide templated double-cage [3X@Pd$_4$**L$^1_8$**] (X = Cl$^-$, Br$^-$) and the triple-catenane {*trans*-[(PdX$_2$)$_2$**L$^1_2$**]}$_3$ (X = Br$^-$). Schematic depiction of the topologies of c) a trefoil knot; d) the Borromean rings and e) the link carrying the systematic description L6n1 that describes the molecular structure of the triple-catenane {*trans*-[(PdBr$_2$)$_2$**L$^1_2$**]}$_3$. Copyright © 2015 WILEY-VCH Verlag GmbH & Co.

Interestingly, the subsequent addition of stoichiometric amounts of halide anions resulted in the formation of interpenetrated double-cages containing halide anions in all of the three pockets. Surprisingly, excess

amounts of the same anion trigged a second structural transition which generating a triply-catenated link structure.

2.2.1 Ligand synthesis and mono-cage assembly

Ligand L^1 was synthesized in three steps starting from carbazole by a Sonogashira cross-coupling reaction of 3,6-dibromo-9-hexyl-carbazole[15] and 3-ethynylpyridine (Figure 2.2a). Monomeric cage [$Pd_2L^1_4$] was obtained stoichiometrically from ligand L^1 by the addition of 0.5 equivalents of [$Pd(CH_3CN)_4$](BF_4)$_2$ in CD_3CN and heating the mixture at 70 °C for 5 h. The characterization was indicated by ^{1}H NMR spectroscopy (Figure 2.3a−b) and ESI mass spectrometry (Figure 2.4a). Single crystals were successfully grown by slow evaporation from acetonitrile solution of the self-assemblies so that the structure of [$Pd_2L^1_4$] was confirmed by single crystal X-ray structure determination (Figure 2.5a). No dimerization into interpenetrated double-cages was observed in this system comparing to the previous work about the formation of cages from slightly longer bis-pyridyl ligands based on tricyclic dibenzosuberone or phenothiazine backbones in the Clever group.[26a,28b,f]
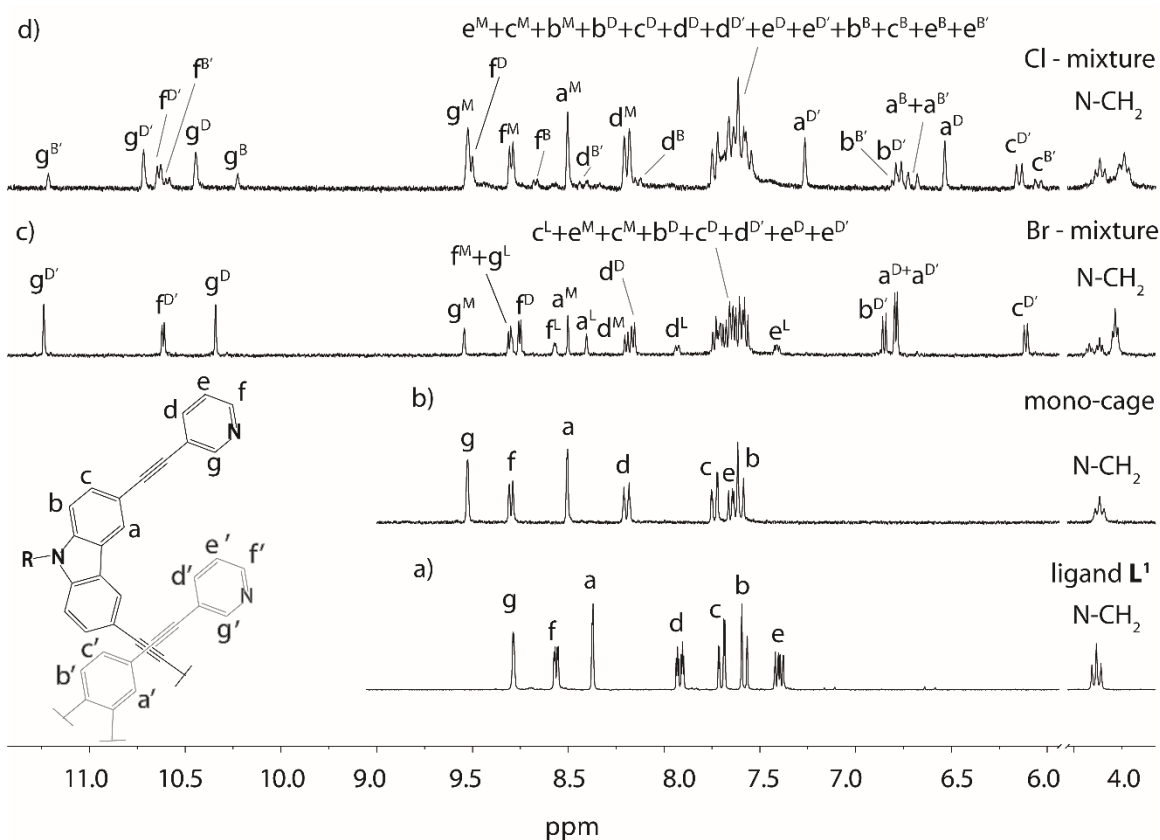

Figure 2.3 ^{1}H NMR spectra of a) ligand L^1; b) mono-cage [$Pd_2L^1_4$] and the mixtures resulting from the reaction of 0.7 mM solutions of [$Pd_2L^1_4$] with c) 1.5 equivalents of bromide and d) 1.0 equivalent of chloride (298K, 500MHz, $N^nBu_4^+$ signals at 0.7−3.1 ppm omitted, L = ligand, M = mono-cage, D = main double-cage, B = minor double-cage [$2Cl+Br@Pd_4L^1_8$]).

2.2.2 Interpenetrated cage assembly

In the previous research of the Clever group,[28e] they have calculated the optimal Pd(pyridine)$_4$−X−Pd(pyridine)$_4$ distances for chloride, bromide and tetrafluoroborate anions equaling to 6.5 Å, 7.0 Å and 8.4 Å, respectively. As the comparison of the length of ligand $\mathbf{L^1}$ with the lengths of the formerly studied systems shown in Figure 2.6, it's able to predict this monomeric but not double cage behavior which is attributed to the fact that, the shorter carbazole-based ligand $\mathbf{L^1}$ gives rise to a smaller cavity which does not allow for the interpenetrated cage unit in the presence of relatively large tetrafluoroborate counter anions.
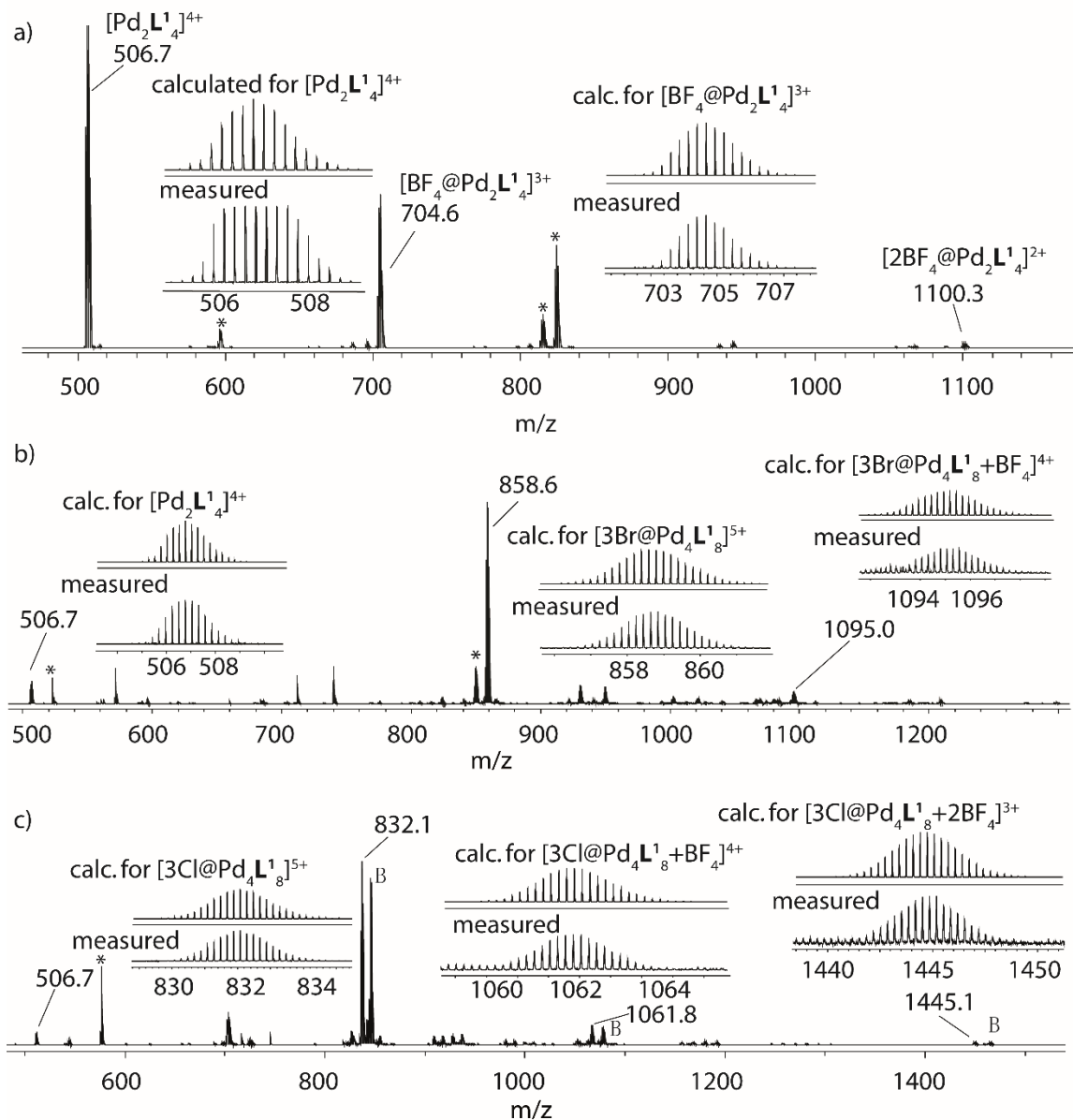

Figure 2.4 ESI-FTICR mass spectra of a) monomeric cage $[n\mathrm{BF_4@Pd_2L^1_4}]^{(4-n)+}$ with $n = 0-2$; b) double-cage $\{[3\mathrm{Br@Pd_4L^1_8}](\mathrm{BF_4})_n\}^{(5-n)+}$ with n = 0−1 and c) double-cage $\{[3\mathrm{Cl@Pd_4L^1_8}](\mathrm{BF_4})_n\}^{(5-n)+}$ with $n = 0-2$ (* = adducts with impurities, $\mathbf{B}$ = double-cage $[(2\mathrm{Cl+Br})@\mathrm{Pd_4L^1_8}]^{5+}$).

Furthermore, previously collected information about the ideal distance between the Pd(pyridine)$_4$-planes and different anions, gave a clue to predict the dimerization from carbazole mono-cages in the presence of smaller anions such as chloride or bromide.[28c,e]
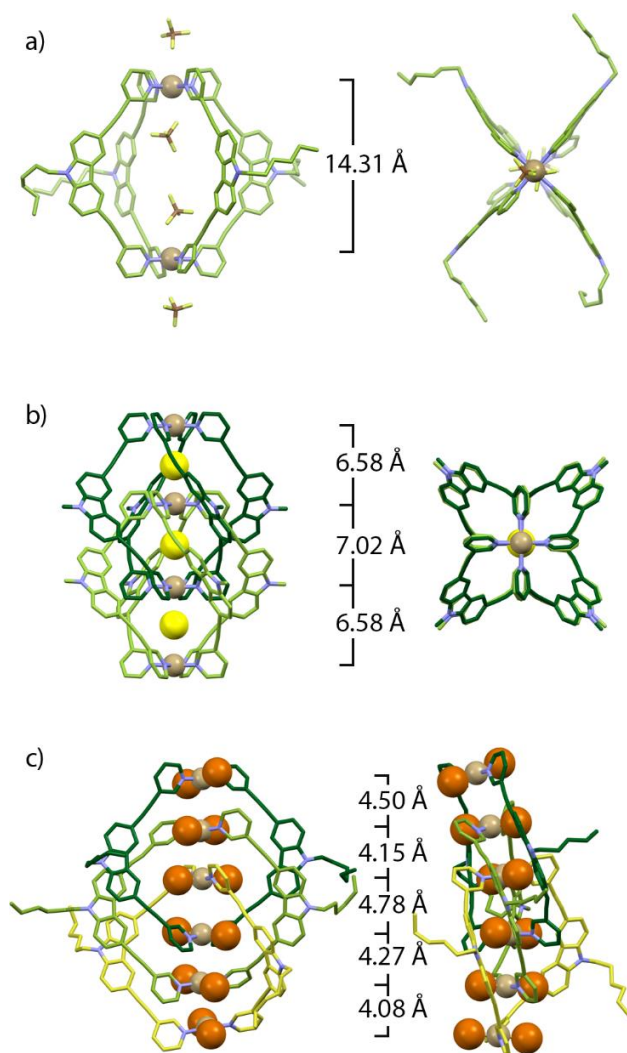

Figure 2.5 a) Single-crystal X-ray structure of the monomeric cage [Pd$_2$L$^1_4$]$^{4+}$ (counter anions = BF$_4^-$); b) DFT-optimized structure of [3Cl@Pd$_4$L$^1_8$]$^{5+}$ and c) X-ray structure of the triple-catenane {*trans*-[(PdBr$_2$)$_2$L$^1_2$]}$_3$. Copyright © 2015 WILEY-VCH Verlag GmbH & Co.

As a fact, the formation of an interpenetrated species [3X@Pd$_4$L$^1_8$] in which three halide anions occupied all the three cavities was indicated by NMR spectroscopy (Figure 2.3c and d) and ESI mass spectrometry (Figure 2.4b and c) after adding 1.5 equivalents of bromide or chloride anions to the mono-cage [Pd$_2$L$^1_4$] solution and heating the reaction mixture for 5 h at 70 °C. On the basic of previous results in the Clever group, double-cage formation is characterized by a two-fold splitting of all ^{1}H NMR signals and distinctive signal shifts of the pyridine protons pointing inside the cage's three pockets. From the high resolution ESI mass spectrum,

the interpenetrated cage was unambiguously identified as the species $[3X@Pd_4L^1_8]^{5+}$, $\{[3X@Pd_4L^1_8]+BF_4\}^{4+}$ and $\{[3X@Pd_4L^1_8]+2BF_4\}^{3+}$.
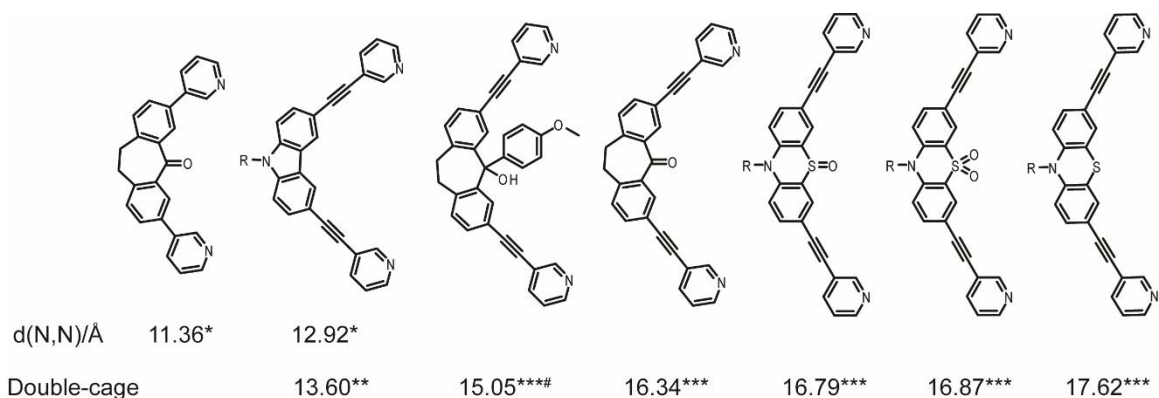

d(N,N)/Å	11.36*	12.92*					
Double-cage			13.60**	15.05***#	16.34***	16.79***	16.87***	17.62***

Figure 2.6 Length of ligand L^1 from DFT calculation and the lengths of the formerly studied systems.[30] *: B3LYP/6-31G* DFT optimization of ligand (conformer with both pyridine-Ns in depicted *endo* position), **: ωB97XD/def2-SVP DFT Model of the chloride-templated double-cage, ***: X-ray structures of the double-cages (in ** and *** the PdN$_4$-plane-to-plane distances are given), #: special case: the bulky group attached to the backbone rather than the N-N distance prevents BF_4^- templation.[28g]

From the analysis of NMR spectra, nevertheless, the double-cages are in equilibrium with the monomeric cage and the free ligand (Figure 2.3c and d). The ratio of the species $[3X@Pd_4L^1_8]$: $[Pd_2L^1_4]$: L^1 was found to be 5 : 3 : 10 for bromide and 5 : 5 : 2 for chloride[31] by NMR spectroscopy. The dependent formation of double-cages upon different halide content was examined by titrating a solution of the halide anions (as their tetrabutylammonium salts in deuterated acetonitrile solution) in a range of 1.5 to 3.0 equivalents for bromide and 0.5 to 2.0 equivalents for chloride in an NMR tube containing the monomeric cage (Figure 2.7). The samples were heated to 70 °C for 5 h after each titration step prior to recording the NMR spectra. As shown in Figure 2.7a, the formation of bromide-templated double-cage reaches its maximum intensity at 1.75 equivalents, further addition of bromide leads to the decrease of the double-cage signal intensities accompanied by consumption of mono-cage (see characteristic signal in blue) and release of free ligand L^1 (see characteristic signal in red). As a similar result in Figure 2.7b, the formation of the desired chloride-templated double-cage reaches its maximum intensity at 1.0 equivalent. In the meantime, another double-cage **B** is formed as a minor component which is identified as mixed chloride/bromide species $[(2Cl+Br)@Pd_4L^1_8](BF_4)_5$ by high resolution mass spectrometry in Figure 2.8. From the simulation, there is another possible composition $\{[3Cl@Pd_4L^1_8]^{5+}+CD_3CN\}$ (in red). However, more thorough evidence against the acetonitrile-containing/associated species is illustrated in (i) the distinct NMR signals of a minor double-cage species, (ii) a negative control experiment using CH_3CN as a solvent instead of CD_3CN and (iii) from the space filling model of the double cage which does not suggest the possibility of acetonitrile co-encapsulation inside the cavities. Further addition of chloride leads to the decrease of the double-cage signal intensities accompanied by consumption of mono-cage (see characteristic signal in blue) and release of free

ligand L^1 (see characteristic signal in red). Fascinatingly, the chloride-templated double-cage ("**D**" in the figure) reacts more readily with excess chloride than double-cage **B** as can be identified when comparing to the relative signal intensities in the spectra upon addition of 1.0 and 1.5 equivalents of bromide.
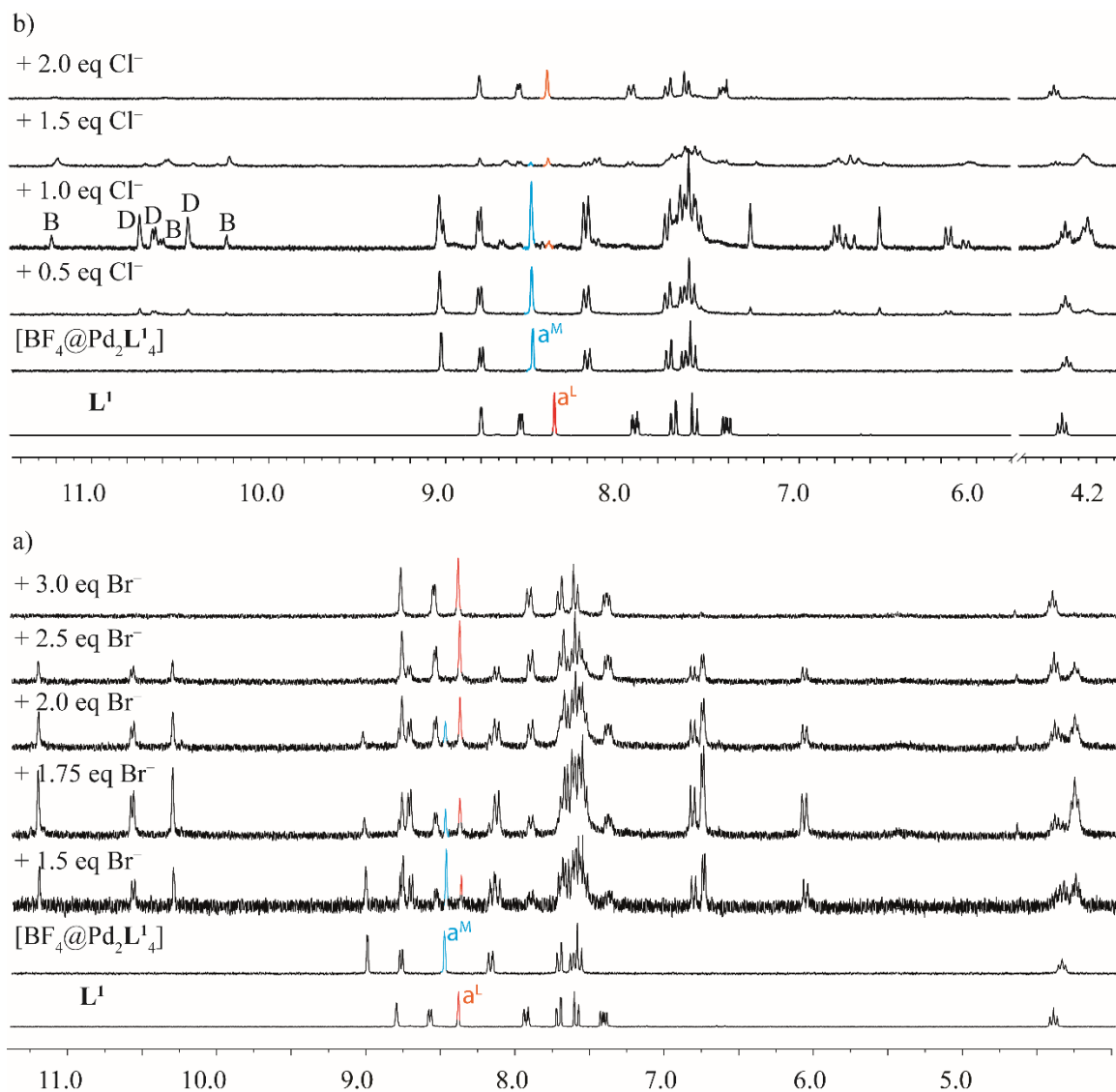
b)

+ 2.0 eq Cl⁻

+ 1.5 eq Cl⁻

+ 1.0 eq Cl⁻

D D D
B   D B B

+ 0.5 eq Cl⁻

$[BF_4@Pd_2L^1_4]$

aᴹ

L^1

aᴸ

| 11.0 | 10.0 | 9.0 | 8.0 | 7.0 | 6.0 | 4.2 |

a)

+ 3.0 eq Br⁻

+ 2.5 eq Br⁻

+ 2.0 eq Br⁻

+ 1.75 eq Br⁻

+ 1.5 eq Br⁻

$[BF_4@Pd_2L^1_4]$

aᴹ

L^1

aᴸ

| 11.0 | 10.0 | 9.0 | 8.0 | 7.0 | 6.0 | 5.0 |

Figure 2.7 ^1H NMR titration (300 MHz, 298 K, CD₃CN) of bromide a) and chloride b) into mono-cage $[Pd_2L^1_4]$ (L = ligand, M = mono-cage).

Since the monomeric cage was obtained quantitatively and no free ligand was present in the solution, the constitution of the major component $[3X@Pd_4L^1_8]$ must be accompanied by a partial ligand liberation by disassembly, even when stoichiometric amounts of halide were added. This phenomenon is in accordance with previously reported observations in the Clever group which showed that other halide-binding (but tetrafluoroborate-templated) double-cages release free ligand upon addition of excess amounts of halide anions.[28b,e] It can be feasibly explained that halide binding inside the cage's cavities competes with the direct

coordination to the square-planar Pd^{II} cations under displacement of up to two of the pyridine donors. The resulting $PdX_2(pyridine)_2$-motif is well known in supramolecular self-assembly.[32]
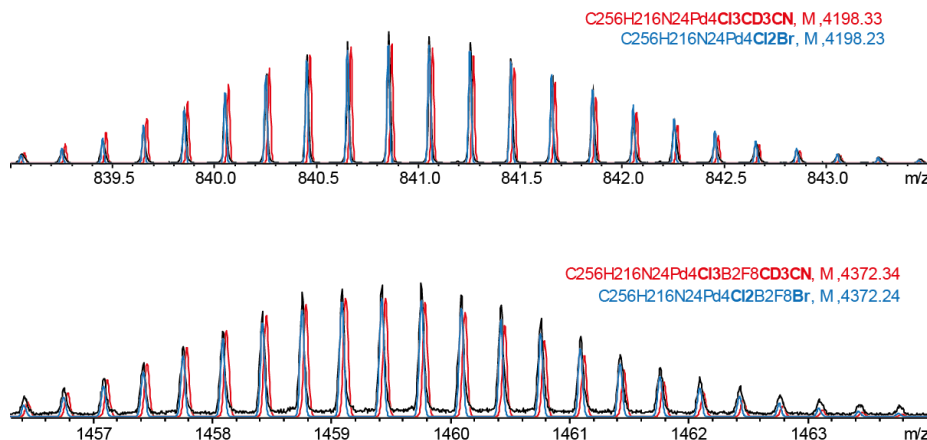

Figure 2.8 ESI-FTICR-HRMS assignment of double-cage **B** in the experimental mass spectrum of the reaction product of mono-cage $Pd_2L^1_4$ with chloride (black) to the calculated composition $[(2Cl+Br)@Pd_4L^1_8]^{5+}$ (blue) as compared to another plausible composition $\{[3Cl@Pd_4L^1_8]^{5+}+CD_3CN\}$ (red).

In addition to the $[Pd_2L^1_4]$ and $[3X@Pd_4L^1_8]$ cages, plausible self-assemblies are the macrocycle *trans*-$[(PdX_2)_2L^1_2]$ and the [2]-catenane $\{trans-[(PdX_2)_2L^1_2]\}_2$ that are formally obtained by substituting two or four ligands from monomeric or dimeric cage with halide substituents, respectively. Owing to the low solubility of these neutral species in polar acetonitrile solution, the observed precipitates can be accounted to some extent.

Unfortunately, no X-ray structure of double cage $[3X@Pd_4L^1_8]$ was obtained, a DFT model of the chloride-templated interpenetrated assembly was constructed according to the acquired spectroscopic results and the crystal structures of reported double-cages in the Clever group using a geometry refined optimization on the ωB97XD/def2-SVP level of theory (Figure 2.5b). Taking the $Pd^{2+}-Cl^--Pd^{2+}$ distance into account, the outcome of this calculation is in quite good agreement with previously published theoretical and experimental researches of relevant double-cage structures.[26a,28]

2.2.3 Triple catenane assembly

To my pleasant surprise, a triply-catenated complex $\{trans-[(PdBr_2)_2L^1_2]\}_3$ was segregated as a single crystal and structurally characterized by X-ray diffraction analysis (Figure 2.5c). In this triply-catenated structure, the bromide-coordinated Pd^{II} nodes carry no net charge[33] which is in the opposite situation comparing with the cage structures discussed above. As a consequence, the non-charged structure could not encapsulate further counter anions and the palladium atoms are capable to reach each other much closer than in the charged double-cages. The intermetallic distances within the structures of $[3X@Pd_4L^1_8]$ and $\{trans-[(PdBr_2)_2L^1_2]\}_3$ are shown in Figure 2.5 so as to interpret this consequence. As shown, the Pd−Pd distance in the chloride-templated double-cage is 6.73 Å on average while the average distance in the triple-catenane

amounts to 4.36 Å. Owing to the significantly longer distance of the latter one compared with twice the van-der-Waals radius of Pd (1.63 Å), the primary control of this particular component should not be attributed to the direct contacts between the metal centers. According to the observation of the structure, six palladium atoms almost stack in linear while the bromide substituents are arrayed in a helical fashion. This inspection reveals that such an arrangement is preferred to other conformations in which the metal centers are arranged in other modus. Based on these observations, the governing cause for undertaking the resulted assembly was attributed to stabilization of π-π-interactions between the ligand backbones, which are optimized in the helical arrangement. As showing in Figure 2.5c, five of the six ligands represent close π-stacking to the neighboring carbazole moieties in the X-ray structure. One ligand is twisted away from its adjacent neighbour, which shows a packing effect ascribed to the adjacent catenane (the depiction of the crystal packing shown in the Experimental Section).

From the topological view, this triply-catenated structure $\{trans$-$[(PdBr_2)_2\mathbf{L^1}_2]\}_3$ is an L6n1 link according to the Thistlethwaite link table.[34] Figure 2.2 illustrates the well-known topologies: trivial name-carrying trefoil knot (Figure 2.2c), Borromean rings (Figure 2.2d), both of these two architectures have been actively researched in another supramolecular subtopic,[35] and molecular structure of the triple-catenane $\{trans$-$[(PdBr_2)_2\mathbf{L^1}_2]\}_3$ which was achieved here (Figure 2.2e). The trefoil knot is composed of only one ring, whereas both other topologies consist of three individual rings. In the Borromean rings, removing any one ring leads to the other two rings immediately separated intact. Regarding of the triply-catenated structure obtained here, nevertheless, all three rings are penetrated to either of the other two and the rest two are still interlocked upon breaking one of the rings. To the best of my knowledge, this topology has never been reported before in the appearance of a metallo-supramolecular self-assembly.[36]

As a result of the description above, the halide anion triggered two distinct actions in this system at different concentrations: on the one hand, it serves as the impetus for the formation of interpenetrated double-cages by templating the dimerization of the precursor monomeric cages. In this situation, three halide anions are encapsulated as guests in the three cavities of the double-cage, thus being tightly sandwiched between the four dicationic palladium metals via coulomb interactions piling up an alternating $Pd^{2+}-X^--Pd^{2+}-X^--Pd^{2+}-X^--Pd^{2+}$ stack. On the other hand, a further structural transformation takes place at a higher concentration of the halide anions. Along with the disassembly of double-cages and partial release of free ligand, a triply interdigitated catenane is formed. Herein, under replacement of two pyridine donors, the halide anions directly bind to the Pd^{II}-centers acting as part of their square-planar coordination sphere.

What should be mentioned here is that, the formation of the interpenetrated double-cage $[3X@Pd_4\mathbf{L^1}_8]$ was attempted directly by reacting the palladium halides $PdCl_2$ or $PdBr_2$ with the ligand $\mathbf{L^1}$. This approach was not successful since these salts would bring too much halide into the system at the beginning. Therefore, this circumstance could compare with the 'halide-overtitrated' state of previous experiment, which supposing the system is in a thermodynamic equilibrium, should not contain double-cages. In fact, the direct reaction of acetonitrile adducts from palladium halides ($PdCl_2$ or $PdBr_2$) with ligand $\mathbf{L^1}$ generated nonpolar products

which were detected to have a much higher solubility in chloroform than the charged mono- and double-cages. Without showing a loss of symmetry in their NMR spectra (Figure 2.9), these complexes can be classified to the uncharged macrocycles *trans*-[(PdX$_2$)$_2$**L**^{1}$_2$] (X = Cl$^-$, Br$^-$).
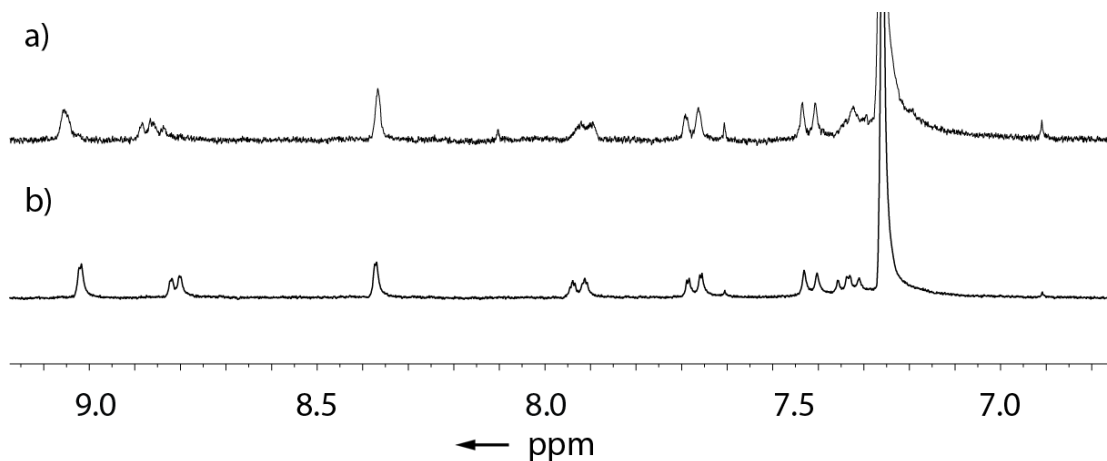

Figure 2.9 ^{1}H NMR (300 MHz, 298 K, CDCl$_3$) spectra of the nonpolar reaction products of a) [PdBr$_2$(CH$_3$CN)$_2$] and b) [PdCl$_2$(CH$_3$CN)$_2$] with ligand **L**^{1} in chloroform.

2.3 Conclusion

In conclusion, it is introduced an transformable system of three novel structures from self-assembly all depended on the same bis-monodentate pyridyl ligand and only varying Pd^{II} to halide ratios from 1 : 0 in case of the monomeric cage [Pd$_2$**L**^{1}$_4$], over 4 : 3 in case of the interpenetrated double-cage [3X@Pd$_4$**L**^{1}$_8$] and further up to 1 : 2 in case of the triple-catenane {*trans*-[(PdBr$_2$)$_2$**L**^{1}$_2$]}$_3$.

What is illuminating, halide anions in the self-assembly of the double-cages obtained here play a considerably different role from Clever's studied double-cages based on the backbones of dibenzosuberone and phenothiazine which were discovered to assemble into interpenetrated dimers in the presence of tetrafluroborate anions as templates. Smaller halide anions were not needed for dimerization but were detected to show up in the outer two pockets kicking out two BF$_4$$^-$ anions from the pre-assembled double-cages with larger binding affinity.[26a, 28b]

In another system in the Clever group, for a ligand derivative, halide anions were indeed required as templates for the formation of double-cages.[28g] The formation here of the halide-templating cages is rather due to the steric hindrance caused by introduction of bulky substituents into the normal ligand backbone than because of the relatively shorted ligands which cannot encapsulate three BF$_4$$^-$ anions sandwiched between four Pd^{II}-centers. In this chapter here, sterically crowding from ligand backbones is not accountable for this extraordinary interpenetration behavior but as an alternative, the length limitation of a little shorter carbazole ligand leads to the conversion of halide-templating entangled cage structure which can uptake smaller halide anions into all three pockets.

Subsequent addition of larger amounts of the same halide triggered further transformation, yielding a distinctive topology, a triply catenated link, in which each Pd^{II} node is *trans*-coordinated by two halides and two pyridine donors from the ligands, which was characterized by X-ray analysis. The acquisition that three different structural complexities are triggered just by a slight concentration change of one anionic additive indicates how molecular compound can be created via a gradual variation of concentration of the corresponding reagents in a supramolecular system.

The observation, that three different self-assembled products are formed by variation of the concentration of a small anionic additive shows that the use of one multifunctional trigger can be sufficient to create a notable degree of complexity in a supramolecular system. The structural rearrangement of artificial self-assemblies demonstrated in this work will serve as a crucial example in the field of supramolecular chemistry.

2.4 Experimental Section

2.4.1 Ligand synthesis
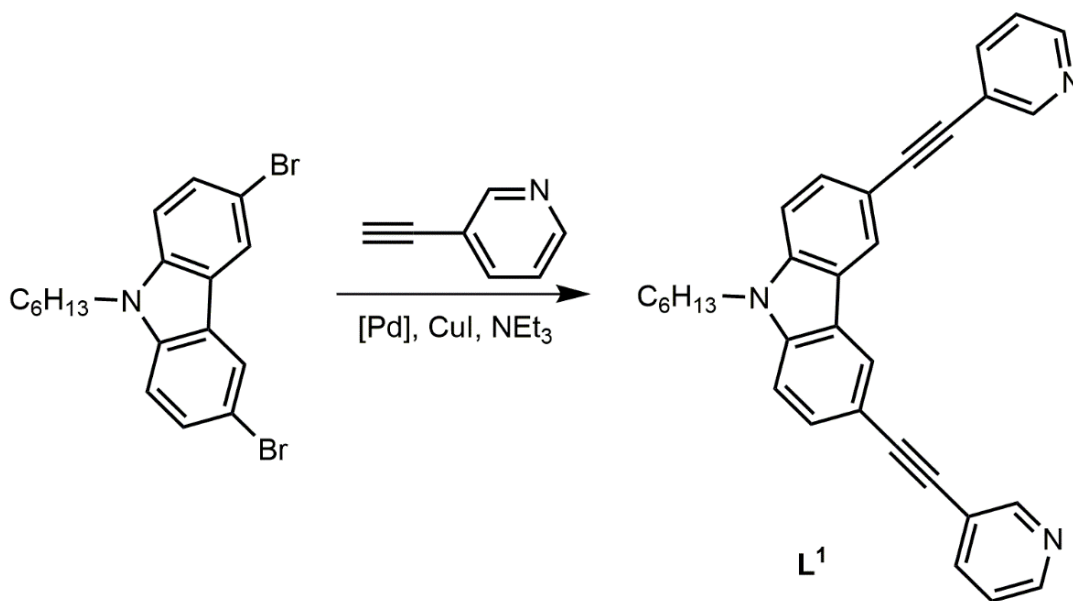
A mixture of 3,6-dibromo-9-hexyl-9*H*-carbazole[1] (814.0 mg, 2 mmol), 3-ethynylpyridine (721.3 mg, 7 mmol) and copper(I) iodide (40 mg, 0.21 mmol) in triethylamine (10 mL) was thoroughly degassed and Pd(PPh$_3$)$_2$Cl$_2$ (70 mg, 0.1 mmol) was added. The mixture was heated under a nitrogen atmosphere at 70 °C for 16 h. Subsequently, the mixture was cooled to room temperature and the solvent was evaporated under reduced pressure. A saturated NH$_4$Cl-solution was added to the residue and the organic components were extracted with CH$_2$Cl$_2$. The organic layer was washed with water and brine, dried over MgSO$_4$, filtrated and evaporated under reduced pressure. The crude residue was purified by flash chromatography on silica gel (*n*-hexane : acetone = 3 : 1) to give **L^1** as a yellow oily product which slowly crystallizes (413.3 mg, 0.91 mmol, 46%).
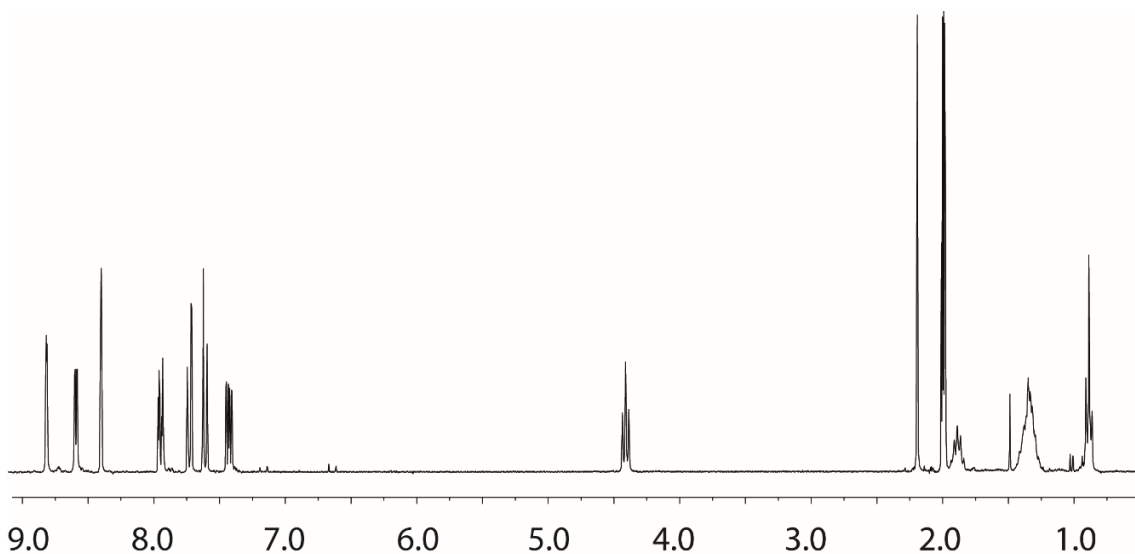
^{1}H NMR (300 MHz, CD$_3$CN): δ [ppm] = 8.78 (d, J = 1.5 Hz, 2H), 8.56 (dd, J = 4.8, 1.5 Hz, 2H), 8.37 (d, J = 0.9 Hz, 2H), 7.92 (dt, J = 7.8, 1.8 Hz, 2H), 7.69 (dd, J = 8.4, 1.5 Hz, 2H), 7.58 (dd, J = 8.4, 0.6 Hz, 2H), 7.40 (ddd, J = 5.7, 4.2, 0.9 Hz, 2H), 4.38 (t, J = 7.2 Hz, 2H), 1.90 – 1.81 (m, 2H), 1.40 – 1.25 (m, 6H), 0.86 (t, J = 6.9 Hz, 3H).
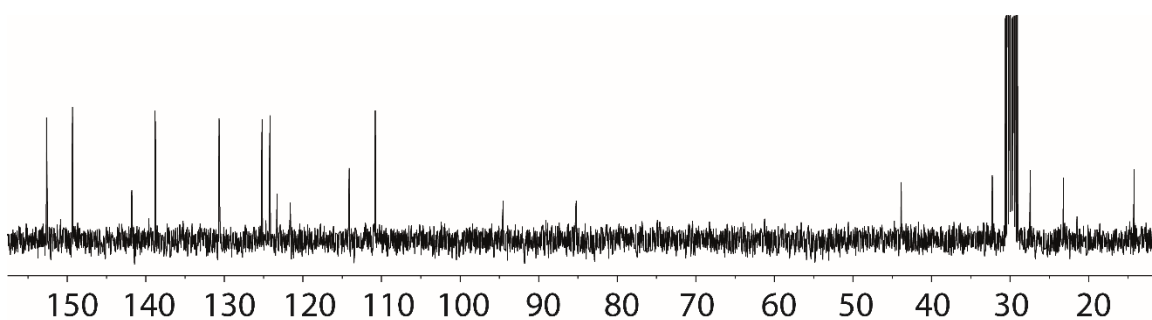
^{13}C NMR (75 MHz, acetone-d_6): δ [ppm] = 152.63, 149.33, 141.78, 138.80, 130.66, 125.20, 124.19, 123.30, 121.61, 114.11, 110.79, 94.51, 85.22, 43.84, 42.25, 29.66, 27.41, 23.21, 14.21.

ESI-FTICR-HRMS calculated for C$_{32}$H$_{27}$N$_3$ [M+H]$^+$ m/z 454.2278, found m/z 454.2266.

2.4.2 Cage syntheses

Cage **1** [Pd$_2$**L^1**$_4$](BF$_4$)$_4$:
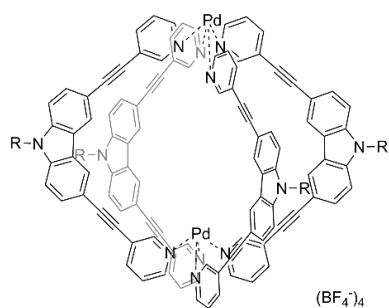
(R represents hexyl chain)

Cage compound **1** was formed in quantitative yield by heating a mixture of ligand **L^1** in CD$_3$CN (930 µL, 1.27 mg, 2.8 µmol) and a solution of [Pd(CH$_3$CN)$_4$](BF$_4$)$_2$ (1.4 µmol, 93 µL of a 15 mM solution in CD$_3$CN) at 70 °C for 5 h to give a 0.7 mM solution of **1**.
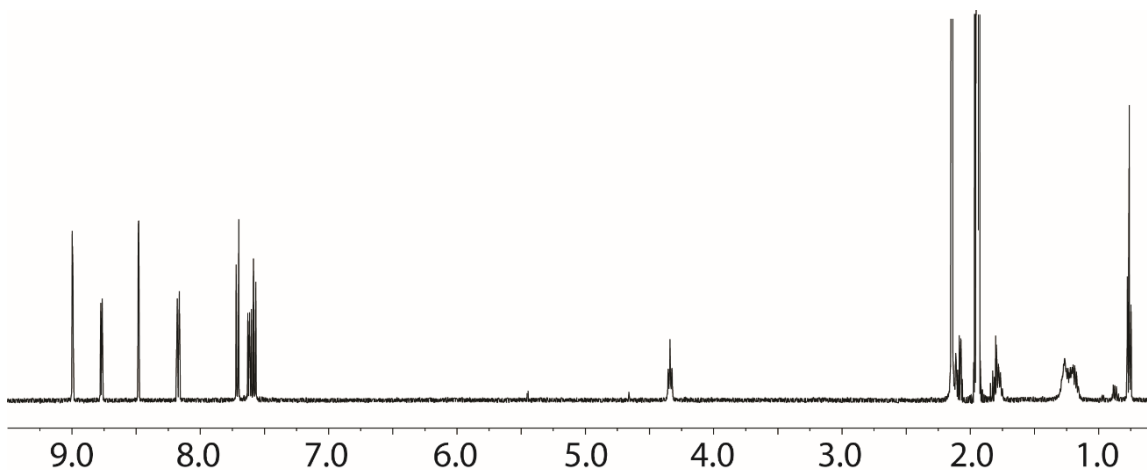
^{1}H NMR (500 MHz, CD$_3$CN): δ [ppm] = 8.99 (d, *J* = 2.0, 8H), 8.77 (dd, *J* = 5.5, 1.0 Hz, 8H), 8.48 (dd, *J* = 1.5 Hz, 0.5 Hz, 8H), 8.17 (dt, *J* = 7.0, 1.0 Hz, 8H), 7.71 (dd, *J* = 8.4, 0.9 Hz, 8H), 7.61 (dd, *J* = 8.0, 6.0 Hz), 7.57 (dd, *J* = 9.0, 0.5 Hz, 8H), 4.34 (t, *J* = 7.0 Hz, 8H), 1.79 – 1.75 (m, 8H), 1.27 – 1.18 (m, 24H), 0.76 (t, *J* = 7.5 Hz, 12H).
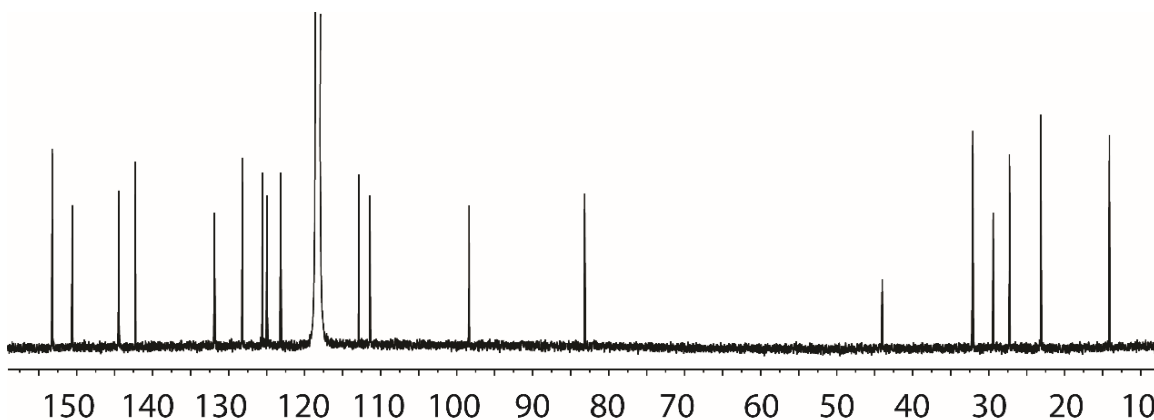
^{13}C NMR (125 MHz, CD$_3$CN): δ [ppm] = 153.21, 150.57, 144.44, 142.28, 131.88, 128.21, 125.57, 124.95, 123.18, 112.86, 111.40, 98.36, 83.16, 44.01, 32.08, 29.42, 27.27, 23.14, 14.12.

ESI-FTICR-HRMS calculated for [C$_{128}$H$_{108}$N$_{12}$Pd$_2$BF$_4$]$^{3+}$ m/z 704.5654, found m/z 704.5631.

Cages **2** [3Br@Pd$_4$**L^1**$_8$](BF$_4$)$_5$ and **3** [3Cl@Pd$_4$ **L^1**$_8$](BF$_4$)$_5$:
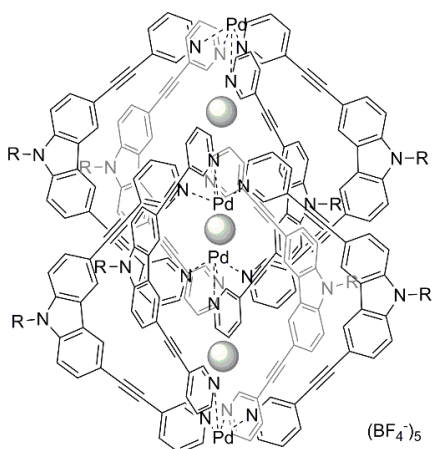
(Grey ball represents Cl$^-$ or Br$^-$, R represents hexyl chain)

Cage compound **2** was formed by heating a mixture of cage **1** (0.35µmol, 500 µL, 0.7 mM) in CD$_3$CN and a solution of N^{n}Bu$_4$Br (0.525 µmol, 60 µL of an 8.75 mM solution in CD$_3$CN) at 70 °C for 5 h to give a solution containing double-cage **2** besides mono-cage **1** and ligand **L^1**.
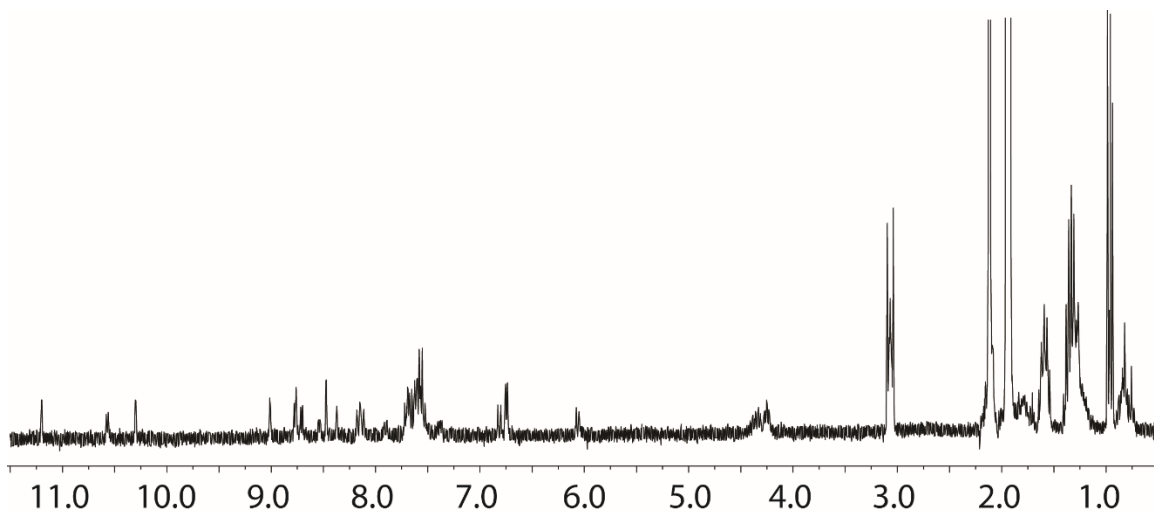
^{1}H NMR signal assignment: see Figure 2.3

ESI-FTICR-HRMS calculated for [C$_{256}$H$_{216}$N$_{24}$Pd$_4$Br$_3$]$^{3+}$ m/z 858.8277, found m/z 858.8372.

Cage compound **3** was formed by heating a mixture of cage **1** (0.35µmol, 500 µL, 0.7 mM) in CD$_3$CN and a solution of N^{n}Bu$_4$Cl (0.35 µmol, 40 µL of an 8.75 mM solution in CD$_3$CN) at 70 °C for 5 h to give a solution containing double-cages **2** and **B** {[(2Cl+Br)@Pd$_4$**L^1**$_8$](BF$_4$)$_5$} besides mono-cage **1** and ligand **L^1**.
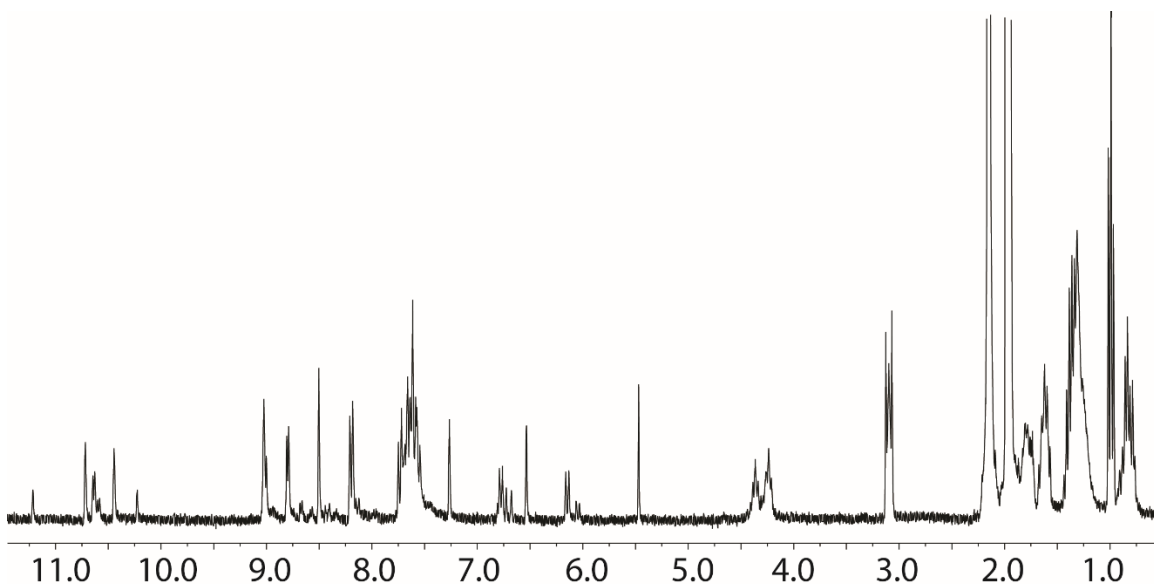
^{1}H NMR signal assignment: see Figure 2.3

ESI-FTICR-HRMS calculated for $[C_{256}H_{216}N_{24}Pd_4Cl_3]^{3+}$ m/z 832.0582, found m/z 832.0600.

Satisfactory ^{13}C NMR spectra of the low-concentration double-cage samples **2**/**3** in their mixture with mono-cage **1**, free ligand $\mathbf{L^1}$ and minor component **B** (in case of the mixture containing **3**) could not be obtained.

2.4.3   Ring/Catenane synthesis

In order to estimate the yield of the ring/catenane species $\{trans\text{-}[(PdBr_2)_2\mathbf{L^1}_2]\}_n$ ($n = 1{-}3$), the halide-induced precipitate stemming from a concentrated reaction mixture (14 mM ligand, 7 mM Pd^{II} source, 14 mM N^{n}Bu$_4$Br) was collected, dried and subjected to elementary analysis, giving the following result: C: 70.49 H: 5.30 N: 7.61 % which fits to a mixture of free ligand and species $\{trans\text{-}[(PdBr_2)_2\mathbf{L^1}_2]\}_n$ ($n = 1{-}3$) in a ratio of 0.546 : 0.454 (based on carbon ratio; H and N values calculated from this value also match reasonably well with H: 5.00, N: 7.70 %). This ratio is close to the expected 1 : 1 ratio for full conversion according to the reaction scheme: $[Pd_2\mathbf{L^1}_4] + 4\ Br^- \rightleftarrows trans\text{-}[(PdBr_2)_2\mathbf{L^1}_2] + 2\ \mathbf{L^1}$.

The mass of the isolated precipitate was with 10.1 mg lower than the expected value of 16.5 mg for this experiment (61 % isolated yield), which it's explained with incomplete precipitation at this concentration and material losses during filtration and recovery of the precipitate.

This experiment, however, does not deliver a yield for the triple-catenane alone, since it does not give any information about the ratio of the species $\{trans\text{-}[(PdBr_2)_2\mathbf{L^1}_2]\}_3$ to the related macrocycle $trans\text{-}[(PdBr_2)_2\mathbf{L^1}_2]$ and the [2]-catenane $\{trans\text{-}[(PdBr_2)_2\mathbf{L^1}_2]\}_2$ which it is expected to form concomitantly.

2.4.4 Further NMR spectroscopy
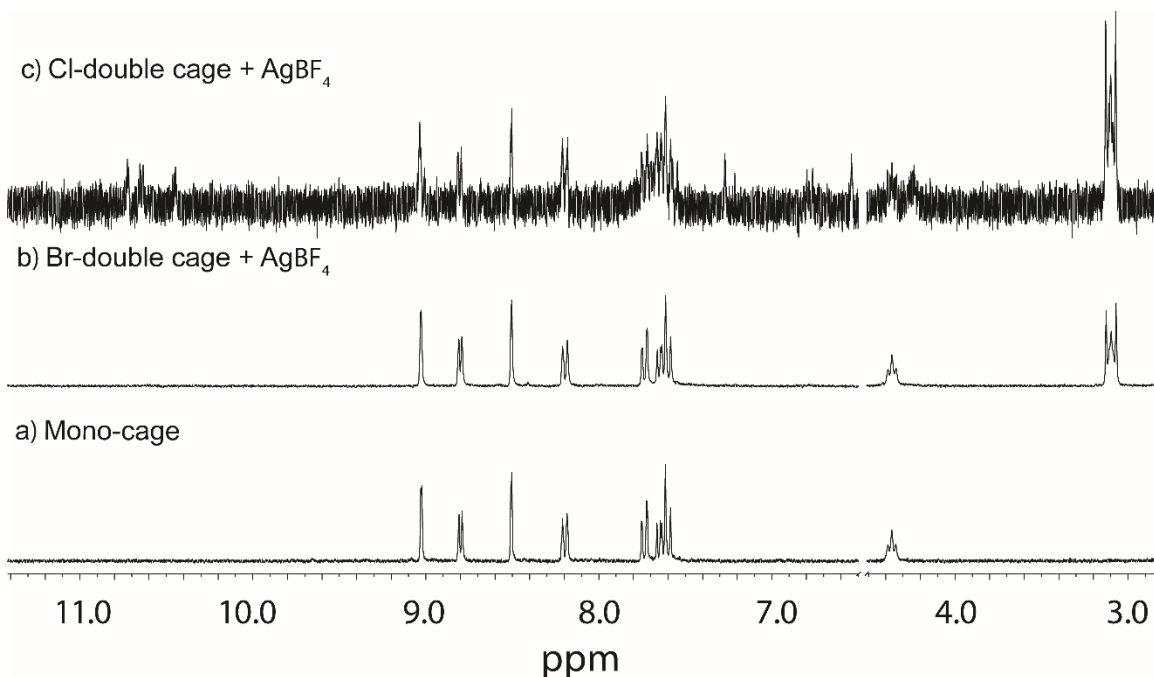
Figure 2.10 ^{1}H NMR (300 MHz, 298 K, CD$_3$CN) spectra upon addition of AgBF$_4$ into b) double-cage **2** showing full reversion into mono-cage **1** and c) double-cage **3** showing only partial conversion back to **1**. Here, double-cage **B** seems to react more readily with the added silver ions than double-cage **3**.

2.4.5 UV-Vis and fluorescence spectroscopy

Further characterization of the ligand and corresponding mono-cage was carried out by UV/Vis and fluorescence spectroscopy (Figures 2.11 and 2.12). Ligand **L**^{1} shows three absorption bands with maxima at 339, 308 and 256 nm. The lowest energy absorption of mono-cage **1** is shifted to longer wavelengths compared to the ligand which is ascribed to the coordination with palladium. In accordance with the fluorescence spectrum shown in Figure 2.12, ligand **L**^{1} shows a strong purple fluorescence upon irradiation with UV light, while mono-cage **L**^{1} barely shows any fluorescence emission which is consistent with the behavior of the related phenothiazine ligands described in the previous work in the Clever group.[26a]

2.4.6 X-ray data of [Pd$_2$**L**$^1_4$](BF$_4$)$_4$ and {*trans*-[(PdBr$_2$)$_2$ **L**$^1_2$]}$_3$

Suitable single crystals for X-ray structural analysis of [Pd$_2$**L**$^1_4$](BF$_4$)$_4$ and {*trans*-[(PdBr$_2$)$_2$**L**$^1_2$]}$_3$ were grown from acetonitrile by slow solvent evaporation. The crystals measurement and structures determination were done by J. Lübben as follows. The crystals were mounted at room temperature in Paratone N inert oil. Single crystal X-ray diffraction data were collected at the Swiss Light Source at beamline PXII. The data were integrated with XDS[38] and converted with the utility program xds2sad by G. M. Sheldrick. An empirical
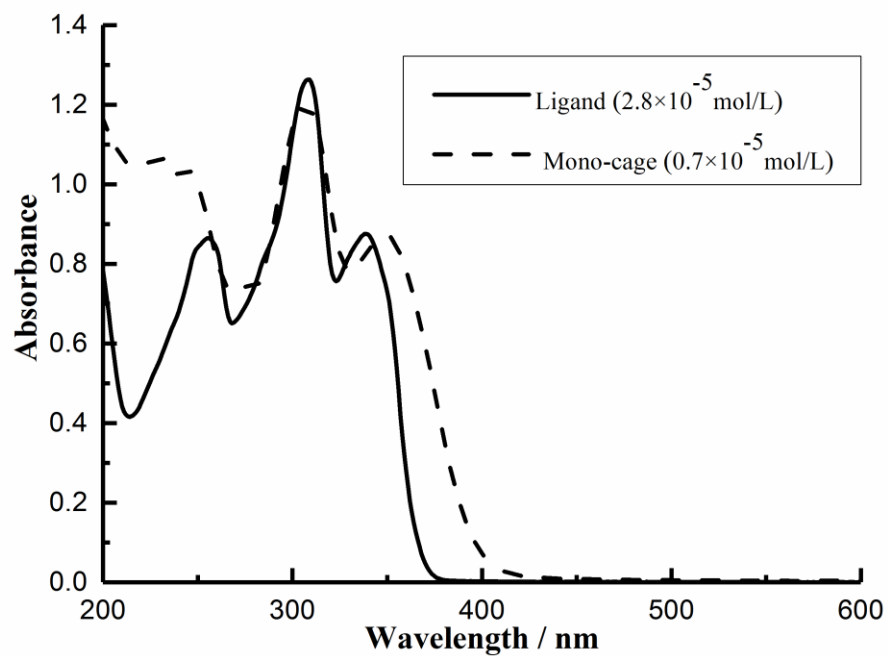
Figure 2.11 UV/Vis spectra of ligand L^1 (2.8×10^{-5} mol/L, solid line) and mono-cage **1** (0.7×10^{-5} mol/L, dashed line).
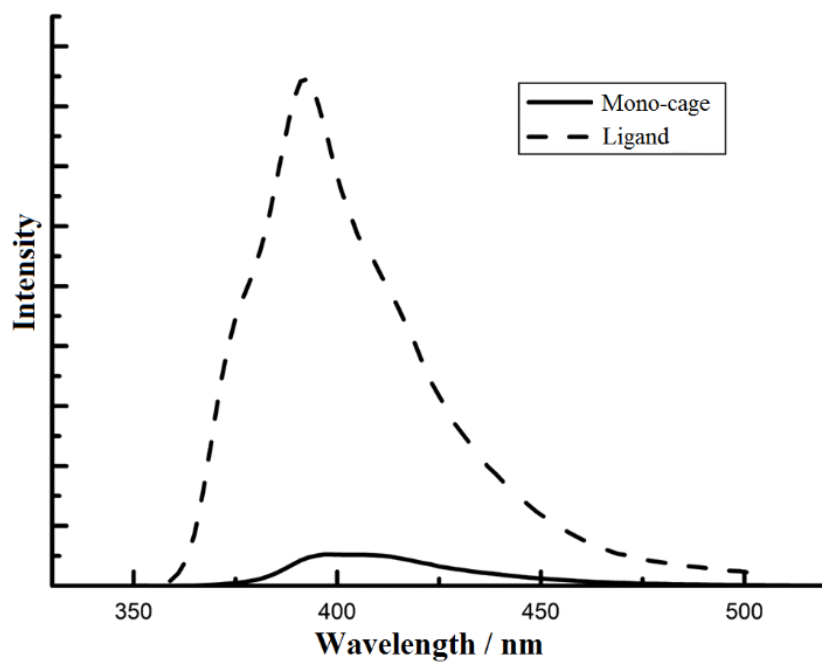
Figure 2.12 Fluorescence spectra of ligand L^1 (2.8×10^{-5} mol/L, dashed line) and mono-cage **1** (0.7×10^{-5} mol/L, solid line). Excitation wavelength: 270 nm.

Compound	$[Pd_2L^1_4](BF_4)_4$	$\{trans\text{-}[(PdBr_2)_2L^1_2]\}_3$
Empirical formula	$C_{128} H_{108} B_4 F_{16} N_{12} Pd_2$	$C_{173.1} H_{118.7} Br_{12} N_{18} Pd_6$ $(C_{192} H_{162} Br_{12} N_{18} Pd_6)$
CCDC no.	1011498	1011499
Molecular weight	2374.31	4048.10
Crystal size [mm]	0.1 x 0.1 x 0.1	0.1 x 0.1 x 0.1
Wavelength [pm]	1.00	1.00
Crystal system	monoclinic	monoclinic
Space group	$P2_1/n$	$P\ 21/n$
a [pm]	15.425(3)	27.787(6)
b [pm]	28.071(6)	23.858(5)
c [pm]	37.184(7)	29.606(6)
α [°]	90	90
β [°]	97.84(3)	107.98(3)
γ [°]	90	90
V [nm^3]	15950(6)	18668(7)
Z	4	4
Temperature [K]	100(2)	100(2)
ρ [Mgm^{-3}]	0.954	1.435
μ [mm^{-1}]	0.696	2.415
F (000)	4672	7917
θ-area [°]	1.3 to 28.5	1.2 to 23.16
Total number of reflect.	76334	34133
Unique reflections	12628	8541
Reflections with $I > 2\sigma(I)$	11492	5736
R_{int}	0.0374	0.1593
Number of restraints	3183	8439
Parameters	1459	2059
$R1$ [$I>2\sigma(I)$]	0.1119	0.2117
$wR2$ [$I>2\sigma(I)$]	0.3382	0.5201
$R1$ [all data]	0.1150	0.2655
$wR2$ [all data]	0.3492	0.5201
GooF	1.756	1.751
Extinction coefficient	-	-
Largest diff. peak / hole max. / min. [$10^3 \cdot e \cdot nm^{-3}$]	+2.11 and -1.44	2.21 and -1.48

Table 2.1 Crystal data and structure refinement for $[Pd_2L^1_4](BF_4)_4$ and $\{trans\text{-}[(PdBr_2)_2L^1_2]\}_3$.

absorption correction with SADABS[39] was applied. Both structures were solved by direct methods.[40] Both structure models were refined against all data by full-matrix least-squares methods on F^2 with the program shelxl2014.[41] All non-hydrogen-atoms were refined with anisotropic displacement parameters. The hydrogen atoms were refined isotopically on calculated positions using a riding model with U_{iso} values constrained to 1.2/1.5 U_{eq} of their parent atoms. The SQUEEZE method provided by the program Platon was used to improve the contrast of the electron density map of structure $[Pd_2L^1_4](BF_4)_4$.[42]
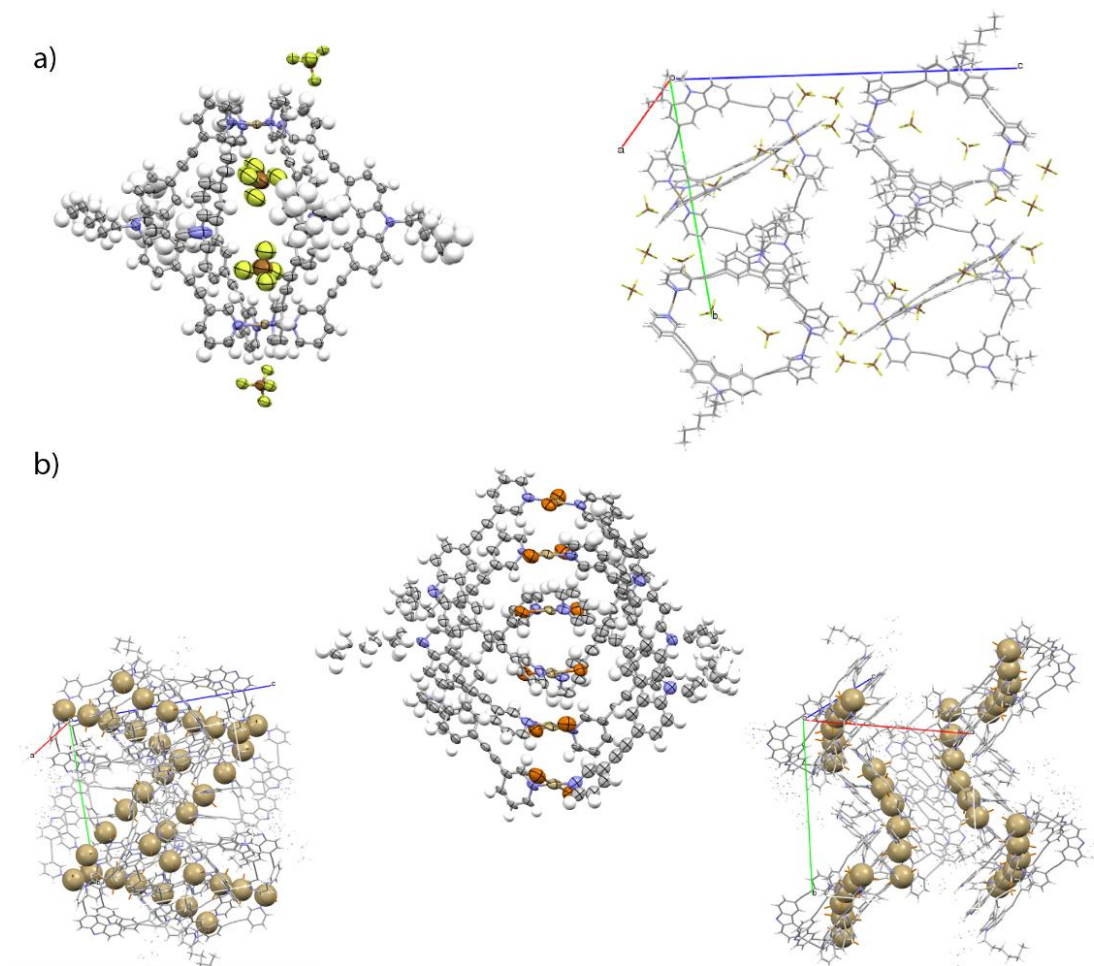
Figure 2.13 Chosen representations of the asymmetric units and the crystal packing of a) $[Pd_2L^1_4](BF_4)_4$ and {*trans*-$[(PdBr_2)_2L^1_2]$}$_3$.

To account for the disorder of the hexyl side chains of compound {*trans*-$[(PdBr_2)_2L^1_2]$}$_3$, a free variable is used to model the occupancy for each side chain. This leads to an incorrect sum formula since the hexyl atoms are only partially occupied. The expected sum formula is given in brackets below the empirical formula.

2.4.7 Geometry optimization of the double-cage structure $[3Cl@Pd_4\mathbf{L^1}_8]^{5+}$ done by G. H. Clever

1. Construction of the double-cage architecture with three chloride anions inside the pockets according to the previously reported X-ray structures of other double cages. Coarse molecular mechanics optimization.

2. Optimization at the semiempirical PM6 level implemented in Gaussian '09.[30]

3. Refined optimization at the ωB97XD/def2-SVP DFT level of theory using the dispersion-corrected ωB97XD functional implemented in Gaussian '09 and the Ahlrichs def2-SVP basis set obtained from the EMSL basis set exchange website https://bse.pnl.gov/bse/portal.[43]

2.5 Reference

[1] a) D. Fiedler, D. H. Leung, R. G. Bergman, K. N. Raymond, *Acc. Chem. Res.* **2005**, *38*, 351; b) M. Yoshizawa, J. K. Klosterman, M. Fujita, *Angew. Chem. Int. Ed.* **2009**, *48*, 3418.

[2] a) J. L. Sessler, P. Gale, W. S. Cho, S. J. Rowan, *Anion Receptor Chemistry (Monographs in Supramolecular Chemistry)*, Royal Society of Chemistry, **2006**; b) K. Bowman-James, A. Bianchi, E. Garcia-España, *Anion Coordination Chemistry*, Wiley, **2012**; c) J. A. Thomas, *Dalton Trans.,* **2011**, *40*, 12005.

[3] a) D. Vriezema, M. Aragones, J. Elemans, J. Cornelissen, A. Rowan, R. Nolte, *Chem. Rev.,* **2005**, *105*, 1445; b) U. H. Brinker, J. Mieusset (Eds.), *Molecular Encapsulation: Organic Reactions in Constrained Systems*, Wiley, **2010**; c) M. J. Wiester, P. A. Ulmann, C. A. Mirkin, *Angew. Chem. Int. Ed.* **2011**, *50*, 114.

[4] M. Fujita, N. Fujita, K. Ogura, K. Yamaguchi, *Nature,* **1999**, *400*, 52.

[5] G. H. Clever, S.Tashiro, M. Shionoya, *Angew. Chem. Int. Ed.* **2009**, *48*, 7010.

[6] J. E. M. Lewis, E. L. Gavey, S. A. Cameron, J. D. Crowley, *Chem. Sci.* **2012**, *3*, 778.

[7] G. H. Clever, M. Shionoya, *Chem. Eur. J.* **2010**, *16*, 11792.

[8] M. Yoshizawa, K. Kumazawa, M. Fujita, *J. Am. Chem. Soc.* **2005**, *127*, 13456.

[9] a) H. Dube, D. Ajami, J. Rebek, *Angew. Chem. Int. Ed.* **2010**, *49*, 3192; b) G. H. Clever, S. Tashiro, M. Shionoya, *J. Am. Chem. Soc.* **2010**, *132*, 9973.

[10] a) R. Quesada, P. A. Gale, *Coord. Chem. Rev.,* **2006**, *250*, 3219; b) *Supramolecular Chemistry of Anions*, ed. A. Bianchi, K. Bowman- James and E. Garcia-España, Wiley-VCH, New York, **1997**; c) P. D. Beer, P. A. Gale, *Angew. Chem. Int. Ed.* **2001**, *40*, 486.

[11] a) J. W. Pflugrath, F. A. Quiocho, *Nature,* **1985**, *314*, 257; b) H. Luecke, F. A. Quiocho, *Nature,* **1990**, *347*, 402; c) R. Dutzler, E. B. Campbell, M. Cadene, B. T. Chait, R. MacKinnon, *Nature,* **2002**, *415*, 287.

[12] a) J. W. Steed, J. L. Atwood, *Supramolecular Chemistry*, 2nd ed., Wiley, Wiltshire, UK, **2009**; b) M. M. Meinholz, E. Carl, E. Kriemen, D. Stalke, *Chem. Commun.* **2011**, 10948.

[13] J. R. Nitschke, *Nature,* **2009**, *462*, 736.

[14] a) J. W. Steed, J. L. Atwood, *Supramolecular Chemistry*, Wiley, **2009**; b) F. Diederich, P. Stang, R. R. Tykwinski (Eds.), *Modern Supramolecular Chemistry: Strategies for Macrocycle Synthesis*, Wiley-VCH, **2008**.

[15] Z. H. Ma, L. C. Chen, J. Q. Ding, L. X. Wang, X. B. Jing, F. S. Wang, *Adv. Mater.* **2011**, *23*, 3726.

[16] a) Q. Liu, W. M. Liu, B. Yao, H. K. Tian, Z. Y. Xie, Y. H. Geng, F. S. Wang, *Macromolecules*, **2007**, *40*(6), 1851; (b) C. Y. Chi, C. Im, V. Enkelmann, A. Ziegler, G. Lieser and G. Wegner, *Chem. Eur. J.* **2005**, *11*, 6833; (c) R. E. Martin and F. Diederich, *Angew. Chem. Int. Ed.* **1999**, *38*, 1355; (d) C. Z. Zhou, T. X. Liu, J. M. Xu and Z. K. Chen, *Macromolecules*, **2003**, *36*(5), 1457.

[17] K. Y. Law, *Chem. Rev.*, **1993**, *93*, 449.

[18] H. C. Gee, C. H. Lee, Y. H. Jeong, W. D. Jang, *Chem. Commun.* **2011**, *47*, 11963.

[19] L. Weber, J. Halama, V. Werner, K. Hanke, L. Bohling, A. Chrostowska, *Eur. J. Inorg. Chem.* **2010**, *34*, 5416.

[20] a) N. Drolet, J. F. Morin, N. Leclerc, S. Wakim, Y. Tao, M. Leclerc, *Adv. Funct. Mater.* **2005**, *15*, 1671; b) Y. B. Song, C. A. Di, Z. M. Wei, T. Y. Zhao, W. Xu, Y. Q. Liu, D. Q. Zhang, D. B. Zhu, *Chem. Eur. J.* **2008**, *14*, 4731; c) S. Cho, J. H. Seo, S. H. Park, S. Beaupré, M. Leclerc, A. J. Heeger, *Adv. Mater.* **2010**, *22*, 1253.

[21] R. H. Partridge, *Polymer*, **1983**, *24*, 733.

[22] B. H. Zhang, G. P. Tan, C. S. Lam, B. Yao, C. L. Ho, L. H. Liu, Z. Y. Xie, W. Y. Wong, J. Q. Ding, L. X. Wang, *Adv. Mater.* **2012**, *24*, 1873.

[23] Z. A. Li, Y. Q. Liu, G. Yu, Y. G. Wen, Y. L. Guo, L. Ji, J. G. Qin, Z. Li, *Adv. Funct. Mater.* **2009**, *19*, 2677.

[24] M. H. Tsai, H. W. Lin, H. C. Su, T. H. Ke, C. C. Wu, F. C. Fang, Y. L. Liao, K. T. Wong, C. I. Wu, *Adv. Mater.* **2006**, *18*, 1216.

[25] a) R. Chakrabarty, P. S. Mukherjee, P. J. Stang, *Chem. Rev.,* **2011**, *111*, 6810; b) M. Fujita, K. Umemoto, M. Yoshizawa, N. Fujita, T. Kusukawa, K. Biradha, *Chem. Commun.* **2001**, 509; c) S. J. Dalgarno, N. P. Power, J. L. Atwood, *Coord. Chem. Rev.,* **2008**, *252*, 825; d) D. Tranchemontagne, Z. Ni, M. O'Keeffe, O. Yaghi, *Angew. Chem. Int. Ed.* **2008**, *47*, 5136; e) M. D. Pluth, K. N. Raymond, *Chem. Soc. Rev.,* **2007**, *36*, 161; f) A. Schmidt, A. Casini, F. E. Kühn, *Coord. Chem. Rev.,* **2014**, *275*, 19; g) M. M. J. Smulders, I. A. Riddell, C. Browne, J. R. Nitschke, *Chem. Soc. Rev.,* **2013**, *42*, 1728; h) R. Custelcean, *Chem. Soc. Rev.,* **2014**, *43*, 1813.

[26] a) M. Frank, J. Hey, I. Balcioglu, Y. S. Chen, D. Stalke, T. Suenobu, S. Fukuzumi, H. Frauendorf, G. H. Clever, *Angew. Chem. Int. Ed.* **2013**, *52*, 10102; b) S. Bivaud, J.-Y. Balandier, M. Chas, M. Allain, S. Goeb, M. Sallé, *J. Am. Chem. Soc.* **2012**, *134*, 11968.

[27] a) M. Han, R. Michel, B. He, Y. S. Chen, D. Stalke, M. John, G. H. Clever, *Angew. Chem. Int. Ed.* **2013**, *52*, 1319; b) T. Murase, S. Sato, M. Fujita, *Angew. Chem. Int. Ed.* **2007**, *46*, 5133.

[28] a) M. Han, D. M. Engelhard, G. H. Clever, *Chem. Soc. Rev.,* **2014**, *43*, 1848; b) S. Freye, J. Hey, A. Torras-Galán, D. Stalke, R. Herbst-Irmer, M. John, G. H. Clever, *Angew. Chem. Int. Ed.* **2012**, *51*, 2191; c)

J. M. Dieterich, G. H. Clever, R. A. Mata, *Phys. Chem. Chem. Phys.* **2012**, *14*, 12746; d) S. Freye, D. M. Engelhard, M. John, G. H. Clever, *Chem. Eur. J.* **2013**, 2114; e) M. Frank, J. M. Dieterich, S. Freye, R. A. Mata, G. H. Clever, *Dalton Trans.,* **2013**, *42*, 15906; f) M. Frank, L. Krause, R. Herbst-Irmer, D. Stalke, G. H. Clever, *Dalton Trans.,* **2014**, *43*, 4587; g) S. Freye, R. Michel, D. Stalke, M. Pawliczek, H. Frauendorf, G. H. Clever, *J. Am. Chem. Soc.* **2013**, *135*, 8476.

[29] For assembly and anion binding of another $[Pd_4L_8]$ double-cage see: a) M. Fukuda, R. Sekiya, R. Kuroda, *Angew. Chem. Int. Ed.* **2008**, *47*, 706; b) R. Sekiya, M. Fukuda, R. Kuroda, *J. Am. Chem. Soc.* **2012**, *134*, 10987.

[30] Gaussian 09, M. J. Frisch, G. W. Trucks, H. B. Schlegel, G. E. Scuseria, M. A. Robb, J. R. Cheeseman, G. Scalmani, V. Barone, B. Mennucci, G. A. Petersson, H. Nakatsuji, M. Caricato, X. Li, H. P. Hratchian, A. F. Izmaylov, J. Bloino, G. Zheng, J. L. Sonnenberg, M. Hada, M. Ehara, K. Toyota, R. Fukuda, J. Hasegawa, M. Ishida, T. Nakajima, Y. Honda, O. Kitao, H. Nakai, T. Vreven, J. A. Montgomery, Jr., J. E. Peralta, F. Ogliaro, M. Bearpark, J. J. Heyd, E. Brothers, K. N. Kudin, V. N. Staroverov, R. Kobayashi, J. Normand, K. Raghavachari, A. Rendell, J. C. Burant, S. S. Iyengar, J. Tomasi, M. Cossi, N. Rega, J. M. Millam, M. Klene, J. E. Knox, J. B. Cross, V. Bakken, C. Adamo, J. Jaramillo, R. Gomperts, R. E. Stratmann, O. Yazyev, A. J. Austin, R. Cammi, C. Pomelli, J. W. Ochterski, R. L. Martin, K. Morokuma, V. G. Zakrzewski, G. A. Voth, P. Salvador, J. J. Dannenberg, S. Dapprich, A. D. Daniels, O. Farkas, J. B. Foresman, J. V. Ortiz, J. Cioslowski and D. J. Fox, Gaussian, Inc., Wallingford CT, **2009**.

[31] For the sake of comparability, 1.5 equivalents of the halide anions were added in both cases. Figure 2.4d shows the spectrum after addition of only 1.0 equivalent of chloride since larger amounts of Cl^- lead to a substantial decrease of the double cage content.

[32] a) S. Hiraoka, Y. Sakata, M. Shionoya, *J. Am. Chem. Soc.* **2008**, *130*, 10058; b) M. J. Mayoral, C. Rest, V. Stepanenko, J. Schellheimer, R. Albuquerque, G. Fernández, *J. Am. Chem. Soc.* **2013**, *135*, 2148; c) Adding even larger amounts of halide anions eventually leads to the formation of $[PdX_4]^{2-}$ as has been shown by Crowley *et al*. [Ref. 6]

[33] This complicated the mass spectrometric analysis and obviously caused low solubility in the polar solvent acetonitrile. Due to the intricate equilibrium situation, presumably also including the formation of the macrocycle *trans*-$[(PdX_2)_2L_2]$ and the [2]-catenane $\{trans$-$[(PdX_2)_2L_2]\}_2$, no yield for the triple-catenated $\{trans$-$[(PdX_2)_2L_2]\}_3$ reaction product could be determined. An overall yield for the formation of all $\{trans$-$[(PdBr_2)_2L_2]\}_n$ (n = 1−3) species by halide-induced precipitation, however, was estimated based on elemental analysis (see the Experimental Information).

[34] a) See the 'knot atlas' on http://katlas.math.toronto.edu/wiki/L6n1; b) D. W. Summers, *Stud. Phys. Theor. Chem.* **1988**, *54*, 67.

[35] a) J.-F. Ayme, J. E. Beves, C. J. Campbell, D. A. Leigh, *Chem. Soc. Rev.,* **2013**, *42*, 1700; b) R. S. Forgan, J.-P. Sauvage, J. F. Stoddart, *Chem. Rev.,* **2011**, *111*, 5434; c) D. M. Engelhard, S. Freye, K. Grohe, M. John, G. H. Clever, *Angew. Chem. Int. Ed.* **2012**, *51*, 4747.

[36] For an example of a metal-templated link with the same topology see: C. Lincheneau, B. Jean-Denis, T. Gunnlaugsson, *Chem. Commun.* **2014**, *50*, 2857.

[37] R. Wang, W. Z. Wang, G. Z. Yang, T. Liu, J. Yu, Y. Jiang, *J. Polym. Sci. Pol. Chem.* **2008**, *46*, 790.

[38] W. Kabsch, *Acta Cryst*. **2010**, *D66*, 125.

[39] G. M. Sheldrick, *SADABS,* Universität Göttingen, Germany, **2000**.

[40] T. R. Schneider, G. M. Sheldrick, *Acta Cryst*. **2002**, *D58*, 1772.

[41] G. M. Sheldrick, G. M. *Acta Crystallogr. Sect. A* **2008**, *64*, 112.

[42] a) A. L. Spek, *J. Appl. Cryst.* **2003**, *36*, 7; b) P. van der Sluis, A. L. Spek, *Acta Cryst.* **1990**, *A46*, 194.

[43] K. L. Schuchardt, B. T. Didier, T. Elsethagen, L. Sun, V. Gurumoorthi, J. Chase, J. Li, T. L. J. Windus, *Chem. Inf. Model.* **2007**, *47*, 1045.

Chapter 3:

Side Chain-Directed Assembly of Heteroleptic *trans*-[Pd₂L₂L′₂] Coordination Cages with Four Picolyl Donors

This chapter details the synthesis of a series of methyl substituted mono-dentate ligands based on carbazole, acridone and phenothiazine backbones and their social self-sorted monomeric cages, which were formed by mixing two different ligands with $[Pd(CH_3CN)_4](BF_4)_2$ in deuterated acetonitrile. The self-assembly of heteroleptic coordination cages was examined by NOESY and DOSY experiments, ESI-MS as well as molecular modeling.

3.1 Introduction

The self-assembly of coordination clusters occurs predominantly from only two types of components: one type of metal ions and ligands. However, in biological processes, functional structures are often assembled from several subcomponents through encoded information.[1] In order to mimic biological systems, achievements on enhancing the complexity and functionality of the metallosupramolecular architectures have been realized by applying multiple ligands or metal ions in coordination-driven self-assembly.[2]

Multi-component self-assembly is well-known as a nonselective process in general so it's formidably challenging to obtain only one discrete structure within a multicomponent system. As a result, several methods have been implemented to control the formation of heteroleptic complexes rather than homogeneous alternatives, such as geometrical constraints,[3,4,5] template-directed organization[6] and orthogonal self-sorting.[7,8] In pioneering studies, Sauvage and coworkers used a topological strategy to guide the selective self-assembly of multicomponent pseudorotaxanes.[9]
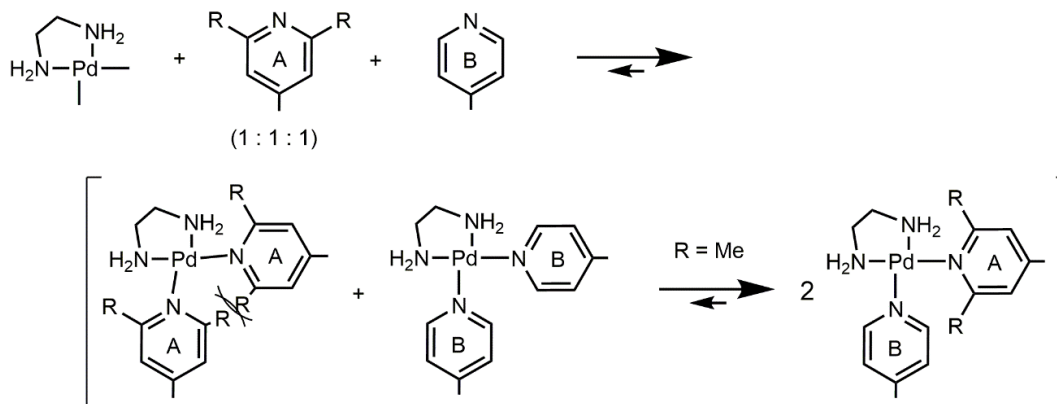
Scheme 3.1 Side chain-directed complementary *cis*-coordination of *p*-substituted pyridine-based ligands (Py^A and Py^B) upon *cis*-protected Pd^II ion in a 1:1:1 ratio. The equilibrium should be pushed toward the right in the case of R = Me.

Fujita and coworkers developed a new strategy as *side chain-directed complementary coordination* (Scheme 3.1) for the selective formation of a unique multicomponent assembly from two kinds of pyridine-based ligands and *cis*-protected Pd[II] ions.[10] From the viewpoint of steric control on coordination, introducing sterically hindered methyl groups to the 2,6-position of Py[A] is expected to yield a heterotopic complex (en)Py[A]Py[B] (en = ethylenediamine) rather than the homotopic ones due to the steric repulsion between the methyl groups of (en)Py[A]$_2$. In their work, a trigonal prism **3.4** was obtained from the assembly of a complementary pair of three linear bidentate ligands **3.2**, two planar *exo*-tridentate ligands **3.3** and six *cis*-protected Pd[II] ions **3.1** (Scheme 3.2). The side chains on ligand **3.2** are pivotal, because homotopic M$_4$L$_4$ square **3.5** composed of **3.1** and 4,4′-bipyridine as well as M$_6$L′$_4$ cage **3.6** composed of **3.1** and **3.3** will be preferably formed without the methyl protection.[10a] In conclusion, methyl groups incorporated to the ligand regulate the formation of multicomponent assemblies from two different ligands with the Pd[II] cations. Kobayashi[11] and Schmittel[12] have also achieved heteroleptic metallosupramolecular complexes by controlling steric constraints.
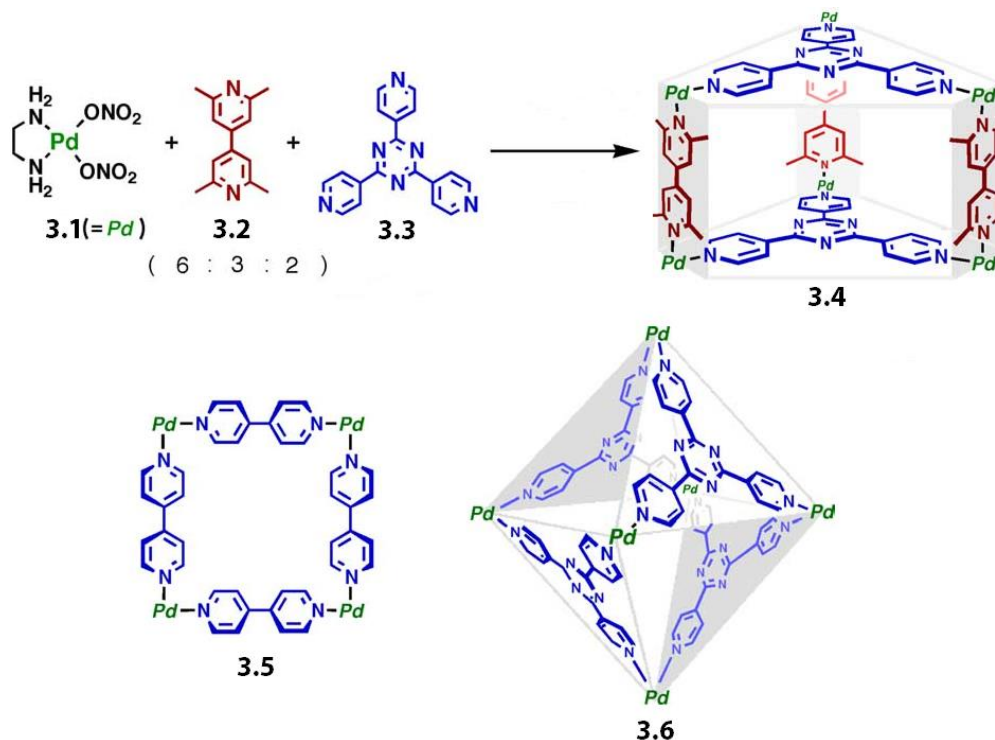
Scheme 3.2 Schematic representation of multicomponent assembly of trigonal prism **3.4** from **3.1**, **3.2** and **3.3** in a 6 : 3 : 2 ratio with chemical structures of trigonal prism **3.5** and M$_4$L$_4$ square **3.6** (Pd = (en)Pd(NO$_3$)$_2$). Copyright © 2005 Elsevier B.V.

Very recently, Stang *et al.* reported a facile approach to access well-defined multicomponent prismatic architectures without the use of any templates.[13] Upon mixing a 90° Pt[II] acceptor, a carboxylate ligand with an appropriate pyridyl donor in a controlled ratio, coordination-driven self-assembly favors the selective generation of a discrete multicomponent structure via charge separation, which facilitates the encapsulation of an aromatic guest, triphenylene (Scheme 3.3). The multi-component complexes described in this study

could also be obtained by a novel supramolecule-supramolecule transformation from homogeneous assemblies.
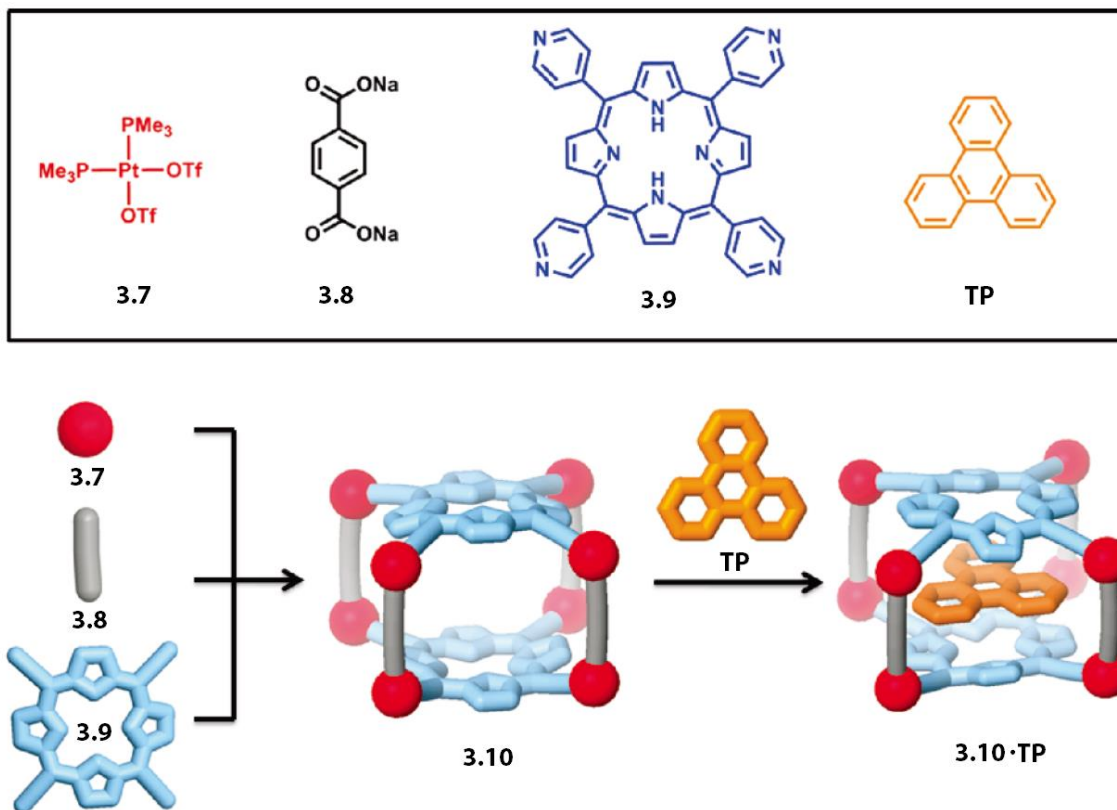
Scheme 3.3 Graphical representation of self-assembly of multicomponent porphyrin cage **3.10** from *cis*-Pt(PMe$_3$)$_2$(OTf)$_2$ (**3.7**), carboxylate **3.8** and pyridyl ligand **3.9** and encapsulation of triphenylene (**TP**). Copyright © 2010 American Chemical Society.

Realization of controlled multi-component self-assembly has been recently achieved by the Clever group. [14] In their research, a bent heteroleptic coordination cage **3.13** was formed not depending on the donor-acceptor interaction or implementation of steric hindrance but by the geometric complementarity of two cautiously designed ligands (Scheme 3.4). It was also demonstrated that this heteroleptic architecture can be obtained via three self-assembly processes: direct combination of the ligands with metal ions, cage-to-cage transformation and ligand triggered cage rearrangement. This template-free formation of a robust cage with a *cis* arrangement of ligands could be applied in developing novel and unique systems with a greater control over the incorporation of multiple functionalities.

Even though various mixed-component supramolecular systems have been reported, the complexity, rational design and synthetic controllability of noncovalent assembly of individual components are still challenging in more advanced applications. Coming up with sufficient molecular information to control selective self-assembly in a multicomponent system remains a demanding issue in modern supramolecular chemistry.

3.11   **3.12**   **3.13**
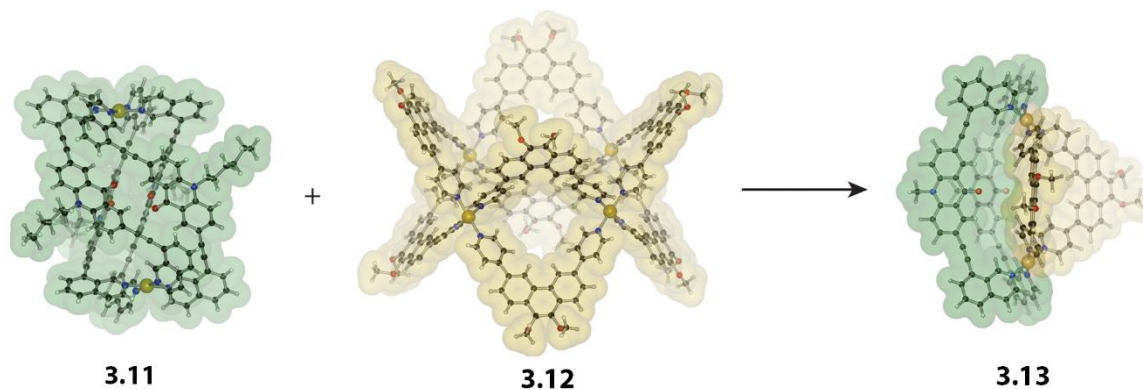
Scheme 3.4 A perspective view of the X-ray crystal structures of homogeneous cage **3.11** and homogeneous box **3.12** and DFT calculated model of heteroleptic cage **3.13**. Copyright © 2016 American Chemical Society.

3.2 Ligand synthesis and assembly based on carbazole backbone

[M_2L_4] coordination cages assembled from bis-monodentate banana-shaped ligands and metal cations (M = Pd, Pt, Cu, Ni) are an archetypal platform to implement functionality, such as light switch-ability,[15] selective guest encapsulation and transport,[16] structural transformation,[17] because of their regularly spatial arrangement of ligands. Due to the possibility of multi-functional supramolecular structures, combining two or more functionalities into one single assembly has attracted considerable attention. In order to approach the social self-sorting behavior in coordination cages, in this chapter, methyl substituents (side chain) are used as bulky groups in different combinations.

At first, based on the carbazole ligand **L¹** mentioned in Chapter 2, ligand **LB** (Scheme 3.5), possessing lutidine groups as bulky groups, was synthesized in the similar way as **L¹** by the Sonogashira cross-coupling reaction using 3-ethynyl-2,6-dimethylpyridine instead of 3-ethynylpyridine. After reacting with the palladium salt [$Pd(CH_3CN)_4$](BF_4)$_2$ in a 2 : 1 ratio, ¹H NMR spectrum showed at least three different species according to the splitting of the methyl groups (Figure 3.1d). ESI-MS revealed signals corresponding to ligand **LB** and very scarce signals assignable to a [Pd**LB**$_2$]²⁺ species. Importantly, the mono-cage peak was not observed (Figure 3.2a) which can be attributed to the steric effect aroused by the methyl groups. In an attempt to get a heteroleptic assembly from two different ligands, ligands **L¹** and **LB** were suspended in CD$_3$CN in ratio of 1 : 1 with 0.5 equivalents of Pd²⁺ heated overnight. From the NMR spectra, the main peaks were assigned to the mono-cage [Pd$_2$**L¹**$_4$]⁴⁺ (Figure 3.1e) and signals corresponding to the cage assembled with different ligands could not be found in the ESI-MS spectrum but only the species [Pd$_2$**L¹**$_4$]⁴⁺ (Figure 3.2b).

An unsymmetrical ligand **LC** was synthesized via two steps of Sonogashira cross-coupling reaction (Scheme 3.5) and was combined with **L¹** attempting to form a social self-sorted cage in the same way as for **LB** discussed above. After mixing **LC** with palladium cations, two species of [Pd**LC**$_2$]²⁺ and [Pd$_2$**LC**$_4$]⁴⁺ were found from the ESI-MS but with very weak signals besides the main protonated [**LC**+H]¹⁺ species. From

the social-assembly, three species were identified from the ESI-MS, including $[Pd_2L^1_4]^{4+}$, $[Pd_2L^1_3LC_1]^{4+}$ and $[Pd_2L^1_2LC_2]^{4+}$. The main signals observed in the ^1H NMR spectrum corresponded to the mono-cage $[Pd_2L^1_4]^{4+}$ (Figure 3.1h). In this case, the social-assembly from different ligands was observed but accompanying with statistical mixtures and narcissistic self-sorting.

LB: $R_1=R_2=R_3=R_4=$ -CH$_3$;
LC: $R_1=R_2=$ -CH$_3$, $R_3=R_4=$ -H;
LD: $R_1=R_4=$ -CH$_3$, $R_2=R_3=$ -H;
LE: $R_1=$ -CH$_3$, $R_2=R_3=R_4=$ -H;
LF: $R_2=R_3=$ -CH$_3$, $R_1=R_4=$ -H.
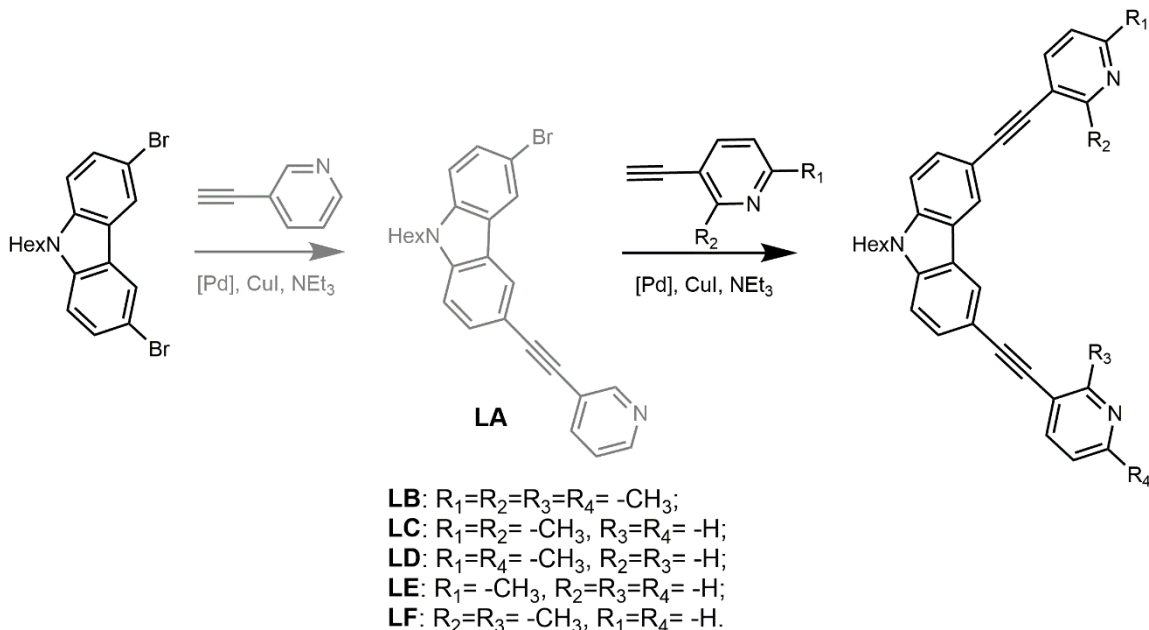
Scheme 3.5 Synthesis of ligands **LB**, **LC**, **LD**, **LE** and **LF** through Sonogashira cross-coupling reaction similar as L^1 described in the second chapter. Ligands **LB**, **LD** and **LF** were synthesized by using 3-ethynyl-2,6-dimethylpyridine, 5-ethynyl-2-methylpyridine and 3-ethynyl-2-methylpyridine instead of 3-ethynyl-pyridine respectively. Ligands **LC** and **LE** were synthesized in two steps: the first step was to obtain **LA** similar as L^1 but reduced the ratio of 1-(3,6-dibromo-9H-carbazol-9-yl)hexan-1-one and 3-ethynylpyridine to 1 : 1.5; the second step was to use 3-ethynyl-2,6-dimethylpyridine and 5-ethynyl-2-methylpyridine respectively coupling with **LA**.

It's supposed that ligands **LB** and **LC**, which contain two methyl groups next to the pyridine nitrogen atom, are too bulky to coordinate with the square planar palladium cations even together with L^1. Another unsymmetrical ligand, **LE**, with only one methyl unit attached on one arm of the ligand was designed and successfully synthesized in the similar way as **LC**. After heating a 2 : 1 mixture of ligand **LE** and $[Pd(CH_3CN)_4](BF_4)_2$ in CD$_3$CN at 70 °C for 8 h, a monomeric cage $[Pd_2LE_4]^{4+}$ was obtained as indicated by ^1H NMR spectroscopy (Figure 3.1j with weak unassignable peaks) and ESI-MS spectrometry (Figure 3.2e). After heating a 1 : 1 : 1 mixture of ligand **LE**, L^1 and $[Pd(CH_3CN)_4](BF_4)_2$ in CD$_3$CN at 70 °C for 8 h, ^1H NMR spectrum (Figure 3.1k) showed a quite complex spectrum and ESI-MS spectrum (Figure 3.2f) showed the presence of a statistical mixture, $[Pd_2L^1_4]^{4+}$, $[Pd_2L^1_3LE]^{4+}$, $[Pd_2L^1_2LE_2]^{4+}$ and $[Pd_2L^1LE_3]^{4+}$. Comparing to the **LC** system, in this case, more species were formed which is attributed to the weaker steric effect. In

consequence, the social self-sorting of supramolecular cages was successfully observed but without strict control over the mixtures.
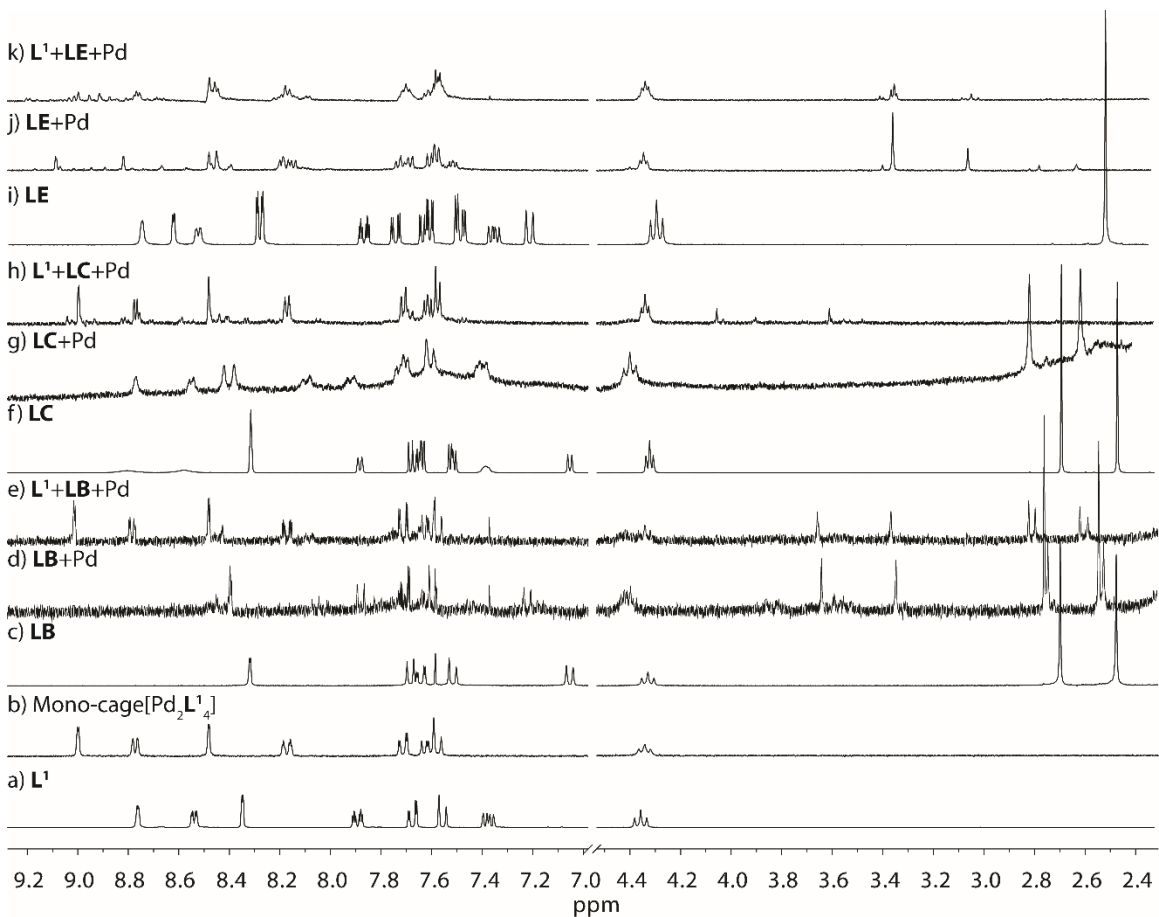
Figure 3.1 ^{1}H NMR spectra of a) L^1; b) mono-cage $[Pd_2L^1_4]^{4+}$; c) **LB**; mixtures resulting from the reaction of d) **LB** with 0.5 equivalents of $[Pd(CH_3CN)_4](BF_4)_2$; e) 1 equivalent of L^1, 1 equivalent of **LB** and 1 equivalent of $[Pd(CH_3CN)_4](BF_4)_2$; f) **LC**; mixtures resulting from the reaction of g) **LC** with 0.5 equivalents of $[Pd(CH_3CN)_4](BF_4)_2$; h) 1 equivalent of L^1, 1 equivalent of **LC** and 1 equivalent of $[Pd(CH_3CN)_4](BF_4)_2$; i) **LE**; and mixtures resulting from the reaction of j) **LE** with 0.5 equivalents of $[Pd(CH_3CN)_4](BF_4)_2$; k)1 equivalent of L^1, 1 equivalent of **LE** and 1 equivalent of $[Pd(CH_3CN)_4](BF_4)_2$ (298K, 500MHz).

In view of the self-sorting experiments described above, ligand L^1 tends to form a homoleptic complex with metal cations, and cannot form a single social self-sorted complex with other ligands in stoichiometry. Ligands **LD** and **LF** were designed and synthesized in the same way as L^1 but using 5-ethynyl-2-methylpyridine and 3-ethynyl-2-methylpyridine instead of 3-ethynylpyridine, respectively. From the two structures of these two ligands, the methyl groups are attached to the *para-* and *ortho-* positions into **LD** and **LF**, respectively. Afterwards, **LD**, **LF** and $[Pd(CH_3CN)_4](BF_4)_2$ in ratio of 1 : 1 : 1 were suspended in CD_3CN and heated for 8 h at 70 °C. ^{1}H NMR spectroscopy and ESI-Mass spectrometry were measured to analyze the system. According to the ESI-MS spectra (Figure 3.4), the mass signal of a mono-cage was observed.

Nevertheless, it's not possible to determine whether a social self-sorting behavior happened or not from ESI-MS in this case because of the same molecular mass of **LD** and **LF**. What's more, no specific information could be extracted from the complicated NMR spectra (Figure 3.3).
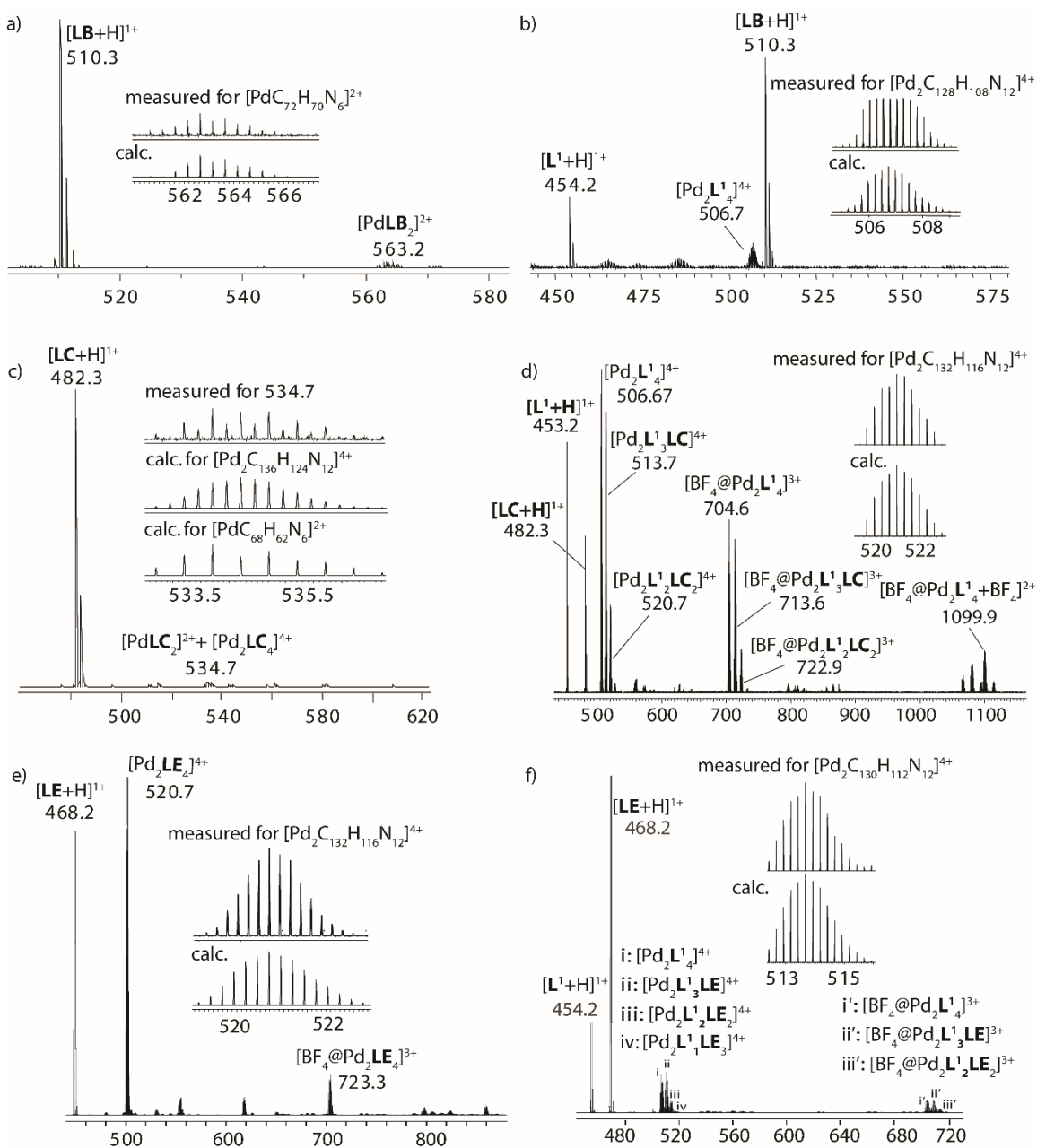
Figure 3.2 ESI-Mass spectra of assemblies from a) **LB**; b) L^1, **LB**; c) **LC**; d) L^1, **LC**; e) **LE**; and f) L^1, **LE** with Pd^{II} cations.
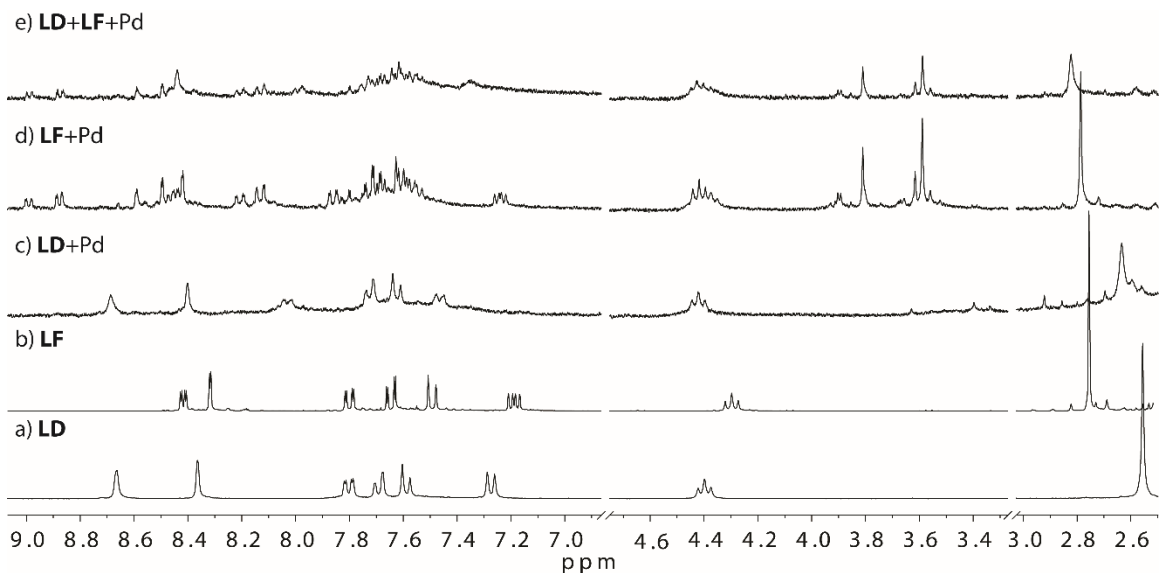
Figure 3.3 ^{1}H NMR spectra of a) **LD**; b) **LF**; mixture resulting from the reaction of c) **LD** and d) **LF** with 0.5 equivalents of [Pd(CH$_3$CN)$_4$](BF$_4$)$_2$; e) 1 equivalent of **LD**, 1 equivalent of **LF** and 1 equivalent of [Pd(CH$_3$CN)$_4$](BF$_4$)$_2$ (298K, 300MHz).
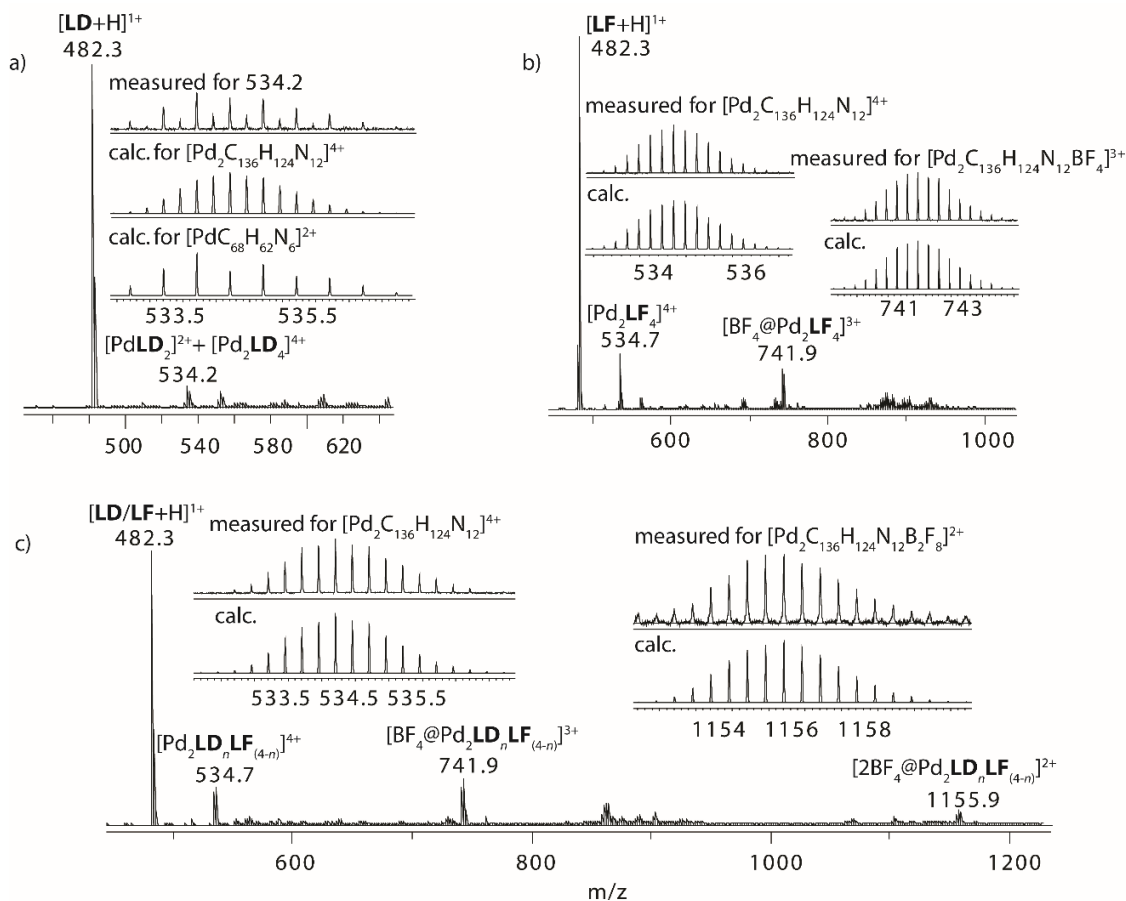
Figure 3.4 ESI-Mass spectra of assemblies from a) **LD**; b) **LF** and c) **LD, LF**, reacting with Pd^{II} cations in stoichiometry (n = 0–4).

3.3 Ligand synthesis and assembly based on acridone and phenothiazine backbones

After the experiments discussed above, ligands based on the carbazole backbone may not be compatible with the formation of uniform heteroleptic assemblies owing to the relatively shorter backbone[17] to some extent. As a result, acridone and phenothiazine backbones came to my mind which were reported before in the Clever group.[18] Ligands **PL¹**, **PL²**, **AL¹**, **AL²** and **AL³** based on picoline functionalities are synthesized via Sonogashira coupling reaction according to the aforementioned route (Scheme 3.6a). Steric hindrance is utilized at the mono-nuclear level by means of an energetically favored alignment of pyridine donors around the Pd[II] center (Scheme 3.6b). From the calculation, the energy of the *anti*-form is 139 kJ/mol lower than the *syn*-form of a Pd(Pic)₄ coordination complex, which means the *anti*-formed Pd(Pic)₄ coordination structure is thermodynamically favorable. This also lays a theoretical foundation on heteroleptic assemblies from ligands with different picoline functionalities.
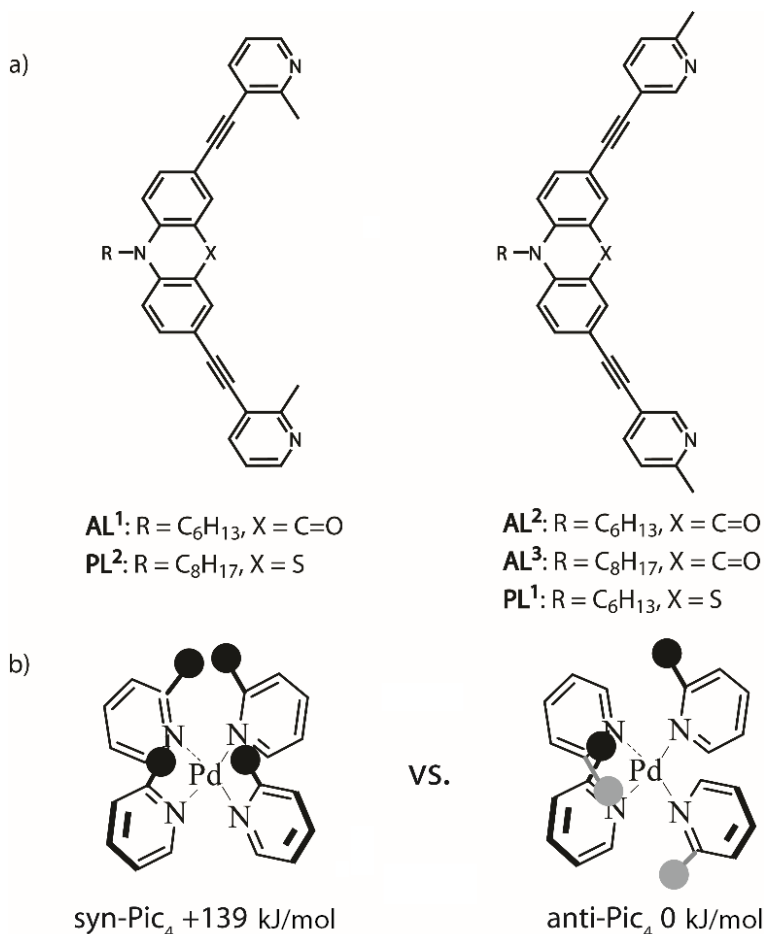
Scheme 3.6 a) Schematic presentation of ligands **PL¹**, **PL²**, **AL¹**, **AL²** and **AL³**; b) Picoline up/down approach. The calculated values highlighted the difference in energy between the *syn*- and *anti*-forms of a Pd(Pic)₄ coordination complex.

To differentiate the heteroleptic assemblies from analogues backbones by mass spectra, different chains were installed into the respective ligand backbones. For example, hexyl chain was attached to form ligand $\textbf{AL}^\textbf{1}$ while octyl chain was attached to form $\textbf{AL}^\textbf{3}$. The structure of these ligands was confirmed by ^{1}H and ^{13}C NMR spectroscopy as well as mass spectrometry.

Initially, it is interesting to study whether the steric hindrance attributed to the assembly from four identically functionalized ligands with Pd^{II} would inhibit cage formation and bring about an intricate mixture. Furthermore it is interesting to find whether the methyl substituent would prevent cage catenation since both of the analog ligands with pyridiyl donors readily form interpenetrated cages with Pd^{II}.[18a,c] Consequently, investigations on the Pd^{II} mediated self-assembly of the acridone-derived ligands, $\textbf{AL}^\textbf{1}$ and $\textbf{AL}^\textbf{3}$, were carried out. It was expected that these two ligands may behave distinctly due to the different spatial conformations of the methyl substituents; in one case, the methyl substituents should point inwardly toward the cavity ($\textbf{AL}^\textbf{1}$) of the cage, while in the second situation ($\textbf{AL}^\textbf{3}$) the methyl groups are expected to point outside the cavity and above the palladium planes of the cage.

Initially, heating a 2 : 1 mixture of $\textbf{AL}^\textbf{1}$ and [Pd(CH$_3$CN)$_4$](BF$_4$)$_2$ at 70 °C for 8 h yielded an involute mixture as revealed by ^{1}H NMR spectroscopy (see further experiments). Nevertheless, the spectrum was significantly simplified when the self-assembly reaction was performed at room temperature. In this case, the ^{1}H NMR spectrum showed the presence of two sets of proton signals, in a 2 : 1 ratio (Figure 3.5c). Further analysis revealed a downfield shift of H$_f$ and the methyl protons signals (H$_g$) relative to the free ligand, indicative of Pd(II) complexation. According to the characteristical shifting of monomeric cage comparing with the corresponding ligand,[15-17] loss of symmetry in this case somehow occurred which caused the signal splitting but without forming a mono-cage structure. Further analysis of the sample by ESI-MS analysis revealed peaks assignable to [Pd$_2$($\textbf{AL}^\textbf{1}$)$_3$]$^{4+}$ assembly (Figure 3.8a). Interestingly, the empty coordination sites of the palladium cations were occupied by CH$_3$CN molecules in solution, as indicated by ESI-MS spectrum. Accordingly, coordinating anion contaminations (F$^-$) which presumably fill this binding site at the Pd^{II} center were found alongside the 3+ and 2+ peaks. ^{1}H−^{1}H NOESY analysis (Figure 3.6) revealed a key cross peak between the two separate H$_f$ signals (refer to Figure 3.7b), which verified the two proton signals arising from two different ligands are in close contact indicating their close proximity within the same molecule. Thus, a C_{2h} symmetry of the [Pd$_2$($\textbf{AL}^\textbf{1}$)$_3$]$^{4+}$ architecture is consistent with the presence of two sets of proton signals in a 2:1 ratio. In this case, two ligands sit at the periphery sharing the same chemical environment and one is situated in the middle possessing a different chemical environment, forming a bow-shaped structure (Figure 3.7a). This was further supported by diffusion-ordered spectroscopy (DOSY) experiment (orange signals in Figure 3.18), which revealed that the two sets of proton signals correspond to the same diffusion coefficient (log D = −9.232, D = 5.86 x 10^{-10}, r = 10.09 Å) indicating they belong to one molecule structure.

On the other hand, stirring a 2 : 1 solution of $\textbf{AL}^\textbf{3}$ with [Pd(CH$_3$CN)$_4$](BF$_4$)$_2$ at room temperature produced three sets of signals of ^{1}H NMR spectrum (Figure 3.5d). COSY and NOESY analysis confirmed that, like for $\textbf{AL}^\textbf{1}$, the peaks present in a 2:1 ratio correspond to a [Pd$_2$($\textbf{AL}^\textbf{3}$)$_3$]$^{4+}$ species. Analysis of the sample by ESI-

MS (Figure 3.8b) revealed signals corresponding to two species: $[Pd_2(AL^3)_3+2CH_3CN]^{4+}$ and $[Pd_2(AL^3)_2+nBF_4]^{(4-n)+}$ (n = 1, 2). The absence of evidence in the ESI-Mass spectrum of a $[Pd_2L_4]$ species suggests that the third set of signals in the ^1H NMR spectrum belongs to the $[Pd_2L_2]$ species.

It is worth noting that bowl-shaped $[Pd_2L_3]^{4+}$ compounds have seldom been reported,[19] while $[Pd_2L_2]^{4+}$ macrocycles are encountered only where the Pd(II) centres possess *cis*-capping ligands[20,21] or *trans*-coordinating halide ligands.[22,23]
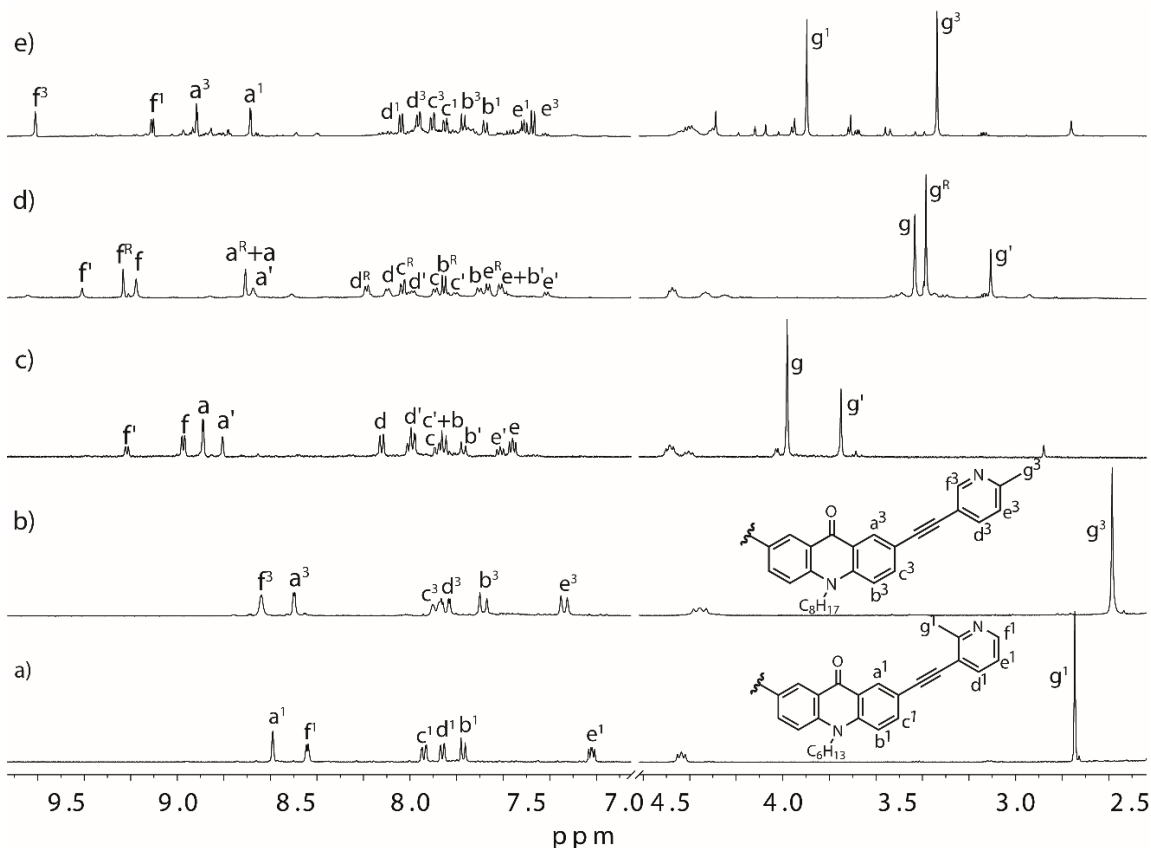
Figure 3.5 ^1H NMR spectra (600 MHz, CD$_3$CN, 293 K) of a) ligand AL^1; b) ligand AL^3; c) bowl-shaped cage $[Pd_2(AL^1)_3]^{4+}$; d) bowl-shaped cage $[Pd_2(AL^3)_3]^{4+}$ and ring $[Pd_2(AL^3)_2]^{4+}$; and e) mono-cage $[Pd_2(AL^1)_2(AL^3)_2]^{4+}$ (^{R} represents ring).

Next, the investigation was focused on the combination of AL^1 and AL^3 to see if there would be social self-sorting behavior. After mixing $[Pd(CH_3CN)_4](BF_4)_2$, AL^1 and AL^3 in a 1 : 1 : 1 ratio in CD$_3$CN and heating overnight, 12 aromatic signals with equal integrations were observed in the ^1H NMR spectrum. These 12 signals can be classified into two sets and each set could be assigned to the shifting of ligands AL^1 and AL^3, respectively, according to the multiplicities of the different picoline groups (Figure 3.5e). From the analysis of ESI-MS, $[Pd_2(AL^1)_2(AL^3)_2+nBF_4]^{(4-n)+}$ (n = 0, 1) species can be observed (Figure 3.8c). Furthermore, DOSY experiment verified that all of the proton signals corresponded to the same diffusion coefficient (Figure 3.10b, *log* D = −9.263, D = 5.46 x 10^{-10}, r = 10.83 Å). In consequence, it was assumed that the coordination of AL^1 and AL^3 with palladium cations resulted a heteroleptic species $[Pd_2(AL^1)_2(AL^3)_2]^{4+}$.
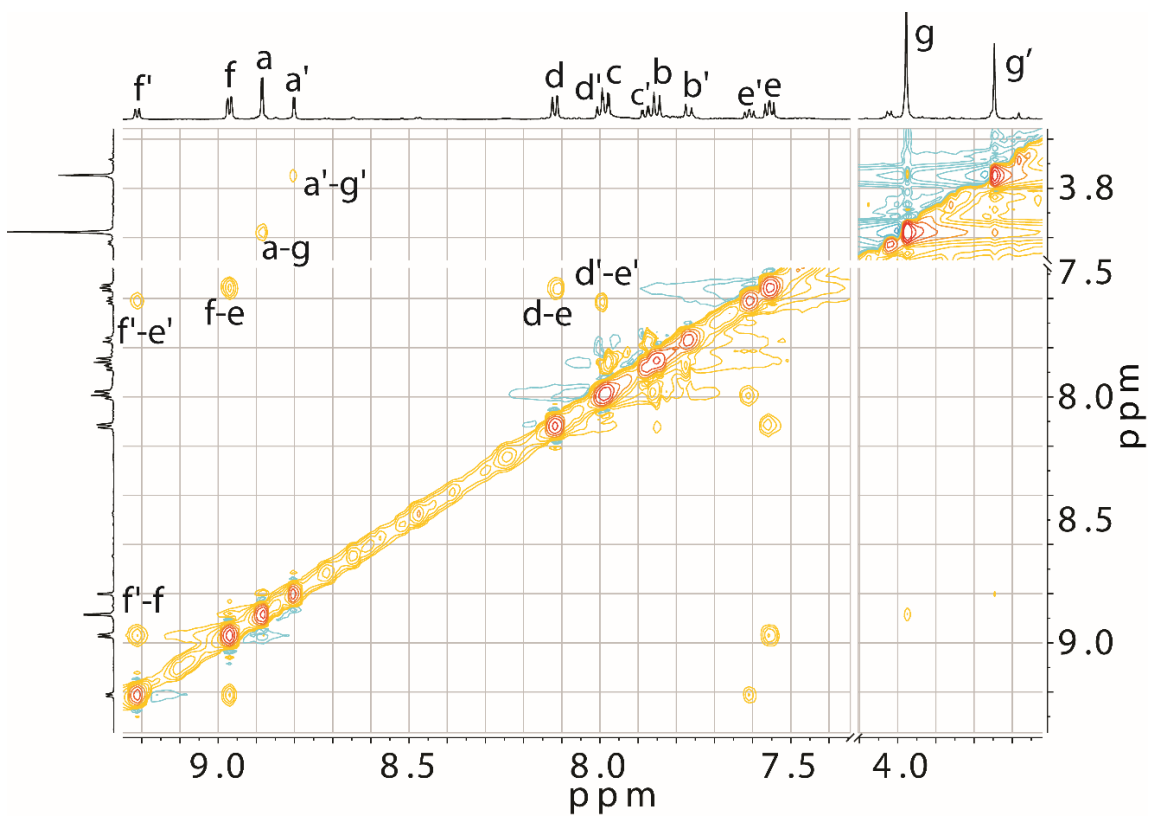
Figure 3.6 ^{1}H–^{1}H NOESY spectrum of bowl-shaped cage $[Pd_2(\mathbf{AL^1})_3]^{4+}$ in CD$_3$CN, for ^{1}H NMR signal assignment: see Figure 3.5.
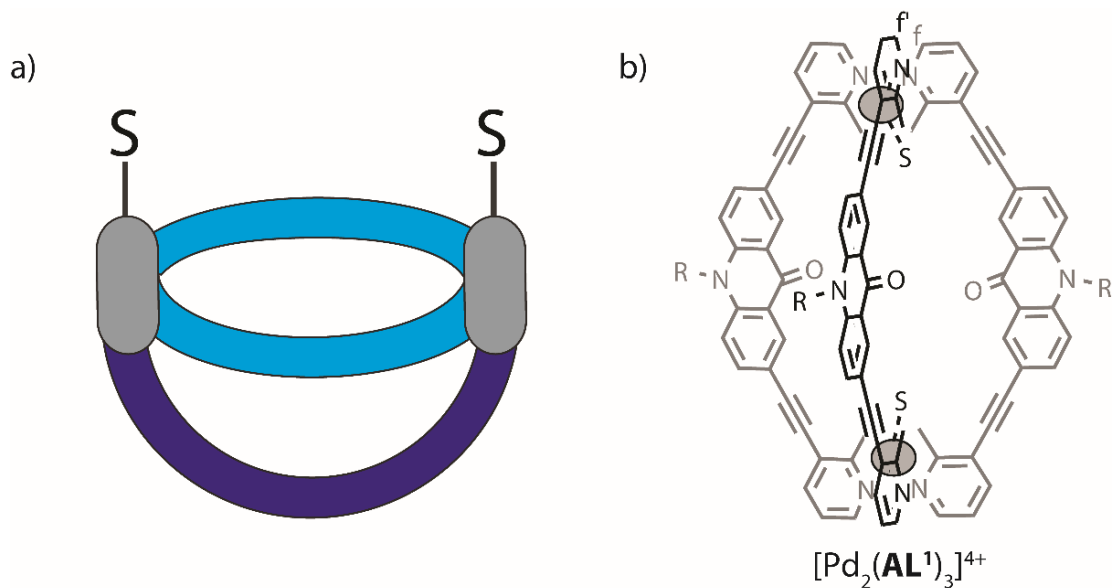
Figure 3.7 a) Graphical representation of bowl-shaped $[M_2L_3]$ architecture (color code: grey, metal; blue, two ligands sitting at the periphery; dark blue, one ligand sitting in the middle); b) bowl-shaped cage $[Pd_2(\mathbf{AL^1})_3]^{4+}$ (grey ball = Pd^{II}, S = solvent, R = –C$_6$H$_{13}$).
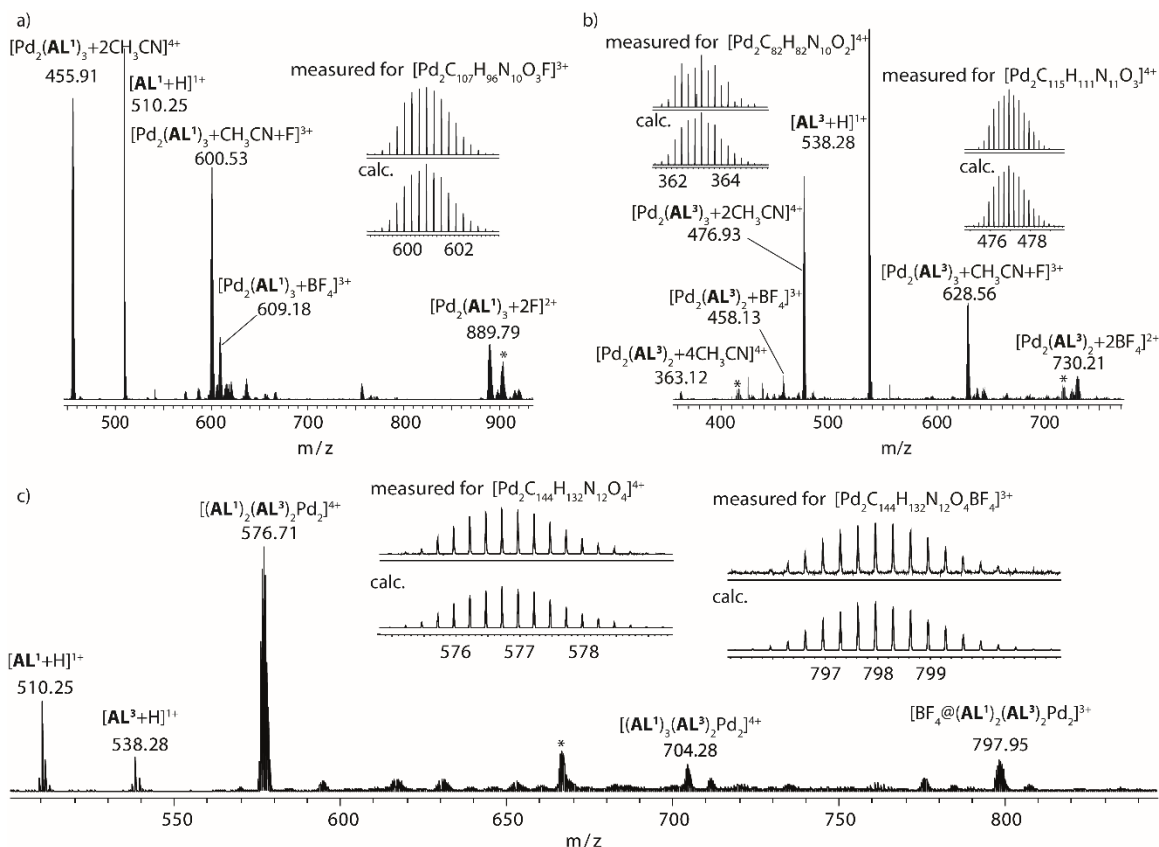
Figure 3.8 ESI-MS spectra of a) bowl-shaped cage $[Pd_2(\textbf{AL}^1)_3]^{4+}$; b) mixture of bowl-shaped cage $[Pd_2(\textbf{AL}^3)_3]^{4+}$ and ring $[Pd_2(\textbf{AL}^3)_2]^{4+}$; c) heteroleptic cage of $[Pd_2(\textbf{AL}^1)_2(\textbf{AL}^3)_2]^{4+}$ (* = adducts with impurities).

According to molecular modelling (Scheme 3.6b), the *anti*-form is more energetically favorable than *syn*-form of a Pd(Pic)$_4$ coordination complex. Therefore, it was expected that the square planar geometry of Pd^{II} with $\textbf{AL}^1$ and $\textbf{AL}^3$ should favor a *syn*-form of the picoline functionalized ligands. Under W. Bloch's endeavor, a crystal structure assembled from four 2-picolines and two palladium cations was obtained but the data was not refined well yet. From the preliminary structure, a *cis*-arrangement of the picoline was presented (Figure 3.9) which was different from my first thought of "*trans*-arrangement". However, it's hard to determine whether the arrangement is *cis* or *trans* just from one single crystal. Further researches are still undergoing in the Clever group. The theoretical calculation was also done but without showing big difference between *cis* and *trans* arrangements. Based on the first supposition, only *trans*-arrangement would be discussed in the following. Since an X-ray structure of heteroleptic cage $[Pd_2(\textbf{AL}^1)_2(\textbf{AL}^3)_2]^{4+}$ could not be obtained, a DFT model of *trans*-$[Pd_2(\textbf{AL}^1)_2(\textbf{AL}^3)_2]^{4+}$ assembly was calculated based on the spectroscopic results and the crystal structures of reported monomeric cages by performing a geometry optimization on the ωB97XD/def2-SVP level of theory (Figure 3.10a). In addition, a ^{1}H–^{1}H NOESY experiment was performed in order to assign the pivotal interligand contacts in heteroleptic cage *trans*-$[Pd_2(\textbf{AL}^1)_2(\textbf{AL}^3)_2]^{4+}$ (Figure 3.11a). It

revealed several evident cross-peaks, especially between the methyl protons (g) and the pyridyl protons (f). The observed contacts are in full agreement with expected contacts measured in the calculated model.

Finally, investigation was made to verify whether picoline functionalization is a general method to combine different backbones in a controlled manner. Interestingly, the Pd-mediated assembly of $\mathbf{AL^1}$ with $\mathbf{PL^1}$ and $\mathbf{AL^2}$ with $\mathbf{PL^2}$ yielded different outcomes. The latter gave a relatively clean spectrum while the former gave a rather complicated spectrum which was hard to analyze. Upon addition of $[Pd(CH_3CN)_4](BF_4)_2$ stoichiometrically into the suspension of $\mathbf{PL^2}$ and $\mathbf{AL^2}$ (1 : 1) in acetonitrile, the color turned from yellow to dark green immediately which changed to orange after heating 8 h at 70 °C. 12 Aromatic protons were provided with the same integration displaying in the ^{1}H NMR spectrum (Figure 3.12c). These 12 signals can be sorted into two sets and each set belonged to the shifting of $\mathbf{AL^2}$ and $\mathbf{PL^2}$, respectively, similar as the case of $\mathbf{AL^1}$ and $\mathbf{AL^3}$. Further characterization of the sample by ESI-MS revealed that the dominant signals were assigned to the $[Pd_2(\mathbf{AL^2})_2(\mathbf{PL^2})_2+n BF_4]^{(4-n)+}$ ($n = 0-2$) species (Figure 3.13). COSY and NOESY experiments were applied to aid and verify the assignments of the ^{1}H NMR spectrum. From the NOESY analysis (Figure 3.14), characteristic cross peaks between the protons of methyl substituents (g) and pyridine protons (f) displayed indicating the adjacent position of the two different ligands in the $[Pd_2\mathbf{L}_2\mathbf{L'}_2]$ assembly. The observed contacts were also consistent with the calculated model shown in Figure 3.10b. Moreover, DOSY analysis (Figure 3.15) confirmed that all the proton signals assigned to the heteroleptic $[Pd_2(\mathbf{PL^1})_2(\mathbf{AL^2})_2]^{4+}$ assembly correspond to the same diffusion coefficient ($log\mathrm{D} = -9.273$, $\mathrm{D} = 5.33 \times 10^{-10}$, r = 11.09 Å). As a result, a social self-sorted assembly $[Pd_2(\mathbf{AL^2})_2(\mathbf{PL^2})_2]^{4+}$ was obtained to a great extent.
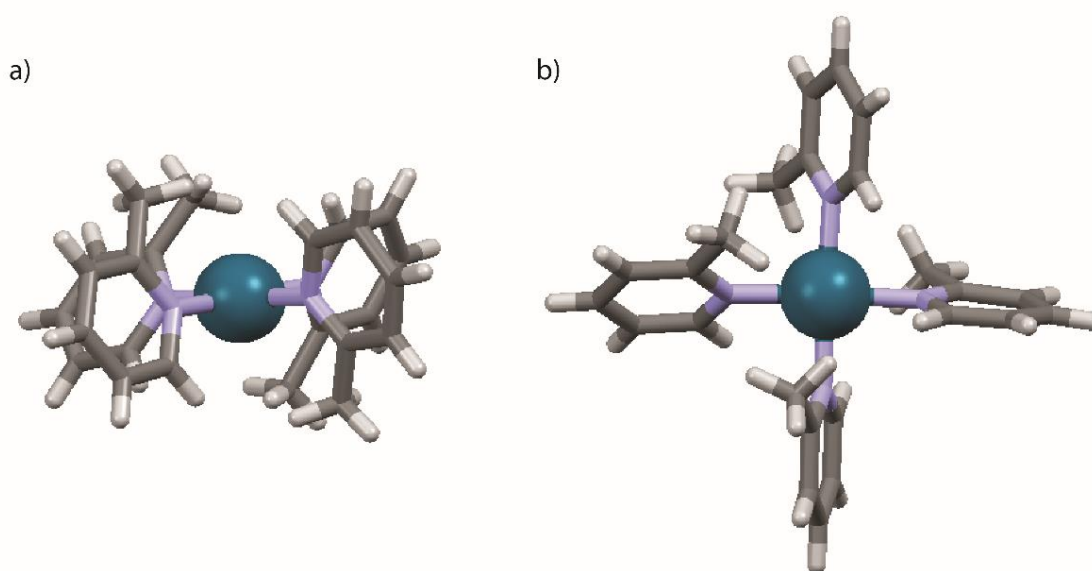
Figure 3.9 Preliminary X-ray structure of assembly from four 2-picolines and two palladium cations a) front view, b) top view. Color code: blue, Pd; purple, N; dark grey, C; grey, H.
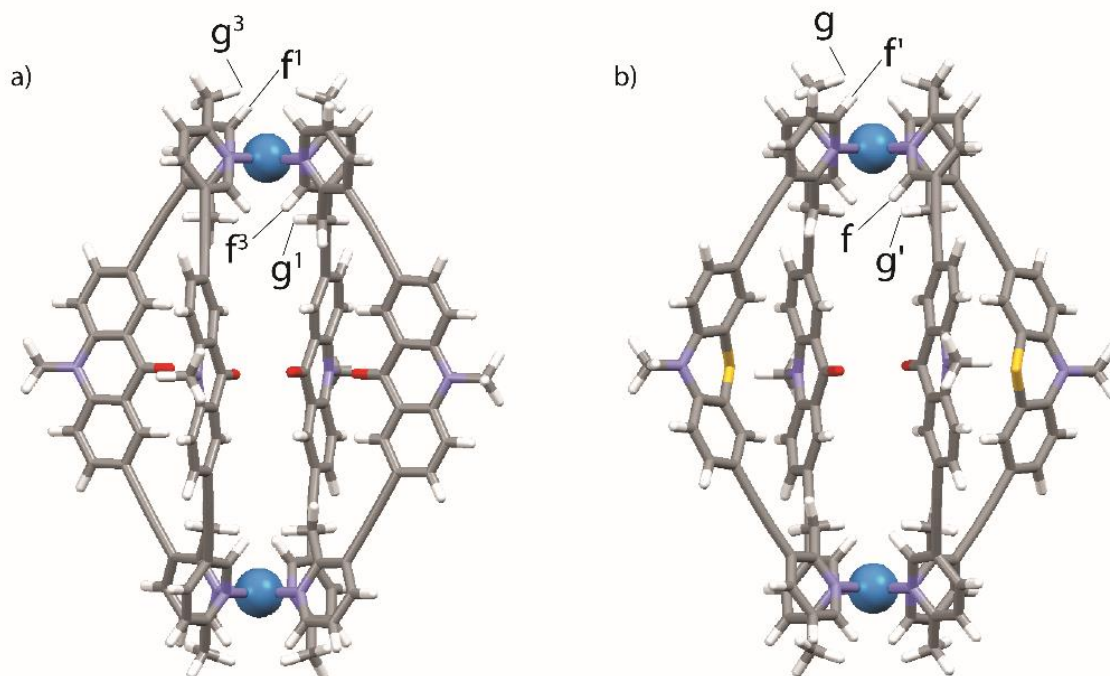
Figure 3.10 DFT-optimized structures of a) heteroleptic cage *trans*-[Pd$_2$(**AL^1**)$_2$(**AL^3**)$_2$]$^{4+}$; b) heteroleptic cage *trans*-[Pd$_2$(**AL^2**)$_2$(**PL^2**)$_2$]$^{4+}$ (for ^{1}H NMR signal assignment: a see Figure 3.5 and b see Figure 3.12). To simplify the calculations, the hexyl and octyl chains of the backbones were replaced with a methyl substitute. Color code: blue, Pd; grey, C; purple, N; red, O; yellow, S; white, H.

Distinctly, when reacting **PL^1** and **AL^1** with Pd^{II} in the same way as **AL^2** and **PL^2** with Pd^{II}, a quite complicated ^{1}H NMR spectrum was obtained presenting multiple overlapping sets of signals. From the comparison spectra, two weak sets of peaks present in the mixture were identified to belong to the species [Pd$_2$(**AL^1**)$_3$]$^{4+}$ (Figure 3.16a). The ESI-MS spectrum also demonstrated the presence of signals from [Pd$_2$(**AL^1**)$_3$]$^{4+}$ assembly (Figure 3.17). However, the assemblies formed from **PL^1** could not be clearly identified. What's more, no signals assignable to a heteroleptic cage could be observed in the ESI-MS spectrum.

To gain insight into the self-sorting phenomena (**AL^2** and **PL^2**, **PL^1** and **AL^1**), DFT calculations of *trans*-[Pd$_2$(**AL^2**)$_2$(**PL^2**)$_2$]$^{4+}$ and *trans*-[Pd$_2$(**AL^1**)$_2$(**PL^1**)$_2$]$^{4+}$ assemblies were performed but without any significant energy difference. Figure 3.18 presents the structures of two kinds of ligands based on acridone and phenothiazine backbones with pyridine groups but not picoline units, respectively. In Figure 3.18d, an apparent bend angle of the phenothiazine backbone was observed comparing with the acridone backbone in Figure 3.18b. Accordingly, it's assumed that, since the phenothiazine backbone is much bending compared with the flat acridone backbone, the geometry of ligands would change a lot when introducing different picoline functionalities into a phenothiazine backbone. As a result, the chemical behaviors displayed quite different when coordinating with palladium ions.
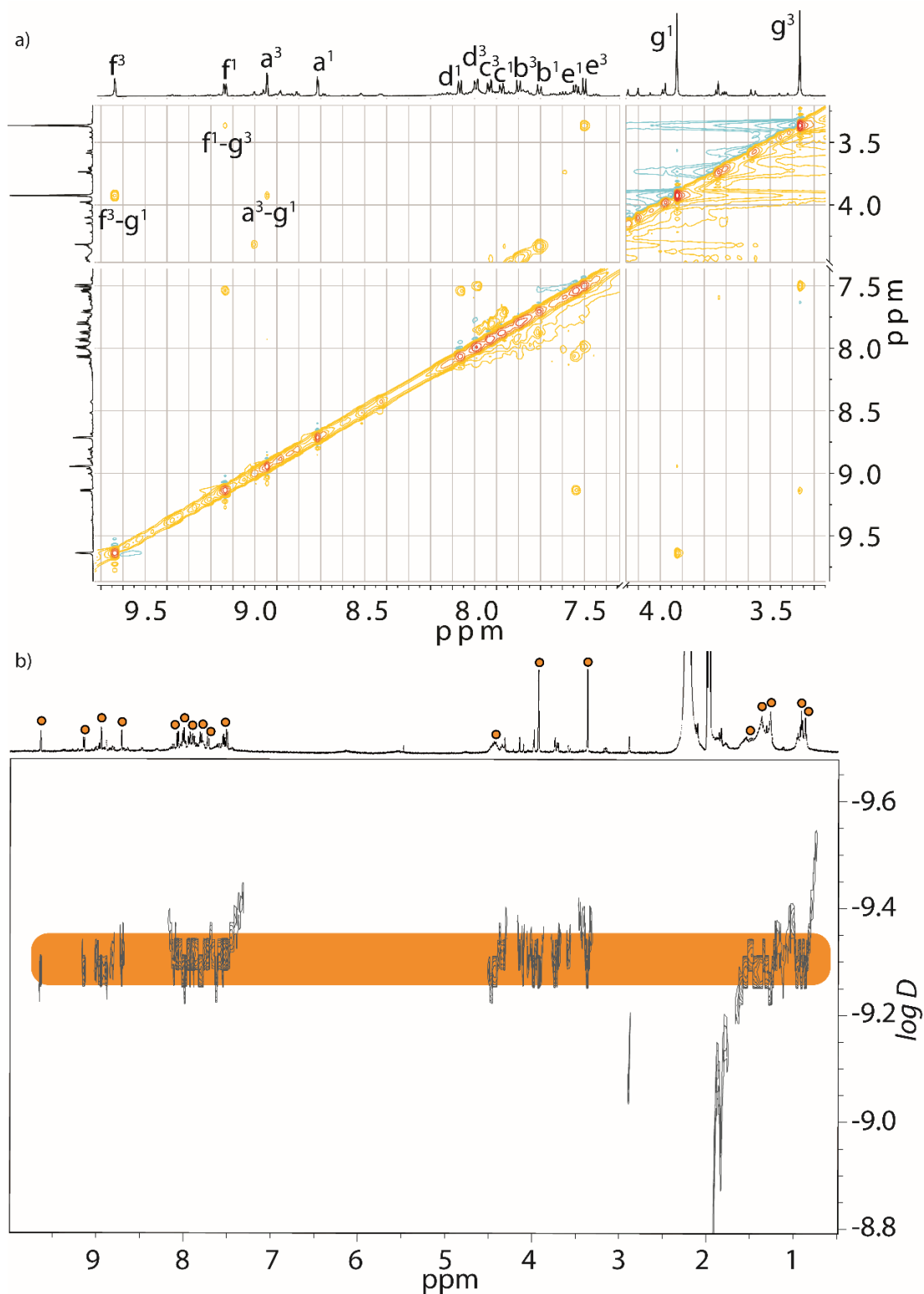
Figure 3.11 a) ^{1}H–^{1}H NOESY spectrum of heteroleptic cage $[Pd_2(\mathbf{AL^1})_2(\mathbf{AL^3})_2]^{4+}$ in CD$_3$CN; b) ^{1}H–^{1}H DOSY spectrum of the heteroleptic cage $[Pd_2(\mathbf{AL^1})_2(\mathbf{AL^3})_2]^{4+}$ (500 MHz/CD$_3$CN, 298K, logD = logarithm of diffusion coefficient D); for ^{1}H NMR signal assignment: see Figure 3.5.
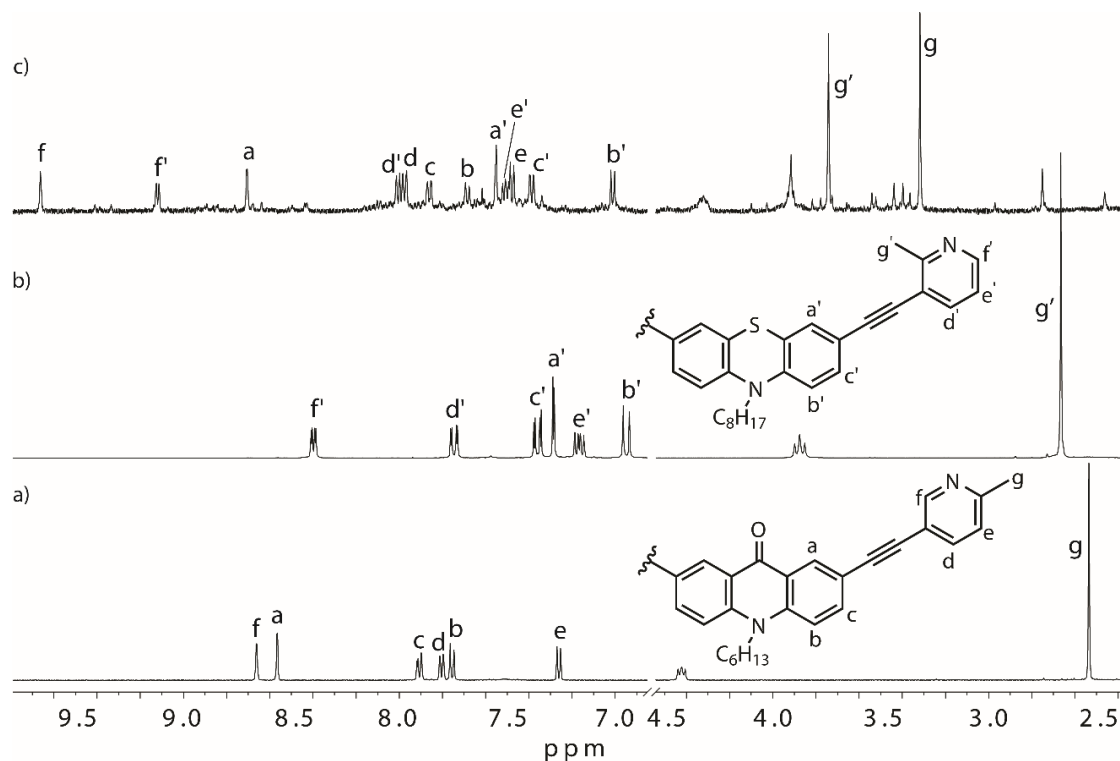
Figure 3.12 ^{1}H NMR spectra (600 MHz, CD$_3$CN, 293 K) of a) ligand **AL^2**, b) ligand **PL^2**, c) heteroleptic cage [Pd$_2$(**AL^2**)$_2$(**PL^2**)$_2$]$^{4+}$.
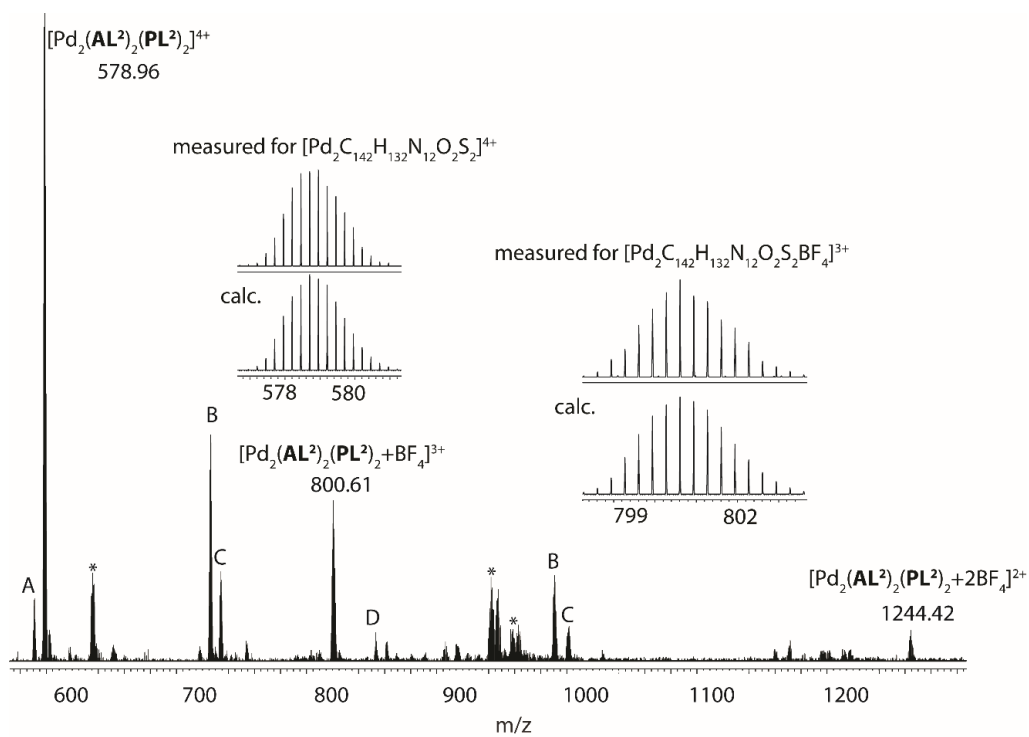
Figure 3.13 ESI-MS spectrum of heteroleptic cage of [Pd$_2$(**AL^2**)$_2$(**PL^2**)$_2$+nBF$_4$]$^{(4-n)+}$, n = 0−2, (A = [Pd$_2$(**AL^2**)$_3$(**PL^2**)$_1$]$^{4+}$, B = [Pd$_2$(**AL^2**)$_3$(**PL^2**)$_2$+mBF$_4$]$^{(4-m)+}$, C = [Pd$_2$(**AL^2**)$_2$(**PL^2**)$_3$+mBF$_4$]$^{(4-m)+}$, D = [Pd$_2$(**AL^2**)$_4$(**PL^2**)$_2$]$^{4+}$, m = 0−1, * = adducts with impurities).
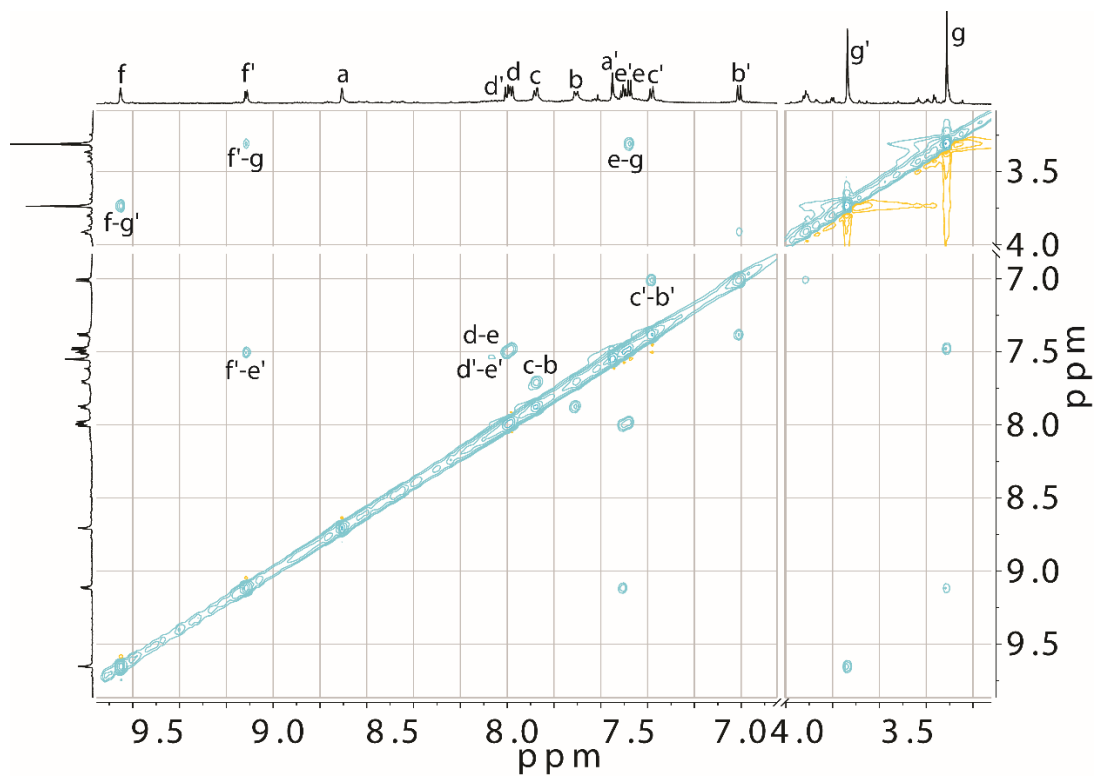
Figure 3.14 ^{1}H–^{1}H NOESY spectrum of the heteroleptic cage $[Pd_2(\mathbf{AL^2})_2(\mathbf{PL^2})_2]^{4+}$ in CD_3CN (only showing aromatic region); ^{1}H NMR signal assignment: see Figure 3.12.
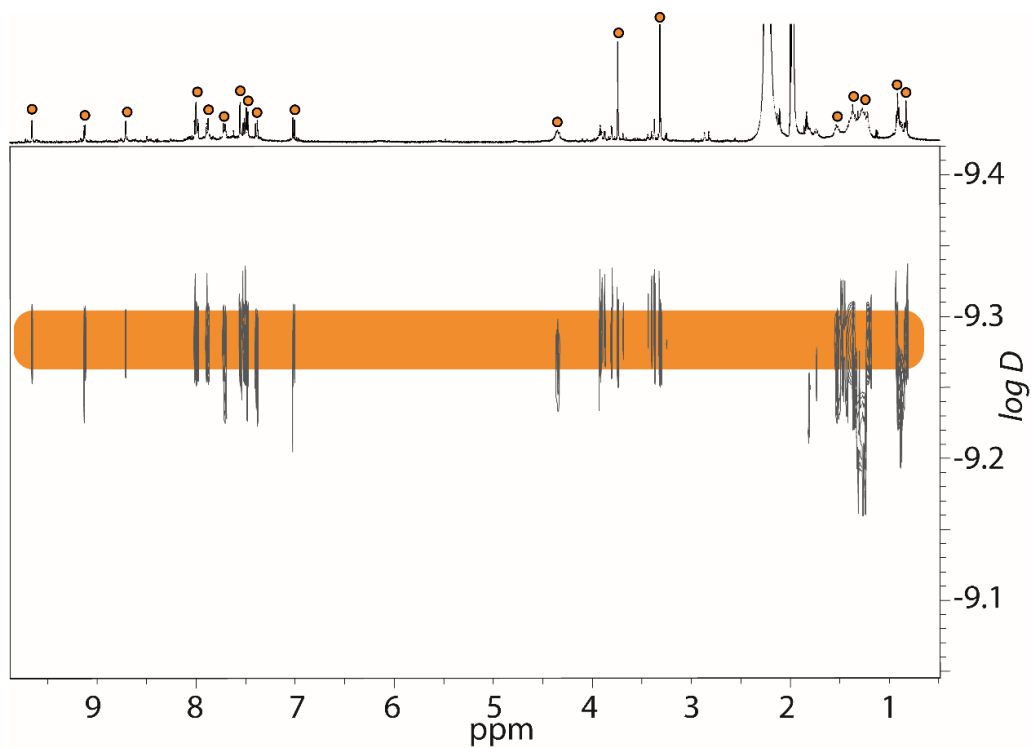
Figure 3.15 ^{1}H–^{1}H DOSY spectrum of the heteroleptic cage $[Pd_2(\mathbf{AL^2})_2(\mathbf{PL^2})_2]^{4+}$ (500 MHz/CD_3CN, 298K, logD = logarithm of diffusion coefficient D).
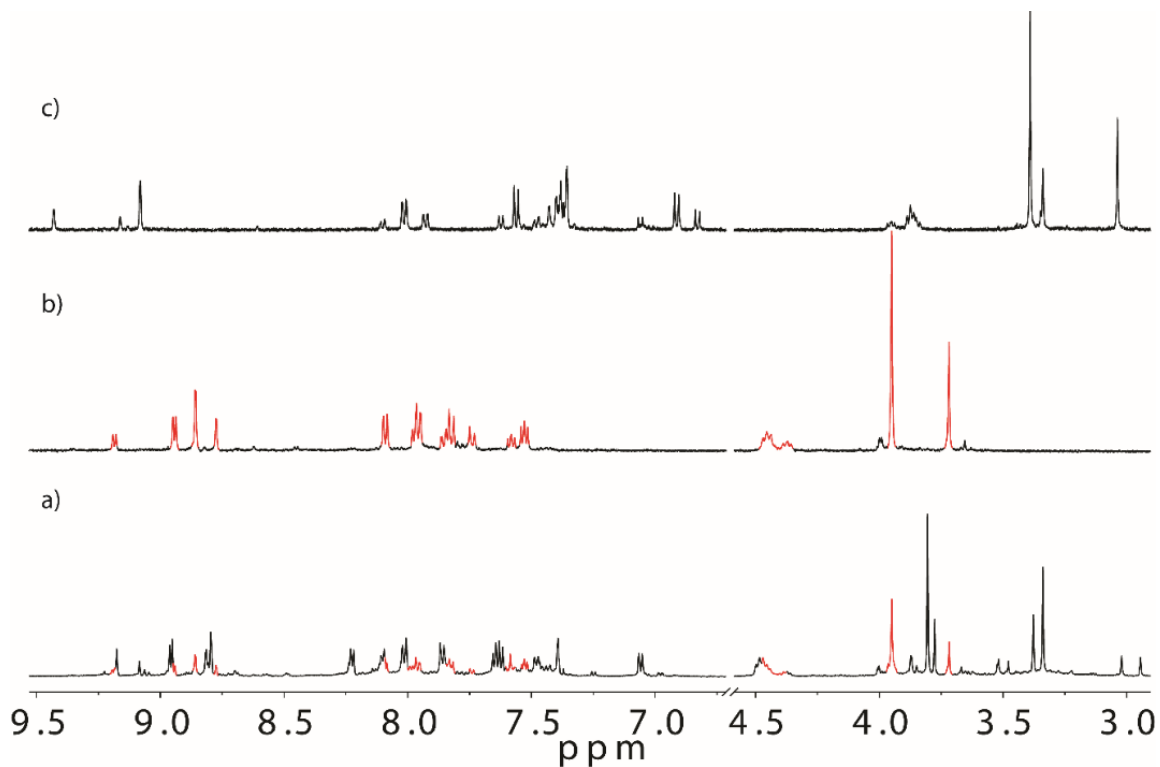
Figure 3.16 Comparison of ^{1}H NMR spectra in CD_3CN of a) assembly from $\mathbf{AL^1}$, $\mathbf{PL^1}$ and Pd^{II}; b) bowl-shaped cage $[Pd_2(\mathbf{AL^1})_3]^{4+}$ and c) mixture of ring $[Pd_2(\mathbf{PL^1})_2]^{4+}$ and bowl-shaped cage $[Pd_2(\mathbf{PL^1})_3]^{4+}$ (298K, 600MHz).
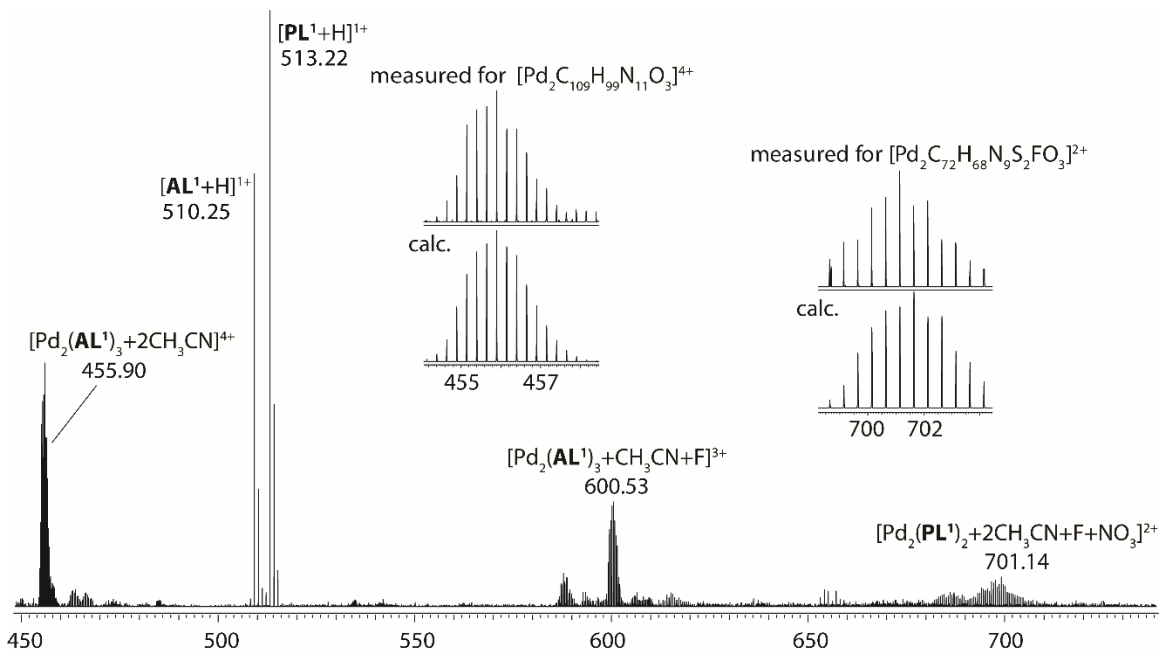
Figure 3.17 ESI-MS spectrum of assembly from $\mathbf{AL^1}$, $\mathbf{PL^1}$ and Pd^{II} cations.
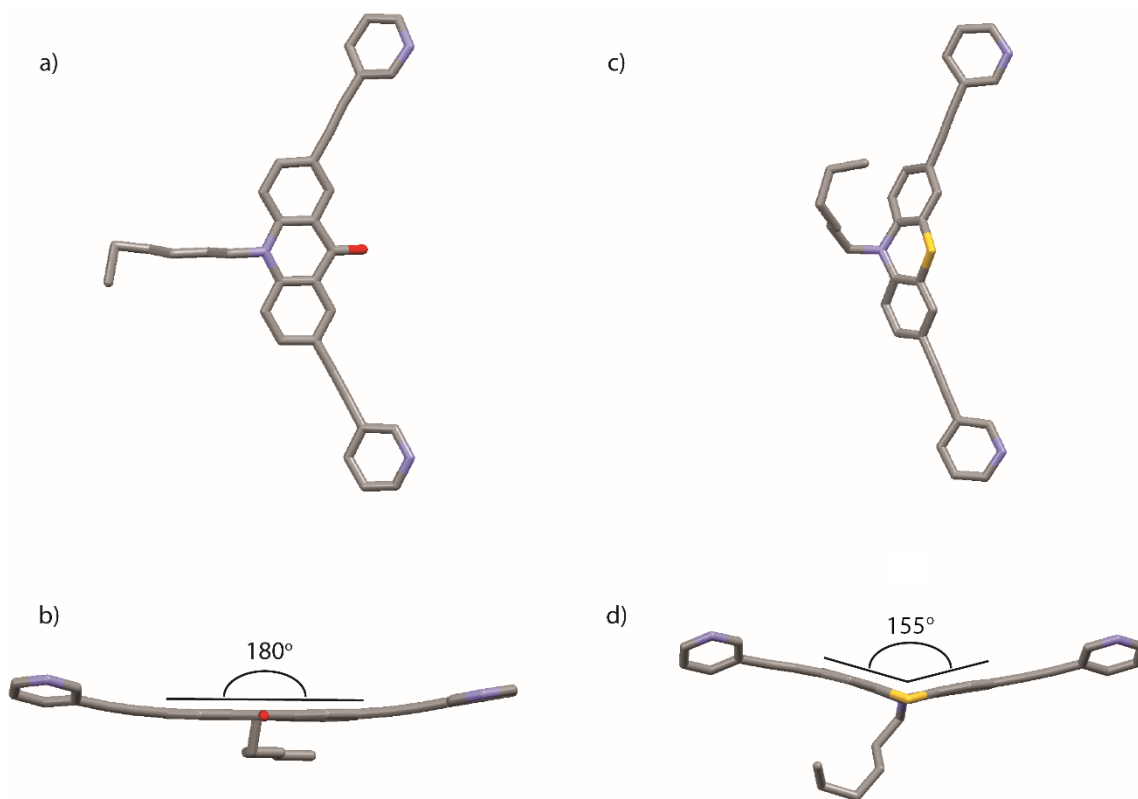
Figure 3.18 Structure of acridone backbone a) front view and b) side view;[18c] and phenothiazine backbone c) front view and d) side view derived from their corresponding cage crystal structures.[24] Color code: grey, C; purple, N; red, O; yellow, S; H omitted for clarity.

3.4 Conclusion

In conclusion, a controlled arrangement of different ligands around the metal centers has been realized when steric constrains were introduced into a heteroleptic coordination environment.

As reported in literature, entropy usually would thwart the self-assembly in multi-components system leading to non-selectively statistical mixtures of products or narcissistic self-sorting. Therefore, approaches to controlling the social self-sorting of different ligands are desperately pursued by supramolecular chemists. In this chapter, a novel route to obtain thermodynamic *trans*-[Pd$_2$L$_2$L′$_2$]$^{4+}$ cages based on picoline functionalized ligands has been described. More inspiringly, two different backbones, acridone and phenothiazine, were successfully combined in one single assembly, thus showcasing that two electronically distinct moieties can be bound together within one controlled conformation.

The heteroleptic complexation presented here could pave the way for accessing new topological architectures and for modifying the electronic and optical properties of the [Pd$_2$L$_4$] framework. A variety of functionalities can be introduced into the target molecule via employing different functionalized precursors in the multicomponent self-assembly process. Furthermore, the discrete void areas in these diverse self-assembly

structures also can be quite helpful in endowing functions for targeted applications such as catalysis, substrate recognition and photoelectrical conversion in the host guest system.

3.5 Experimental section

Unless otherwise stated, all chemicals were obtained from commercial sources and used as received. 3-ethynyl-2,6-dimethylpyridine (**P1**), 3-ethynyl-2-methylpyridine (**P2**) and 5-ethynyl-2-methylpyridine (**P3**) were prepared according to literature procedures.[25] All ligands were synthesized via Sonogashira cross coupling reaction described as follows. Electrospray ionization (ESI) mass spectra were recorded on a Bruker Apex IV ESI-FTICR Mass Spectrometer with a dual electrospray ionization source. GPC purification of all ligands was performed on a 3AI LC-9210 II NEXT.

3.5.1   Ligand synthesis
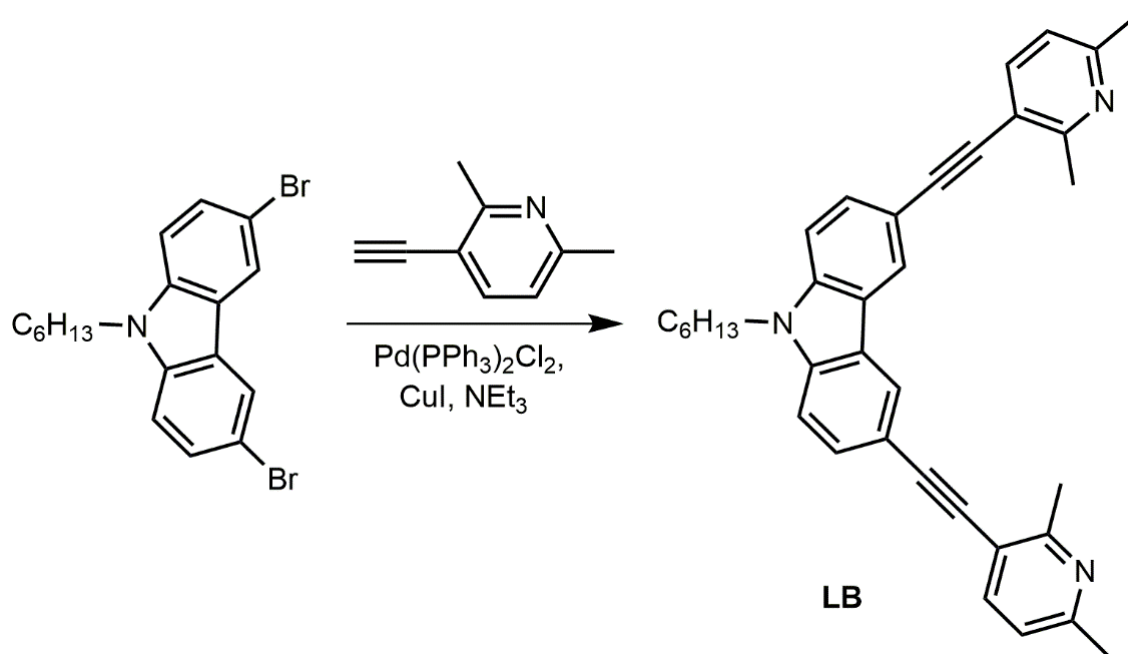
3,6-bis[(2,6-dimethylpyridin-3-yl)ethynyl]-9-hexyl-9H-carbazole (LB) was synthesized in the same way as **L**[1] in the Chapter 2 using **P1** instead of 3-ethinylpyridine. Yield: 68.4%.
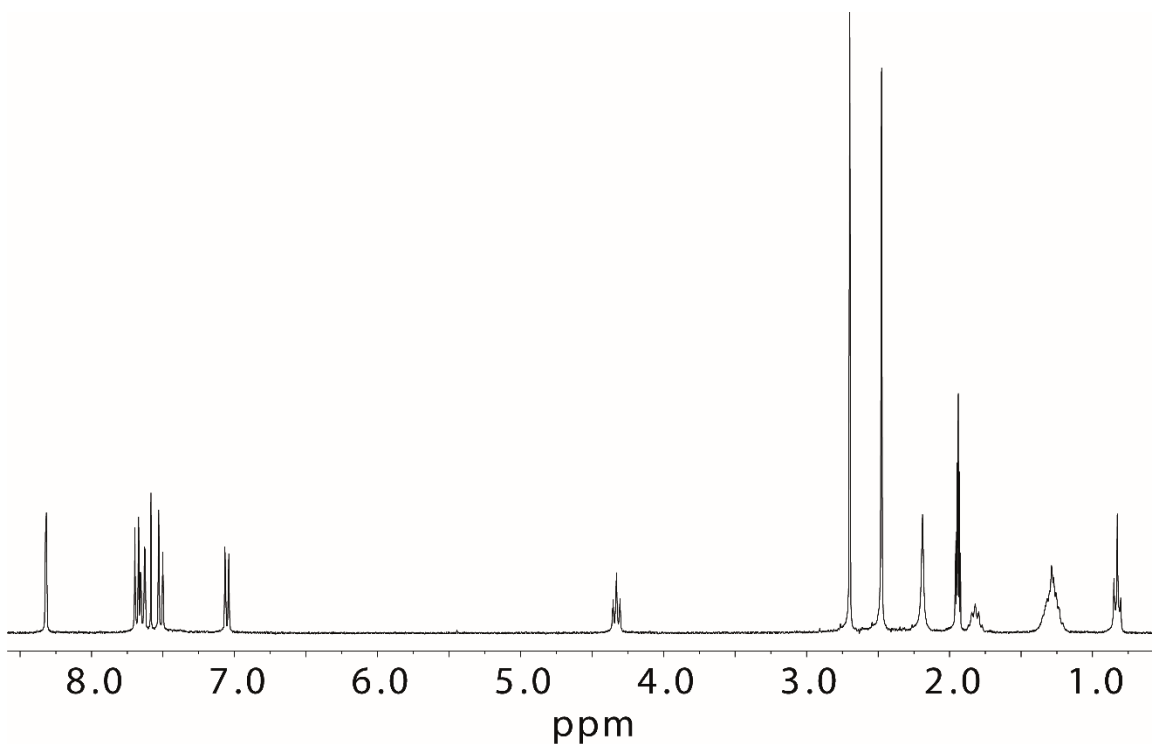
^{1}H NMR (300 MHz, CD$_3$CN) δ [ppm] = 8.32 (d, J = 1.5 Hz, 2H), 7.74 – 7.58 (m, 4H), 7.51 (d, J = 8.6 Hz, 2H), 7.06 (d, J = 7.9 Hz, 2H), 4.32 (t, J = 7.2 Hz, 2H), 2.74 (s, 6H), 2.53 (d, J = 8.3 Hz, 6H), 1.88 – 1.77 (m, 2H), 1.30 (p, J = 9.4, 8.8 Hz, 6H), 0.85 (d, J = 6.7 Hz, 3H).
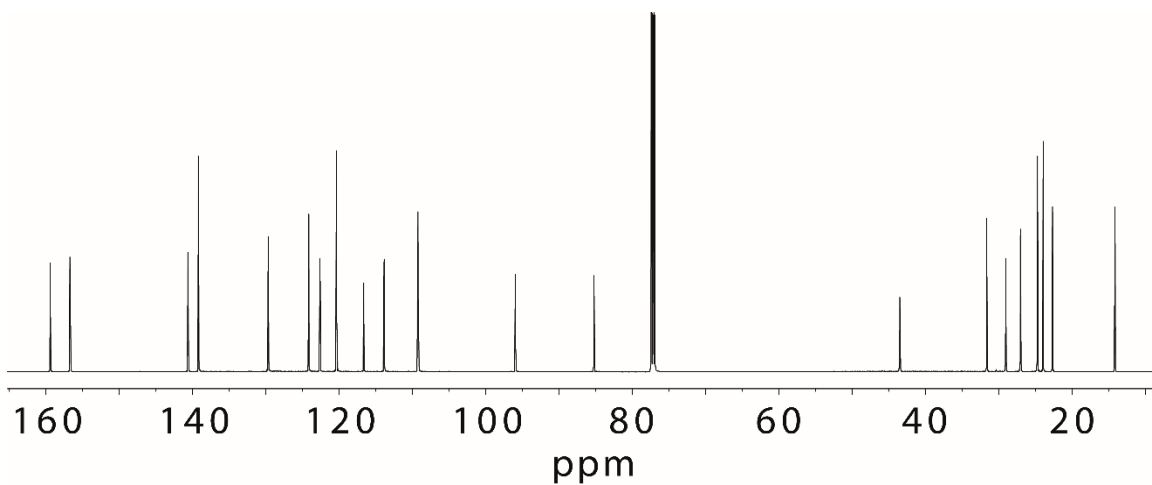
^{13}C NMR (150 MHz, CDCl$_3$) δ [ppm] = 159.43, 156.72, 140.63, 139.19, 129.69, 124.13, 122.59, 120.34, 116.64, 113.85, 109.22, 95.93, 85.22, 43.48, 31.63, 29.04, 27.02, 24.71, 23.91, 22.64, 14.12.

ESI-FTICR-HRMS calculated for C$_{36}$H$_{36}$N$_3$ [M+H]$^+$ m/z 510.2909, found m/z 510.2904.
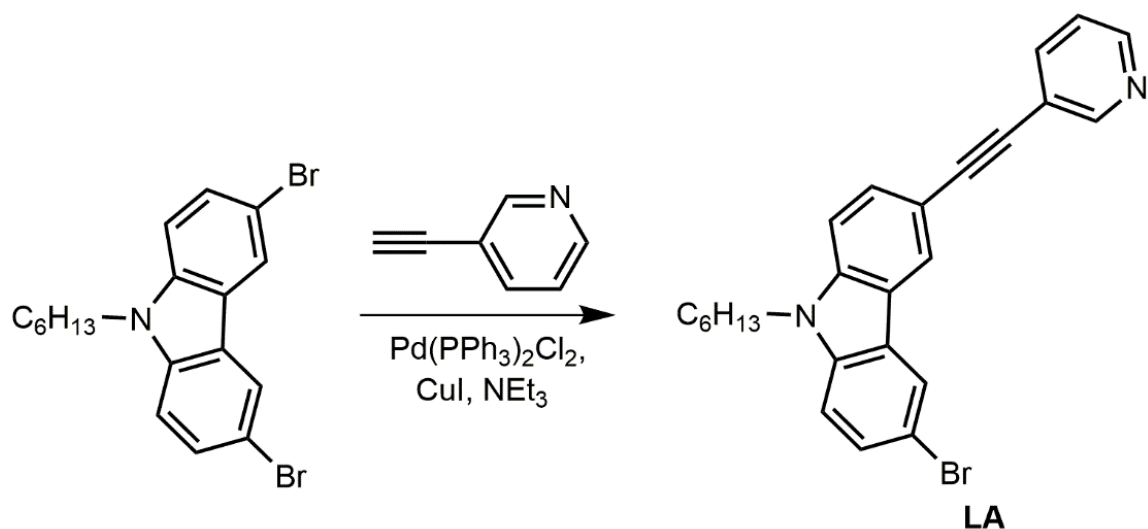
*1-[3-bromo-6-(pyridin-3-ylethynyl)-9H-carbazol-9-yl]hexan-1-one (**LA**)* was synthesized in the same way as **L^1** in the Chapter 2, only reducing 3-ethinylpyridine from 3.5 mmol to 1.8 mmol (318.9 mg, 0.7 mmol, 37.7%).
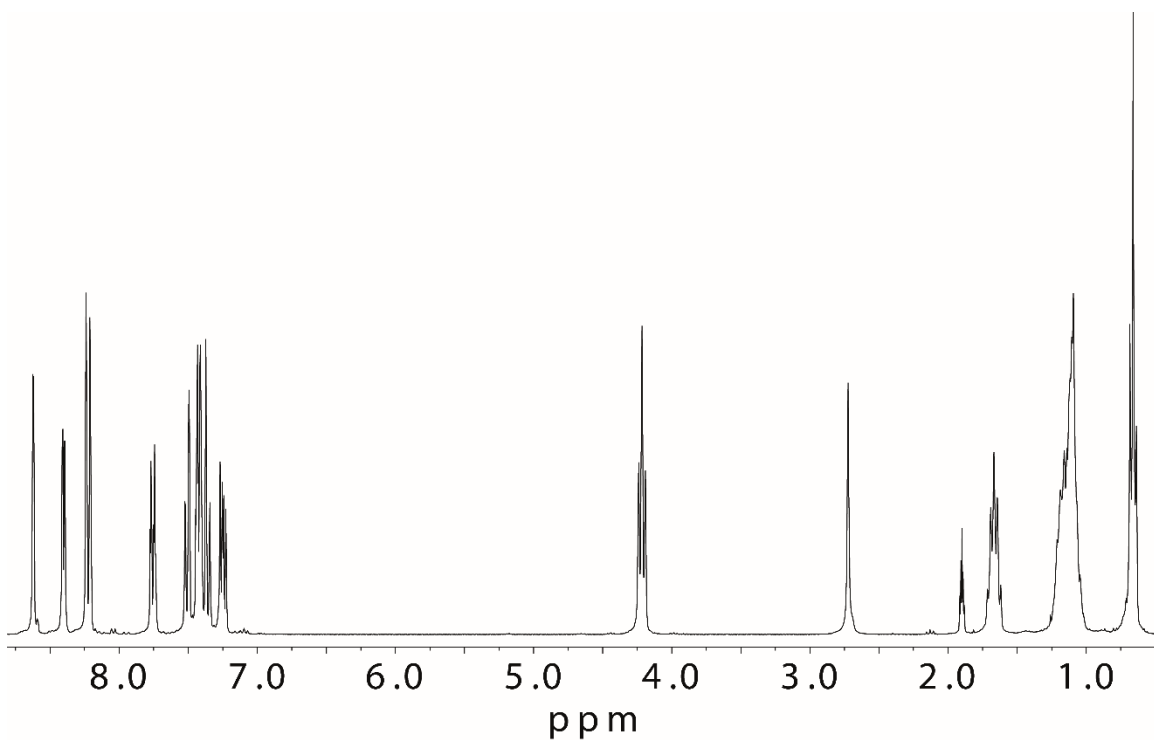
^{1}H NMR (300 MHz, Acetone-d_6) δ [ppm] = 8.62 (dd, J = 2.3, 0.9 Hz, 1H), 8.40 (dd, J = 4.8, 1.7 Hz, 1H), 8.22 (dd, J = 8.7, 1.7 Hz, 2H), 7.76 (dt, J = 7.9, 2.0 Hz, 1H), 7.51 (dd, J = 8.5, 1.6 Hz, 1H), 7.48 – 7.31 (m, 2H), 7.35 (d, J = 8.0 Hz, 1H), 7.25 (ddd, J = 8.0, 4.8, 0.8 Hz, 1H), 4.22 (t, J = 7.2 Hz, 2H), 1.72 – 1.61 (m, 2H), 1.17 – 1.09 (m, 6H), 0.67 (t, J = 7.0 Hz, 3H).
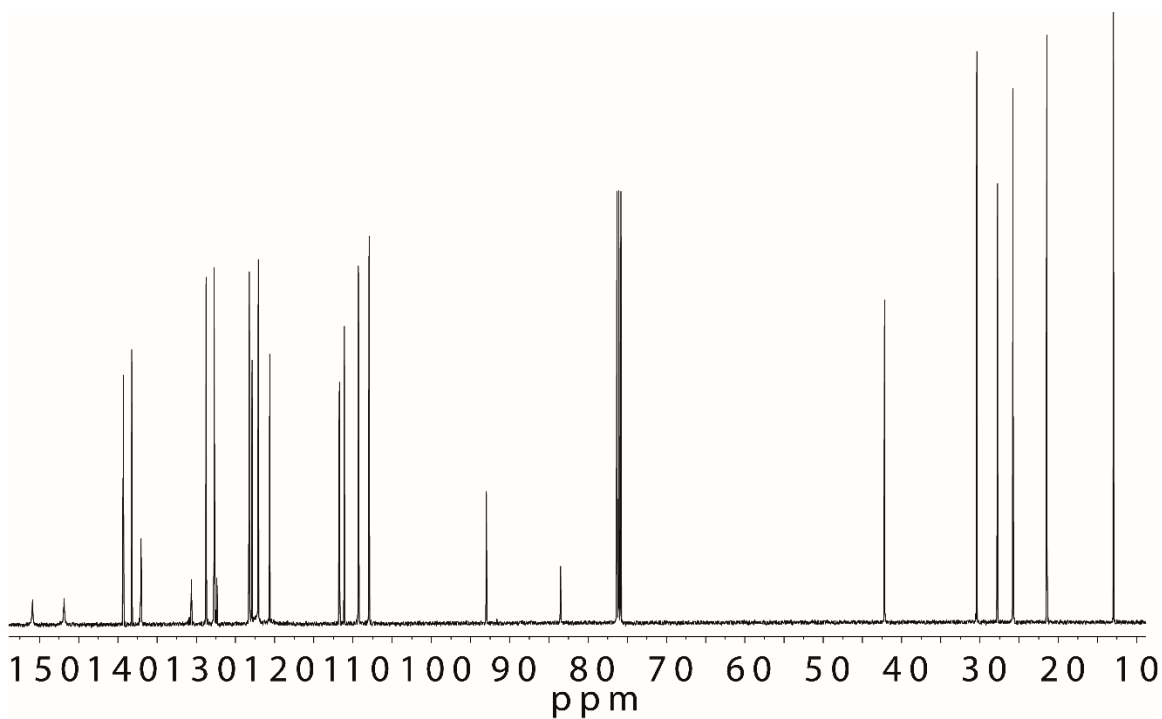
^{13}C NMR (100 MHz, CDCl$_3$) δ [ppm] = 151.97, 147.96, 140.24, 139.15, 138.03, 129.69, 128.65, 124.13, 123.80, 123.00, 122.93, 121.56, 120.92, 112.72, 112.05, 110.24, 108.88, 93.96, 84.45, 43.07, 31.36, 28.70, 26.74, 22.44, 13.93.

ESI-FTICR-HRMS calculated for C$_{25}$H$_{24}$N$_2$Br [M+H]$^+$ m/z 431.1136, found m/z 431.1123.
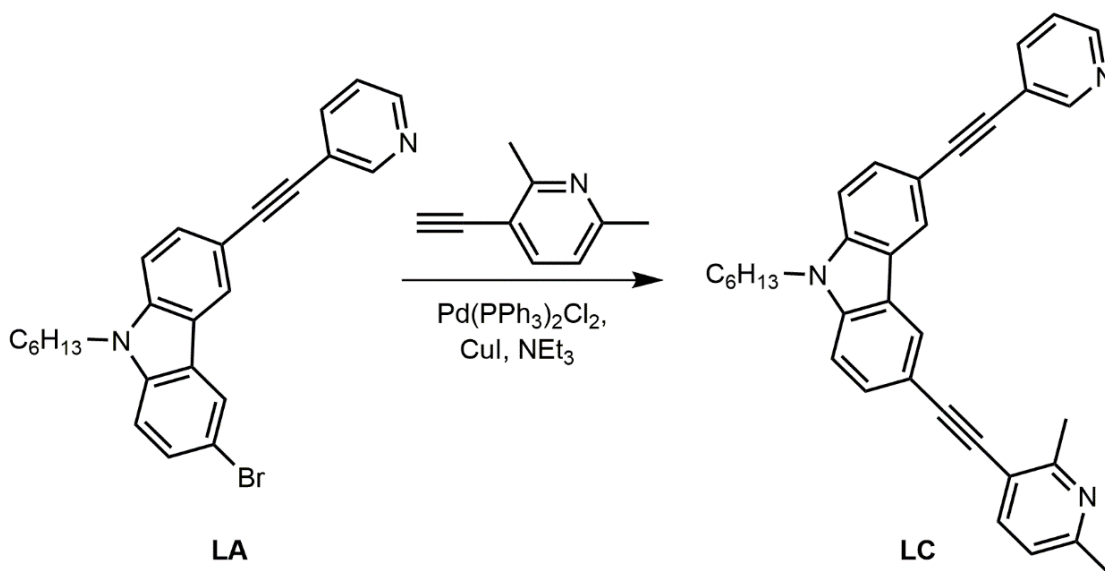
*3-[(2,6-dimethylpyridin-3-yl)ethynyl]-9-hexyl-6-(pyridin-3-ylethynyl)-9H-carbazole (**LC**) was synthesized via Sonogashira coupling reaction same as **L^1** but using **LA** and **P1** as the starting materials, yield: 80.7%.*
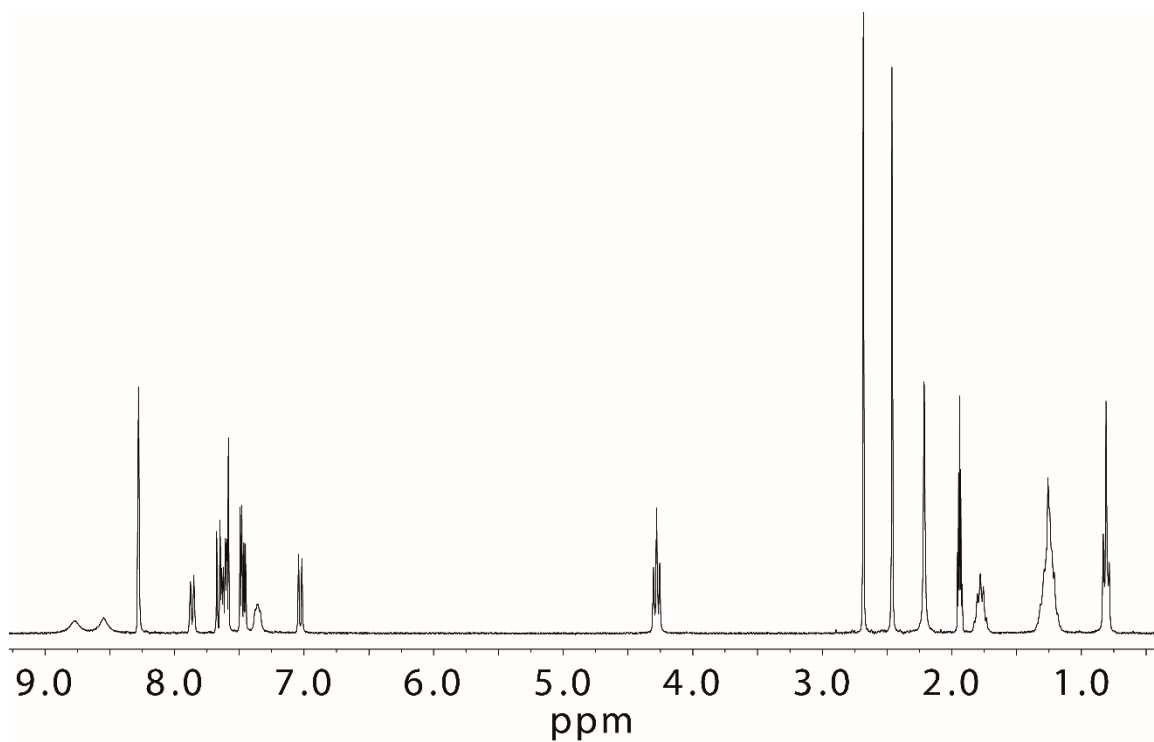
^{1}H NMR (300 MHz, CD$_3$CN) δ [ppm] = 8.77 (s, 1H), 8.55 (s, 1H), 8.28 (dq, J = 1.5, 0.8 Hz, 2H), 7.86 (d, J = 7.9 Hz, 1H), 7.66 (d, J = 7.9 Hz, 1H), 7.63 (ddd, J = 3.8, 1.6, 0.8 Hz, 1H), 7.62 – 7.59 (m, 1H), 7.49 (dd, J = 3.7, 0.8 Hz, 1H), 7.46 (dt, J = 3.7, 0.8 Hz, 1H), 7.35 (d, J = 7.9 Hz, 1H), 7.03 (d, J = 7.9 Hz, 1H), 4.28 (t, J = 7.2 Hz, 2H), 2.68 (s, 3H), 2.46 (s, 3H), 1.78 (t, J = 7.2 Hz, 2H), 1.25 – 1.23 (m, 6H), 0.86 – 0.75 (m, 3H).
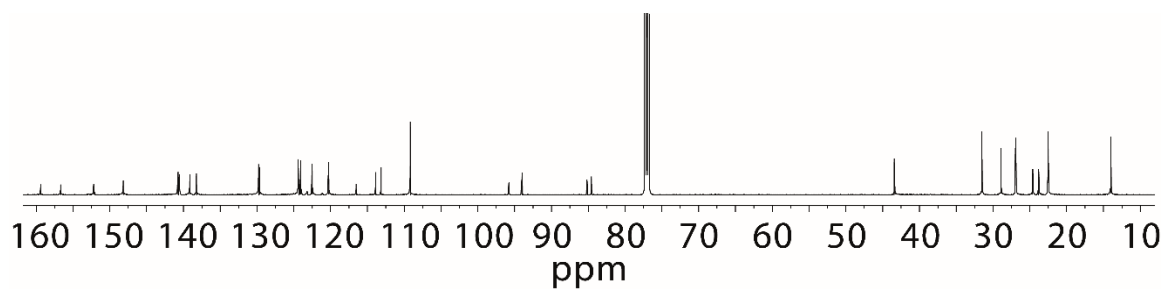
^{13}C NMR (150 MHz, CDCl$_3$) δ [ppm] = 159.37, 156.66, 152.19, 148.17, 140.73, 140.58, 139.13, 138.24, 129.79, 129.66, 124.42, 124.06, 122.51, 120.26, 116.53, 113.85, 113.14, 109.17, 95.78, 93.96, 85.16, 84.58, 43.43, 31.53, 28.95, 26.93, 24.62, 23.81, 22.55, 14.01.

ESI-FTICR-HRMS calculated for C$_{34}$H$_{32}$N$_3$ [M+H]$^+$ m/z 482.2596, found m/z 482.2583.
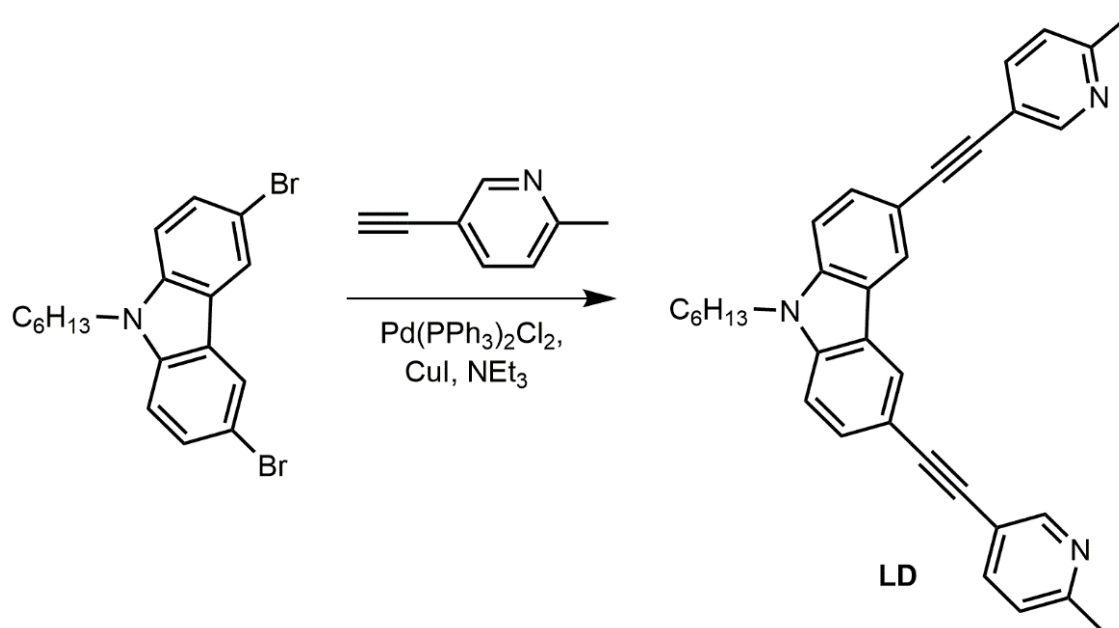
9-hexyl-3,6-bis[(6-methylpyridin-3-yl)ethynyl]-9H-carbazole (LD) was synthesized was synthesized in the same way as **L¹** in the Chapter 2 using **P2** instead of 3-ethinylpyridine. Yield: 72.3%.
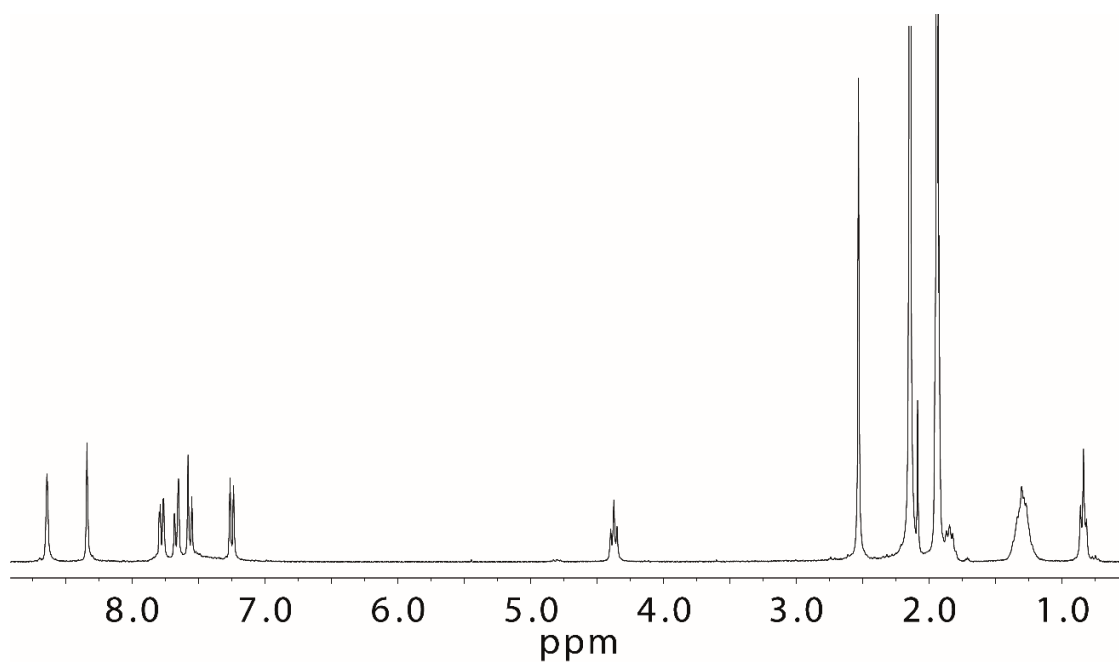
^{1}H NMR (300 MHz, CD₃CN) δ [ppm] = 8.64 (s, 2H), 8.34 (s, 2H), 7.78 (dd, J = 8.0, 2.2 Hz, 2H), 7.67 (dd, J = 8.5, 1.6 Hz, 2H), 7.57 (d, J = 8.6 Hz, 2H), 7.25 (d, J = 8.1 Hz, 2H), 4.37 (t, J = 7.2 Hz, 2H), 2.53 (s, 6H), 1.91– 1.81 (m, 2H), 1.41– 1.23 (m, 6H), 0.88 – 0.78 (t, J = 6.8 Hz, 3H).
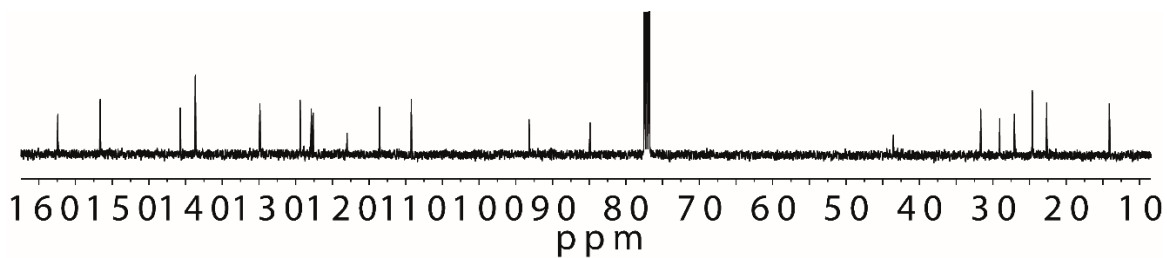
^{13}C NMR (100 MHz, CDCl$_3$) δ [ppm] = 157.41, 151.62, 140.74, 138.67, 129.87, 124.39, 122.86, 122.61, 117.99, 113.55, 109.25, 93.20, 84.87, 43.54, 31.63, 29.06, 27.05, 24.61, 22.66, 14.11.

ESI-FTICR-HRMS calculated for C$_{34}$H$_{32}$N$_3$ [M+H]$^+$ m/z 482.2596, found m/z 482.2573.
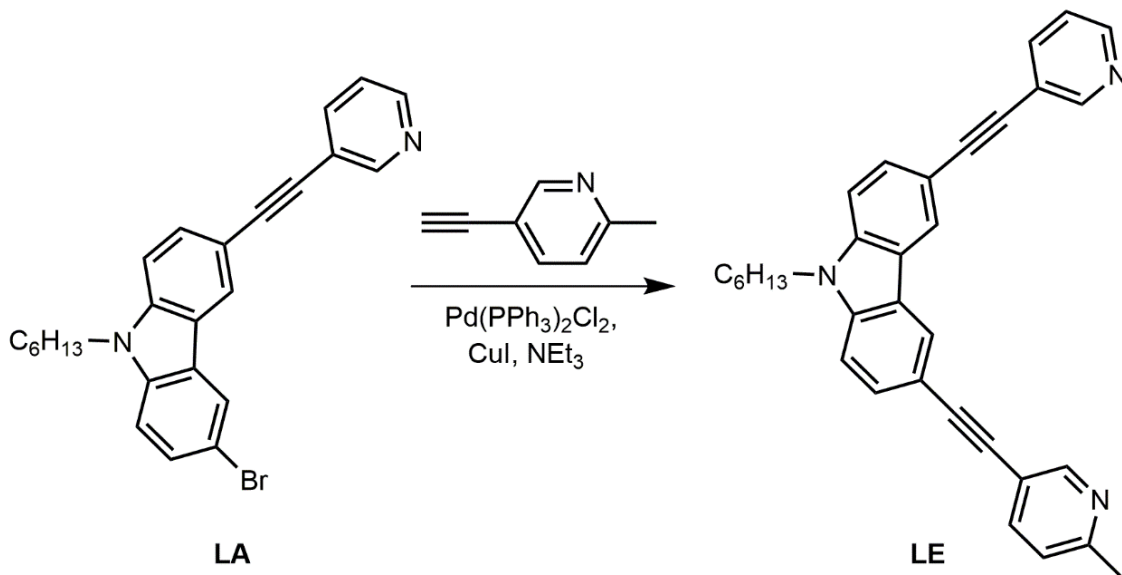
*9-hexyl-3-[(6-methylpyridin-3-yl)ethynyl]-6-(pyridin-3-ylethynyl)-9H-carbazole (**LE**)* was synthesized via Sonogashira coupling reaction same as **L^1** but using **LA** and **P2** as the starting materials, yield: 62.7%.
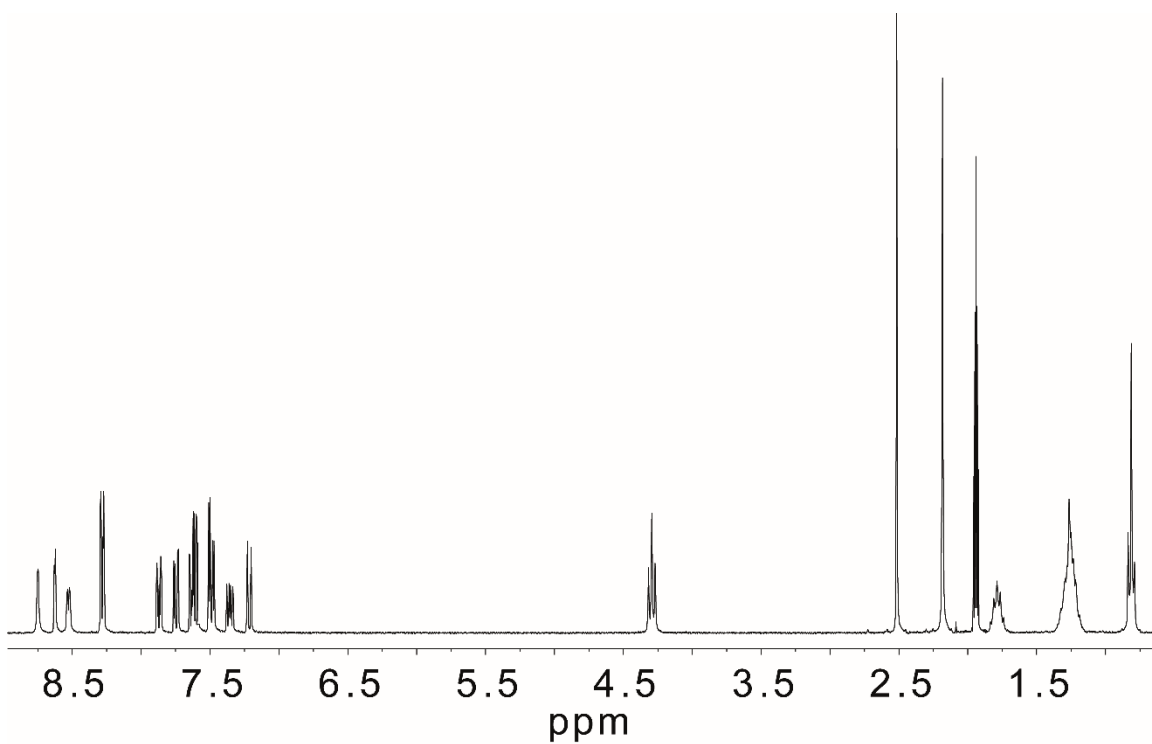
^{1}H NMR (300 MHz, CD$_3$CN) δ [ppm] = 8.77 (d, J = 2.1 Hz, 1H), 8.65 (dd, J = 2.1, 0.8 Hz, 1H), 8.55 (dd, J = 4.9, 1.6 Hz, 1H), 8.31 (ddd, J = 5.9, 1.6, 0.7 Hz, 2H), 7.89 (dddd, J = 8.0, 2.2, 1.7, 0.5 Hz, 1H), 7.77 (dd, J = 8.0, 2.3 Hz, 1H), 7.65 (ddd, J = 8.5, 5.7, 1.6 Hz, 2H), 7.54 – 7.52 (m, 1H), 7.50 (dd, J = 2.8, 0.7 Hz, 1H), 7.38 (ddd, J = 7.9, 4.9, 0.9 Hz, 1H), 7.24 (ddt, J = 8.0, 1.0, 0.5 Hz, 1H), 4.32 (t, J = 7.2 Hz, 2H), 2.54 (s, 3H), 1.86 – 1.76 (m, 2H), 1.37 – 1.20 (m, 6H), 0.89 – 0.77 (t, J = 7.1 Hz, 3H).
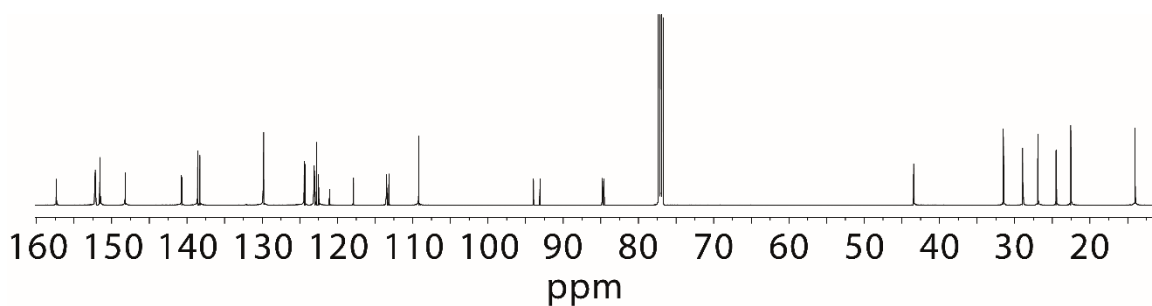
^{13}C NMR (150 MHz, CDCl$_3$) δ [ppm] = 157.31, 152.19, 151.51, 148.18, 140.72, 140.63, 138.57, 138.28, 129.80, 124.39, 124.29, 123.08, 122.77, 122.51, 122.47, 121.03, 117.85, 113.48, 113.16, 109.17, 93.96, 93.04, 84.79, 84.57, 43.43, 31.52, 28.95, 26.94, 24.51, 22.55, 14.01.

ESI-FTICR-HRMS calculated for C$_{33}$H$_{30}$N$_3$ [M+H]$^+$ m/z 468.2440, found m/z 468.2421.
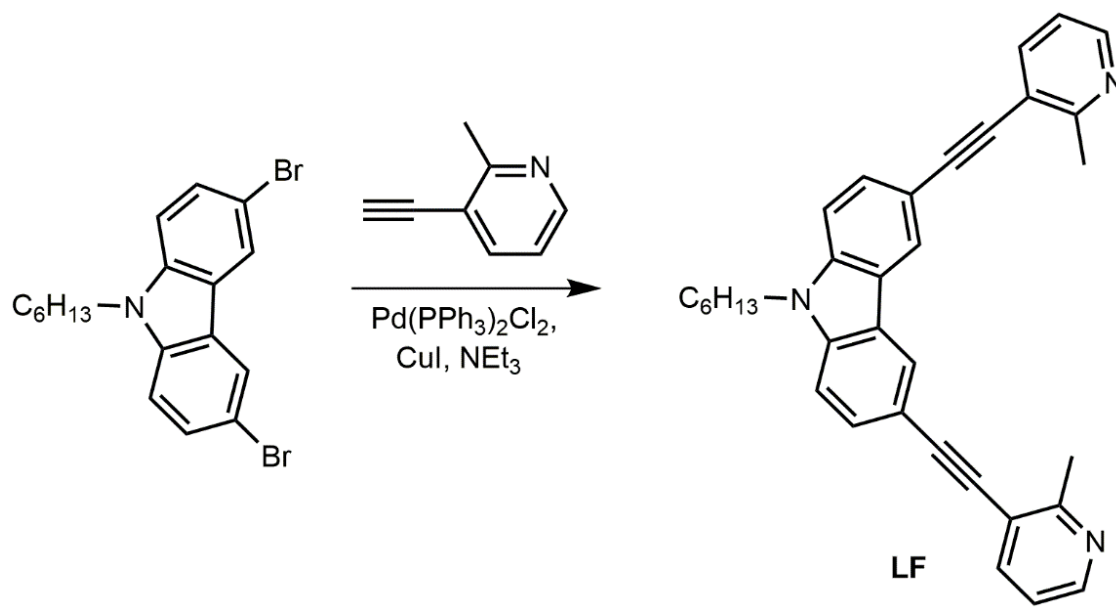
*9-hexyl-3,6-bis[(2-methylpyridin-3-yl)ethynyl]-9H-carbazole (**LF**)* was synthesized was synthesized in the same way as **L¹** in the Chapter 2 using **P3** instead of 3-ethinylpyridine. Yield: 37.0%.
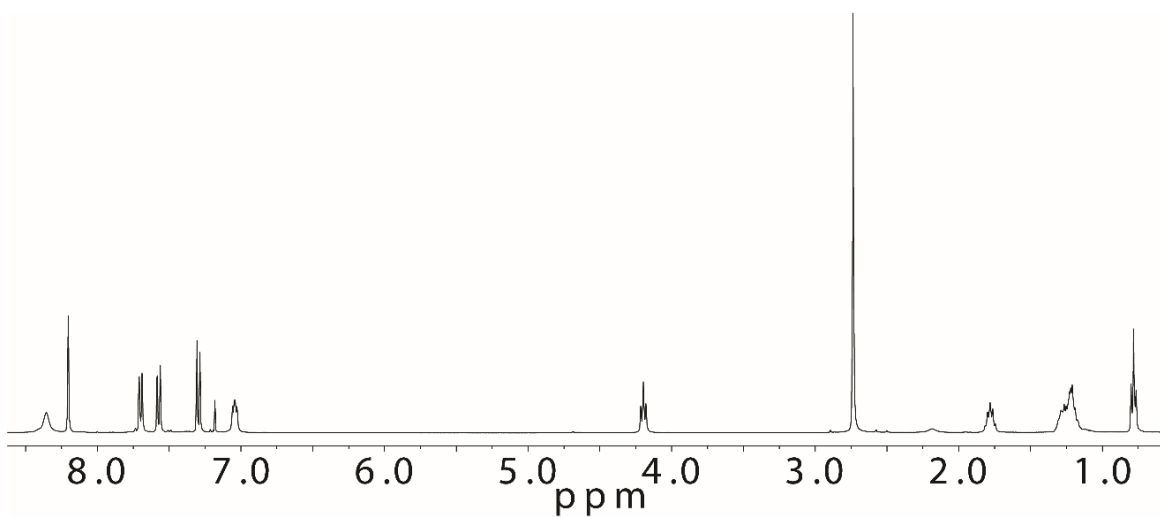
^{1}H NMR (400 MHz, CDCl₃) δ [ppm] = 8.36 (s, 2H), 8.20 (d, *J* = 1.5 Hz, 2H), 7.70 (dd, *J* = 7.8, 1.6 Hz, 2H), 7.57 (dd, *J* = 8.4, 1.6 Hz, 2H), 7.30 (d, *J* = 8.5 Hz, 2H), 7.04 (dd, *J* = 7.8, 4.8 Hz, 2H), 4.20 (t, *J* = 7.2 Hz, 2H), 2.74 (s, 6H), 1.84 – 1.75 (m, 2H), 1.32 – 1.16 (m, 6H), 0.78 (t, *J* = 6.9 Hz, 3H).
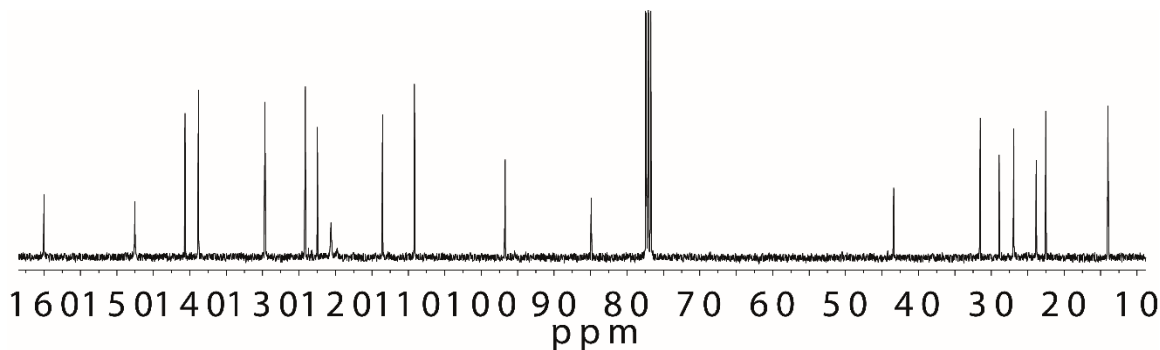
^{13}C NMR (100 MHz, CDCl$_3$) δ [ppm] = 160.01, 147.55, 140.66, 138.82, 129.69, 124.15, 122.50, 120.64, 113.56, 109.18, 96.73, 84.91, 77.27, 43.40, 31.52, 28.93, 26.91, 23.85, 22.53, 14.00.

ESI-FTICR-HRMS calculated for C$_{34}$H$_{32}$N$_3$ [M+H]$^+$ m/z 482.2596, found m/z 482.2575.

Synthesis of 10-hexyl-2,7-bis[(2-methylpyridin-3-yl)ethynyl]acridin-9(10H)-one (AL^1):
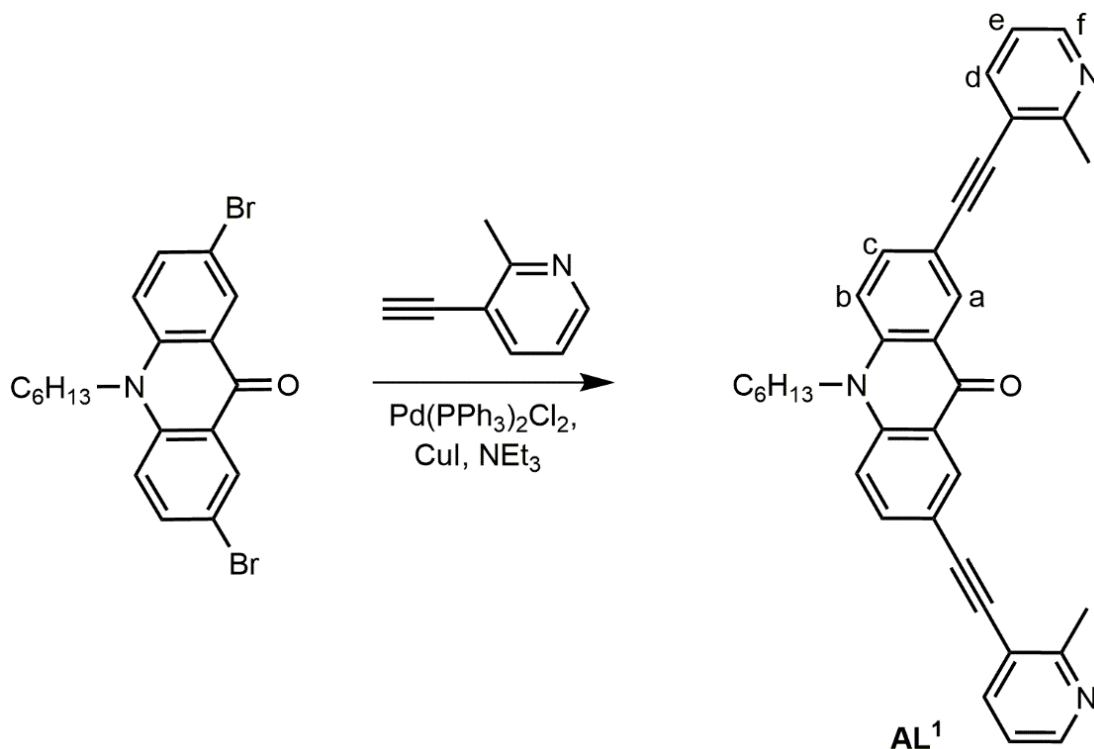
A mixture of 2,7-dibromo-10-hexylacridin-9(10*H*)-one[18c] (152.95 mg, 0.35 mmol), 3-ethynyl-2-methyl-pyridine (122.85 mg, 1.05 mmol), copper (I) iodide (7.60 mg, 0.04 mmol) and Pd(PPh$_3$)$_2$Cl$_2$ (14.04 mg, 0.02 mmol) in triethylamine (8 mL) was thoroughly degassed. The mixture was heated under nitrogen atmosphere at 70 °C for 24 h. The mixture was cooled to room temperature and the solvent was evaporated under reduced pressure. A saturated NH$_4$Cl-solution was added to the residue and the organic components were extracted with CH$_2$Cl$_2$. The organic layer was washed with water and brine, dried over MgSO$_4$, filtrated and evaporated

90

under reduced pressure. The crude residue was purified by flash chromatography on silica gel (*n*-hexane : ethylacetate = 1 : 3) and then by GPC to give **AL¹** as a yellow solid product (20.36 mg, 0.04 mmol, 11.0%).
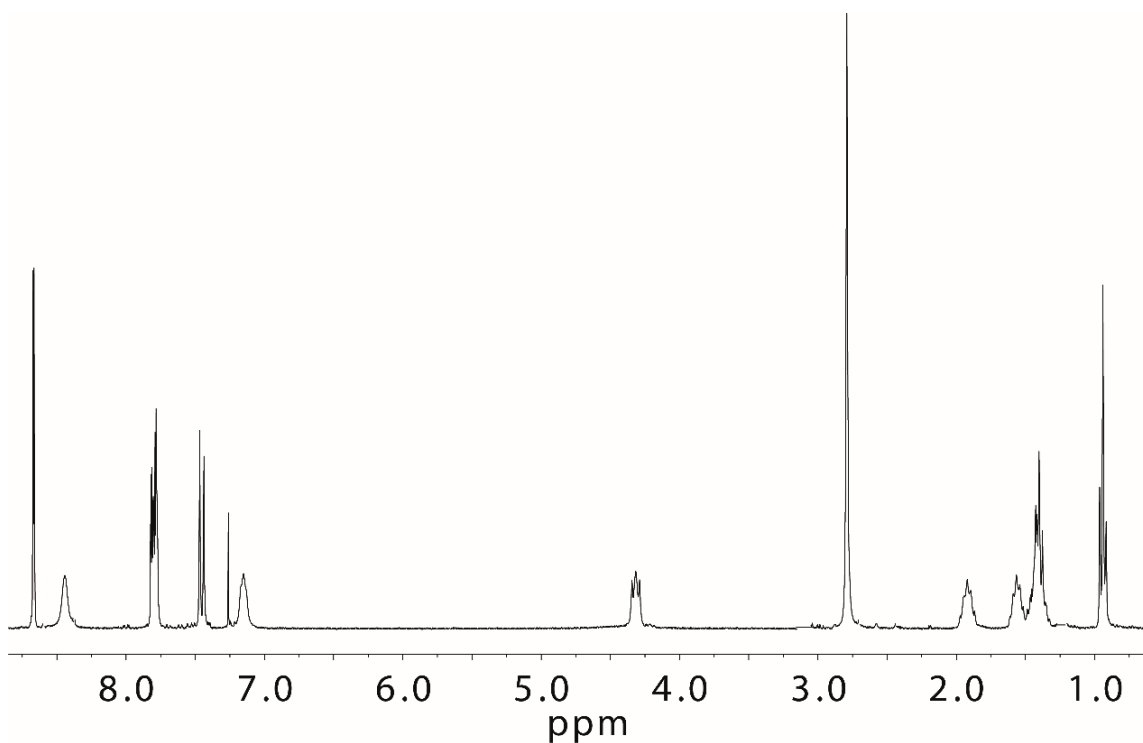

¹H NMR (300 MHz, CDCl₃) δ [ppm] = 8.67 (d, *J* = 2.1 Hz, H_a), 8.44 (s, H_f), 7.80 (dd, *J* = 8.9, 2.2 Hz, H_c), 7.79 (d, *J* = 7.4 Hz, H_d), 7.45 (d, *J* = 9.0 Hz, H_b), 7.15 (s, H_e), 4.32 (t, *J* = 7.9 Hz, 2H), 2.79 (s, 6H), 1.99 – 1.83 (m, 2H), 1.62 – 1.54 (m, 2H), 1.50 – 1.32 (m, 4H), 0.98 – 0.91 (t, *J* = 6.9 Hz 3H).
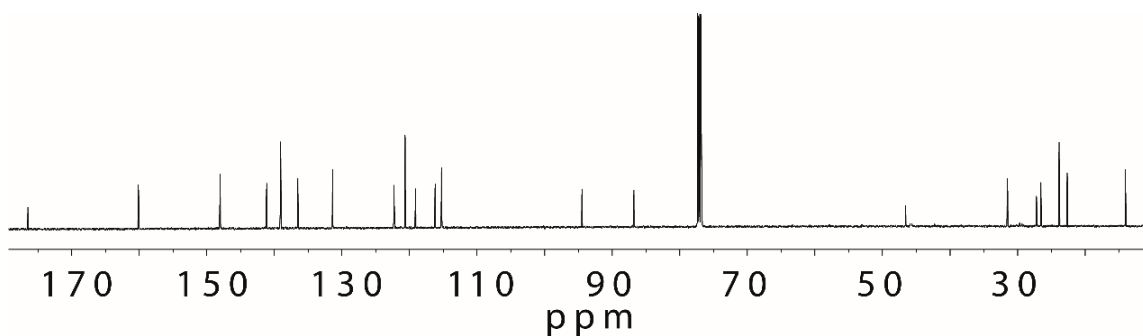
¹³C NMR (125 MHz, CDCl₃) δ [ppm] = 176.57, 160.21, 148.11, 141.23, 139.17, 136.61, 131.45, 122.39, 120.72, 119.18, 116.29, 115.35, 94.56, 86.87, 46.65, 31.56, 27.27, 26.63, 23.92, 22.73, 14.11.

ESI-FTICR-HRMS calculated for $C_{35}H_{32}N_3O$ [M+H]⁺ m/z 510.2545, found m/z 510.2541.

Synthesis of 10-hexyl-2,7-bis[(6-methylpyridin-3-yl)ethynyl]acridin-9(10H)-one (AL²):
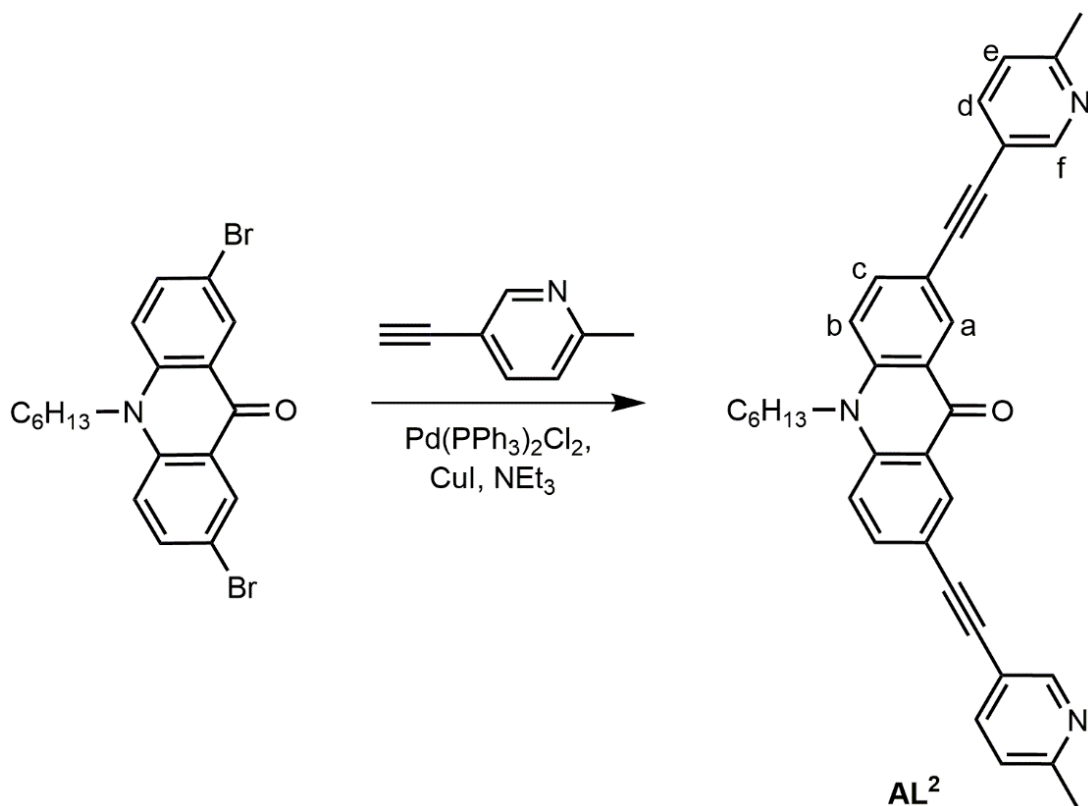
A mixture of 2,7-dibromo-10-hexylacridin-9(10*H*)-one (130.00 mg, 0.30 mmol), 5-ethynyl-2-methylpyridine (105.44 mg, 0.90 mmol), copper (I) iodide (5.71 mg, 0.03 mmol) and Pd(PPh$_3$)$_2$Cl$_2$ (14.04 mg, 0.02 mmol) in triethylamine (6 mL) was thoroughly degassed. The mixture was heated under nitrogen atmosphere at 70 °C for 24 h. The mixture was cooled to room temperature and the solvent was evaporated under reduced pressure. A saturated NH$_4$Cl-solution was added to the residue and the organic components were extracted with CH$_2$Cl$_2$. The organic layer was washed with water and brine, dried over MgSO$_4$, filtrated and evaporated under reduced pressure. The crude residue was purified by flash chromatography on silica gel (*n*-hexane : ethylacetate = 1 : 3) and then by GPC to give **AL²** as a yellow solid product (40.16 mg, 0.08 mmol, 26.3%).
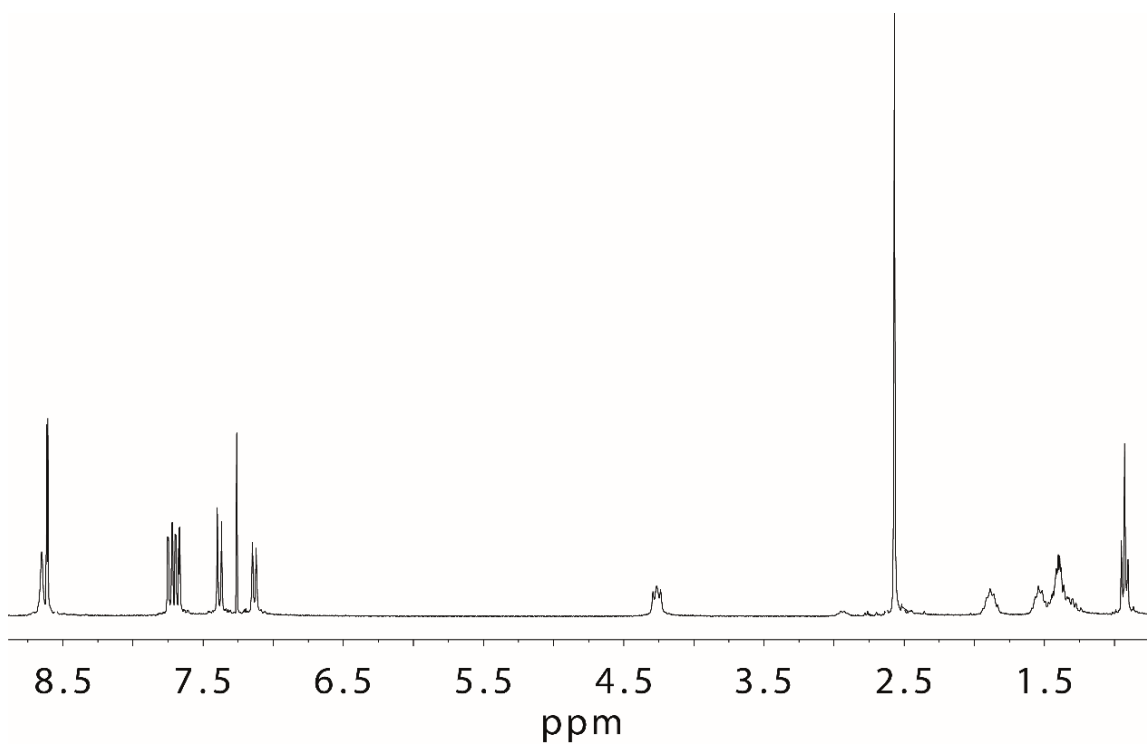
^{1}H NMR (300 MHz, CDCl$_3$) δ [ppm] = 8.65 (s, H$_f$), 8.61 (d, J = 2.1 Hz, H$_a$), 7.74 (dd, J = 9.0, 2.2 Hz, H$_c$), 7.68 (dd, J = 8.0, 2.2 Hz, H$_d$), 7.38 (d, J = 9.0 Hz, H$_b$), 7.13 (d, J = 8.0 Hz, H$_e$), 4.26 (t, J = 8.4 Hz, 2H), 2.57 (s, 6H), 1.92 – 1.84 (m, 2H), 1.56 – 1.50 (m, 2H), 1.34 – 1.42 (m, 4H), 0.96 – 0.90 (t, J = 7.0 Hz, 3H).
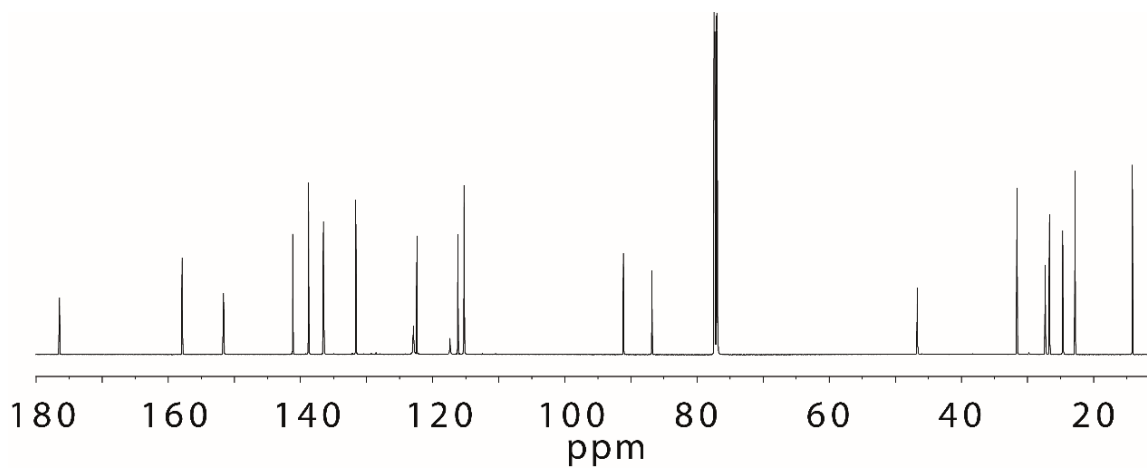
^{13}C NMR (150 MHz, CDCl$_3$) δ [ppm] = 176.47, 157.91, 151.65, 141.18, 138.79, 136.53, 131.64, 122.92, 122.39, 117.38, 116.21, 115.27, 91.14, 86.84, 46.66, 31.59, 27.30, 26.68, 24.67, 22.77, 14.13.

ESI-FTICR-HRMS calculated for C$_{35}$H$_{32}$N$_3$O [M+H]$^+$ m/z 510.2545, found m/z 510.2527.

Synthesis of 2,7-bis[(6-methylpyridin-3-yl)ethynyl]-10-octylacridin-9(10H)-one (AL³):
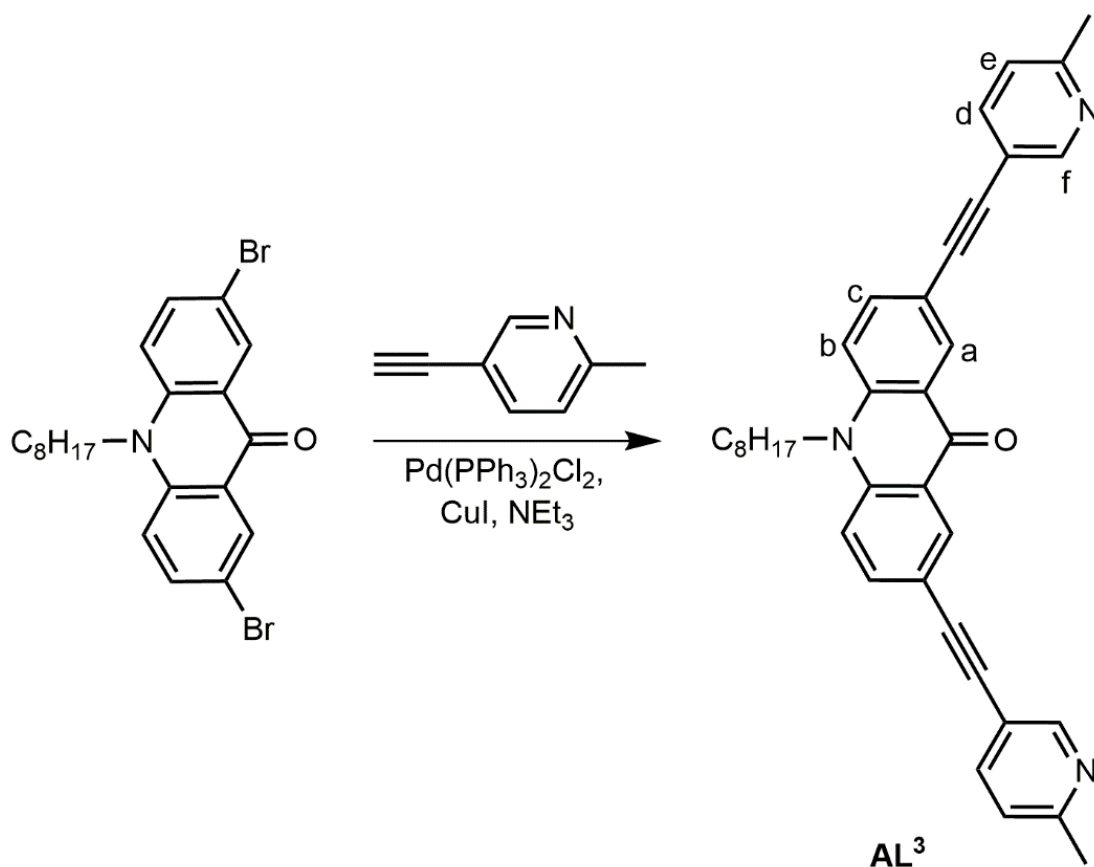
A mixture of 2,7-dibromo-10-octylacridin-9(10*H*)-one[18c] (148.80 mg, 0.32 mmol), 5-ethynyl-2-methyl-pyridine (112.46 mg, 0.96 mmol), copper (I) iodide (7.60 mg, 0.04 mmol) and Pd(PPh$_3$)$_2$Cl$_2$ (14.04 mg, 0.02 mmol) in triethylamine (8 mL) was thoroughly degassed. The mixture was heated under nitrogen atmosphere at 70 °C for 24 h. The mixture was cooled to room temperature and the solvent was evaporated under reduced pressure. A saturated NH$_4$Cl-solution was added to the residue and the organic components were extracted with CH$_2$Cl$_2$. The organic layer was washed with water and brine, dried over MgSO$_4$, filtrated and evaporated under reduced pressure. The crude residue was purified by flash chromatography on silica gel (*n*-hexane : ethylacetate = 1 : 3) and then by GPC to give **AL³** as a yellow solid product (49.21 mg, 0.09 mmol, 28.6%).
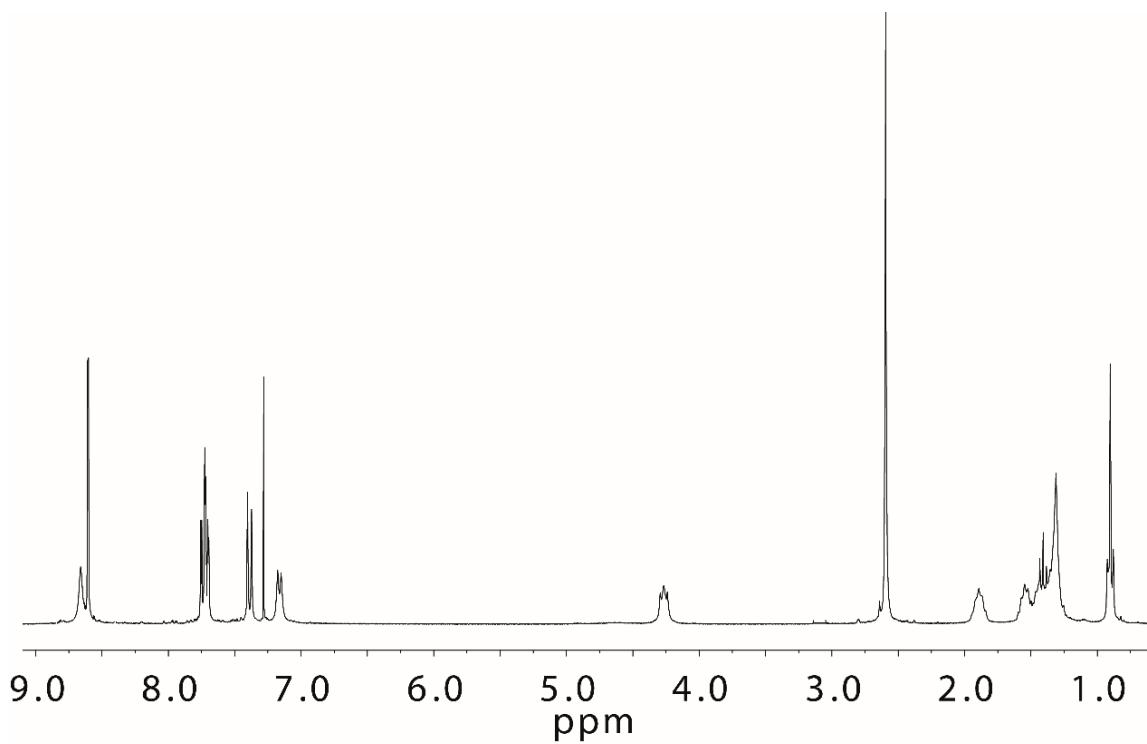
^{1}H NMR (300 MHz, CDCl$_3$) δ [ppm] = 8.64 (s, H$_f$), 8.58 (d, J = 2.2 Hz, H$_a$), 7.70 (dd, J = 2.2, 1.1 Hz, H$_c$), 7.68(dd, J = 15.9, 2.2 Hz, H$_d$), 7.37 (d, J = 9.1 Hz, H$_b$), 7.14 (d, J = 8.0 Hz, H$_e$), 4.24 (t, J = 8.4 Hz, 2H), 2.57 (s, 6H), 1.85 (m, 2H), 1.53 (m, 2H), 1.45 – 1.22 (m, 8H), 0.92 – 0.85 (t, J = 6.4 Hz, 3H).
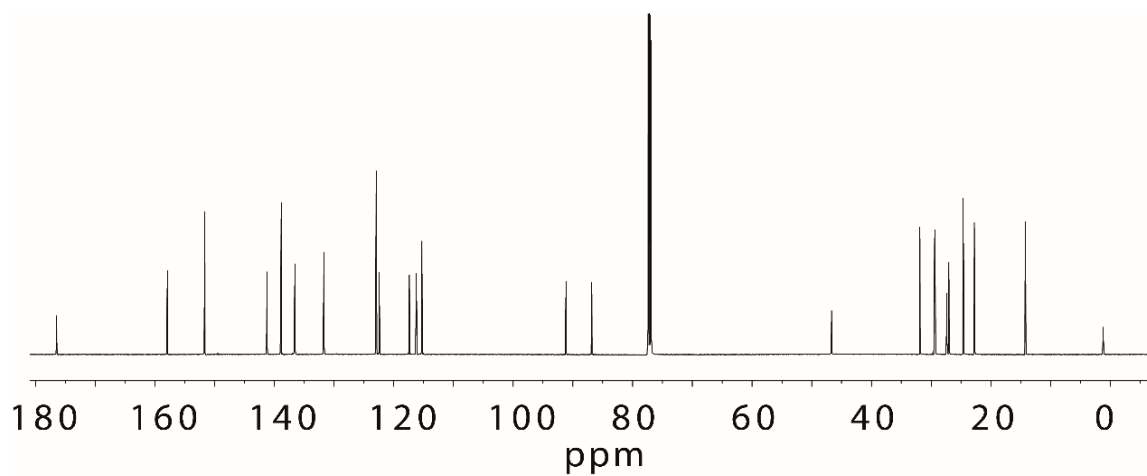
^{13}C NMR (150 MHz, CDCl$_3$) δ [ppm] = 157.90, 151.65, 141.22, 138.84, 136.56, 131.70, 122.92, 122.44, 117.39, 116.24, 115.29, 91.16, 86.84, 46.67, 31.88, 29.42, 27.34, 27.02, 24.65, 22.76, 14.23, 1.15.

ESI-FTICR-HRMS calculated for C$_{37}$H$_{36}$N$_3$O [M+H]$^+$ m/z 538.2858, found m/z 538.2841.

Synthesis of 10-hexyl-3,7-bis[(6-methylpyridin-3-yl)ethynyl]-10H-phenothiazine (PL¹):
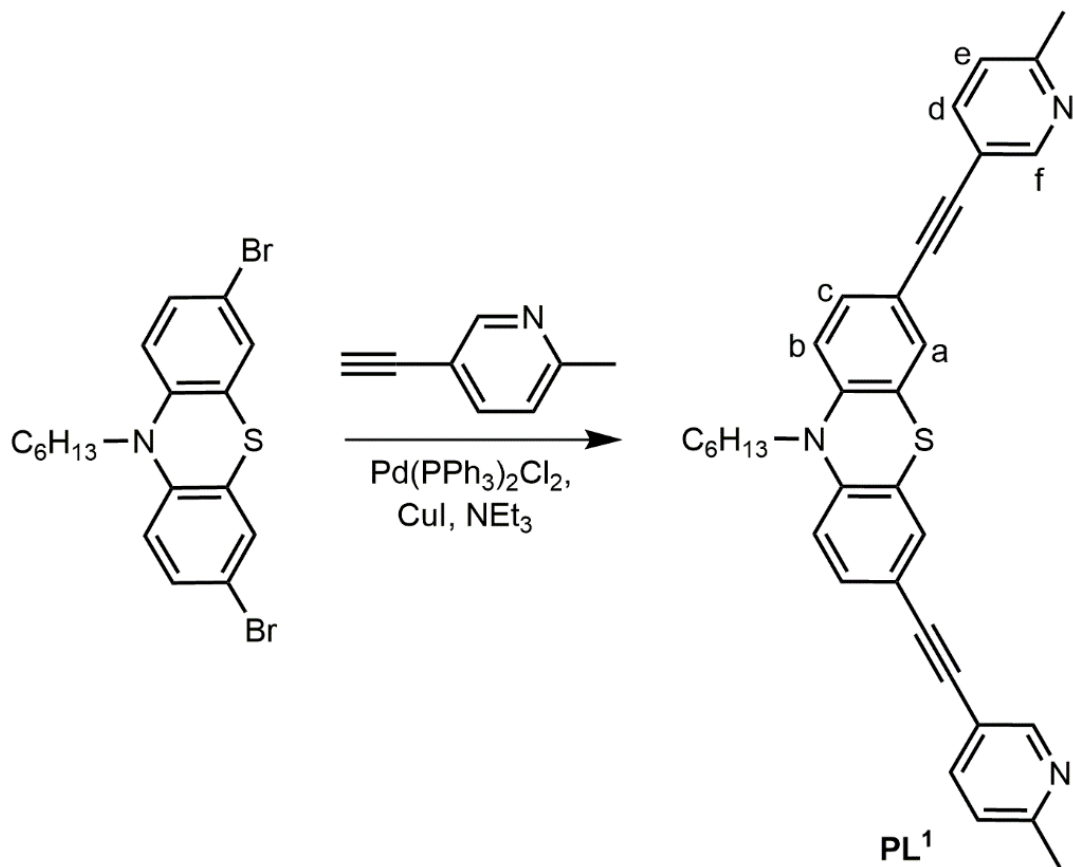
A mixture of 3,7-dibromo-10-hexyl-10*H*-phenothiazine[18a] (147.07 mg, 0.33 mmol), 5-ethynyl-2-methyl-pyridine (117.15 mg, 1.00 mmol), copper (I) iodide (7.60 mg, 0.04 mmol) and Pd(PPh$_3$)$_2$Cl$_2$ (14.04 mg, 0.02 mmol) in triethylamine (8 mL) was thoroughly degassed. The mixture was heated under nitrogen atmosphere at 70 °C for 24 h. The mixture was cooled to room temperature and the solvent was evaporated under reduced pressure. A saturated NH$_4$Cl-solution was added to the residue and the organic components were extracted with CH$_2$Cl$_2$. The organic layer was washed with water and brine, dried over MgSO$_4$, filtrated and evaporated under reduced pressure. The crude residue was purified by flash chromatography on silica gel (*n*-hexane : ethylacetate = 3 : 1) and then by GPC to give **PL¹** as a yellow oily product (39.78 mg, 0.08 mmol, 23.5%).
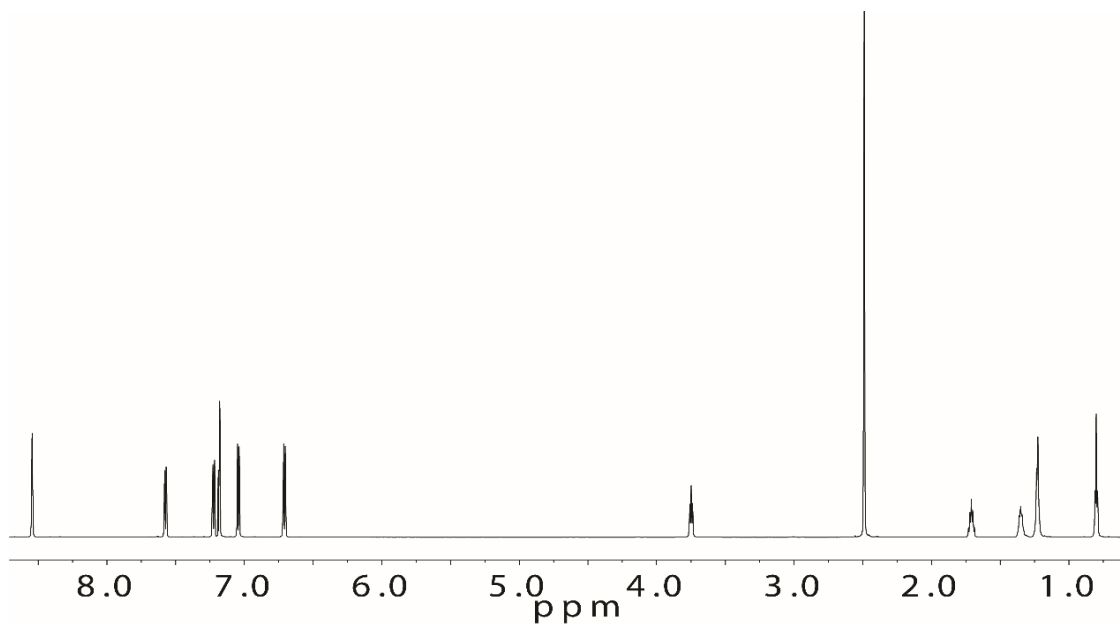
^{1}H NMR (700 MHz, CDCl$_3$) δ [ppm] = 8.54 (d, J = 2.3 Hz, H$_f$), 7.57 (dd, J = 8.0, 2.2 Hz, H$_d$), 7.22 (dd, J = 8.4, 2.0 Hz, H$_c$), 7.18 (d, J = 2.1 Hz, H$_a$), 7.04 (d, J = 8.0 Hz, H$_e$), 6.71 (d, J = 8.5 Hz, H$_b$), 3.75 (t, J = 7.3 Hz, 2H), 2.49 (s, 6H), 1.79 – 1.70 (m, 2H), 1.46 – 1.37 (m, 2H), 1.26 – 1.19 (m, 4H), 0.80 (t, J = 7.1 Hz, 3H).
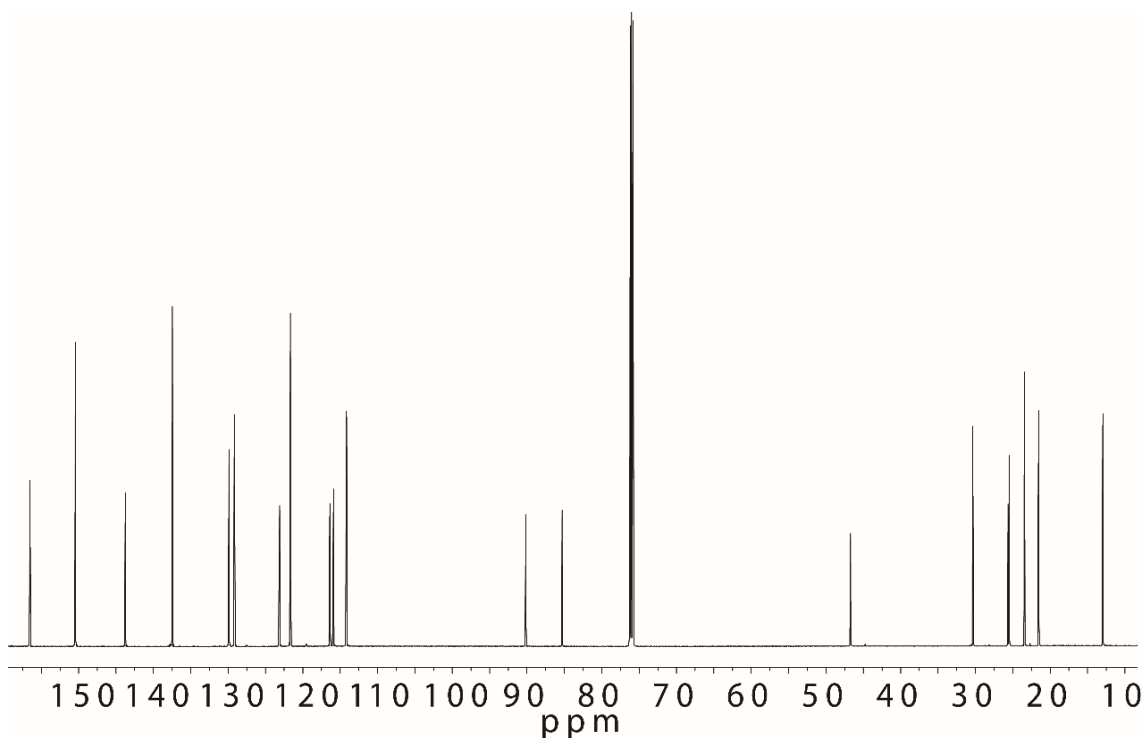

^{13}C NMR (175 MHz, CDCl$_3$) δ [ppm] =157.65, 151.57, 144.89, 138.61, 131.02, 130.30, 124.24, 122.80, 117.53, 117.03, 115.30, 91.29, 86.44, 47.86, 31.50, 26.78, 26.61, 24.61, 22.69, 14.10.

ESI-FTICR-HRMS calculated for C$_{34}$H$_{32}$N$_3$S [M+H]$^+$ m/z 514.2317, found m/z 514.2301.

Synthesis of 3,7-bis[(2-methylpyridin-3-yl)ethynyl]-10-octyl-10H-phenothiazine (PL²):
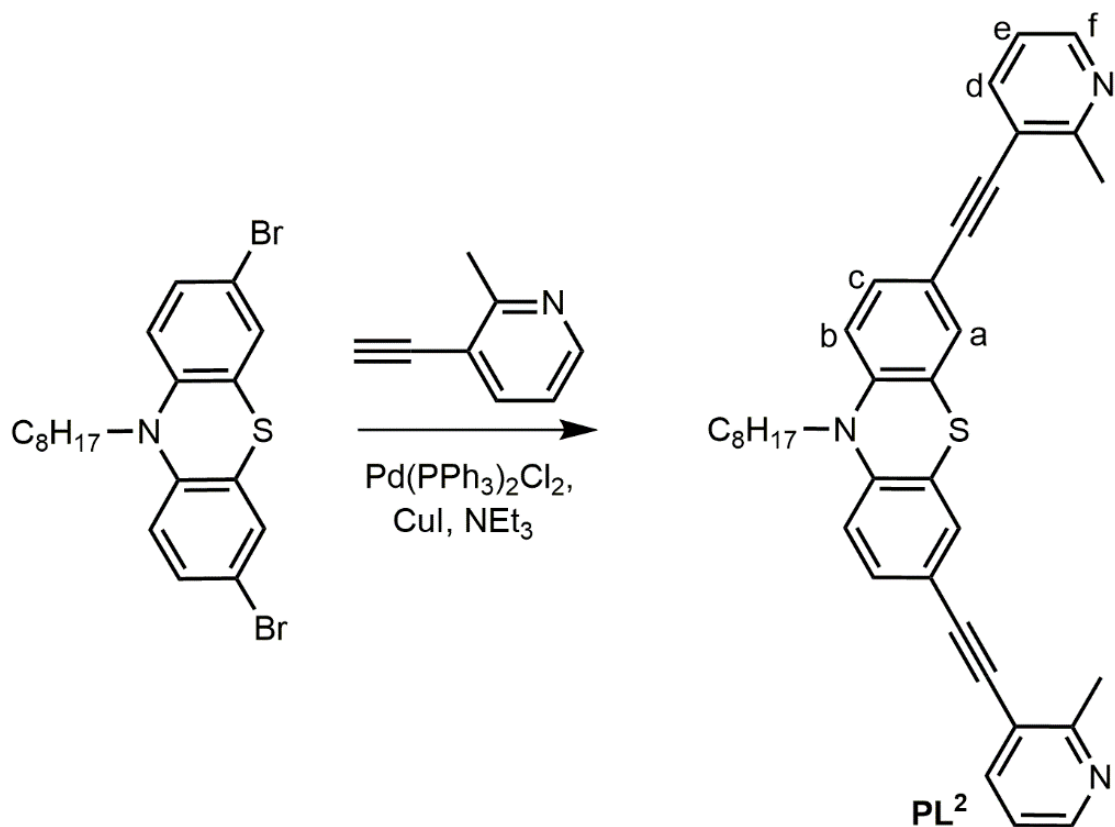
A mixture of 3,7-dibromo-10-octyl-10*H*-phenothiazine[18a] (200.54 mg, 0.43 mmol), 3-ethynyl-2-methyl-pyridine (150.00 mg, 1.28 mmol), copper (I) iodide (7.60 mg, 0.04 mmol) and Pd(PPh$_3$)$_2$Cl$_2$ (14.04 mg, 0.02 mmol) in triethylamine (10 mL) was thoroughly degassed. The mixture was heated under nitrogen atmosphere at 70 °C for 24 h. The mixture was cooled to room temperature and the solvent was evaporated under reduced pressure. A saturated NH$_4$Cl-solution was added to the residue and the organic components were extracted with CH$_2$Cl$_2$. The organic layer was washed with water and brine, dried over MgSO$_4$, filtrated and evaporated under reduced pressure. The crude residue was purified by flash chromatography on silica gel (*n*-hexane : ethylacetate = 3 : 1) and then by GPC to give **PL²** as a yellow oily product (101.43 mg, 0.19 mmol, 43.6%).
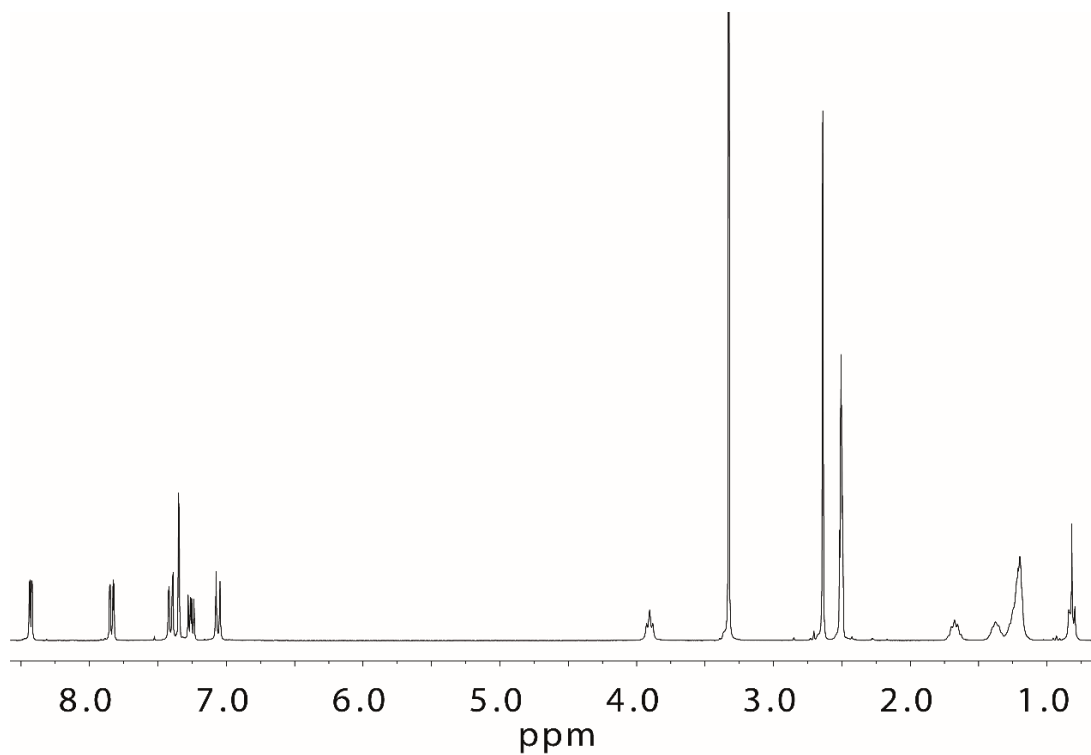
^{1}H NMR (300 MHz, DMSO-d_6) δ [ppm] = 8.43 (dd, J = 4.9, 1.7 Hz, H$_f$), 7.84 (dd, J = 7.8, 1.8 Hz, H$_d$), 7.41 (dd, J = 8.4, 2.0 Hz, H$_c$), 7.35 (d, J = 1.9 Hz, H$_a$), 7.26 (ddd, J = 7.8, 4.9, 0.7 Hz, H$_e$), 7.06 (d, J = 8.6 Hz, H$_b$), 3.90 (t, J = 6.9 Hz, 2H), 2.64 (s, 6H), 1.72 – 1.61 (m, 2H), 1.40 – 1.3 (m, 2H), 1.29 – 1.14 (m, 8H), 0.82 (t, J = 6.7 Hz, 3H);
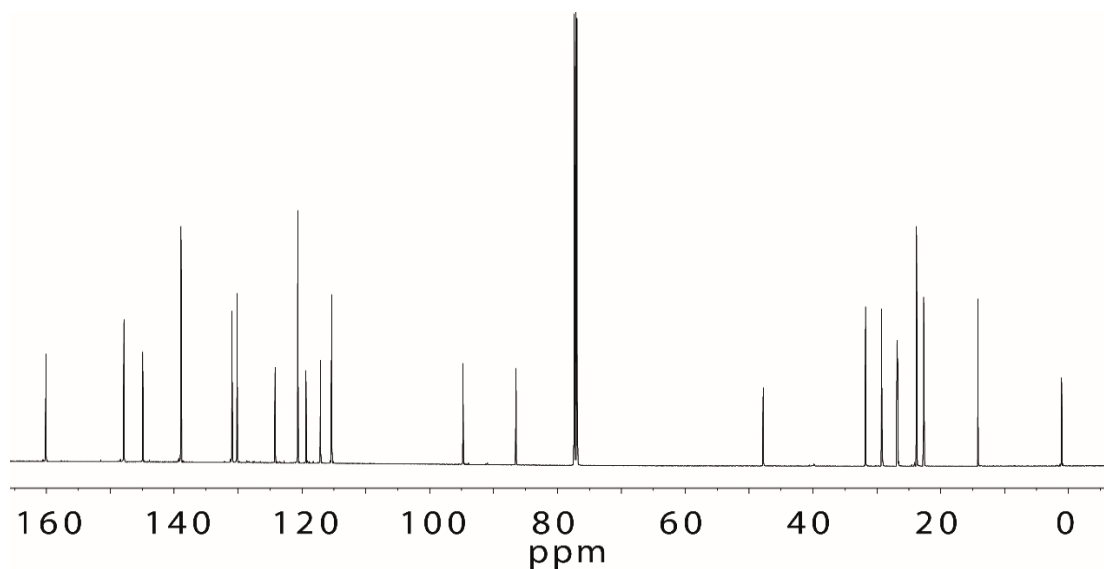
^{13}C NMR (150 MHz, CDCl$_3$) δ [ppm] = 160.05, 147.85, 144.92, 138.92, 130.95, 130.14, 124.20, 120.65, 119.37, 117.07, 115.33, 94.79, 86.47, 47.80, 31.78, 29.25, 26.85, 26.72, 23.79, 22.68, 14.17, 1.09.

ESI-FTICR-HRMS calculated for C$_{36}$H$_{36}$N$_3$S [M+H]$^+$ m/z 542.2630, found m/z 542.2595.

3.5.2 Self-assembly of ligands with palladium(II) cations

Bowl-shaped cage $[Pd_2(AL^1)_3]^{4+}$:
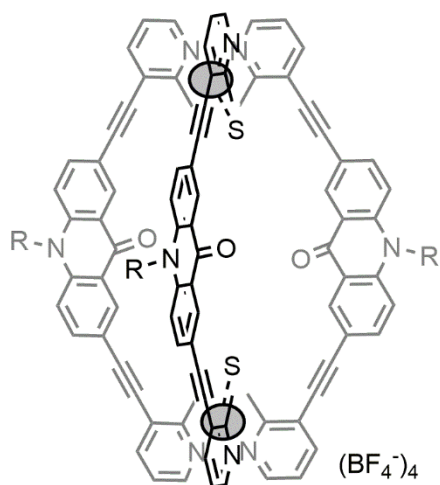
(Grey ball represents Pd^{II}, S represents solvent, R represents hexyl chain)

Cage $[Pd_2(AL^1)_3]^{4+}$was formed by stirring a mixture of ligand AL^1 in CD_3CN (930 µL, 1.43 mg, 2.8 µmol) and a solution of $[Pd(CH_3CN)_4](BF_4)_2$ (1.4 µmol, 139 µL of a 15 mM solution in CD_3CN) at room temperature for 8 h to give a solution of $[Pd_2(AL^1)_3]^{4+}$.
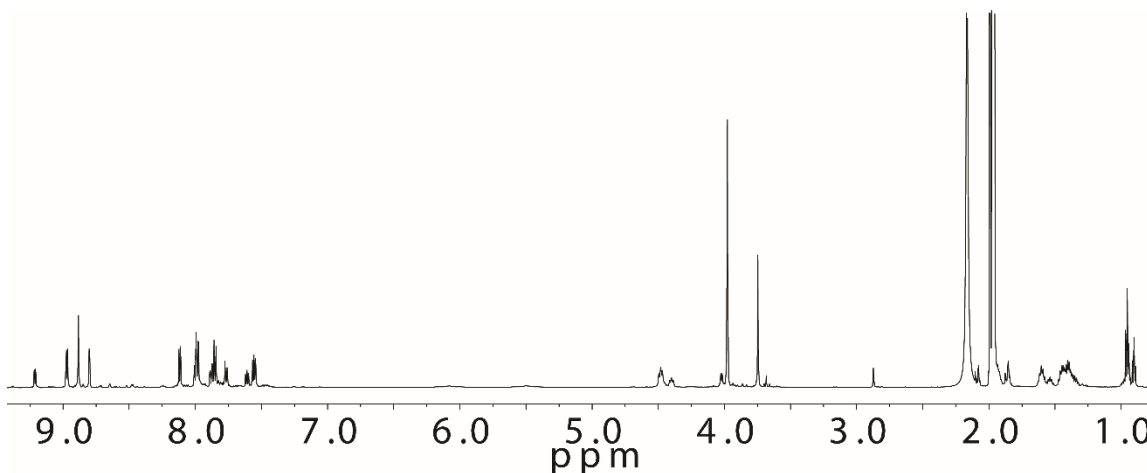
^{1}H NMR (600 MHz, CD_3CN) δ [ppm] = 9.21 (dd, J = 6.3, 1.3 Hz, 2H), 8.97 (dd, J = 6.1, 1.4 Hz, 4H), 8.88 (d, J = 2.2 Hz, 4H), 8.80 (d, J = 2.2 Hz, 2H), 8.12 (dd, J = 7.7, 1.3 Hz, 4H), 8.01 (d, J = 1.2 Hz, 2H), 7.98 (dd, J = 9.1, 2.2 Hz, 4H), 7.88 (dd, J = 8.9, 2.3 Hz, 4H), 7.85 (d, J = 9.0 Hz, 4H), 7.77 (d, J = 9.0 Hz, 2H), 7.61 (t, J = 7.2 Hz, 2H), 7.56 (t, J = 6.8 Hz, 4H), 4.48 (t, J = 8.4 Hz, 4H), 4.40 (t, J = 8.2 Hz, 2H), 3.98 (s, 12H), 3.75 (s, 6H), 1.60 – 1.54 (m, 6H), 1.47 – 1.33 (m, 18H), 0.95 (t, J = 7.1 Hz, 6H), 0.90 (d, J = 7.1 Hz, 3H).
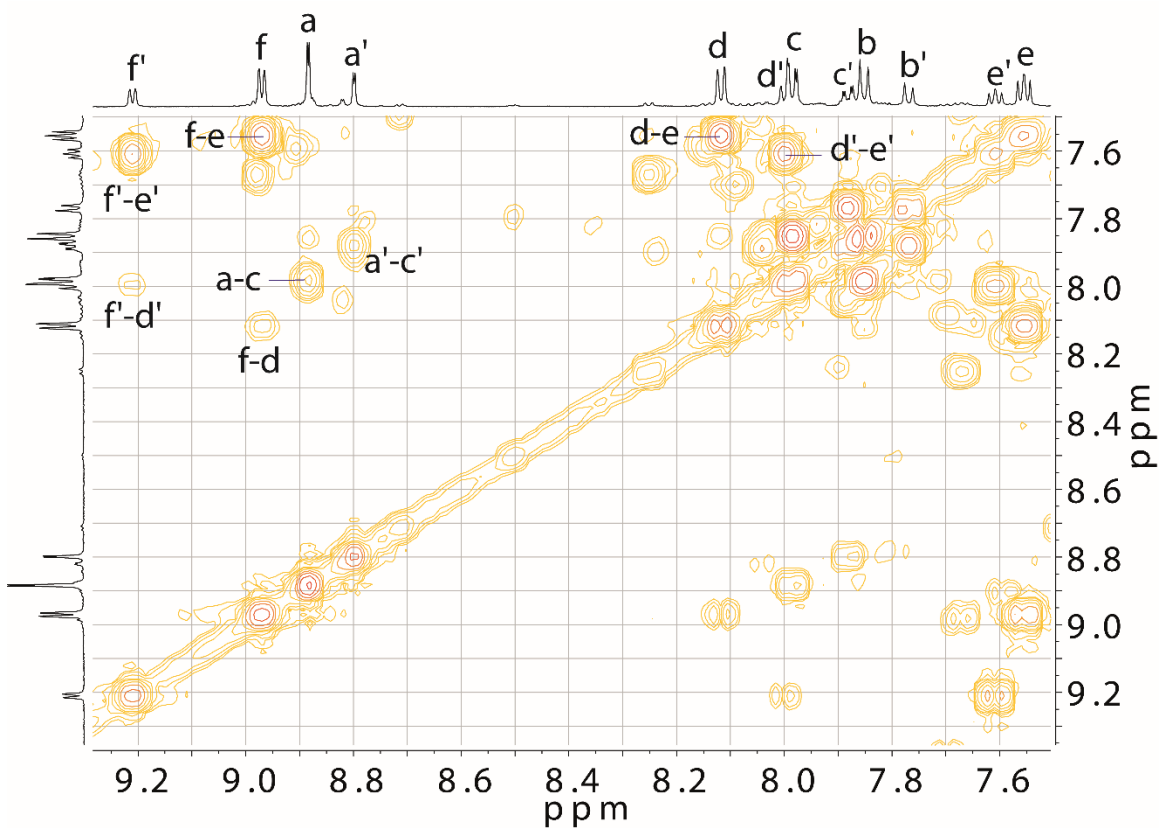
^{1}H–^{1}H COSY spectrum (600 MHz/CD$_3$CN) of [Pd$_2$(**AL**^{1})$_3$]$^{4+}$ (only showing aromatic region), for ^{1}H NMR ascriptions refer to **AL**^{1} structure.

ESI-FTICR-HRMS calculated for [C$_{105}$H$_{93}$N$_9$O$_3$Pd$_2$BF$_4$]$^{3+}$ m/z 609.5179, found m/z 609.5300.

Mixture of bowl-shaped cage [Pd$_2$(**AL**^{1})$_3$]$^{4+}$containing free ligand **AL**^{1}:

Heating a mixture of ligand **AL**^{1} in CD$_3$CN (930 µL, 1.43 mg, 2.8 µmol) and a solution of [Pd(CH$_3$CN)$_4$](BF$_4$)$_2$ (1.4 µmol, 93 µL of a 15 mM solution in CD$_3$CN) at 70 °C for 8 h gave a mixture of [Pd$_2$(**AL**^{1})$_3$]$^{4+}$ and ligand **AL**^{1}.
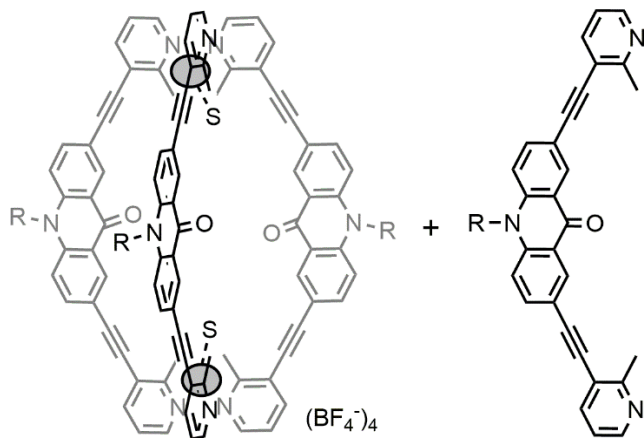
(Grey ball represents Pd^{II}, S represents solvent, R represents hexyl chain)
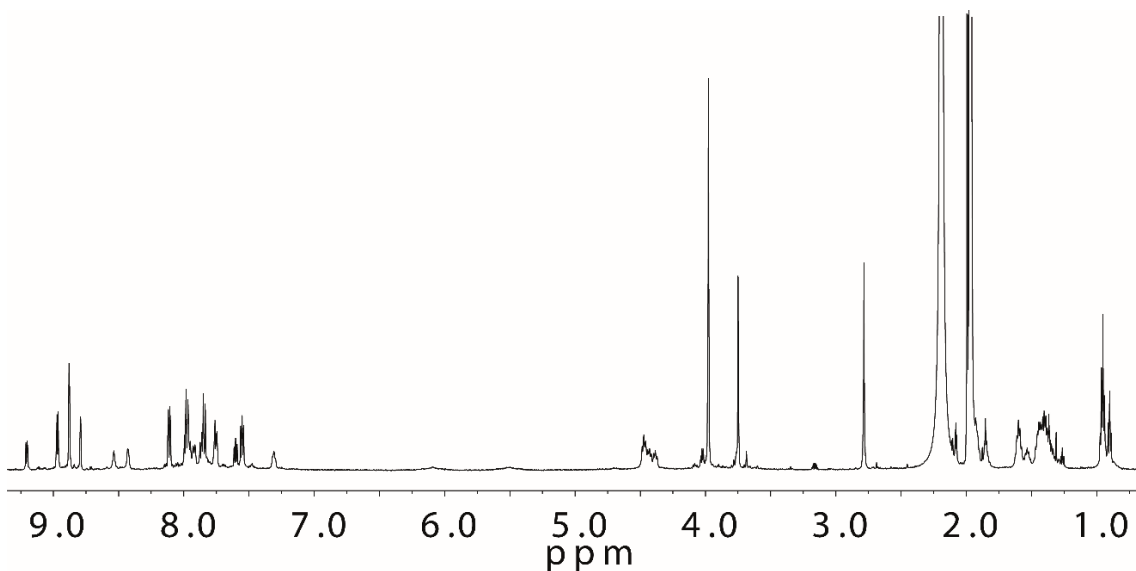
^{1}H NMR (600 MHz, CD$_3$CN) δ [ppm] = 9.21 (dd, J = 6.4, 1.3 Hz, 2H), 8.97 (dd, J = 6.1, 1.4 Hz, 4H), 8.88 (d, J = 2.2 Hz, 4H), 8.79 (d, J = 2.2 Hz, 2H), 8.54 (s, 2H), 8.43 (d, J = 4.9 Hz, 2H), 8.11 (dd, J = 7.8, 1.3 Hz, 4H), 8.00 – 7.94 (m, 8H), 7.92 (d, J = 8.5 Hz, 2H), 7.87 (dd, J = 8.9, 2.2 Hz, 2H), 7.84 (d, J = 9.0 Hz, 4H), 7.76 (dd, J = 9.1, 3.0 Hz, 4H), 7.60 (t, J = 6.8 Hz, 2H), 7.55 (t, J = 6.9 Hz, 4H), 7.30 (t, J = 6.1 Hz, 2H), 4.47 (t, J = 8.2 Hz, 4H), 4.43 (t, J = 8.2 Hz, 2H), 4.39 (d, J = 7.9 Hz, 2H), 3.98 (s, 12H), 3.75 (s, 6H), 2.79 (s, 6H), 1.60 – 1.54 (m, 8H), 1.52 – 1.48 (m, 2H), 1.48 – 1.23 (m, 30H), 0.96 (td, J = 7.2, 3.7 Hz, 12H), 0.90 (t, J = 7.0 Hz, 3H).
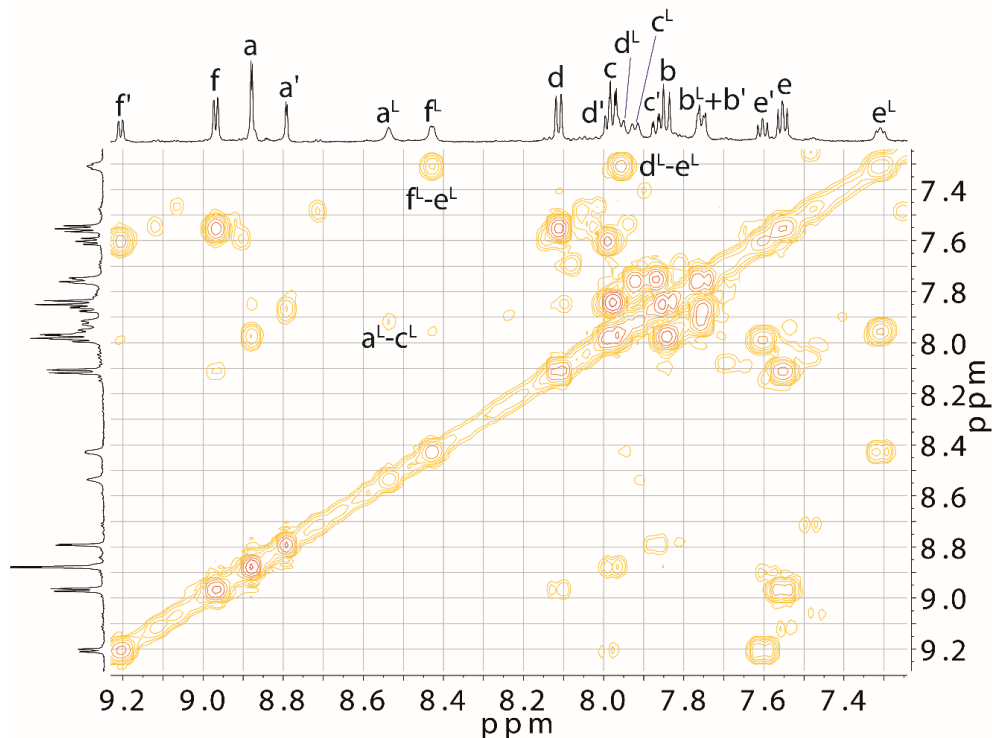
^{1}H–^{1}H COSY spectrum (600 MHz, CD$_3$CN) of mixture of [Pd$_2$(**AL**^{1})$_3$]$^{4+}$ and **AL**^{1} (only showing aromatic region, ^{L} peaks represent ligand **AL**^{1}), for ^{1}H NMR ascriptions refer to **AL**^{1} structure.
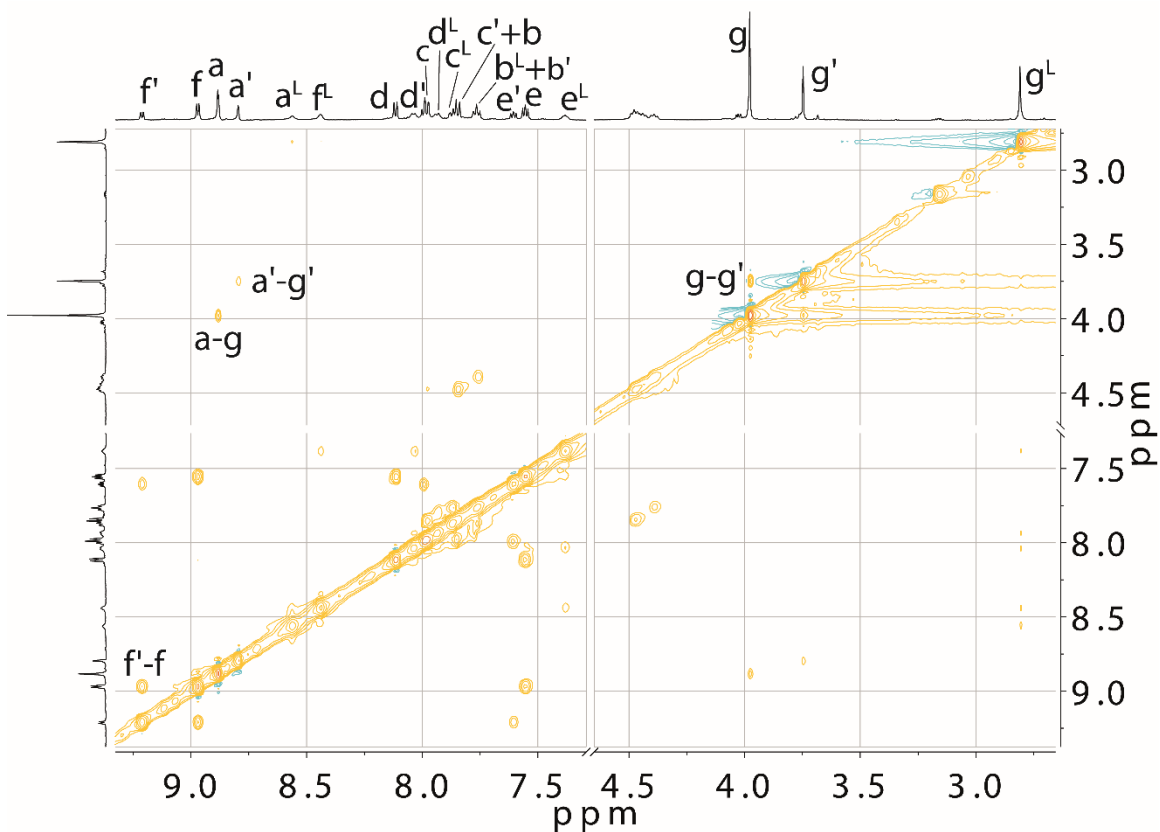
^{1}H–^{1}H NOESY spectrum (600 MHz/CD$_3$CN) of mixture of [Pd$_2$(**AL^1**)$_3$]$^{4+}$ and **AL^1** (–C$_6$H$_{13}$ signals at 0.5–2.5 ppm omitted, ^{L} peaks represent ligand **AL^1**), for ^{1}H NMR ascriptions refer to **AL^1** structure.

Mixture of ring [Pd$_2$(**AL^3**)$_2$]$^{4+}$ and bowl-shaped cage [Pd$_2$(**AL^3**)$_3$]$^{4+}$:
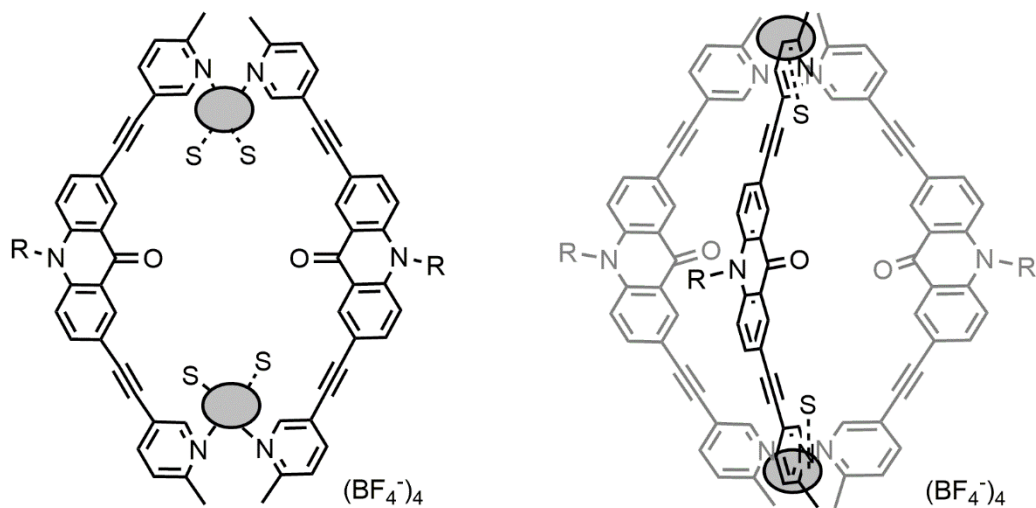
(Grey ball represents Pd^{II}, S represents solvent, R represents octyl chain)

Stirring a mixture of ligand **AL³** in CD₃CN (930 µL, 1.50 mg, 2.8 µmol) and a solution of [Pd(CH₃CN)₄](BF₄)₂ (1.4 µmol, 93 µL of a 15 mM solution in CD₃CN) at room temperature for 8 gave a mixture of [Pd₂(**AL³**)₂]⁴⁺ and [Pd₂(**AL³**)₃]⁴⁺.
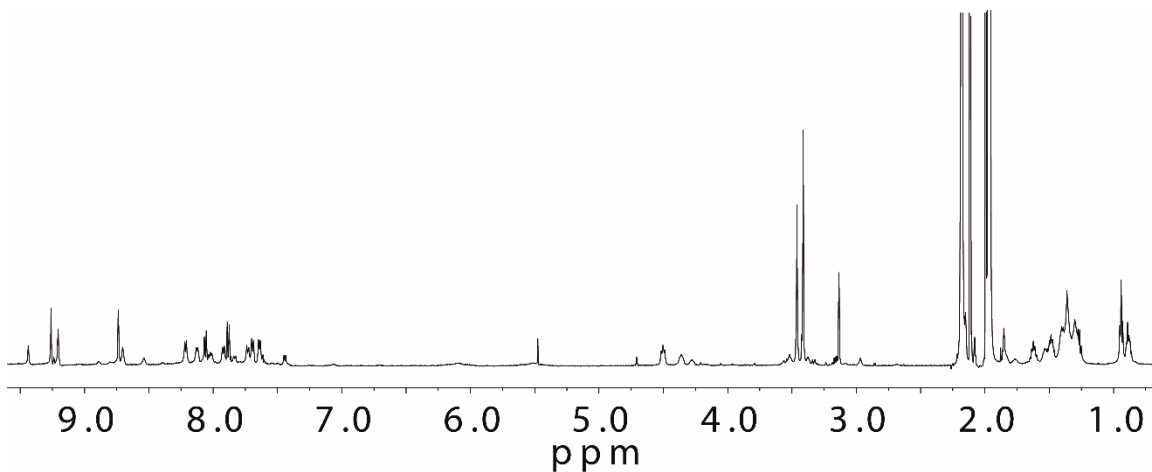
¹H NMR (600 MHz, CD₃CN) δ [ppm] = 9.41 (s, 2H), 9.23 (s, 4H), 9.18 (s, 4H), 8.71 (d, J = 2.2 Hz, 4H), 8.67 (s, 4H), 8.51 (s, 2H), 8.19 (d, J = 8.0 Hz, 4H), 8.10 (d, J = 7.9 Hz, 4H), 8.03 (dd, J = 8.9, 2.2 Hz, 4H), 7.99 (d, J = 8.3 Hz, 2H), 7.89 (d, J = 8.8 Hz, 4H), 7.85 (d, J = 8.9 Hz, 4H), 7.80 (d, J = 8.5 Hz, 2H), 7.70 (d, J = 9.0 Hz, 4H), 7.67 (d, J = 8.1 Hz, 4H), 7.61 (d, J = 8.0 Hz, 4H), 7.42 (d, J = 8.2 Hz, 2H), 4.48 (t, J = 8.0 Hz, 4H), 4.33 (t, J = 8.0 Hz, 4H), 4.25 (t, J = 7.3 Hz, 4H), 3.43 (s, 12H), 3.39 (s, 12H), 3.11 (s, 6H), 1.62 – 1.56 (m, 2H), 1.51 – 1.44 (m, 6H), 1.37 – 1.27 (m, 22H), 0.91 (t, J = 6.8 Hz, 6H), 0.87 – 0.83 (m, 9H).
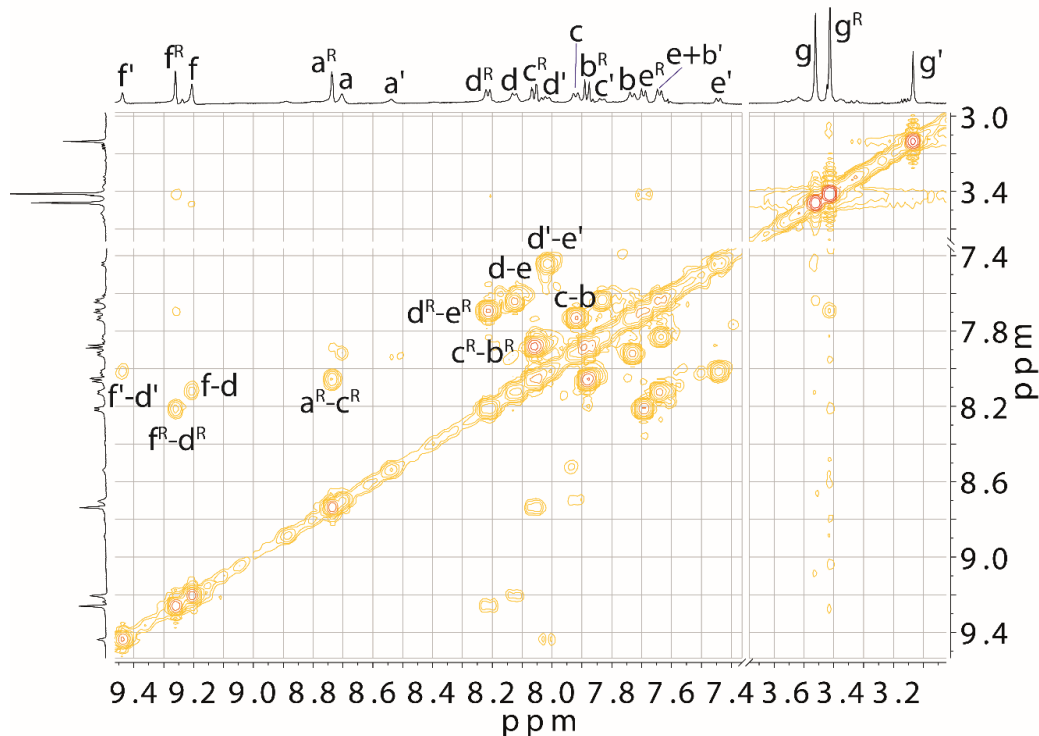
¹H–¹H COSY spectrum (600 MHz, CD₃CN) of mixture of [Pd₂(**AL³**)₂]⁴⁺ and [Pd₂(**AL³**)₃]⁴⁺ (–C₈H₁₇ signals at 0.7–3.0 ppm omitted, [R] peaks represent [Pd₂(**AL³**)₂]⁴⁺), for ¹H NMR ascriptions refer to **AL³** structure.
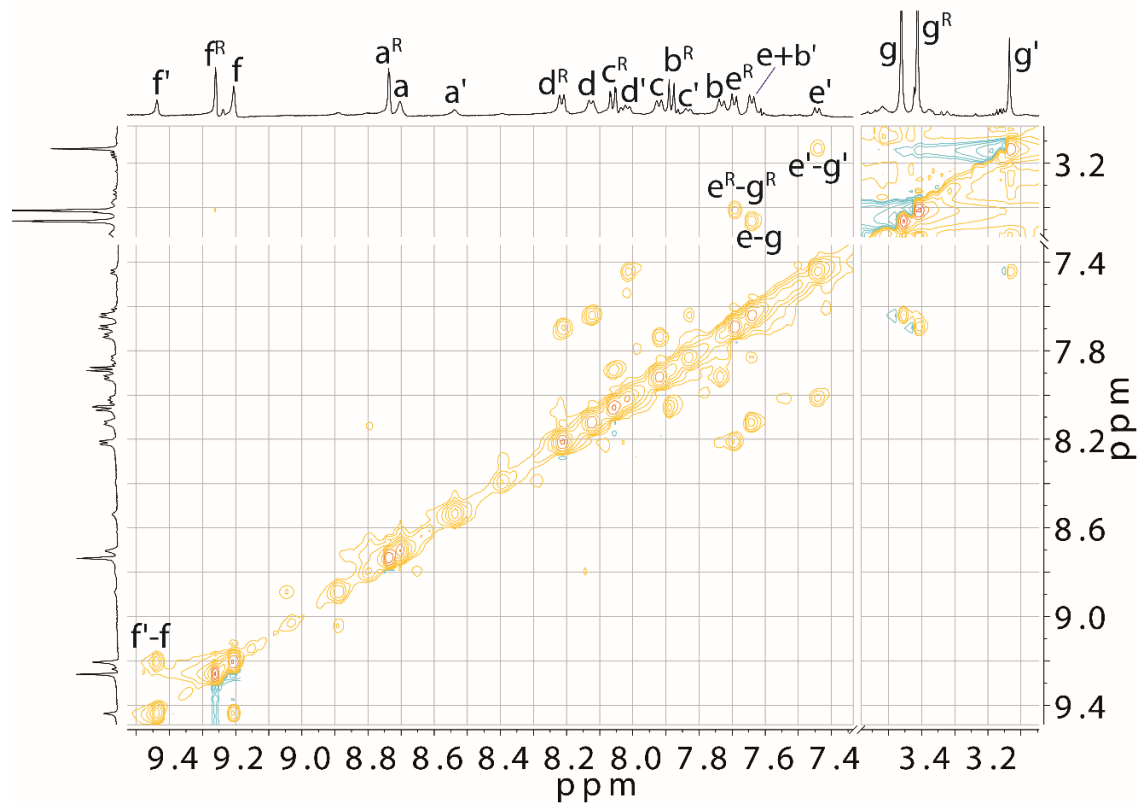
^{1}H–^{1}H NOESY spectrum (600 MHz, CD$_3$CN) of mixture of [Pd$_2$(**AL^3**)$_2$]$^{4+}$ and [Pd$_2$(**AL^3**)$_3$]$^{4+}$ (–C$_8$H$_{17}$ signals at 0.7–3.0 ppm omitted, ^{R} peaks represent [Pd$_2$(**AL^3**)$_2$]$^{4+}$), for ^{1}H NMR ascriptions refer to **AL^3** structure.

ESI-FTICR-HRMS calculated for [C$_{82}$H$_{82}$N$_{10}$O$_2$Pd$_2$]$^{4+}$ m/z 363.1177, found m/z 363.1209; for [C$_{115}$H$_{111}$N$_{11}$O$_3$Pd$_2$]$^{4+}$ m/z 476.9242, found m/z 476.9285.

Heteroleptic cage [Pd$_2$(**AL^1**)$_2$(**AL^3**)$_2$]$^{4+}$:
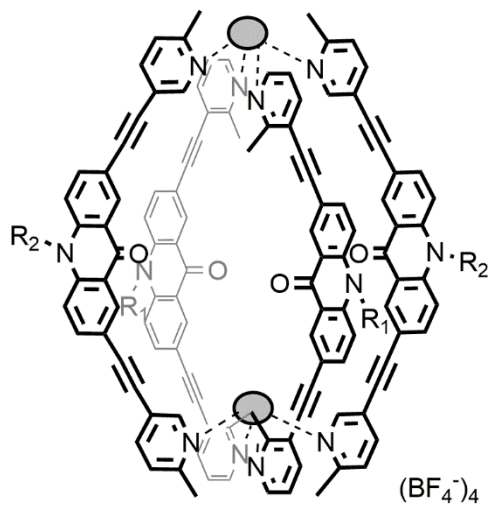
(Grey ball represents Pd^{II}, S represents solvent, R$_1$ represents hexyl chain, R$_2$ represents octyl chain)

Heteroleptic cage $[Pd_2(AL^1)_2(AL^3)_2]^{4+}$ was formed by heating a mixture of ligand AL^1 in CD_3CN (930 µL, 1.43 mg, 2.8 µmol), AL^3 in CD_3CN (930 µL, 1.50 mg, 2.8 µmol) and a solution of $[Pd(CH_3CN)_4](BF_4)_2$ (1.4 µmol, 186 µL of a 15 mM solution in CD_3CN) at 70 °C overnight.
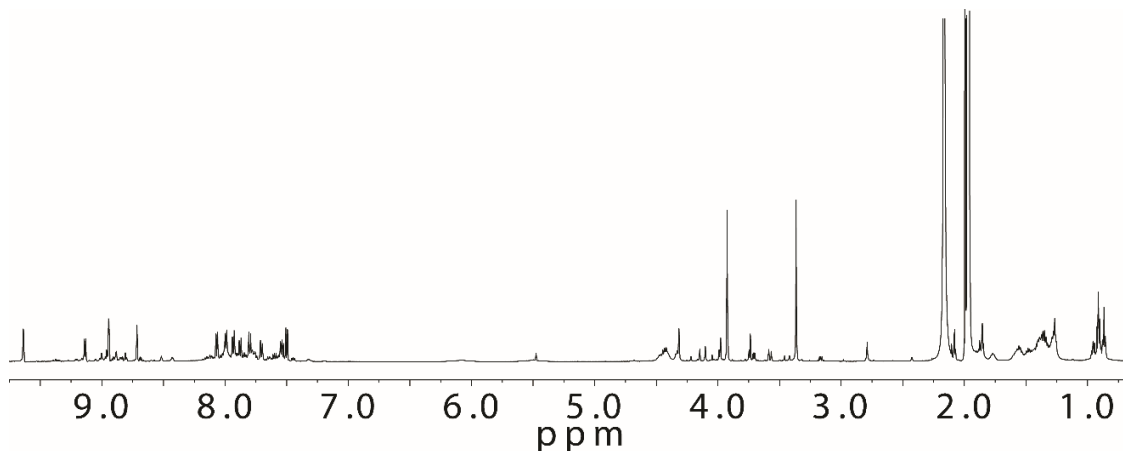
^{1}H NMR (600 MHz, CD_3CN) δ [ppm] = 9.64 (d, J = 1.9 Hz, 4H), 9.13 (dd, J = 6.1, 1.4 Hz, 4H), 8.94 (d, J = 2.2 Hz, 4H), 8.71 (d, J = 2.2 Hz, 4H), 8.07 (dd, J = 7.7, 1.3 Hz, 4H), 7.99 (dd, J = 8.0, 1.8 Hz, 4H), 7.93 (dd, J = 8.9, 2.3 Hz, 4H), 7.88 (dd, J = 8.9, 2.2 Hz, 4H), 7.80 (d, J = 9.0 Hz, 4H), 7.71 (d, J = 9.0 Hz, 4H), 7.55 – 7.52 (m, 4H), 7.50 (d, J = 8.2 Hz, 4H), 4.49 – 4.38 (m, 4H), 4.34 – 4.31 (m, 4H), 3.92 (s, 12H), 3.37 (s, 12H), 1.79 – 1.74 (m, 2H), 1.61 – 1.53 (m, 4H), 1.50 – 1.41 (m, 2H), 1.41 – 1.30 (m, 28H), 1.30 – 1.25 (m, 4H), 0.91 (t, J = 7.4 Hz, 6H), 0.87 (t, J = 6.6 Hz, 6H).
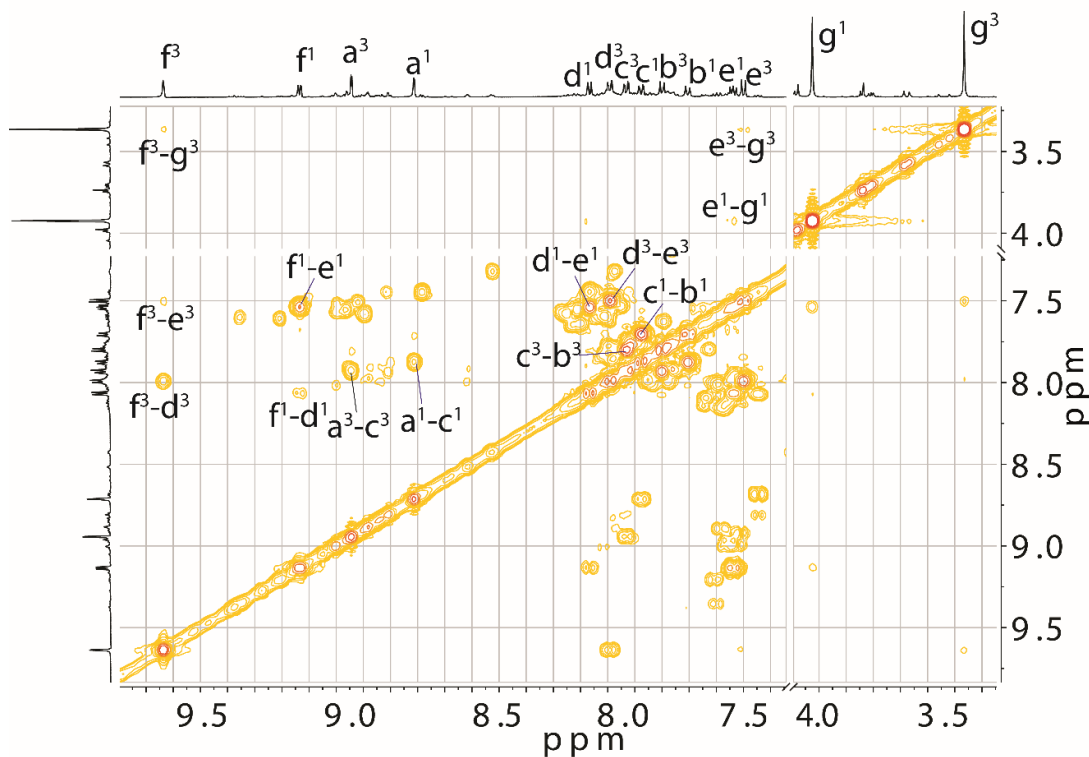
^{1}H–^{1}H COSY spectrum (600 MHz, CD_3CN) of $[Pd_2(AL^1)_2(AL^3)_2]^{4+}$ (–C_6H_{13} and –C_8H_{17} signals at 0.7–3.4 ppm omitted, ^{1} represent AL^1, ^{3} represents AL^3, for ^{1}H NMR ascriptions refer to AL^1 and AL^3 structures.
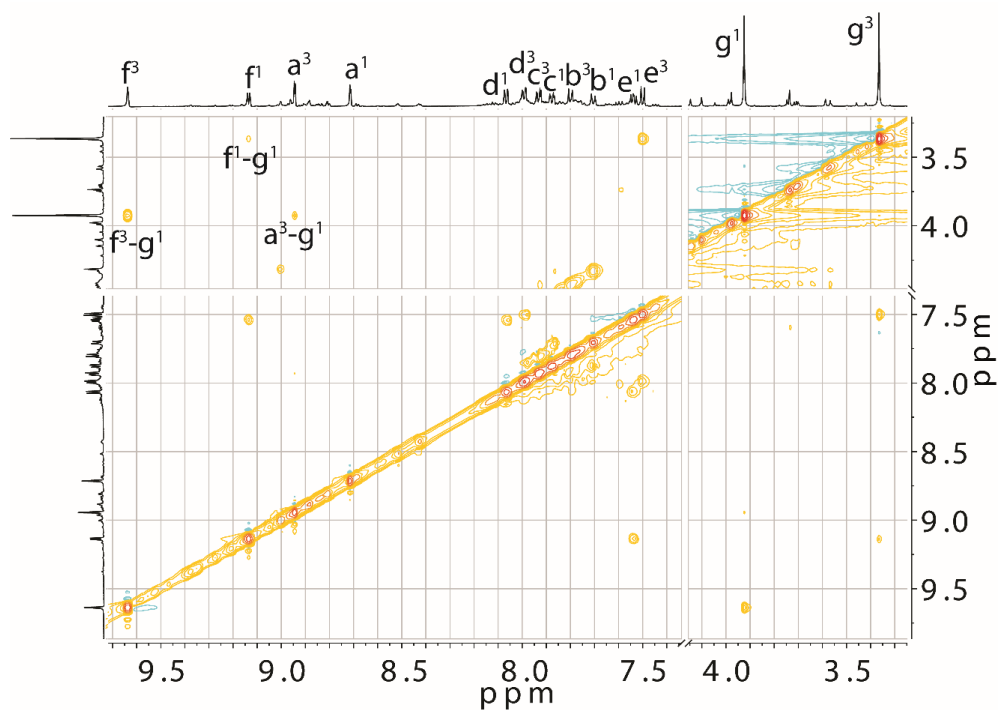
^{1}H–^{1}H NOESY spectrum (600 MHz, CD$_3$CN) of [Pd$_2$(**AL^1**)$_2$(**AL^3**)$_2$]$^{4+}$ (–C$_6$H$_{13}$ and –C$_8$H$_{17}$ signals at 0.7–3.4 ppm omitted), [1] represent **AL^1**, [3] represents **AL^3**, for ^{1}H NMR ascriptions refer to **AL^1** and **AL^3** structures.

ESI-FTICR-HRMS calculated for [C$_{144}$H$_{132}$N$_{12}$O$_4$Pd$_2$]$^{4+}$ m/z 576.7150, found m/z 576.7140.

Mixture of ring [Pd$_2$(**PL^1**)$_2$]$^{4+}$ and bowl-shaped cage [Pd$_2$(**PL^1**)$_3$]$^{4+}$:
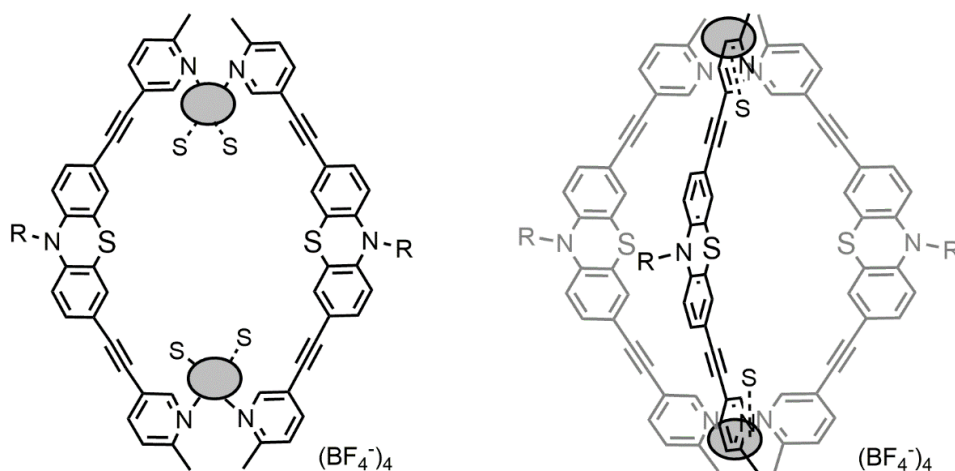
(Grey ball represents Pd^{II}, S represents solvent, R represents hexyl chain)

Stirring a mixture of ligand **PL^1** in CD$_3$CN (930 μL, 1.44 mg, 2.8 μmol) and a solution of [Pd(CH$_3$CN)$_4$](BF$_4$)$_2$ (1.4 μmol, 93 μL of a 15 mM solution in CD$_3$CN) at room temperature overnight gave a mixture of [Pd$_2$(**PL^1**)$_2$]$^{4+}$ and [Pd$_2$(**PL^1**)$_3$]$^{4+}$.
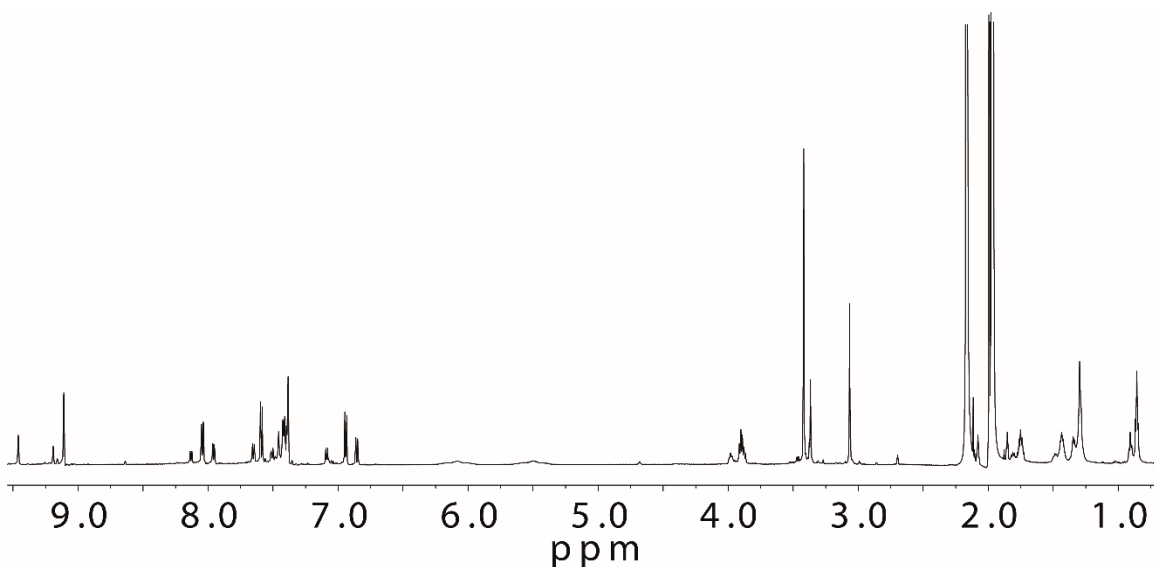
^{1}H NMR (600 MHz, CD$_3$CN) δ [ppm] = 9.46 (s, 4H), 9.19 (s, 2H), 9.11 (s, 8H), 8.13 (dd, J = 8.1, 1.8 Hz, 2H), 8.04 (dd, J = 8.1, 1.9 Hz, 8H), 7.96 (dd, J = 8.2, 1.8 Hz, 4H), 7.65 (d, J = 8.2 Hz, 2H), 7.59 (d, J = 8.2 Hz, 8H), 7.51 (dt, J = 8.6, 2.6 Hz, 2H), 7.46 (s, 4H), 7.43 – 7.40 (m, 16H), 7.40 – 7.37 (m, 10H), 7.08 (d, J = 8.4 Hz, 2H), 6.94 (d, J = 8.5 Hz, 8H), 6.86 (d, J = 8.5 Hz, 4H), 3.98 (t, J = 7.7 Hz, 2H), 3.91 – 3.87 (m, 12H), 3.42 (s, 24H), 3.37 (s, 6H), 3.07 (s, 12H), 1.82 – 1.79 (m, 2H), 1.78 – 1.72 (m, 8H), 1.51 – 1.39 (m, 16H), 1.36 – 1.26 (m, 30H), 0.91 (t, J = 6.8 Hz, 6H), 0.87 – 0.83 (m, 15H).
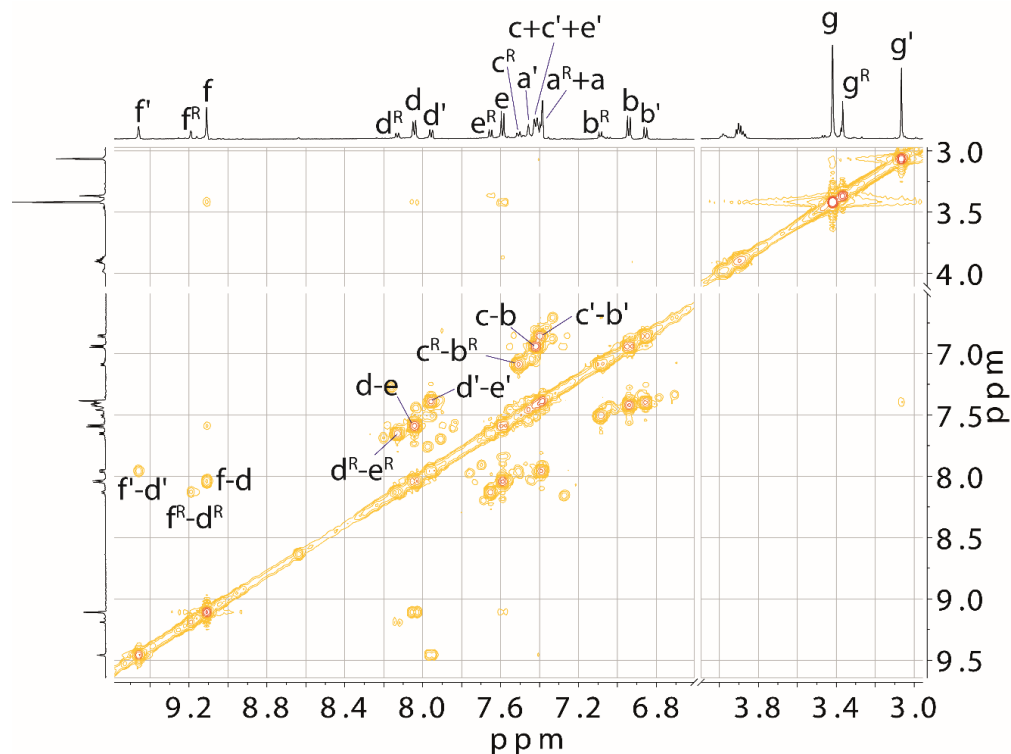
^{1}H–^{1}H COSY spectrum (600 MHz, CD$_3$CN) of mixture of [Pd$_2$(**PL^1**)$_2$]$^{4+}$ and [Pd$_2$(**PL^1**)$_3$]$^{4+}$ (–C$_6$H$_{13}$ signals at 0.7–3.0 ppm omitted, ^{R} peaks represent [Pd$_2$(**PL^1**)$_2$]$^{4+}$), ^{1}H NMR ascriptions refer to **PL^1** structure.

ESI-FTICR-HRMS calculated for $[C_{72}H_{68}N_9S_2Pd_2FO_3]^{2+}$ m/z 700.6400, found m/z 700.6480; for $[C_{102}H_{93}N_9S_3Pd_2]^{4+}$ m/z 438.3719, found m/z 438.3701.

Bowl-shaped cage $[Pd_2(\mathbf{PL^2})_3]^{4+}$:
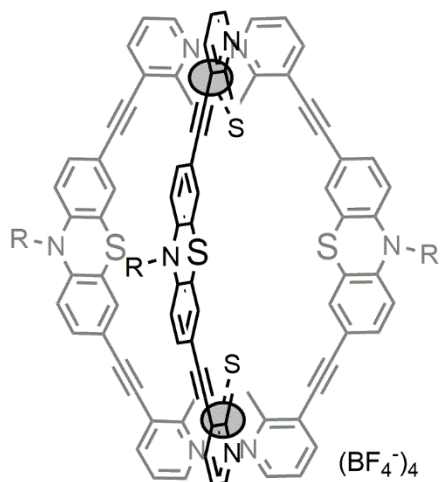
(Grey ball represents Pd^{II}, S represents solvent, R represents octyl chain)
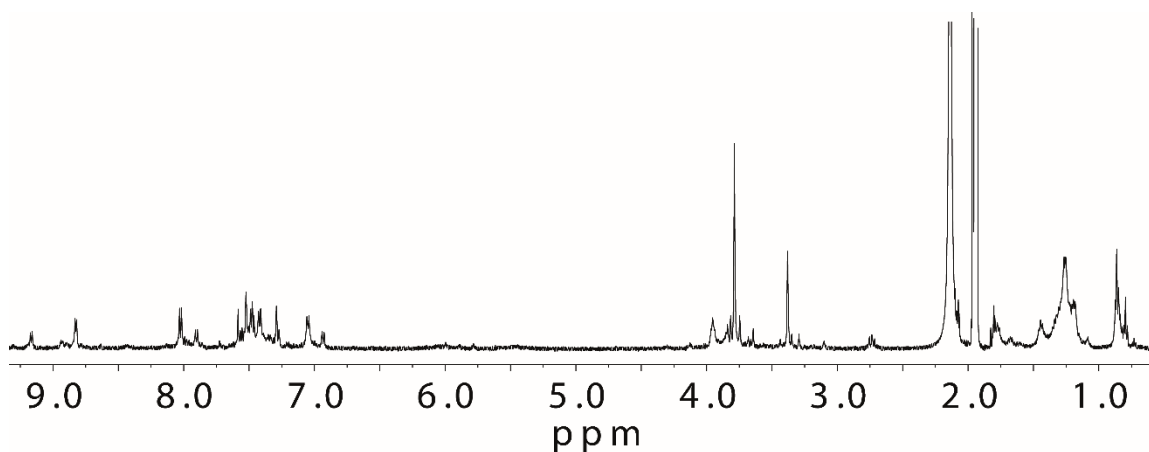
The assembly from $\mathbf{PL^2}$ with Pd^{II} gave a rather complicated spectrum in which two main sets of peaks could be found and roughly assigned as the bowl-shaped cage $[Pd_2(\mathbf{PL^2})_3]^{4+}$ (see Figure 3.22d). This species can be verified by ESI-MS spectra in Figure 3.23b.

ESI-FTICR-HRMS calculated for $[C_{108}H_{105}N_9S_3Pd_2]^{4+}$ m/z 459.4018, found m/z 459.3936.

Heteroleptic cage $[Pd_2(\mathbf{AL^2})_2(\mathbf{PL^2})_2]^{4+}$:
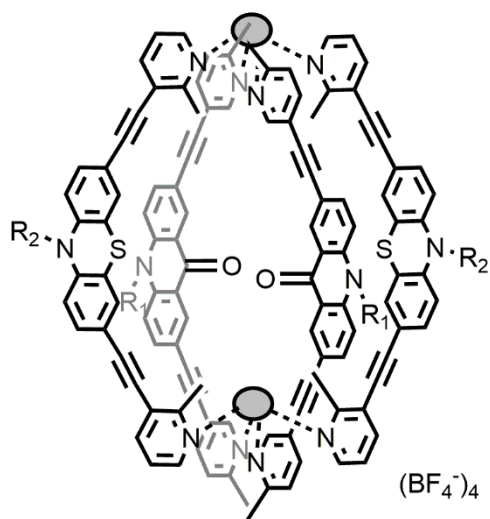
(Grey ball represents Pd^{II}, S represents solvent, R_1 represents hexyl chain, R_2 represents octyl chain)

Heteroleptic cage $[Pd_2(\mathbf{AL^2})_2(\mathbf{PL^2})_2]^{4+}$ was formed by heating a mixture of ligand $\mathbf{AL^2}$ in CD_3CN (930 µL, 1.43 mg, 2.8 µmol), $\mathbf{PL^2}$ in CD_3CN (930 µL, 1.52 mg, 2.8 µmol) and a solution of $[Pd(CH_3CN)_4](BF_4)_2$ (1.4 µmol, 186 µL of a 15 mM solution in CD_3CN) for 8 h.
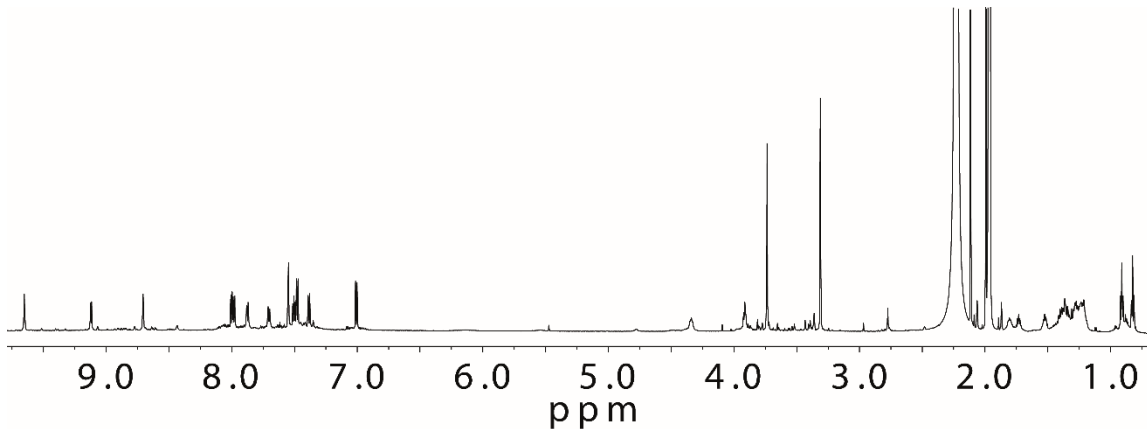
^{1}H NMR (700 MHz, CD_3CN) δ [ppm] = 9.65 (d, J = 2.0 Hz, 4H), 9.12 (dd, J = 6.2, 1.4 Hz, 4H), 8.71 (d, J = 2.1 Hz, 4H), 8.00 (dd, J = 7.8, 1.3 Hz, 4H), 7.98 (dd, J = 8.1, 1.8 Hz, 4H), 7.87 (dd, J = 8.8, 2.2 Hz, 4H), 7.70 (d, J = 9.0 Hz, 4H), 7.55 (d, J = 2.0 Hz, 4H), 7.50 (dd, J = 7.7, 6.2 Hz, 4H), 7.48 (d, J = 8.1 Hz, 4H), 7.38 (dd, J = 8.3, 2.0 Hz, 4H), 7.01 (d, J = 8.4 Hz, 4H), 4.34 (t, J = 8.1 Hz, 4H), 3.91 (t, J = 7.6 Hz, 4H), 3.74 (s, 12H), 3.31 (s, 12H), 1.83 – 1.78 (m, 2H), 1.75 – 1.71 (m, 2H), 1.55 – 1.50 (m, 4H), 1.41 – 1.32 (m, 6H), 1.30 – 1.18 (m, 6H), 0.91 (t, J = 7.1 Hz, 6H), 0.83 (t, J = 7.0 Hz, 6H).
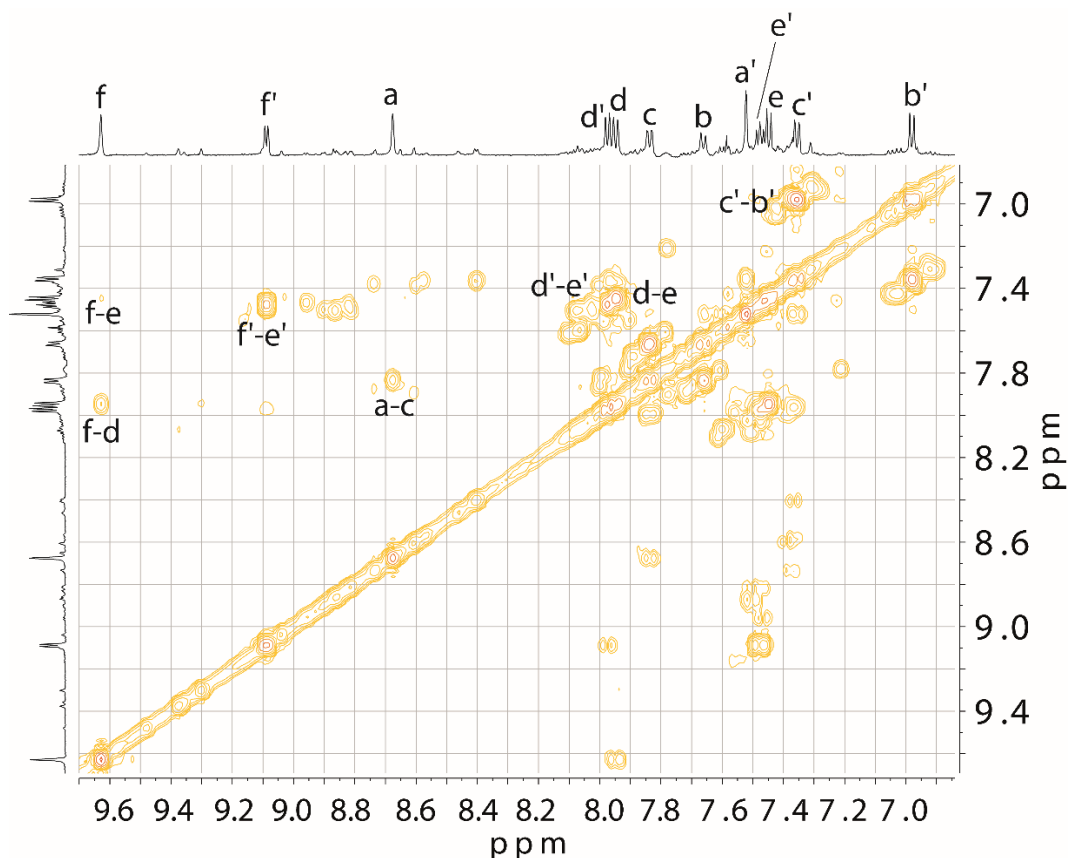
$^1H–^1H$ COSY spectrum (600 MHz/CD$_3$CN) of [Pd$_2$(**AL^2**)$_2$(**PL^2**)$_2$]$^{4+}$ (only showing aromatic region), for ^1H NMR ascriptions refer to Figure 3.12.

ESI-FTICR-HRMS calculated for [C$_{142}$H$_{132}$N$_{12}$O$_2$ S$_2$Pd$_2$]$^{4+}$ m/z 578.7035, found m/z 578.7060.

3.5.3   Further experiments

Heating the already formed sample of [Pd$_2$(**AL^1**)$_3$]$^{4+}$ to 70 °C for 8 h resulted three sets of proton signals (Figure 3.19c). Two sets belong to [Pd$_2$(**AL^1**)$_3$]$^{4+}$ assembly (marked as X) and the rest set was marked as X^L. According to the characteristic proton shifting of momeric cage[15,16a,17,18d] or bowl-shaped cage discussed above, this set of X^L signals which showing a very slight shift was not supposed due to Pd^{II} complexation. However, DOSY experiment confirmed the set of X^L signals (green signals in Figure 3.21) possesses a different diffusion efficient (*log* D = –8.955, D = 11.09 x 10^{-10} m^{2}s^{-1}, r = 5.33 Å) from the [Pd$_2$(**AL^1**)$_3$]$^{4+}$ species (*log* D = –9.232, D = 5.86 x 10^{-10} m^{2}s^{-1}, r = 10.09 Å). Comparing the values of hydrodynamic radii of two different species, it's assumed that the X^L signals can't be attributed to the monomeric cage [Pd$_2$(**AL^1**)$_4$]$^{4+}$ even there is a weak signal of [Pd$_2$(**AL^1**)$_4$]$^{4+}$ species presenting in the mass spectrum (Figure 3.20). As a result, it's supposed that the set of X^L signals belong to the free ligand **AL^1** showing slight shifting in the presence of palladium cations or coordination assembly.
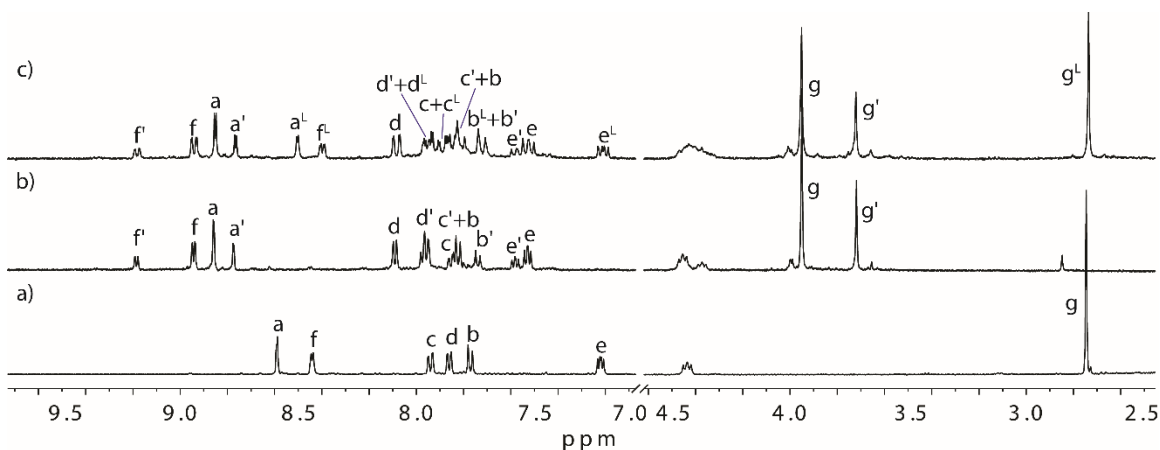
Figure 3.19 ^{1}H NMR spectra (600 MHz, CD$_3$CN, 293 K) of a) ligand **AL^1**; b) bowl-shaped cage [Pd$_2$(**AL^1**)$_3$]$^{4+}$; c) bowl-shaped cage [Pd$_2$(**AL^1**)$_3$]$^{4+}$ and ligand **AL^1** (^{1}H NMR ascriptions refer to **AL^1** structure, ^{L} represnets ligand **AL^1**).
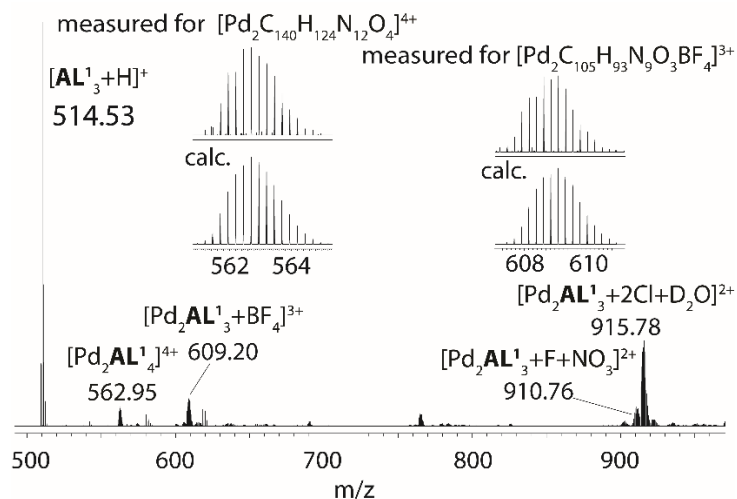

Figure 3.20 ESI-Mass spectra of assembly from **AL^1** with Pd^{II} under heating condition.

Since there is a considerable difference between the phenothiazine and acridone backbone aforementioned, it draws interest to investigate whether this difference would influence the assembly from these ligands with metal cations. Homoleptic assemblies from **PL^1** and **PL^2** were, however, analogous to that observed for the acridone ligands. Reacting **PL^1** with [Pd(CH$_3$CN)$_4$](BF$_4$)$_2$ in a 2:1 ratio at 298 K gave a 4:1 mixture of [Pd$_2$(**PL^1**)$_3$]$^{4+}$ and [Pd$_2$(**PL^1**)$_2$]$^{4+}$ by ^{1}H NMR spectroscopy (Figure 3.22c). The presence of these species were also confirmed by ESI-MS (Figure 3.23a) and through the relevant contacts observed in the NOESY spectrum (Figure 3.24). Under similar conditions, **PL^2** and [Pd(CH$_3$CN)$_4$](BF$_4$)$_2$ gave a single species, which was identified as [Pd$_2$(**PL^2**)$_3$]$^{4+}$ by NMR spectroscopy (Figue 3.22d) and ESI-MS (Figure 3.23b).

After heating the mixture of **PL^1**, **PL^2** and [Pd(CH$_3$CN)$_4$](BF$_4$)$_2$ (1 : 1 : 1) in CD$_3$CN at 70 °C for 8h, a complicated ^{1}H NMR spectrum (Figure 3.22e) was obtained showing highly overlapping area which was too hard to analyze. From the ESI-MS spectra (Figure 3.23c) weak signal of mono-cage [Pd$_2$(**PL^1**)$_2$(**PL^2**)$_2$]$^{4+}$ was
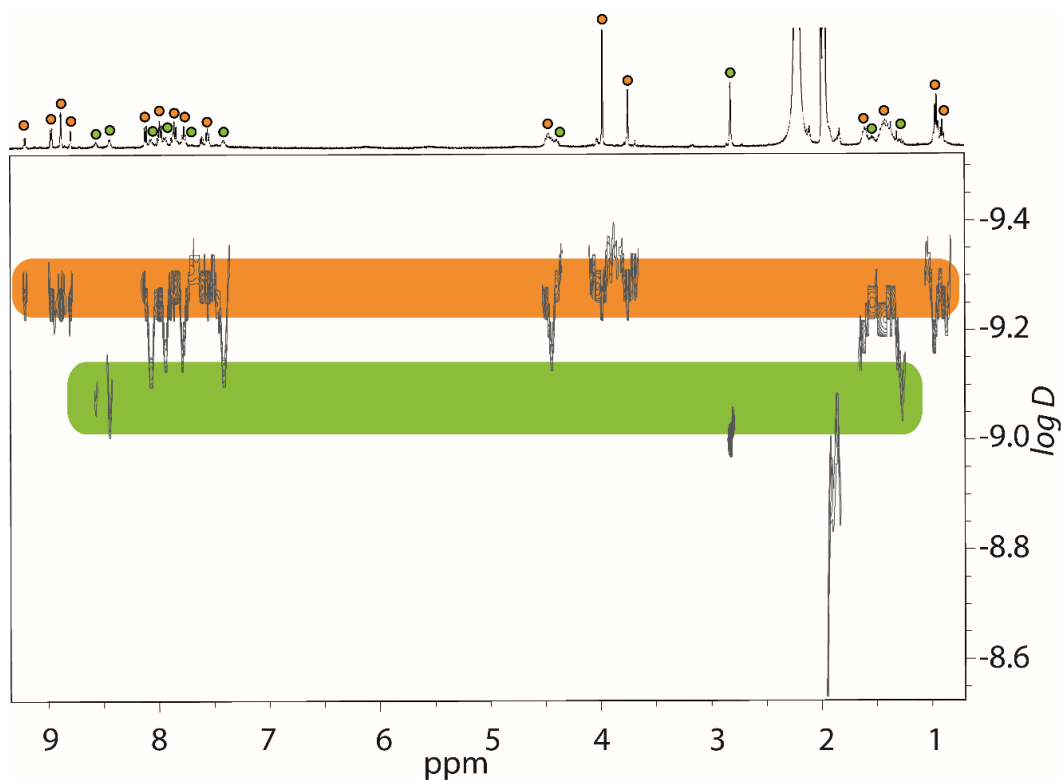
Figure 3.21 ^{1}H–^{1}H DOSY spectrum of mixture of bowl-shaped cage [Pd$_2$(**AL^1**)$_3$]$^{4+}$ (orange) and ligand **AL^1** (green) (500 MHz/CD$_3$CN, 298K, *log*D = logarithm of diffusion coefficient D).
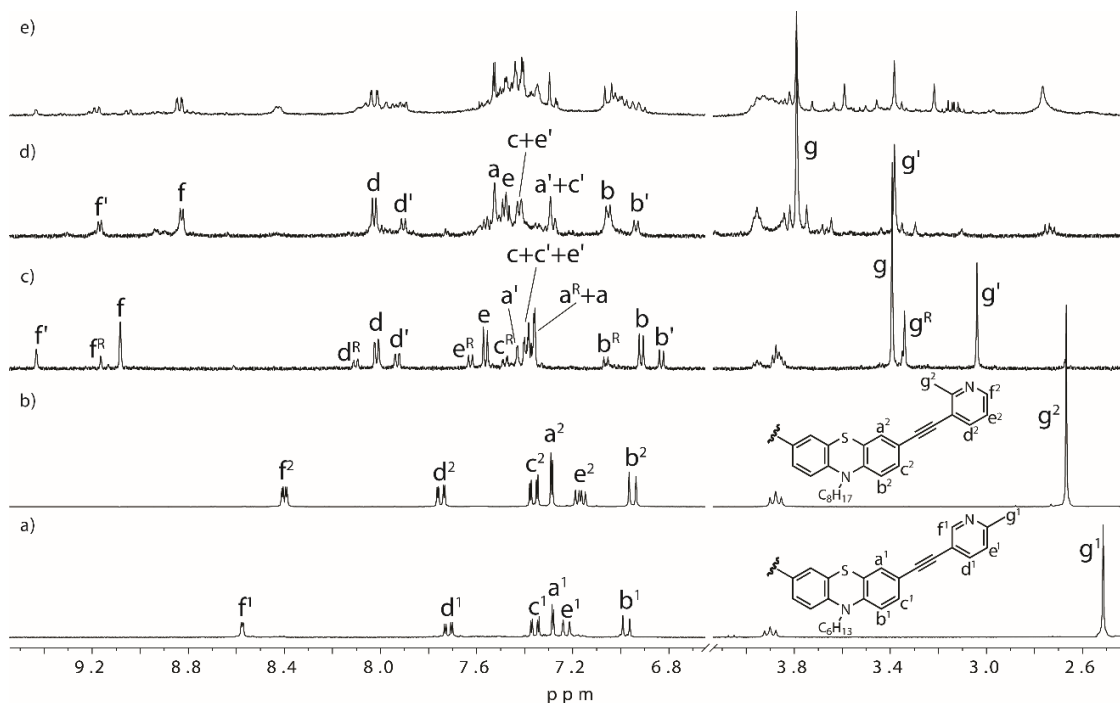

Figure 3.22 ^{1}H NMR spectra (500 MHz, CD$_3$CN, 293 K) of a) **PL^1**, b) **PL^2** and c) bowl-shaped cage [Pd$_2$(**PL^1**)$_3$]$^{4+}$ and ring [Pd$_2$(**PL^1**)$_2$]$^{4+}$; d) bowl-shaped cage [Pd$_2$(**PL^2**)$_3$]$^{4+}$; e) assembly **PL^1**, **PL^2** with Pd^{II} in ratio of 1 : 1 : 1 (^{R} represnets ring).

found accompanied with many impurities. In this case, the heteroleptic assembly seems not favoured comparing to the acidone system which may originate from the bent nature of the phenothiazine backbone.
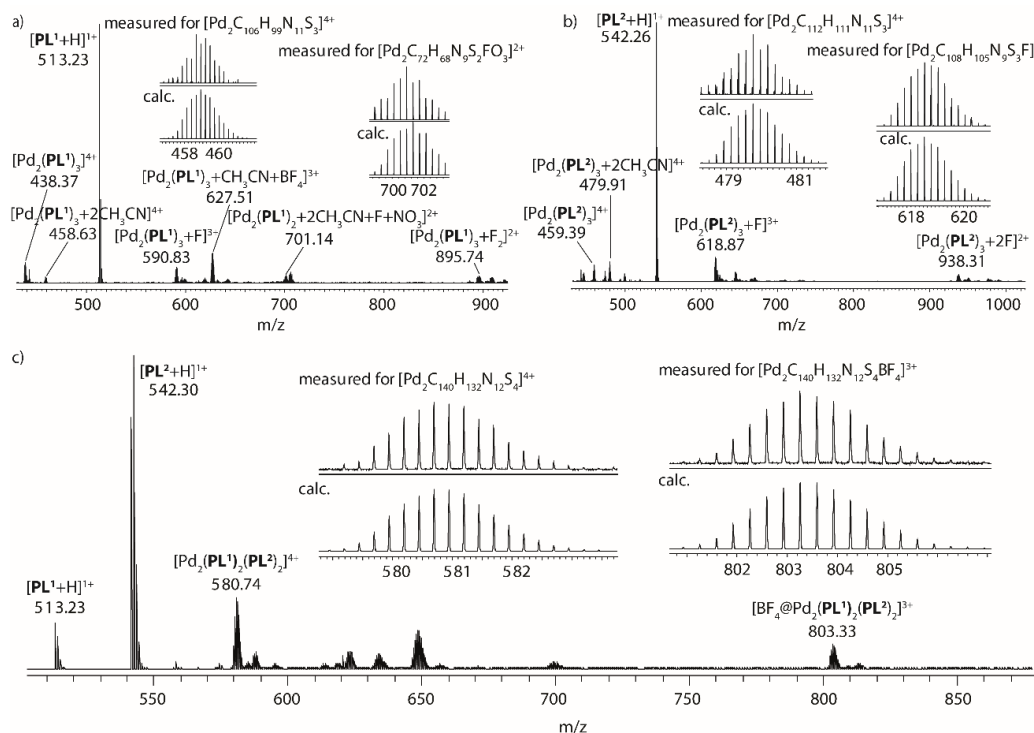

Figure 3.23 ESI-Mass spectra of assembly from a) PL^1, b) PL^2 and c) PL^1 and PL^2 with Pd^{II}.
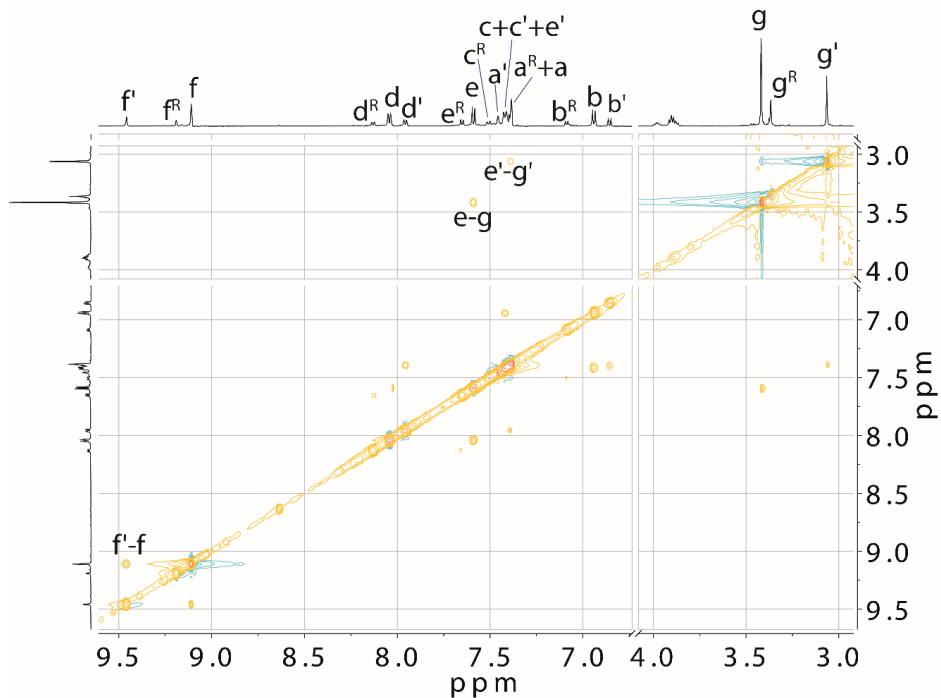

Figure 3.24 ^1H–^1H NOESY spectrum (600 MHz, CD_3CN) of mixture of $[Pd_2(PL^1)_2]^{4+}$ and $[Pd_2(PL^1)_3]^{4+}$ (–C_6H_{13} signals at 0.7–3.0 ppm omitted, ^{R} peaks represent $[Pd_2(PL^1)_2]^{4+}$), ^1H NMR ascriptions refer to PL^1 structure.

3.6 Reference

[1] a) C. Abad-Zapatero, S. S. Abdel-Meguid, J. E. Johnson, A. G. W. Leslie, I. Rayment, M. G. Rossmann, D. Suck and T. Tsukihara, *Nature*, **1980**, *286*, 33; b) M. G. Rossmann, E. Arnold, J. W. Erickson, *et al.*, *Nature*, **1985**, *317*, 145; c) M. Groll, L. Dizel, J. Lowe, D. Stock, M. Bochter, H. D. Bartunik and R. Huber, *Nature*, **1997**, *386*, 463.

[2] a) S. De, K. Mahata, M. Schmittel, *Chem. Soc. Rev.,* **2010**, *39*, 1555; b) M. L. Saha, S. De, S. Pramanik, M. Schmittel, *Chem. Soc. Rev.,* **2013**, *42*, 6860; c) S. Mukherjee, P. S. Mukherjee, *Chem. Commun.* **2014**, *50*, 2239; d) H. Li, Z. J. Yao, D. Liu, G. X. Jin, *Coord. Chem. Rev.,* **2015**, *293*, 139; e) Z. He, W. Jiang, C. A. Schalley, *Chem. Soc. Rev.,* **2015**, *44*, 779; f) G. R. Newkome, C. N. Moorefield, *Chem. Soc. Rev.,* **2015**, *44*, 3954.

[3] a) A. M. Garcia, D. M. Bassani, J.-M. Lehn, G. Baum, D. Fenske, *Chem. Eur. J.* **1999**, *5*, 1234; b) S. P. Argent, H. Adams, T. Riis-Johannessen, J. C. Jeffery, L. P. Harding, M. D. Ward, *J. Am. Chem. Soc.* **2006**, *128*, 72; c) N. K. Al-Rasbi, I. S. Tidmarsh, S. P. Argent, H. Adams, L. P. Harding, M. D. Ward, *J. Am. Chem. Soc.* **2008**, *130*, 11641.

[4] a) Y. R. Zheng, B. H. Northrop, H. B. Yang, L. Zhao, P. J. Stang, *J. Org. Chem.* **2009**, *74*, 3554; b) J. R. Li, H. C. Zhou, *Angew. Chem. Int. Ed.* **2009**, *48*, 8465; c) J. R. Li, H. C. Zhou, *Nat. Chem.* **2010**, *2*, 893; d) J. L. Wang, X. Li, X. Lu, I. F. Hsieh, Y. Cao, C. N. Moorefield, C. Wesdemiotis, S. Z. D. Cheng, G. R. Newkome, *J. Am. Chem. Soc.* **2011**, *133*, 11450.

[5] a) X. Lu, X. Li, Y. Cao, A. Schultz, J. L. Wang, C. N. Moorefield, C. Wesdemiotis, S. Z. D. Cheng, G. R. Newkome, *Angew. Chem. Int. Ed.* **2013**, *52*, 7728; b) R. Sarkar, K. Guo, C. N. Moorefield, M. J. Saunders, C. Wesdemiotis, G. R. Newkome, *Angew. Chem. Int. Ed.* **2014**, *53*, 12182; c) Q. F. Sun, S. Sato, M. Fujita, *Angew. Chem. Int. Ed.* **2014**, *53*, 13510.

[6] a) Y. Kubota, S. Sakamoto, K. Yamaguchi, M. Fujita, Proc. *Natl. Acad. Sci. U. S. A.* **2002**, *99*, 4854; b) K. Kumazawa, K. Biradha, T. Kusukawa, T. Okano, M. Fujita, *Angew. Chem. Int. Ed.* **2003**, *42*, 3909.

[7] a) H. B. Yang, K. Ghosh, B. H. Northrop, Y. R. Zheng, M. M. Lyndon, D. C. Muddiman, P. J. Stang, *J. Am. Chem. Soc.* **2007**, *129*, 14187; b) Y. Liu, A. Bruneau, J. He, Z. Abliz, *Org. Lett.* **2008**, *10*, 765; c) G. Koshkakaryan, K. Parimal, J. He, X. Zhang, Z. Abliz, A. H. Flood, Y. Liu, *Chem. Eur. J.* **2008**, *14*, 10211.

[8] a) Z. Y. Li, Y. Zhang, C. W. Zhang, L. J. Chen, C. Wang, H. Tan, Y. Yu, X. Li, H. B. Yang, *J. Am. Chem. Soc.* **2014**, *136*, 8577; b) S. Li, J. Huang, F. Zhou, T. R. Cook, X. Yan, Y. Ye, B. Zhu, B. Zheng, P. J. Stang, *J. Am. Chem. Soc.* **2014**, *136*, 5908; c) Y. Ye, S. P. Wang, B. Zhu, T. R. Cook, J. Wu, S. Li, P. J. Stang, *Org. Lett.* **2015**, *17*, 2804; d) P. Wei, X. Yan, F. Huang, *Chem. Soc. Rev.,* **2015**, *44*, 815.

[9] a) J.-P. Sauvage, J. Weiss, *J. Am. Chem. Soc.* **1985**, *107*, 6108; b) J. F. Nierengarten, C. O. Dietrich-Buchecker, J.-P. Sauvage, *J. Am. Chem. Soc.* **1994**, *116*, 375; c) D. A. Amabilino, C. O. Dietrich-Buchecker, J.-P. Sauvage, *J. Am. Chem. Soc.* **1996**, *118*, 3285; d) N. Solladie, J.-C. Chambron, J.-P. Sauvage, *J. Am. Chem. Soc.* **1999**, *121*, 3684.

[10] a) M. Yoshizawa, M. Nagao, K. Kumazawa, M. Fujita, *J. Organomet. Chem.* **2005**, *690*, 5383; b) M. Yoshizawa, J. Nakagawa, K. Kumazawa, M. Nagao, M. Kawano, T. Ozeki, M. Fujita, *Angew. Chem. Int. Ed.*

2005, *44*, 1810; c) Y. Yamauchi, M. Fujita, *Chem. Commun.* **2010**, *46*, 5897; d) Y. Yamauchi, M. Yoshizawa, M. Akita, M. Fujita, *J. Am. Chem. Soc.* **2010**, *132*, 960.

[11] M. Yamanaka, Y. Yamada, Y. Sei, K. Yamaguchi, K. Kobayashi, *J. Am. Chem. Soc.* **2006**, *128*, 1531.

[12] a) M. Schmittel, A. Ganz, *Chem. Commun.* **1997**, 999; b) M. Schmittel, A. Ganz, D. Fenske, *Org. Lett.* **2002**, *4*, 2289; c) M. Schmittel, H. Ammon, V. Kalsani, A. Wiegrefe, C. Michel, *Chem. Commun.* **2002**, 2566; d) M. Schmittel, V. Kalsani, D. Fenske, A. Wiegrefe, *Chem. Commun.* **2004**, *5*, 490; (e) M. Schmittel, V. Kalsani, J. W. Bats, *Inorg. Chem.* **2005**, *44*, 4115; f) M. Schmittel, K. Mahata, *Angew. Chem. Int. Ed.* **2008**, *47*, 5284; g) M. Schmittel, K. Mahata, *Inorg. Chem.* **2009**, *48*, 822; h) J. Fan, J. W. Bats, M. Schmittel, *Inorg. Chem.* **2009**, *48*, 6338; i) K. Mahata, M. Schmittel, *J. Am. Chem. Soc.* **2009**, *131*, 16544.

[13] Y. R. Zheng, Z. Zhao, M. Wang, K. Ghosh, J. B. Pollock, T. R. Cook and P. J. Stang, *J. Am. Chem. Soc.* **2010**, *132*, 16873.

[14] W. M. Bloch, Y. Abe, J. J. Holstein, C. M. Wandtke, B. Dittrich, G. H. Clever, *J. Am. Chem. Soc.* **2016**, *138*, 13750.

[15] M. Han, R. Michel, B. He, Y. S. Chen, D. Stalke, M. John, G. H. Clever, *Angew. Chem. Int. Ed.* **2013**, *52*, 1319.

[16] a) S. Freye, R. Michel, D. Stalke, M. Pawliczek, H. Frauendorf, G. H. Clever, *J. Am. Chem. Soc.* **2013**, *135*, 8476; b) M. Yoshizawa, M. Tamura, M. Fujita, *Angew. Chem. Int. Ed.* **2007**, *46*, 3874.

[17] R. Zhu, J. Lübben, B, Dittrich, G. H. Clever, *Angew. Chem. Int. Ed.* **2015**, *54*, 2796.

[18] a) M. Frank, J. Hey, I. Balcioglu, Y. S. Chen, D. Stalke, T. Suenobu, S. Fukuzumi, H. Frauendorf, G. H. Clever, *Angew. Chem. Int. Ed.* **2013**, *52*, 10102; b) M. Frank, L. Krause, R. H. Irmer, D. Stalke, G. H. Clever, *Dalton Trans.,* **2013**, *42*, 15906.; c) S. Löffler, J. Lübben, L. Krause, D. Stalke, B. Dittrich, G. H. Clever, *J. Am. Chem. Soc.* **2015**, *137*, 1060; d) S. Löffler, J. Lübben, A. Wuttke, R. A. Mata, M. John, B. Dittrich, G. H. Clever, *Chem. Sci.* **2016**, *7*, 4676.

[19] Shivakumaraiah, N. M. N. Gowda, *J. Chem. Res.* **2005**, *3,* 505.

[20] S.-Y.Chang, H.-Y. Jang, K.-S. Jeong, *Chem. Eur. J.* **2004**, *10*, 4358.

[21] T. Rama, C. Alvariño, O. Domarco, C. Platas-Iglesias, V. Blanco, M. D. García, C. Peinador, J. M. Quintela, *Inorg. Chem.* **2016**, *55*, 2290.

[22] Q. Zhang, L. He, J.-M. Liu, W. Wang, J. Zhang, C.-Y. Su, *Dalton Trans.,* **2010**, *39*, 11171.

[23] F. A. Pereira, T. Fallows, M. Frank, A. Chen, G. H. Clever, *Z. Anorg. Allg. Chem.* **2013,** *639,* 1598.

[24] M. Frank, L. Krause, R. Herbst-Irmer, D. Stalke, G. H. Clever, *Dalton Trans.,* **2014**, *43*, 4587.

[25] E. Bosch, C. L. Barnes, *Organometallics* **2000**, *19*, 5522.

Chapter 4:

Self-Assembled Coordination Cages Based on Multi-Dentate Ligands

In this chapter, a self-assembled [Pd$_3$**L^2**$_4$] cage was achieved and dimerized into an interpenetrated cage [5Cl@Pd$_6$**L^2**$_8$] upon addition of 2.5 equivalents of halide anions (X = Cl$^-$, Br$^-$). The formation and characterization of these two different structures are comprehensively explained by NMR spectroscopy, ESI-MS spectrometry and X-ray structures (molecular modeling showing in the following because the refinement of the structures has not been completed yet). Related experiments were also done with one unsymmetrical ligand **L^3** based on both carbazole and acridone backbones and a relatively longer ligand **L^4** based on three carbazole backbones.

4.1 Introduction

Self-assembly of cage-like complexes[1,2] from organic ligands and transition metal ions has become a chasing theme of supramolecular chemistry because of not only their fascinating architectures but also their promising applications in catalysis,[3] recognition,[4] separation[5] and drug delivery systems.[6]

In the last few decades, extensive research has been carried out on discrete supramolecular assemblies M$_x$**L**$_y$.[7,8] The use of metal ions with suitable coordination geometry and multidentate binding subunits open avenues towards a range of novel structures with special properties. Structural variation of the coordination cages was realized by varying the metal-to-ligand ratio without the use of a template or guest in the Chang group.[9] As they reported, the self-assembly from an "E-shaped" tris-monodentate ligand bis(pyridin-3-ylmethyl) pyridine-3,5-dicarboxylate, **4.1**, and Pd^{II} at ratios of 1 : 2 and 3 : 4 yielded exclusive formations of the "spiro-type" [Pd$_2$(**4.1**)$_2$] macrocycle and the quadruple-stranded "double-decker" [Pd$_3$(**4.1**)$_4$] coordination cage, respectively (Figure 4.1). Furthermore, complexes [Pd$_2$(**4.1**)$_2$] and [Pd$_3$(**4.1**)$_4$] are interconvertible when proper amounts of Pd^{II} or ligand **4.1** are added. The fresh structure of [Pd$_3$(**4.1**)$_4$] could encapsulate two halide ions (F$^-$, Cl$^-$, or Br$^-$), one in each of the cavities. This kind of [Pd$_3$**L**$_4$] architecture has also been reported by Pfeffer in collaboration with the Clever group. In their system, four tris-monodentate fused [6]polynorbornane-based ligands assembled into [Pd$_3$**L**$_4$] cages with palladium ions which were demonstrated by ^{1}H NMR spectra, HRMS and simulated by PM6 geometry optimization.[10]

Coordination cage [M$_6$**L**$_8$] is a commom species which usually possesses an octahedral or spherical structure in which six metal ions occupy the apexes and eight ligands lay on the eight sides.[11,12] As an example from the Shionoya group, the novel disk-shaped tris-monodentate ligand **4.2** was obtained comprising of a central hexaphenylbenzene core whose six 4-substituted peripheral rings alternate between 3-pyridyl and methyl

groups. The ligand **4.2** formed 10 structurally equivalent coordination cages $[M_6(\textbf{4.2})_8]^{12+}$ with a series of transition metal ions via self-assembly processes (Figure 4.2).[11d] Since the metal ions at the six apexes can be replaced with preservation of the architecture, the metal-dependent functions such as magnetic, redox, optical and dynamic properties can be anticipated in the further research. Size- or shaped-selective dynamic molecular recognition and metal-triggered chemical reactions are possible applications due to the large hollow structure surrounded by organic and inorganic components. Very recently, Crowley reported multicavity $[Pd_n\textbf{L}_4]^{2n+}$ (n = 2 − 4) cages based on long backbone ligands with segregated guest binding in different designed internal cavities.[13]
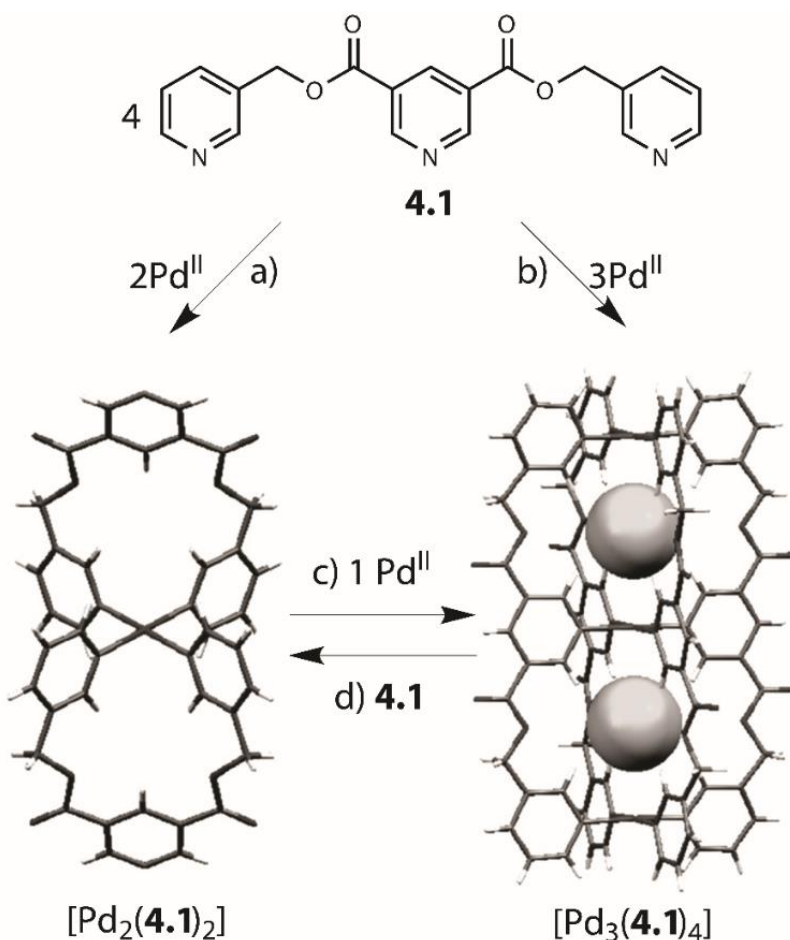
Figure 4.1 Metal-to-ligand stoichiometrically controlled exclusive synthesis of self-assembled a) "spiro-type" $[Pd_2(\textbf{4.1})_2]$, and b) "double-decker" $[Pd_3(\textbf{4.1})_4]$; Synthesis of c) complex $[Pd_3(\textbf{4.1})_4]$ from $[Pd_2(\textbf{4.1})_2]$, and d) complex $[Pd_2(\textbf{4.1})_2]$ from $[Pd_3(\textbf{4.1})_4]$, using additional amounts of Pd^{II} or ligand through dynamic reorganization processes. Copyright © 2014 WILEY-VCH Verlag GmbH & Co.

In this chapter, a new self-assembly interpenetrated $[M_6\textbf{L}_8]$ cage is obtained from eight tris-monodentate ligands based on two carbazole backbones with six square-planar-coordinated Pd^{II} ions which possesses five cavities that can each encapsulate a halide anion.
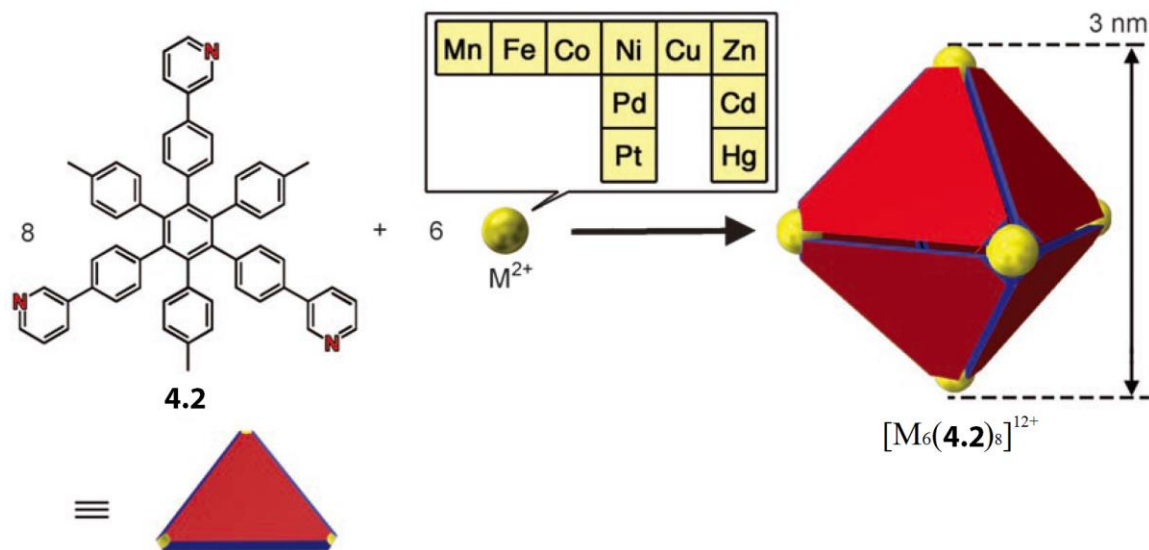
Figure 4.2 Schematic representation of the formation of $[M_6(\mathbf{4.2})_8]^{12+}$ coordination capsules formed from eight disk-shaped tris-monodentate ligands **4.2** and six divalent d^5–d^{10} transition-metal ions, M^{2+}. Copyright © 2006 WILEY-VCH Verlag GmbH & Co.

4.2 Ligand synthesis and self-assembly

Pertaining to those well shape-forming structures and their fascinating functionalities introduced above, it was anticipated that extending our supramolecular assembly from bis-monodentate ligands to multi-dentate ligands would provide such structures along with multi-functionalities. As a result, the design and successful synthesis of two tris-monodentate ligands, $\mathbf{L^2}$ (Figure 4.3) and $\mathbf{L^3}$ (Scheme 4.1) and one quadruple-monodentate ligand $\mathbf{L^4}$ (Scheme 4.2) are herein reported, in addition to the studies on their self-assembly behavior with metal cations.

Initially, the tris-pyridyl ligand $\mathbf{L^2}$ based on two carbazole backbones was synthesized and reacted with the palladium salt $[Pd(CH_3CN)_4](BF_4)_2$ to obtain a stable peanut-shaped cage $[Pd_3\mathbf{L^2}_4]$ which contains three metals and two pockets which can encapsulate at least two BF_4^- anions (Figure 4.2). At the first thought, polymerization could take place when half parts from two peanut-shaped cages interpenetrated each other in the presence of small halide anions. Interestingly, the subsequent addition of halide anions brought about the formation of interpenetrated cage $[Pd_6\mathbf{L^2}_8]$ from two peanut-shaped cages containing five pockets which are all occupied by halide anions.

4.2.1   Synthesis of ligand $\mathbf{L^2}$ and cages assembly

Ligand $\mathbf{L^2}$ was synthesized by a Sonogashira cross-coupling reaction of ligand **LA** introduced in Chapter 3 and 3,5-diethynylpyridine (Figure 4.3). Peanut-shaped cage $[Pd_3\mathbf{L^2}_4]$ was obtained stoichiometrically from

ligand L^2 treated with 0.75 equivalents of $[Pd(CH_3CN)_4](BF_4)_2$ in CD_3CN and heating the mixture at 70 °C for 5 h. The formation was indicated by the shift of signals observed in ^1H NMR spectroscopy (Figure 4.4a, b) and occurrence of peaks for the species $[Pd_3L^2_4]^{6+}$, $[Pd_3L^2_4+BF_4]^{5+}$, $[Pd_3L^2_4+2BF_4]^{4+}$, $[Pd_3L^2_4+3BF_4]^{3+}$ in the high resolution ESI mass spectrum (Figure 4.5a).
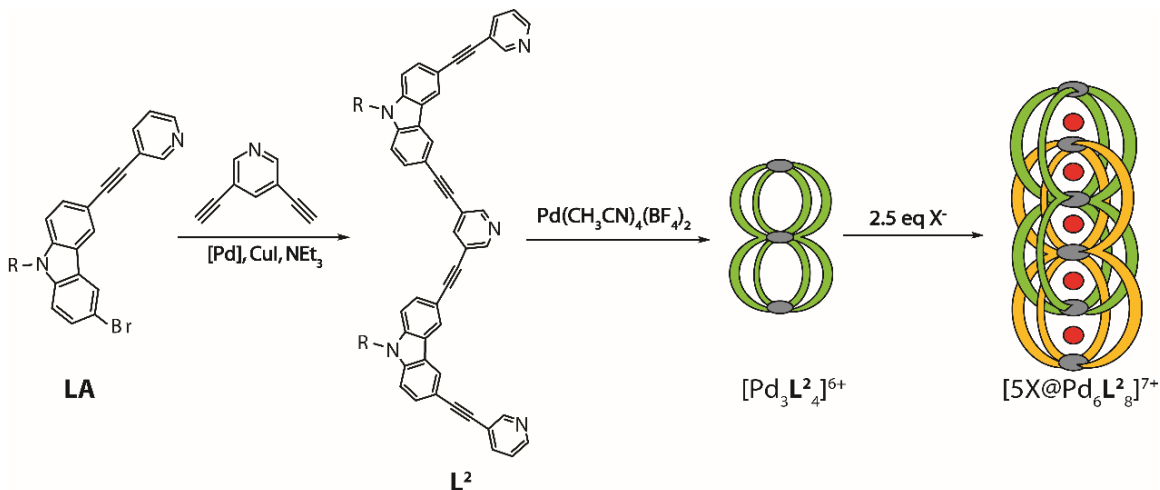

Figure 4.3 Synthesis of ligand L^2: 3,5-diethynylpyridine, CuI, $Pd(PPh_3)_2Cl_2$, NEt_3, 90 °C and stepwise assembly of the peanut-shaped cage $[Pd_3L^2_4]$ with the halide templated interpenetrated cage $[5X@Pd_6L^2_8]$ (X = Cl$^-$, Br$^-$).
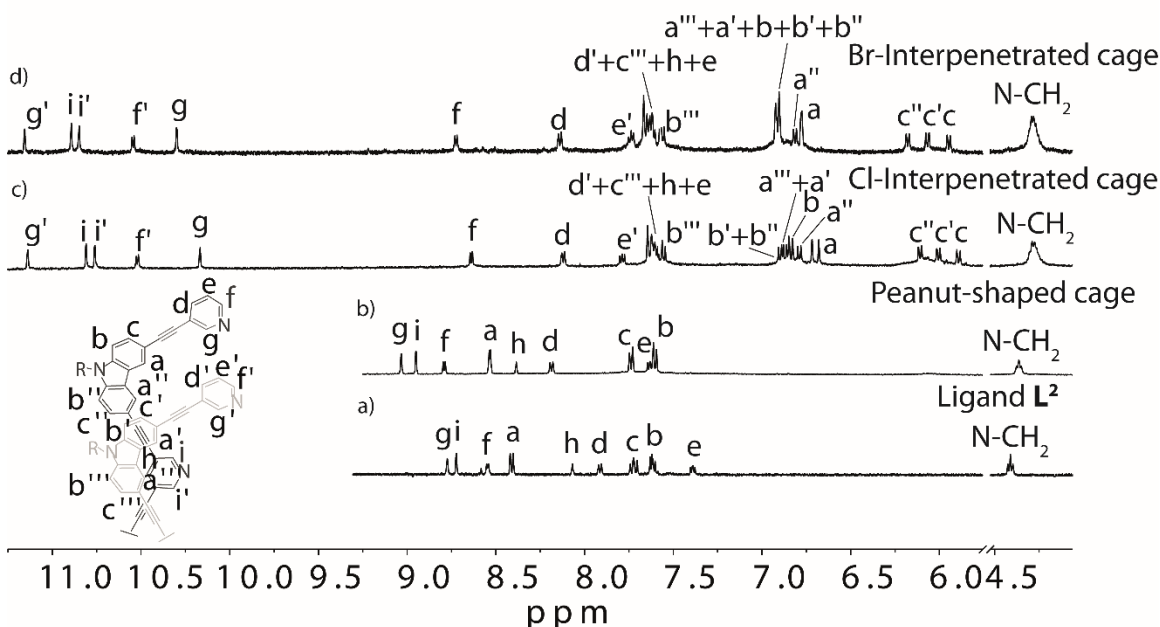
Figure 4.4 ^1H NMR spectra of a) ligand L^2; b) peanut-shaped cage $[Pd_3L^2_4]$ and interpenetrated cages $[Pd_6L^2_8]$ resulting from the reaction of 0.7 mM solutions of $[Pd_3L^2_4]$ with 2.5 equivalents of c) chloride and d) bromide in CD_3CN (298K, 500MHz, $N^nBu_4^+$ signals from 0.7−4.0 ppm omitted).
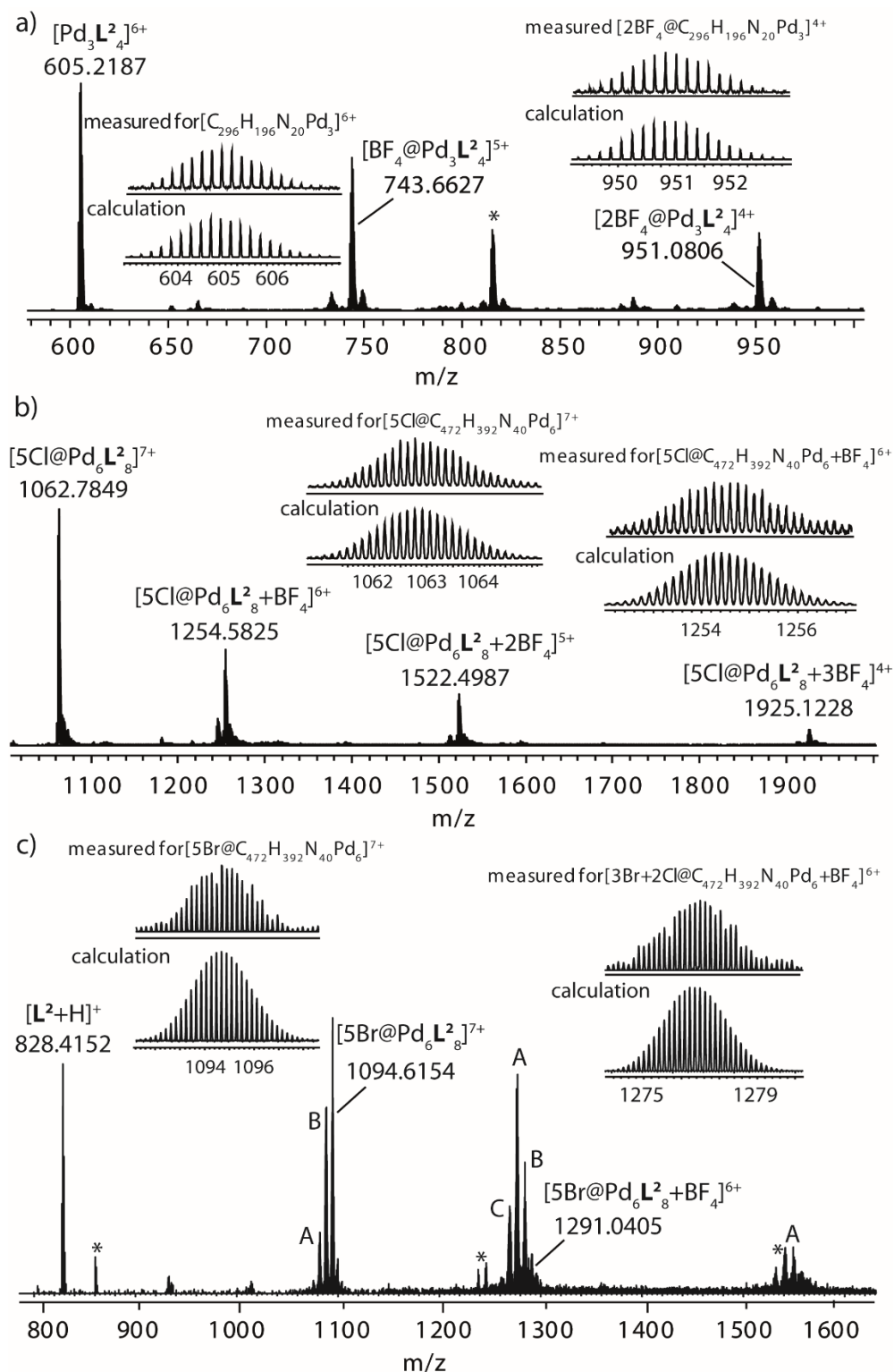
Figure 4.5 ESI-FTICR mass spectra of a) peanut-shaped cage $[n\mathrm{BF_4}@\mathrm{Pd_3L^2_4}]^{(6-n)+}$ with $n = 0-2$; b) interpenetrated-cage $\{[5\mathrm{Cl}@\mathrm{Pd_6L^2_8}]+n\mathrm{BF_4}\}^{(7-n)+}$ with $n = 0-3$ and c) interpenetrated-cage $\{[5\mathrm{Br}@\mathrm{Pd_6L^2_8}]+n\mathrm{BF_4}\}^{(7-n)+}$ with $n = 0-1$ (A = $[(3\mathrm{Br}+2\mathrm{Cl})@\mathrm{Pd_6L^2_8}+n\mathrm{BF_4}]^{(7-n)+}$ with $n = 0-2$, B = $[(4\mathrm{Br}+\mathrm{Cl})@\mathrm{Pd_6L^2_8}+n\mathrm{BF_4}]^{(7-n)+}$ with $n = 0-1$, C = $[(2\mathrm{Br}+3\mathrm{Cl})@\mathrm{Pd_6L^2_8}+\mathrm{BF_4}]^{6+}$, * = adducts with impurities).
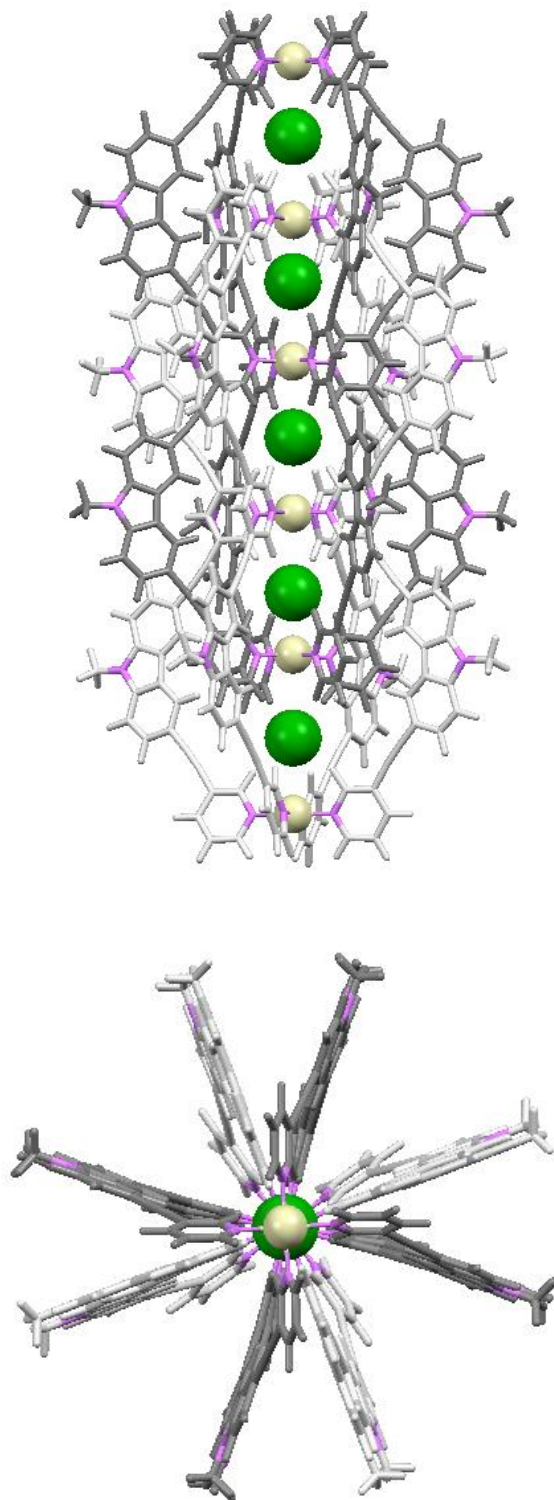
Figure 4.6 Side and top view of the geometry optimized structures of [5Cl@Pd$_6$**L**$^2_8$] (PM6), to simplify the calculations, the hexyl chain of carbazole backbones was replaced with a methyl substitute, color code: light yellow, Pd; green, Cl; purple, N.

As introduced in Chapter 2, the interpenetrated species of [3X@Pd$_4$L$^1_8$] was formed after addition of halide anions into the monomeric cage [Pd$_2$L$^1_4$]. Herein, after adding 2.5 equivalents of halide anions into the peanut-shaped cage [Pd$_3$L$^2_4$] solution and heating the reaction mixture at 70 °C for 5 h, the highly symmetric, interpenetrated species [5X@Pd$_6$L$^2_8$] was obtained stoichiometrically in which five halide anions occupied all of the five cavities. The structure of [5X@Pd$_6$L$^2_8$] was deduced by the splitting and relative chemical shifts of ^{1}H NMR signals, NOESY NMR analysis and was also assisted by molecular modelling. Intercatenated cage [Pd$_6$L$^2_8$] is characterized by a loss of symmetry in the ^{1}H NMR spectrum (Figure 4.4c and 4.4d). From the result of high resolution ESI mass spectrometry (Figure 4.5b and 4.5c), the interpenetrated cage can be unambiguously singled out by the signals for the species [5X@Pd$_6$L$^1_8$]$^{7+}$, {[5X@Pd$_6$L$^2_8$]+BF$_4$}$^{6+}$, {[5X@Pd$_6$L$^2_8$]+2BF$_4$}$^{5+}$ and {[5X@Pd$_6$L$^2_8$]+3BF$_4$}$^{4+}$.

From analysis of the NMR spectra of the interpenetrated cages (Figure 4.4c and 4.4d), the pyridine protons are splitting into two sets of signals except proton h which possesses only one chemical environment. As we can see, distinctive signal shifts of these pyridine protons pointing inside the cage's five pockets are identical to other reports in the Clever group.[14] However, a four-fold splitting of NMR signals from the carbazole backbones is envisaged in the NMR spectra which is consistent with the anticipated cage structure.

Since an X-ray structure of cage [5X@Pd$_6$L$^2_8$] has not be refined completely yet, the metallosupramolecular structure was supported by geometry optimization on the semiempirical PM6 level of theory[15] by using the software Gaussian 09[16] according to the acquired spectroscopic results and the crystal structures of reported self-assembly cages[14,18] in the Clever group (Figure 4.6). The mass spectrometric data of [Pd$_6$L$^2_8$] (Figure 4.5b) was in agreement with the calculated structure as well.

4.2.2 UV-Vis spectroscopy

Further characterization of the ligand and corresponding self-assembly cages was carried out by UV/Vis spectroscopy (Figures 4.7). Ligand **L^2** shows four absorption bands with maxima at 216 nm, 249 nm, 309 nm and 341 nm. The absorptions of the peanut-cage and interpenetrated cage shift slightly compared with the ligand which was attributed to coordination with the Pd^{II} metal ions.

4.2.3 Design and synthesis of tris-monodentate ligand **L^3**

As described in Chapter 2, the halide anions play an important role in the structure transformation.[17] Two monomeric cages interpenetrated with each other forming a dimeric cage where three halide anions sitting in the three cavities. From the reported work by Clever *et al*,[20] self-assembled interpenetrated cages from a bis-monodentate ligand based on the acridone backbone and Pd^{II} cations can convert into a new cage which encapsulate two small chloride anions in the outer two pockets and one tetrafluoroborate anion in the central pocket. It has also been presented in previous chapter that, the multicomponent, selective self-assembly is an essential phenomenon in many biological systems.[18,19] Chapter 3 shows that a significant amount of efforts

is required to achieve low symmetry coordination cages, by employing different ligands with steric constraints around the metal centers.

What will happen when two different backbones combine together forming one single unsymmetrical ligand? A possible metallo-supramolecular polymer is shown in Figure 4.8, representing a self-assembly only from the same backbone to form an endless framework after adding the appropriate templating anions into the system.

An unsymmetrical ligand L^3, containing two different backbone fragments (carbazole and acridone), was synthesized via the Sonogashira cross-coupling reaction of 1-{3-[(5-bromopyridin-3-yl)ethynyl]-6-(pyridin-3-ylethynyl)-9H-carbazol-9-yl}hexan-1-one and 10-hexanoyl-2-(pyridin-3-ylethynyl)-7[(trimethylsilyl)-ethynyl]acridin-9(10H)-one in the ratio of 1 : 1 which was introduced in detail in the following (Scheme 4.1). Characterization was completed using NMR spectroscopy and mass spectrometry.
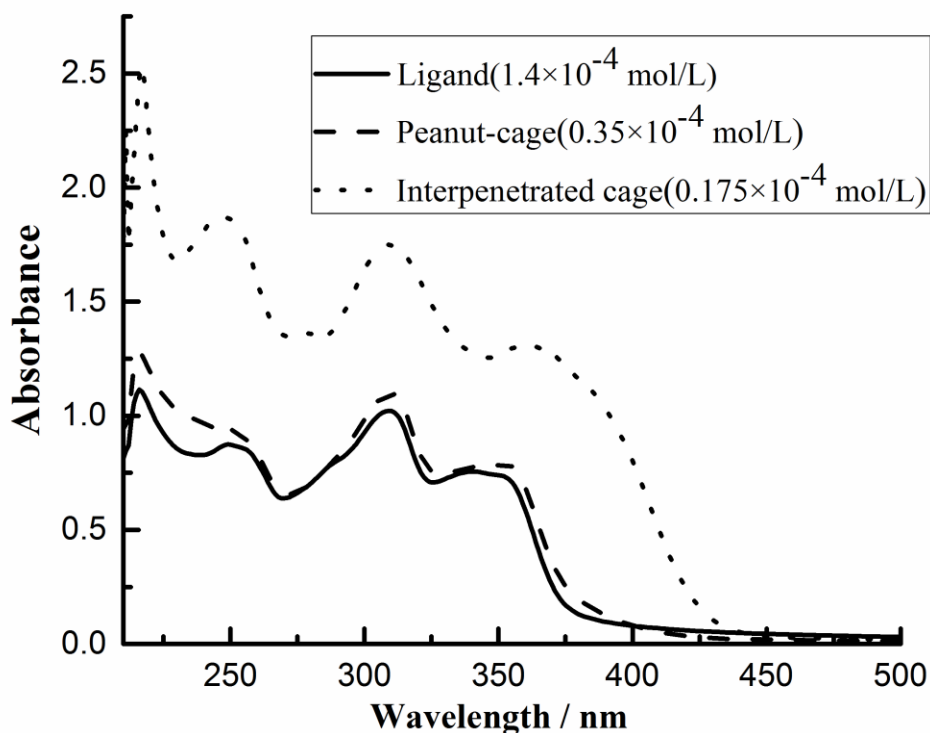
Figure 4.7 UV/Vis spectra of ligand L^2 (1.4×10^{-4} mol/L, solid line), peanut-cage (0.35×10^{-4} mol/L, dashed line) and Cl−interpenetrated cage (0.175×10^{-4} mol/L, dotted line).
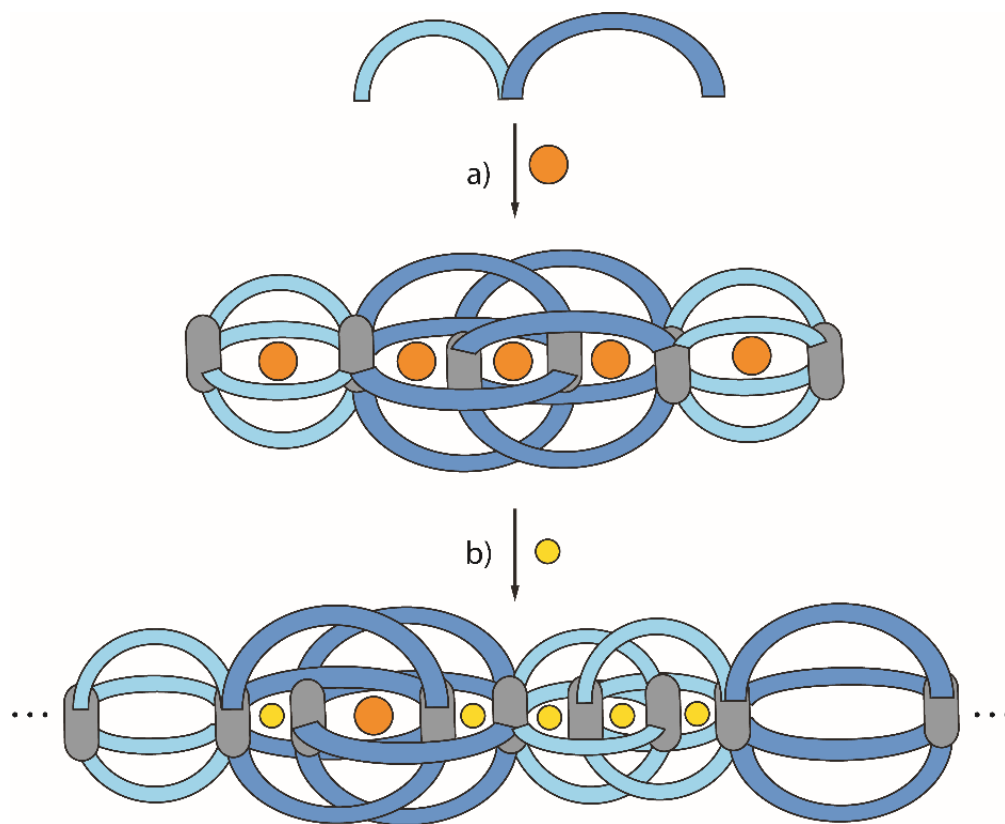
Figure 4.8 Graphical representations of proposed products: a) interpenetrated cages in the presence of large anions such as tetrafluoroborate anions and b) supramolecular polymer self-assembly in the presence of small anions such as halides from unsymmetrical ligand, orange ball represents large anions and yellow ball represents small anions.
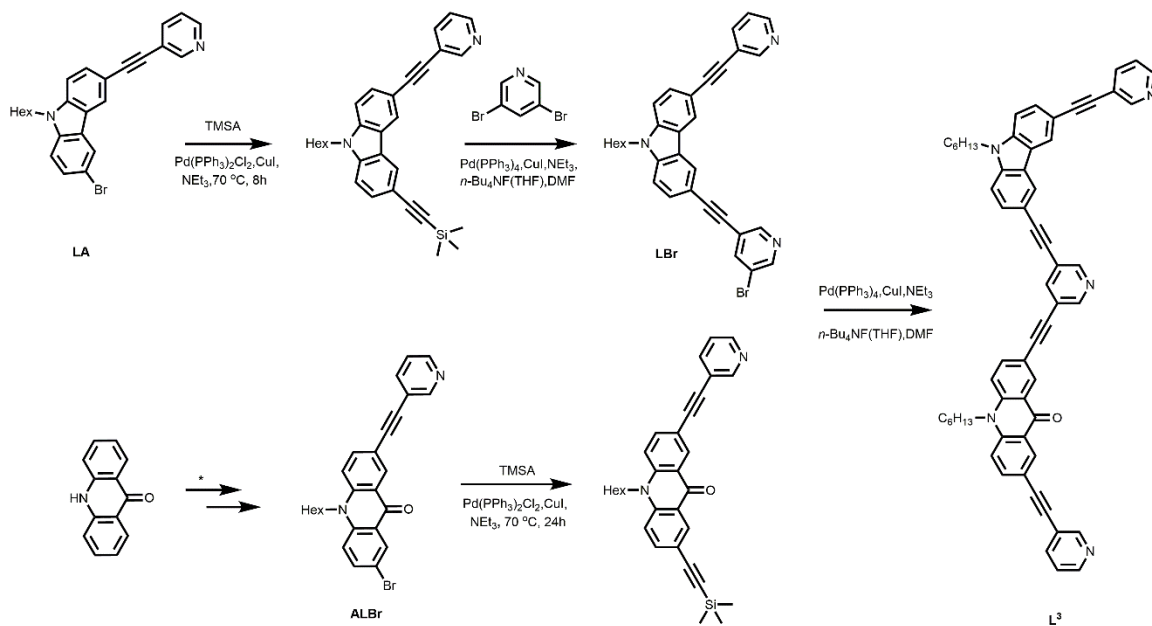
Scheme 4.1 Synthesis of the ligand $\mathbf{L^3}$, *: according to the literature.[18]

4.2.4 Self-assembly on ligand L^3

Heating a colorless solution of ligand L^3 and 0.75 equivalents of $[Pd(CH_3CN)_4](BF_4)_2$ in CD_3CN for 8 h at 70 °C produced a brown solution. The ^1H NMR spectrum presented broad signals which showed almost no signals (Figure 4.9b). It remained the same even heating much longer. In order to improve the reaction, conditions employing microwave irradiation were also trialed but the ^1H NMR spectrum again showed broad and weak signals which were too difficult to analyze (Figure 4.9c). It could be explained that intricate aggregations occurred in the presence of such a complex ligand and Pd^{II} cations. The ligand was not free in that solution but probably forms undefined Pd-L aggregate clusters.[21]

Furthermore, ESI-FTICR mass spectroscopy was done to investigate the composition of the system which turned out that there are two minor species of charged complexes, 7+ and 6+, besides the main signal of protonated ligand (Figure 4.10). These two charged species are composed of six palladium cations and eight ligands L^3 together with five or six tetrafluoroborate anions, respectively. This kind of $[Pd_6L_8]$ compound could be explained that, in the presence of tetrafluoroborate anions, two sets of longer acridone units interpenetrated each other similar as reported in the literature[20] and the shorter carbazole unit assembled into mono-cage similar as introduced in Chapter 2, arising from the five pockets that can each encapsulate an anion (Figure 4.8a). In order to realize the assumption in Figure 4.8b, halides such as chloride or bromide anions are added into the solution and heated overnight. Both the NMR spectroscopy and mass spectrometry gave no indication of larger assemblies.

As a result, the polymer assumption was not realized in this way which may be explained as entropy favors smaller compact structures with a minimum number of components rather than the polymeric structures.
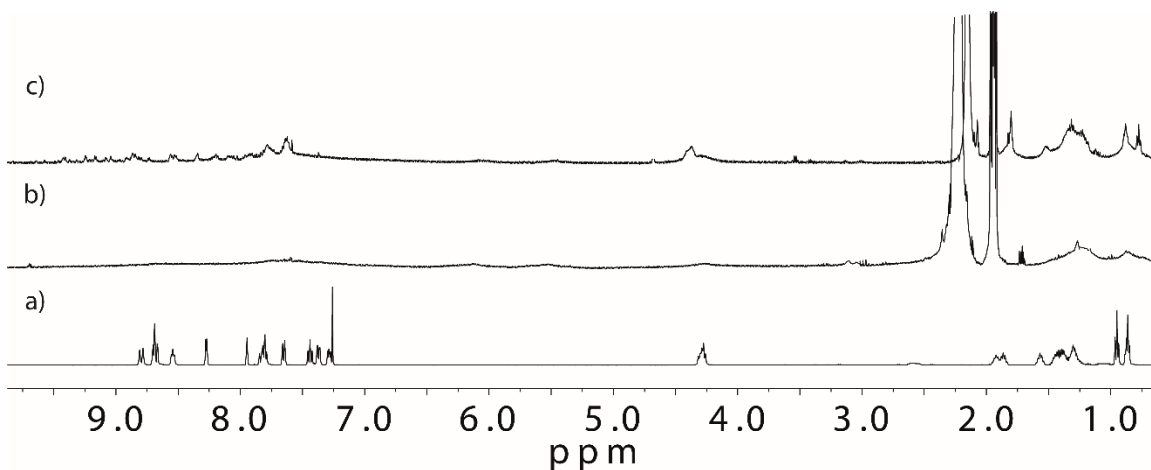
Figure 4.9 ^1H NMR spectra of a) ligand L^3 in $CDCl_3$; b) ligand L^3 and 0.75 equivalents of $[Pd(CH_3CN)_4](BF_4)_2$ heating at 70 °C for 8 h in CD_3CN; c) ligand L^3 and 0.75 equivalents of $[Pd(CH_3CN)_4](BF_4)_2$ under microwave reaction (70 °C, 150 W, 30 min) in CD_3CN.
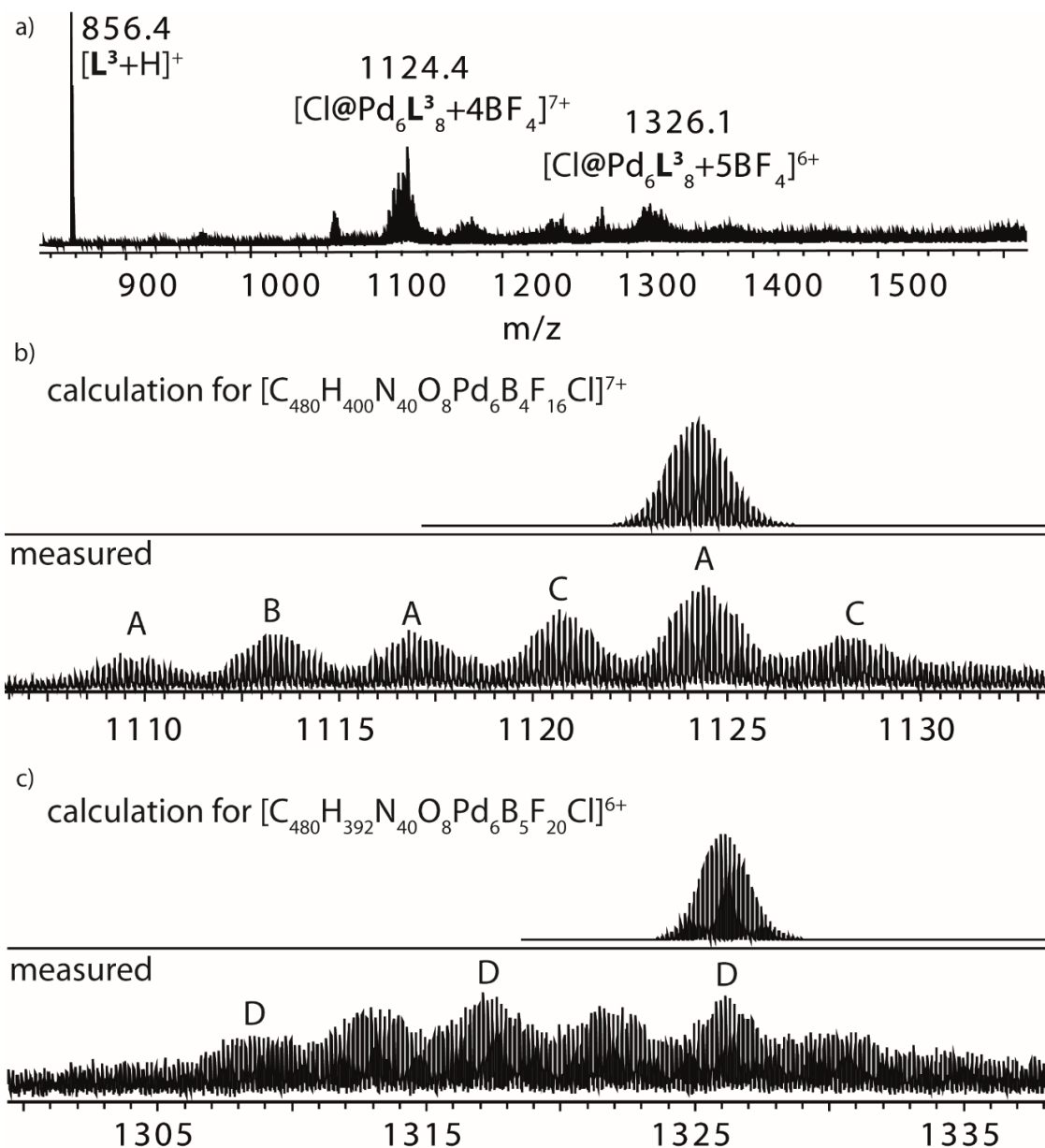
Figure 4.10 ESI-FTICR mass spectrum of reaction mixture a) whole spectrum; b) calculated (top) and measured (bottom) 7+ charged species (A = $[n\text{Cl}@\text{Pd}_6\mathbf{L^3}_8+(5−n)\text{BF}_4]^{7+}$ n = 1−3, B = $[(2\text{Cl}+\text{NO}_3)@\text{Pd}_6\mathbf{L^3}_8+2\text{BF}_4]^{7+}$, C = $[n\text{NO}_3@\text{Pd}_6\mathbf{L^3}_8+(5−n)\text{BF}_4]^{7+}$, n = 1 or 3; and c) calculated (top) and measured (bottom) 6+ charged species (D = $[n\text{Cl}@\text{Pd}_6\mathbf{L^3}_8+(6−n)\text{BF}_4]^{6+}$ n = 1−3).

4.2.5 Self-assembly on ligand $\mathbf{L^4}$

In addition, a longer ligand $\mathbf{L^4}$ containing three carbazole backbones was obtained via several steps of Sonogashira cross-coupling reaction (Scheme 4.2) and was characterized by NMR spectroscopy and mass spectrometry. The self-assembly behavior was investigated by combining ligand $\mathbf{L^4}$ and $[\text{Pd}(\text{CH}_3\text{CN})_4](\text{BF}_4)_2$ in the ratio of 1:1 in deuterated DMF. After heating the mixture solution at 70 °C overnight, a clear NMR

spectrum was obtained presenting down field shifting which was attributed to the coordination with the palladium cations (Figure 4.11). From the high resolution ESI mass spectroscopy, a triple-cavity cage was identified as the species $[nBF_4@Pd_4L^4{}_4]^{(8-n)+}$ ($n = 0-3$) (Figure 4.12). The disassembly and reassembly of this elongated ligand with Pd^{II} seems quite difficult after adding smaller halide anions into the system. The NMR spectrum only showed several broad and weak peaks upon addition chloride anions to the triple-cavity cage.
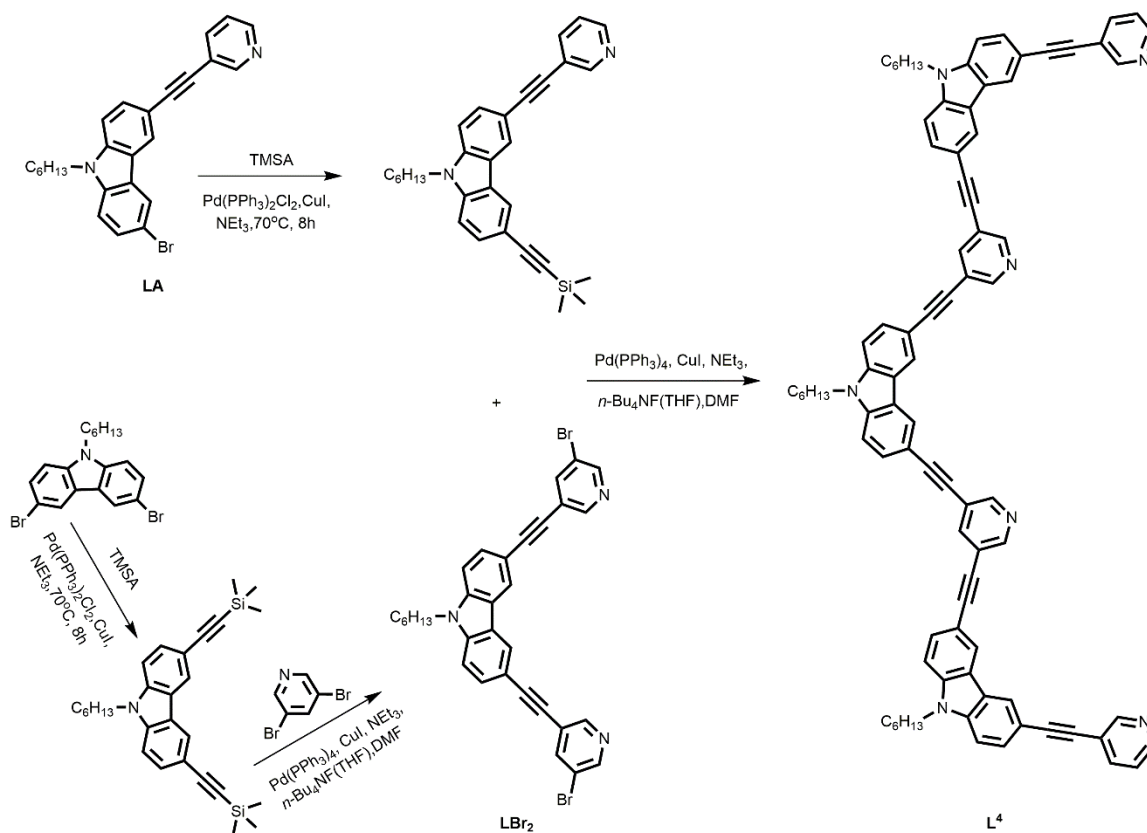
Scheme 4.2 Synthesis of the ligand L^4.

4.3 Conclusion

In conclusion, three novel multi-dentate pyridyl ligands were successfully synthesized and fully characterized which shows thriving potential as precursors in supramolecular chemistry.

According to the literature, the architecture of $[M_6L_8]$ assemblies always present a hollow molecular sphere in which six metal ions occupy the apexes and eight ligands lay on the eight adjoining edges. In this work, an innovative structural transformation is achieved by varying anions of different size: from a symmetrical peanut-shaped self-assembly $[M_3L^2{}_4]$ to a unique interpenetrated $[M_6L^2{}_8]$ cage possessing five cavities instead
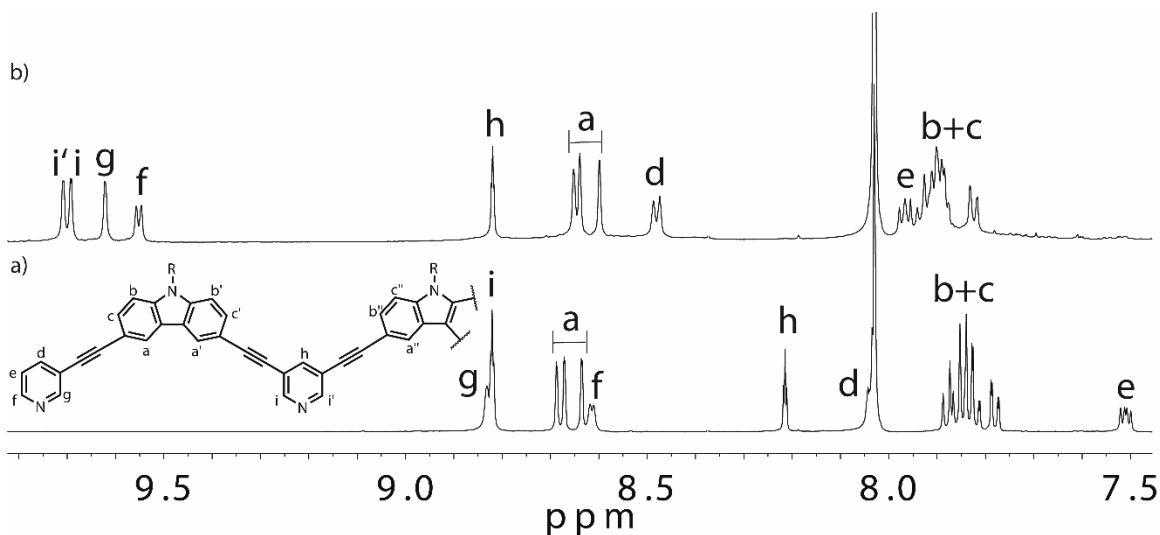
Figure 4.11 ^{1}H NMR spectra of a) ligand $\mathbf{L^4}$; b) triple-cavity cage [Pd$_4$L$^4_4$] in DMF-d_7, 298K, 600MHz.
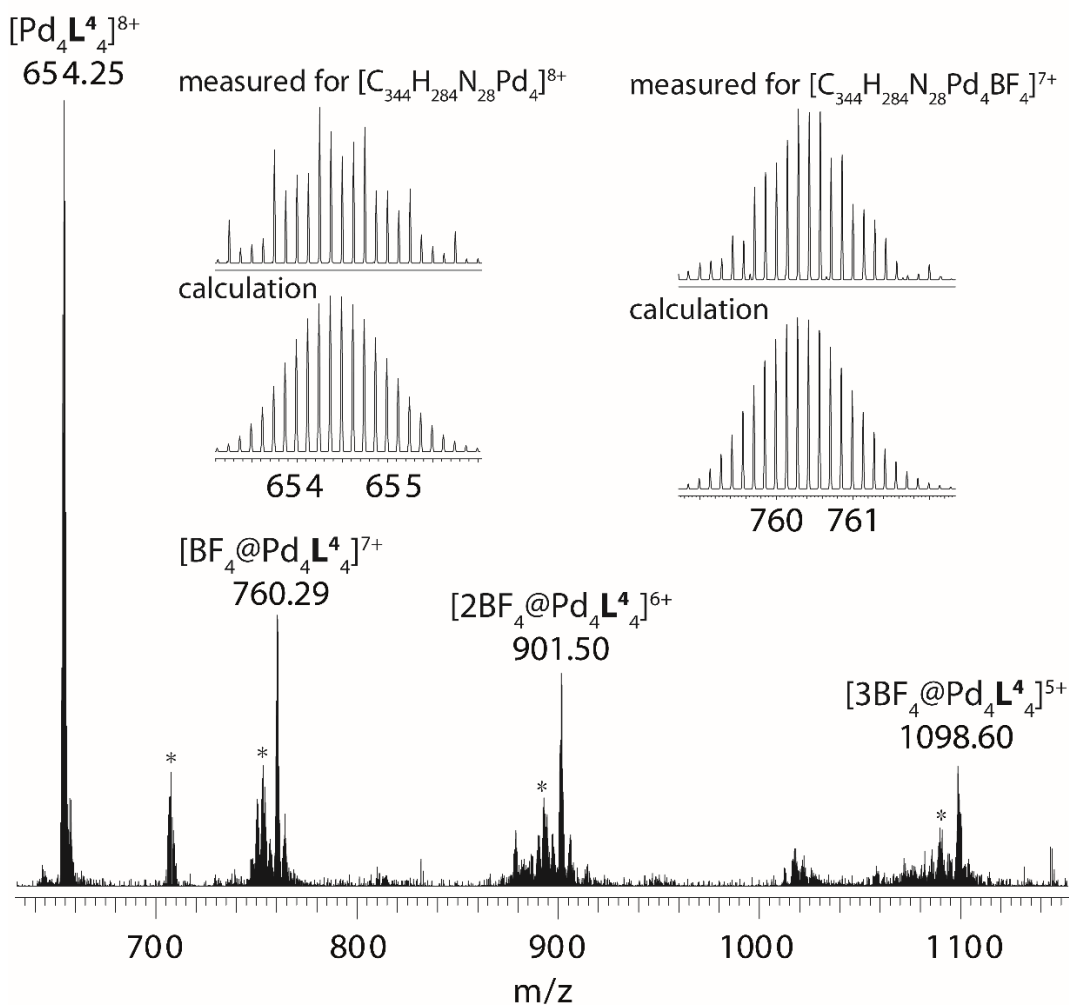
Figure 4.12 ESI-FTICR mass spectra of the triple-cavity cage [nBF$_4$@Pd$_4$L$^4_4$]$^{(8-n)+}$ with n = 0−3 (* = adducts with impurities).

of the typical octahedral structure that possesses a single cavity. Due to its densely packed and multi-pocket framework, the hexa-nuclear [$M_6L^2_8$] architecture is extremely promising in host-guest binding cooperativity.

Even though the self-assembly of discrete structures from ligands L^3 and L^4 was not so straightforward and led to polymeric mixtures/aggregates, the unique and beautiful composition of these two ligands still warrant further investigation for their potential applications in supramolecular self-assembly. Indeed, related research is currently underway in the Clever group.

4.4 Experimental section

4.4.1 Ligand synthesis
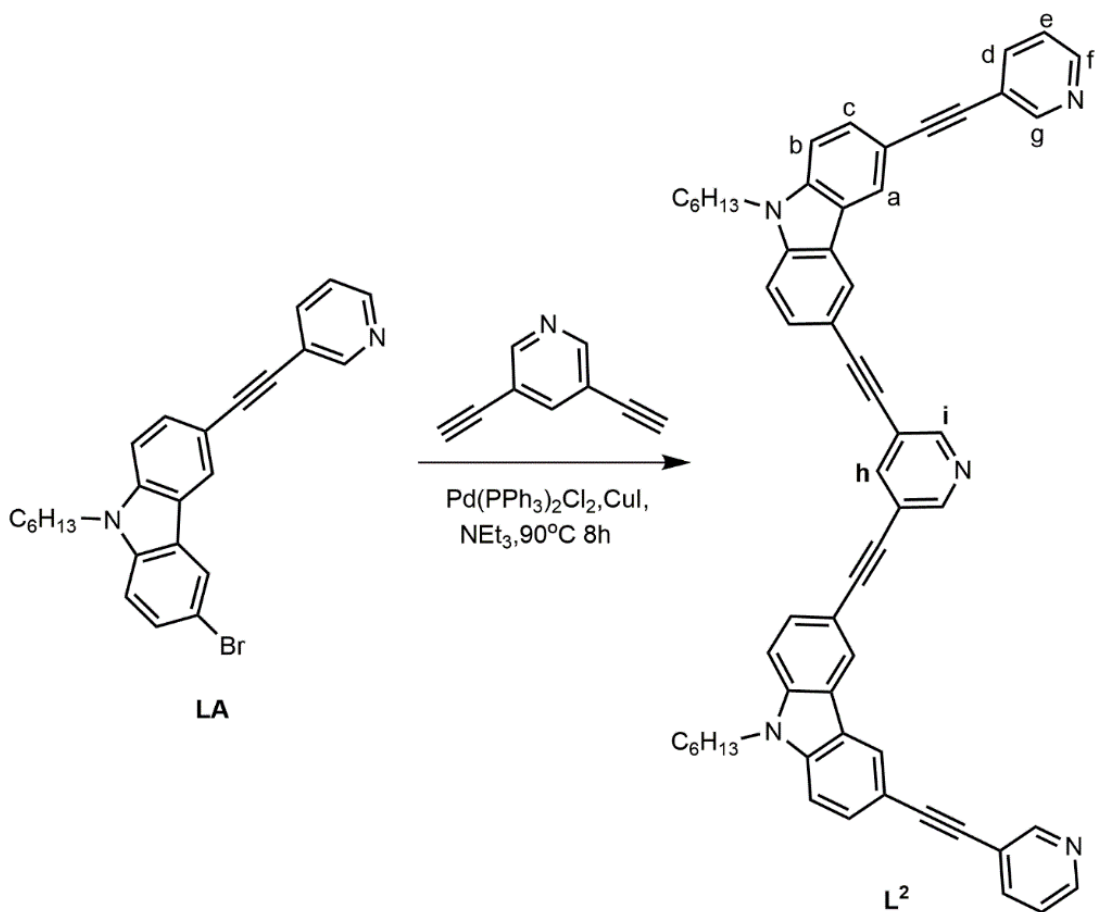
3,5-Bis{[9-hexyl-6-(pyridin-3-ylethynyl)-9H-carbazol-3-yl]ethynyl}pyridine (*L²*) was synthesized via Sonogashira coupling reaction same as L^1 in Chapter 2 using **LA** which was introduced in Chapter 3 and 3,5-diethynylpyridine[22] as starting materials. Yield, 37.5%.
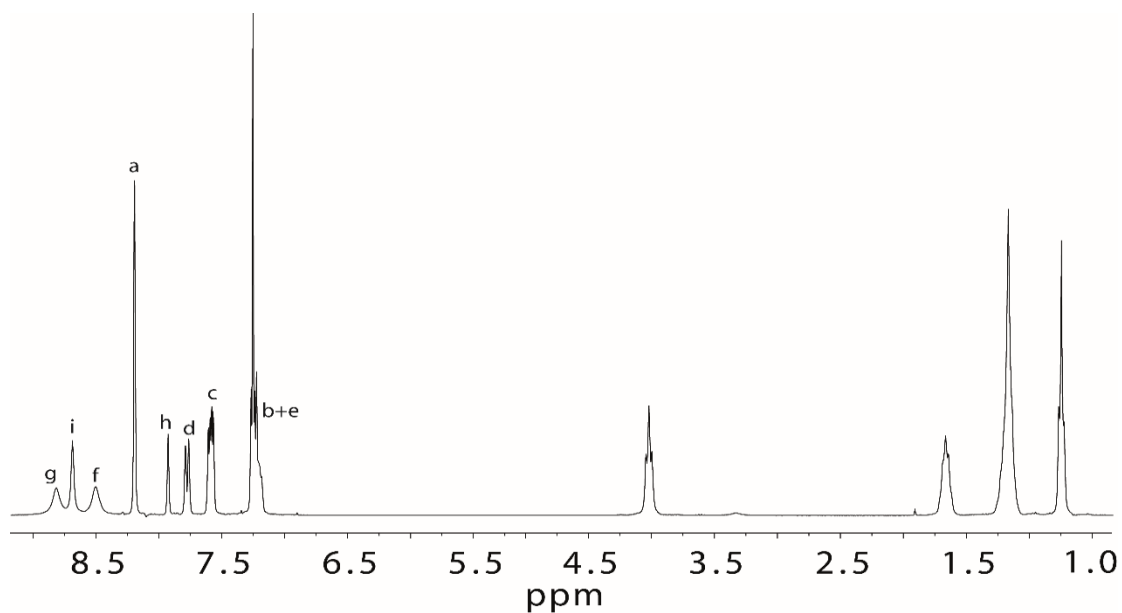
^{1}H NMR (300 MHz, CDCl$_3$): δ [ppm] = 8.82 (s, 2H), 8.69 (s, 2H), 8.51 (s, 2H), 8.20 (s, 4H), 7.93 (s, 1H), 7.78 (d, J = 7.4 Hz, 2H), 7.59 (dd, J = 8.5, 4.8 Hz, 4H), 7.27 (d, J = 3.8 Hz, 4H), 7.24 (d, J = 4.2 Hz, 2H), 4.11 (t, J = 7.1 Hz, 2H), 1. 08 – 1.70 (m, 4H), 1.32 – 1.17 (m, 12H), 0.84 (t, J = 6.5 Hz, 6H).
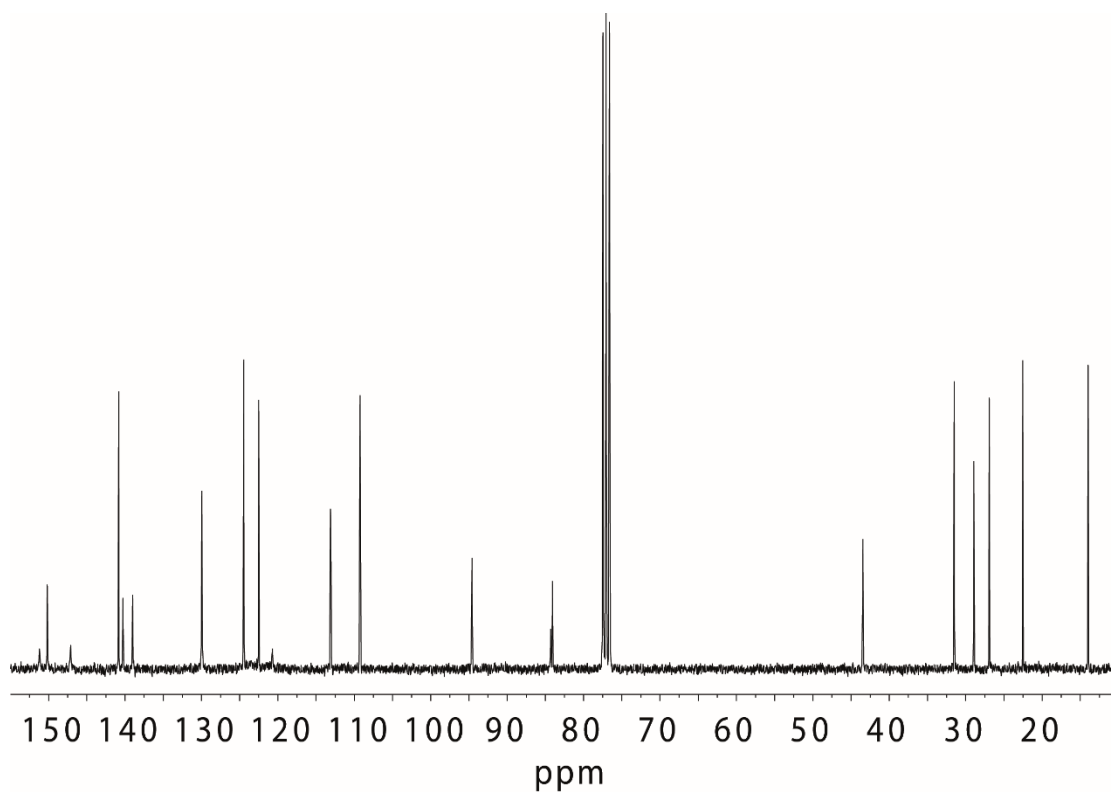
^{13}C NMR (75 MHz, CDCl$_3$): δ [ppm] = 151.30, 150.28, 147.23, 140.94, 140.38, 139.13, 130.07, 130.03, 124.58, 122.62, 120.82, 113.23, 113.18, 109.36, 94.77, 94.71, 84.42, 84.19, 43.57, 31.63, 29.05, 27.04, 22.65, 14.10.

ESI-FTICR-HRMS calculated for C$_{59}$H$_{50}$N$_5$ [M+H]$^+$ m/z 828.4086, found m/z 828.4066.
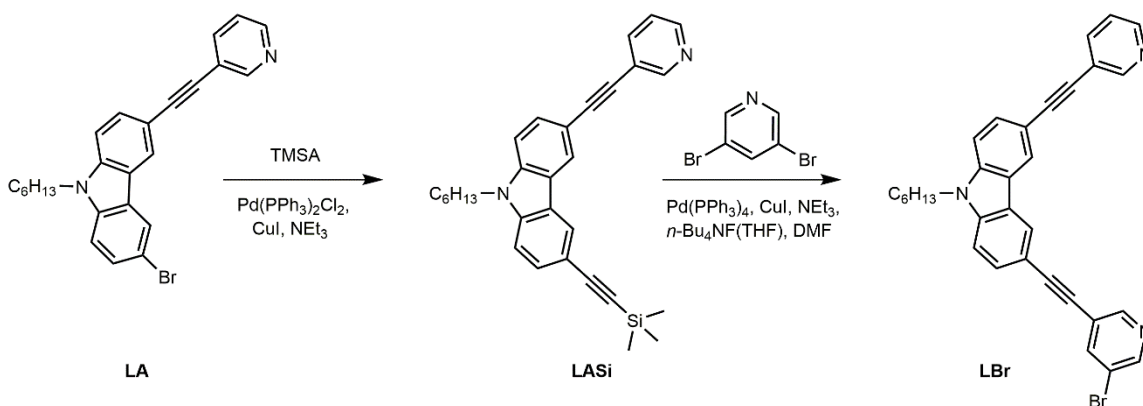
1-{3-[(5-bromopyridin-3-yl)ethynyl]-6-(pyridin-3-ylethynyl)-9H-carbazol-9-yl}hexan-1-one *(LBr)* was synthesized from LASi (1166.58 mg, 2.60 mmol) via Sonogashira coupling reaction with 3,5-dibromopyridine (686.99 mg, 2.90 mmol), copper(I) iodide (57.13 mg, 0.30 mmol), Pd(PPh3)4 (173.33 mg, 0.15mmol) and trimethylamine (0.44 mL, 3.10mmol) in DMF (18.00 mL). The mixture was thoroughly degassed and heated under a nitrogenatmosphere slowly to 85 °C. N^nBu_4F (756.35 mg, 2.86 mmol) in THF (3.00 mL) was added dropwise into the mixture over half an hour. TLC analysis demonstrated the reaction to be complete after N^nBu_4F addition. The reaction mixture was filtered through Celite and partitioned between ethyl acetate and 0.1 N HCl. The organic layer was washed with H_2O, dried over $MgSO_4$, and evaporated in vacuo. The residue was purified by flash chromatography on silica gel (*n*-hexane : ethylacetate = 2 : 1) to give LBr as a yellow solid product (1102.24 mg, 2.07 mmol, 79.6 %). LASi was used to synthesis LBr directly after Sonogashira reaction from LA with trimethylsilyl acetylene.
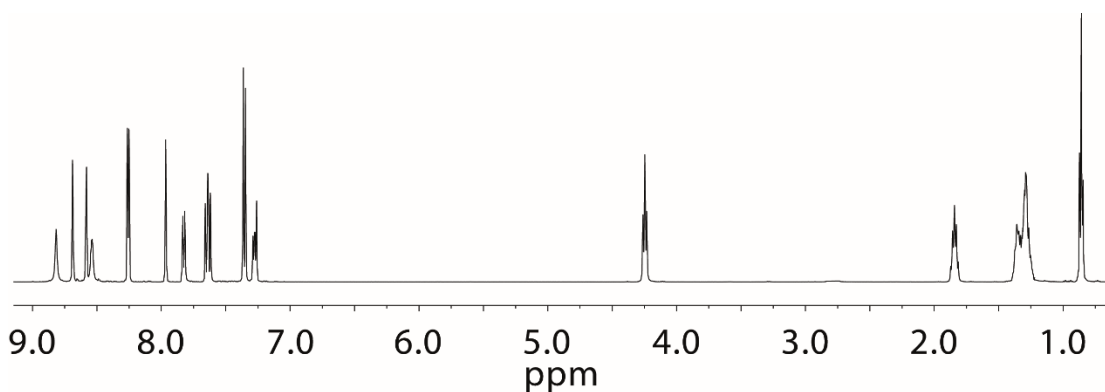
^{1}H NMR (500 MHz, CDCl3) δ [ppm] = 8.82 (s, 1H), 8.69 (d, *J* = 1.8 Hz, 1H), 8.58 (d, *J* = 2.2 Hz, 1H), 8.54 (d, *J* = 4.7 Hz, 1H), 8.26 (dd, *J* = 6.0, 1.5 Hz, 2H), 7.97 (t, *J* = 2.0 Hz, 1H), 7.83 (dt, *J* = 7.9, 1.9 Hz, 1H), 7.64 (ddd, *J* = 11.4, 8.5, 1.6 Hz, 2H), 7.36 (d, *J* = 8.5 Hz, 2H), 7.27 (dd, *J* = 8.5, 5.5 Hz, 1H), 4.25 (t, *J* = 7.3 Hz, 2H), 1.85 (q, *J* = 7.3 Hz, 2H), 1.41 – 1.22 (m, 6H), 0.86 (t, *J* = 6.9 Hz, 3H).
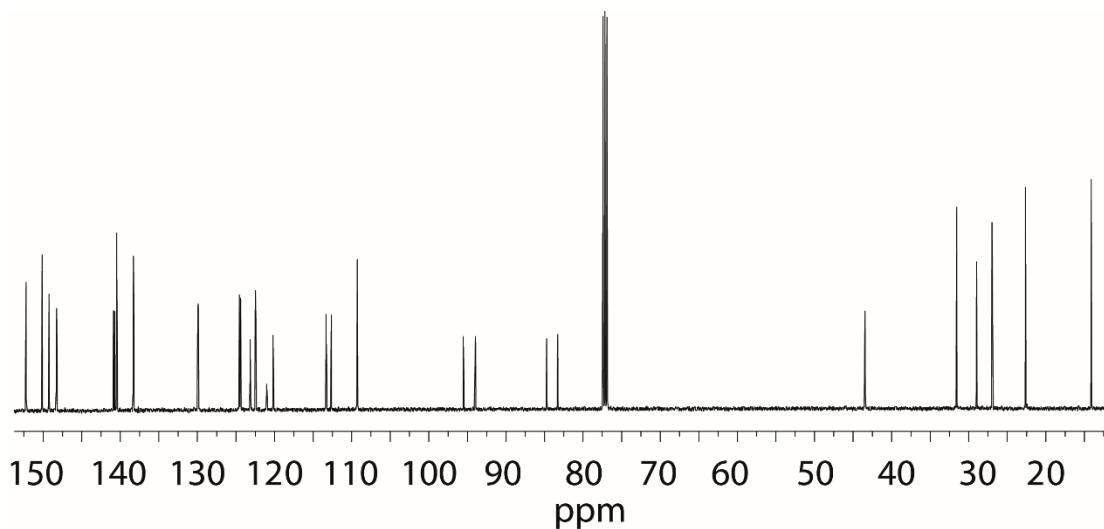
^{13}C NMR (125 MHz, CDCl$_3$) δ [ppm] = 152.21, 150.13, 149.24, 148.25, 140.87, 140.71, 140.47, 138.29, 129.95, 129.89, 124.55, 124.40, 123.14, 122.49, 122.42, 121.01, 120.19, 113.33, 112.65, 109.27, 109.26, 95.52, 93.94, 84.72, 83.29, 43.45, 31.57, 28.99, 26.98, 22.62, 14.11.
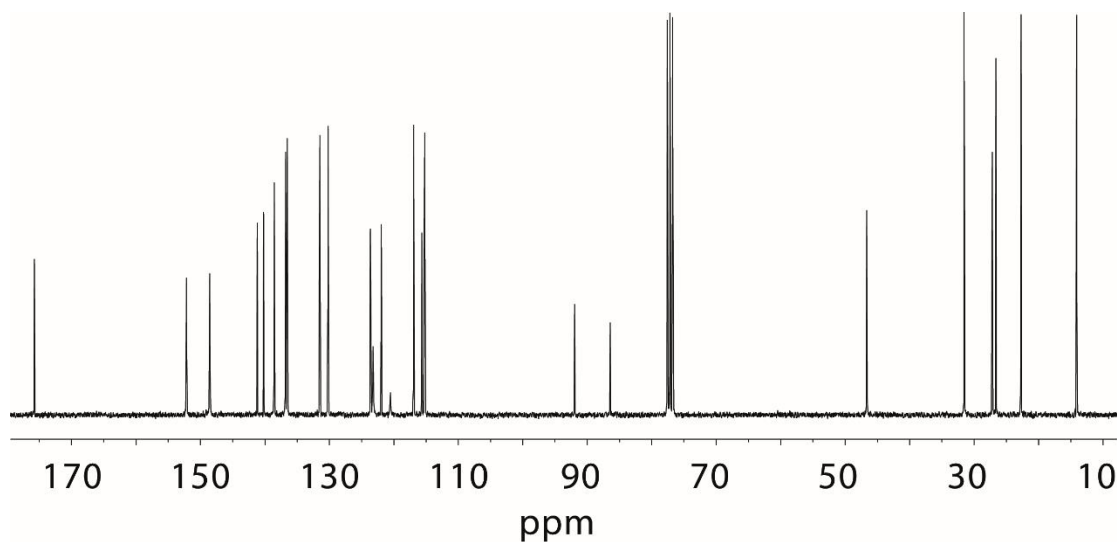
ESI-FTICR-HRMS calculated for C$_{32}$H$_{27}$N$_3$Br [M+H]$^+$ m/z 532.1388, found m/z 532.1402.
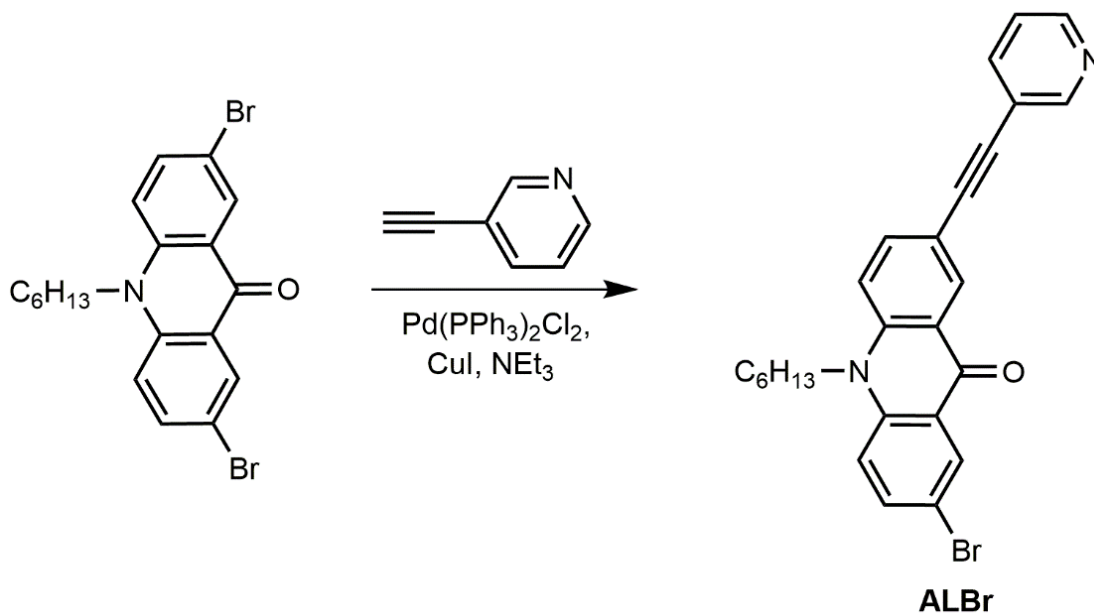
*2-Bromo-10-hexanoyl-7-(pyridin-3-ylethynyl)acridin-9(10H)-one (**ALBr**)* was synthesized via Sonogashira coupling reaction similar as **LA** in Chapter 3. Yield: 30.9%.
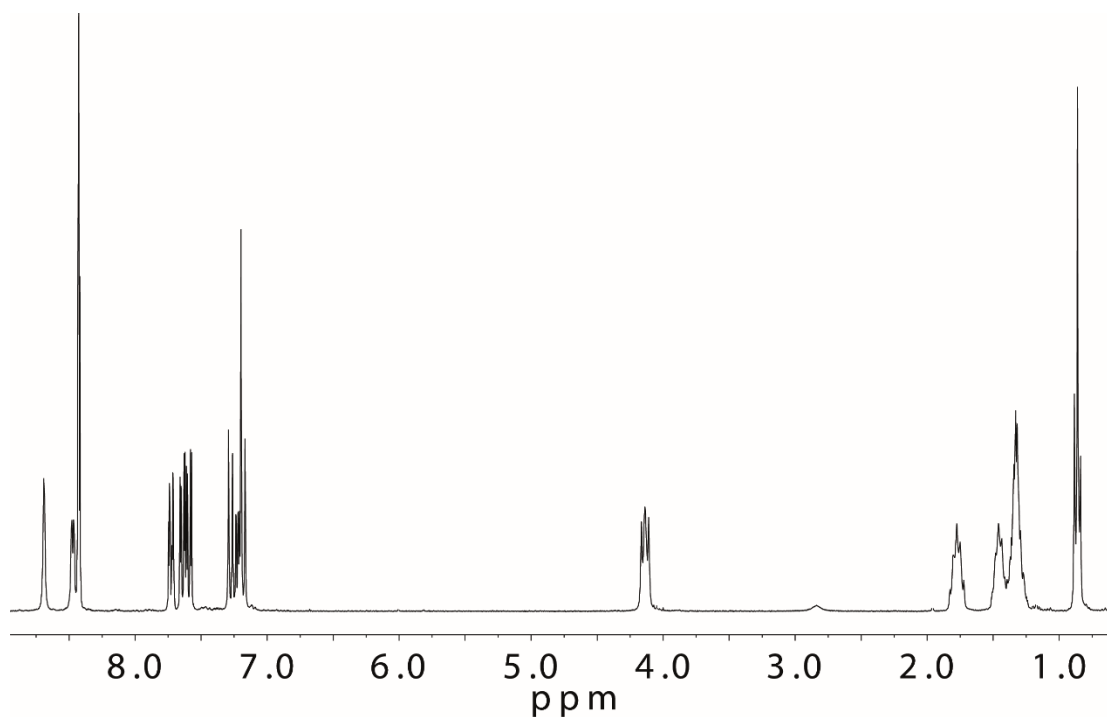
^{1}H NMR (300 MHz, CDCl$_3$) δ [ppm] = 8.75 (s, 1H), 8.53 (dd, J = 5.22, 1.74 Hz, 1H), 8.49 (t, J = 2.19Hz, 2H), 7.79 (dt, J = 7.9, 1.9 Hz, 1H), 7.70 (dd, J = 8.90, 2.16 Hz, 1H), 7.65 (dd, J = 9.17, 2.54 Hz, 1H), 7.34 (d, J = 9.10 Hz, 1H), 7.28 (ddd, J = 7.70, 4.85, 0.79 Hz, 1H), 7.24 (d, J = 8.02 Hz, 1H), 4.20 (t, J = 7.97 Hz, 2H), 1.91 – 1.75 (m, 2H), 1.51 (q, J = 7.1 Hz, 2H), 1.46 – 1.32 (m, 6H), 0.91 (t, J = 6.89 Hz, 3H).

^{13}C NMR (75 MHz, CDCl$_3$) δ [ppm] = 175.76, 152.17, 148.56, 141.18, 140.19, 138.55, 136.80, 136.53, 131.49, 130.21, 123.64, 123.23, 121.93, 120.54, 116.92, 115.67, 115.23, 115.13, 91.96, 86.44, 46.65, 31.55, 27.18, 26.61, 22.72, 14.09.

ESI-FTICR-HRMS calculated for C$_{26}$H$_{25}$N$_2$BrO [M+H]$^+$ m/z 459.1072, found m/z 459.1091.
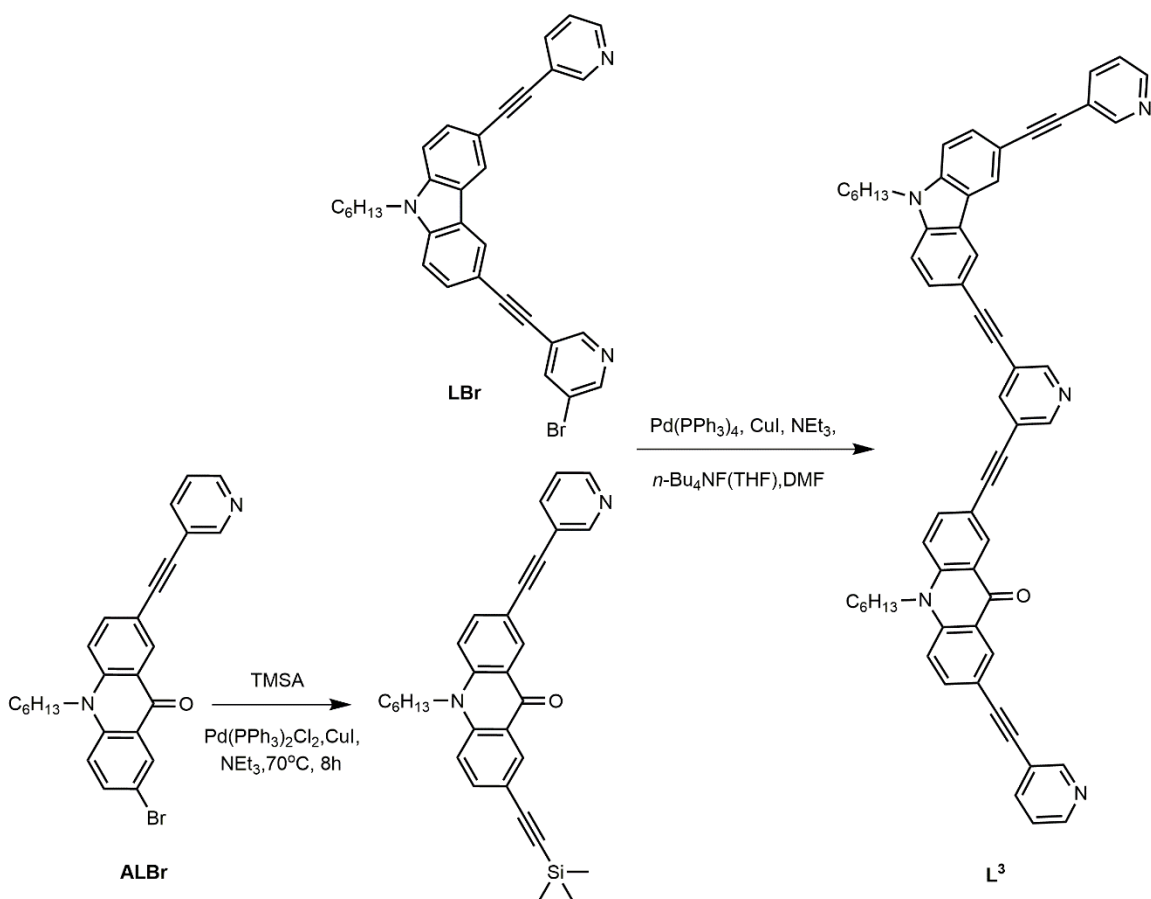
10-hexyl-2-{{5-{[9-hexyl-6-(pyridin-3-ylethynyl)-9H-carbazol-3-yl]ethynyl}pyridin-3-yl}ethynyl}7(pyridin-3-ylethynyl)acridin-9(10H)-one (**L³**) was synthesized via the modified Sonogashira coupling reaction similar as **LBr** but heated overnight. Yield: 85.4%.
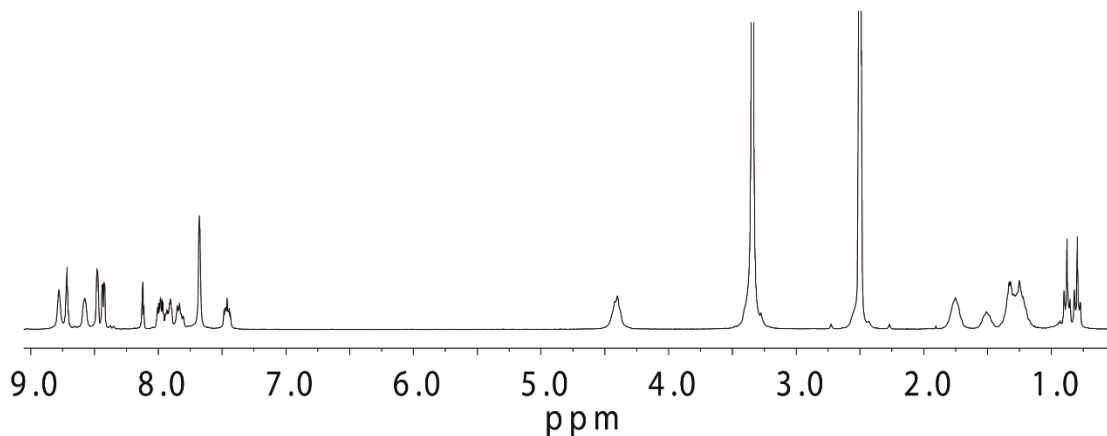
^{1}H NMR (300 MHz, DMSO-d_6) δ [ppm] = 8.78 (s, 2H), 8.72 (t, J = 2.0 Hz, 2H), 8.58 (s, 2H), 8.48 (dt, J = 3.0, 1.2 Hz, 2H), 8.43 (dd, J = 4.6, 2.2 Hz, 2H), 8.12 (t, J = 2.2 Hz, 1H), 7.99 (ddt, J = 8.0, 4.0, 1.9 Hz, 2H), 7.92 (ddd, J = 9.0, 3.5, 2.1 Hz, 2H), 7.83 (dd, J = 9.3, 4.9 Hz, 2H), 7.68 (dd, J = 2.5, 1.2 Hz, 4H), 7.46 (dddd,

$J = 7.7, 4.9, 2.7, 0.9$ Hz, 2H), 4.41 (t, $J = 7.3$ Hz, 4H), 1..87 – 1.75 (m, 4H), 1.59 – 1.51(m, 2H), 1.37 – 1.20 (m, 10H), 0.88 (t, $J = 7.5$ Hz, 3H), 0.79 (m, $J = 6.4$ Hz, 3H).
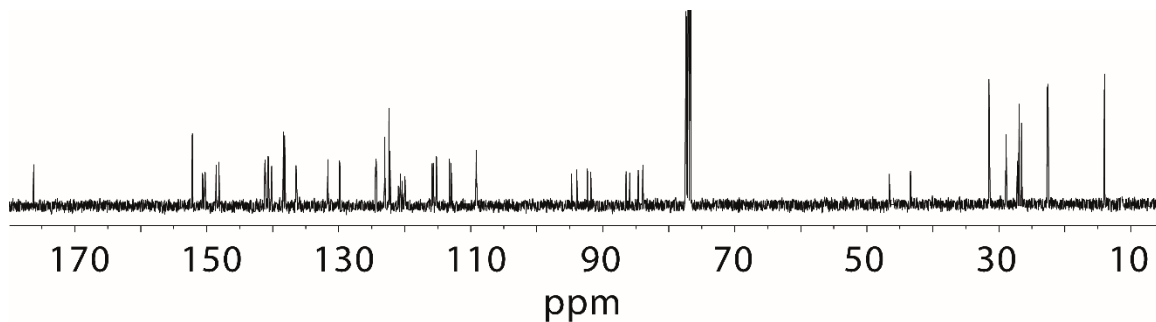
^{13}C NMR (100 MHz, CDCl$_3$) δ [ppm] = 176.32, 152.29, 152.24, 150.73, 150.33, 148.67, 148.25, 141.30, 141.23, 140.81, 140.73, 140.27, 138.47, 138.30, 136.58, 136.51, 131.79, 131.73, 129.98, 129.91, 124.49, 124.41, 123.15, 122.50, 122.37, 122.35, 121.08, 120.77, 120.46, 120.07, 115.96, 115.78, 115.30, 113.32, 113.06, 109.26, 94.85, 94.03, 92.42, 91.90, 86.58, 86.02, 84.72, 84.03, 77.36, 46.69, 43.48, 31.60, 31.58, 29.01, 27.27, 27.01, 26.67, 22.77, 22.64, 14.12, 14.09.
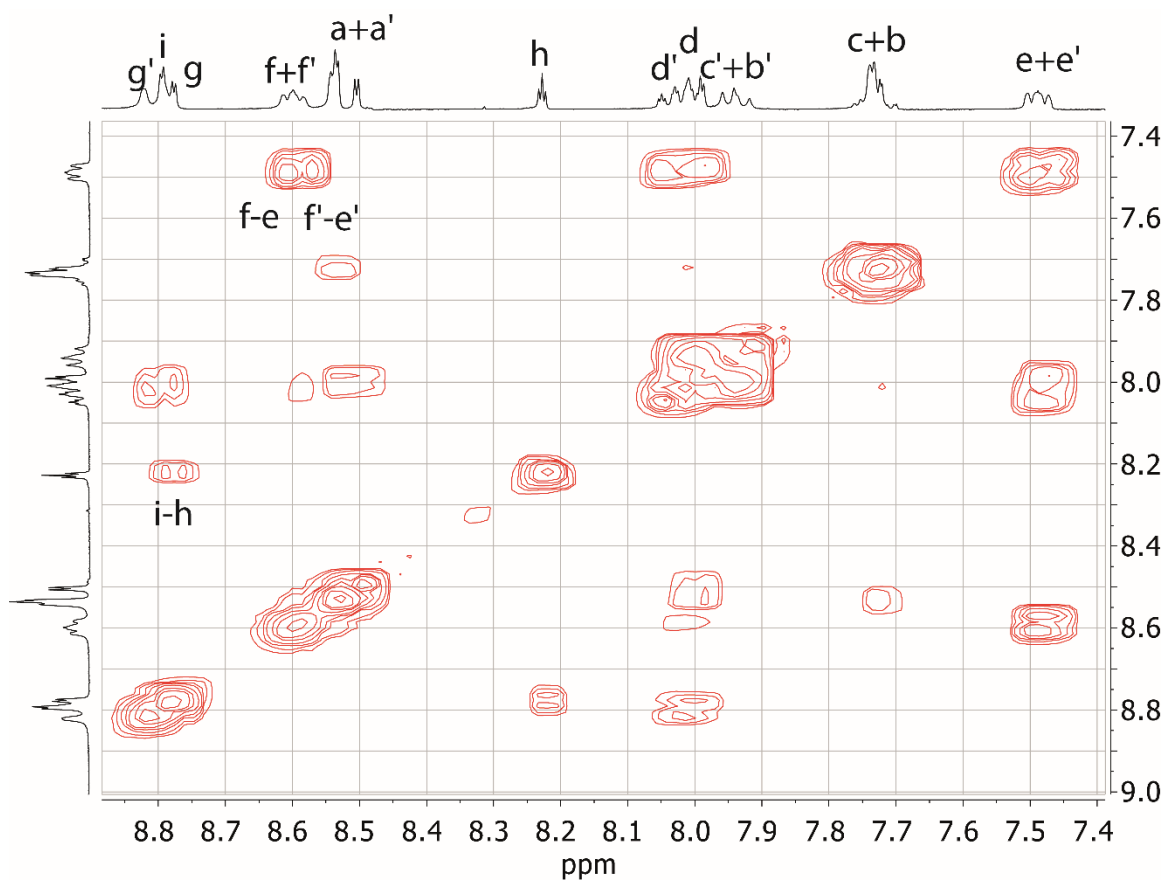
^{1}H–^{1}H COSY spectrum of **L^3** in DMSO-d_6, only showing aromatic region.

ESI-FTICR-HRMS calculated for C$_{60}$H$_{50}$N$_5$O [M+H]$^+$ m/z 856.4010, found m/z 856.3966.
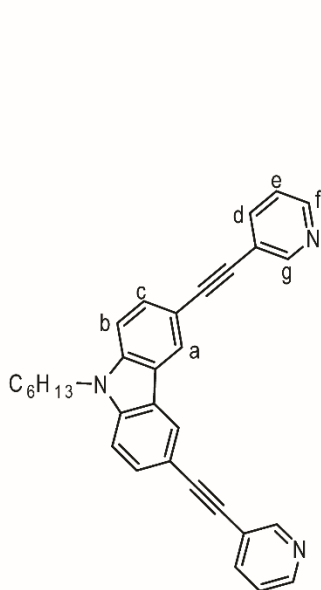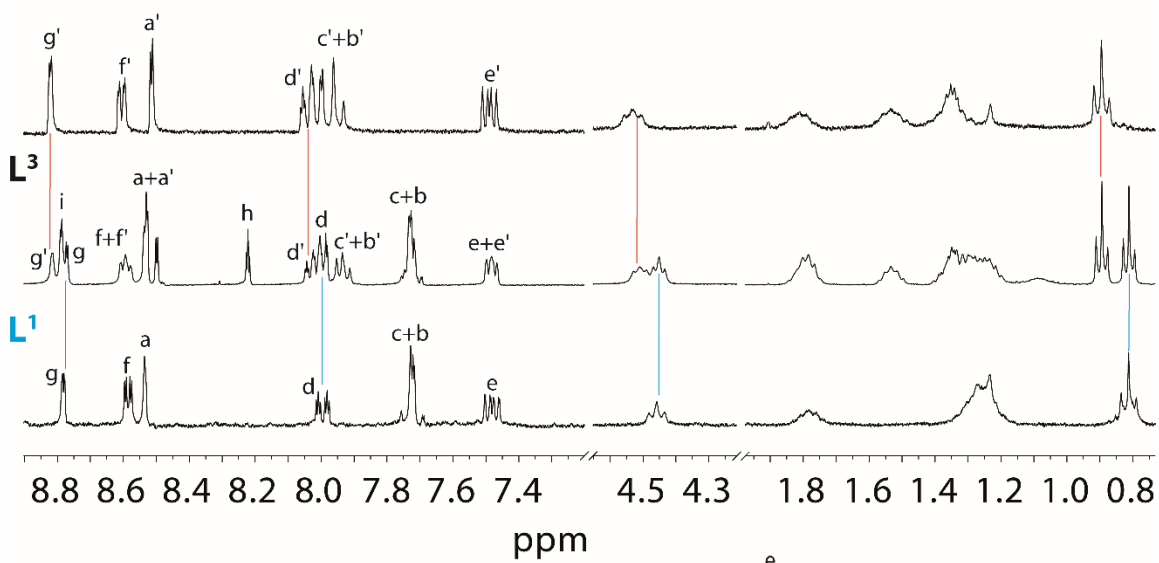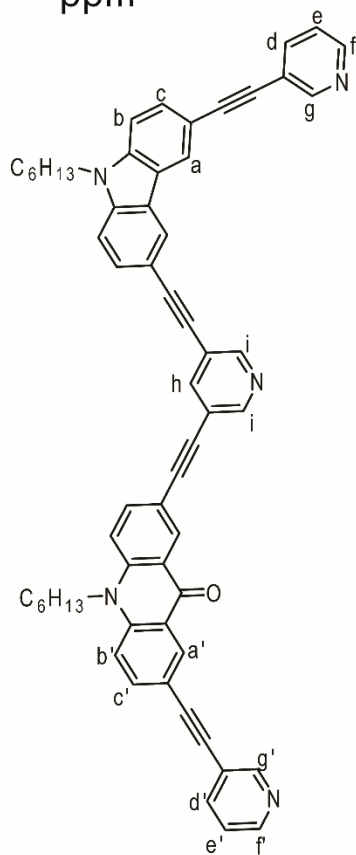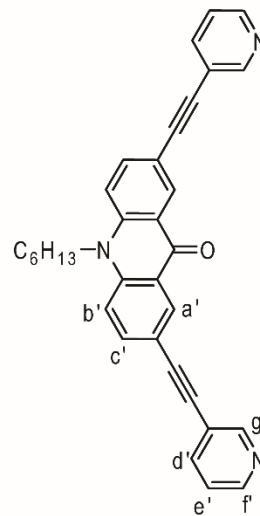
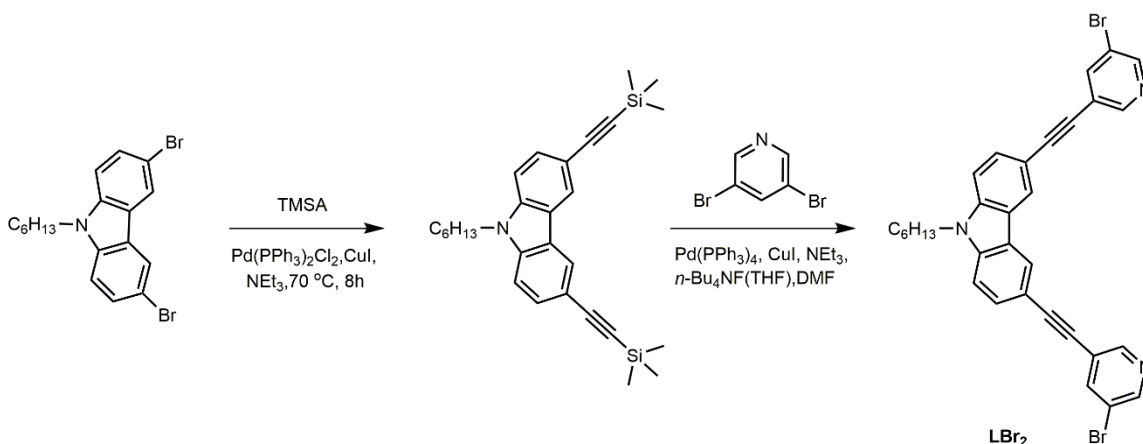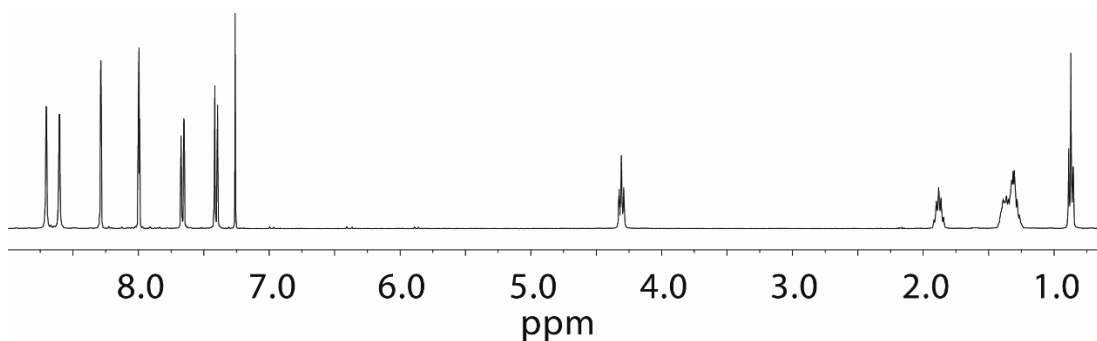Comparison of ^{1}H NMR spectra of L^1, L^3 and acridone-L in DMSO-d_6.

*3,6-Bis[(5-bromopyridin-3-yl)ethynyl]-9-hexyl-9H-carbazole (**LBr₂**)* was synthesized via the modified Sonogashira coupling reaction similar as **LBr** but using 3,6-dibromo-9-hexyl-9H-carbazole as the starting material. Yield: 19.3%.


^{1}H NMR (400 MHz, CDCl₃) δ [ppm] = 8.70 (d, J = 1.7 Hz, 2H), 8.60 (d, J = 2.2 Hz, 2H), 8.29 (d, J = 1.4 Hz, 2H), 8.00 (t, J = 2.0 Hz, 2H), 7.66 (dd, J = 8.5, 1.6 Hz, 2H), 7.41 (d, J = 8.5 Hz, 2H), 4.31 (t, J = 7.3 Hz, 2H), 1.94 – 1.87 (m, 2H), 1.43 – 1.24 (m, 3H), 0.87 (t, J = 7.0 Hz, 2H).
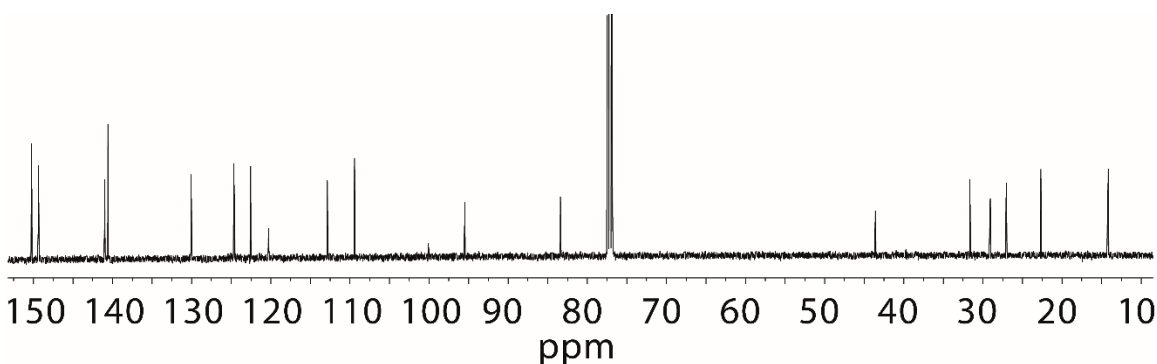

^{13}C NMR (125 MHz, CDCl₃) δ [ppm] = 150.22, 149.37, 141.00, 140.58, 130.07, 124.64, 122.54, 120.27, 112.86, 109.42, 100.10, 95.46, 83.39, 77.36, 43.58, 31.64, 29.06, 27.05, 22.68, 14.15.

ESI-FTICR-HRMS calculated for C₃₂H₂₆N₃Br₂ [M+H]$^+$ m/z 612.0473, found m/z 612.0491.
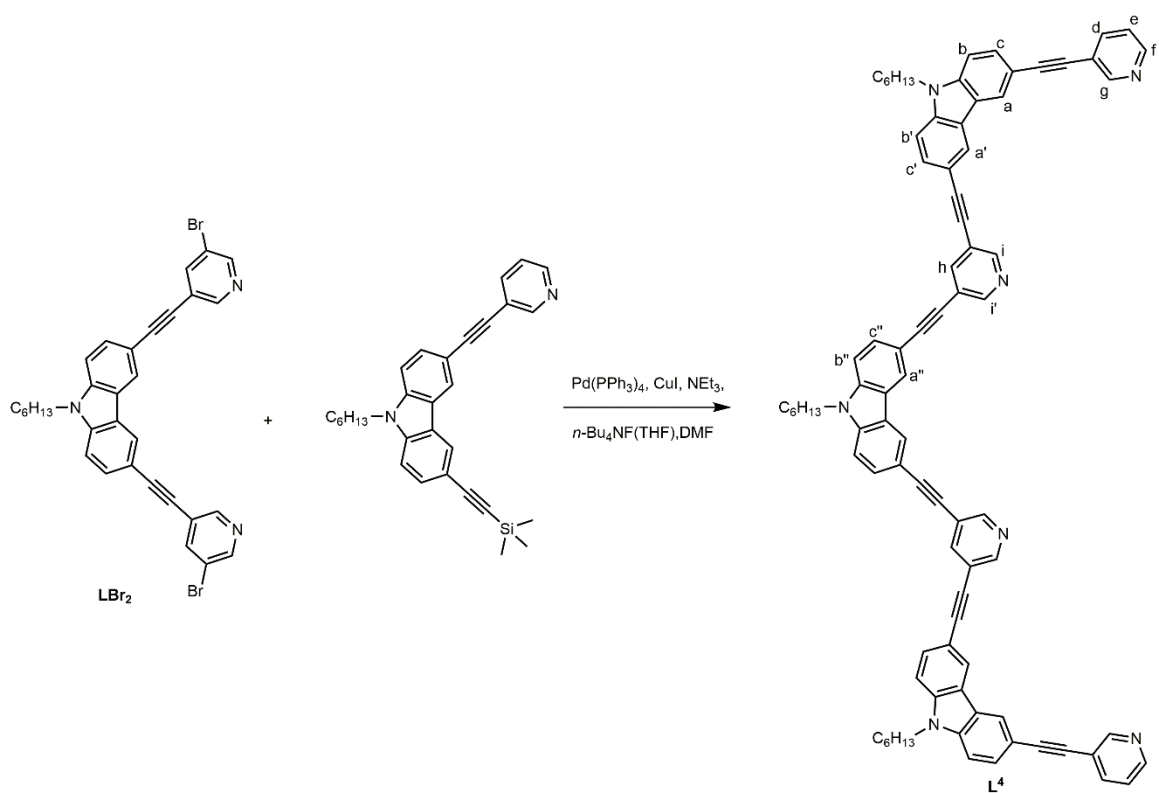
6,6'-{{[(9-hexyl-9H-carbazole-3,6-diyl)bis(ethyne-2,1-diyl)]bis(pyridine-5,3-diyl)}bis(ethyne-2,1diyl)}-bis [9-hexyl-3-(pyridin-3-ylethynyl)-9H-carbazole] (L⁴) was synthesized via the modified Sonogashira coupling reaction similar as **L³** using **LBr₂** and 9-hexyl-3-(pyridin-3-ylethynyl)-6-((trimethylsilyl)ethynyl)-9*H*-carbazole obtained in the aforementioned step. Yield: 63.0%.
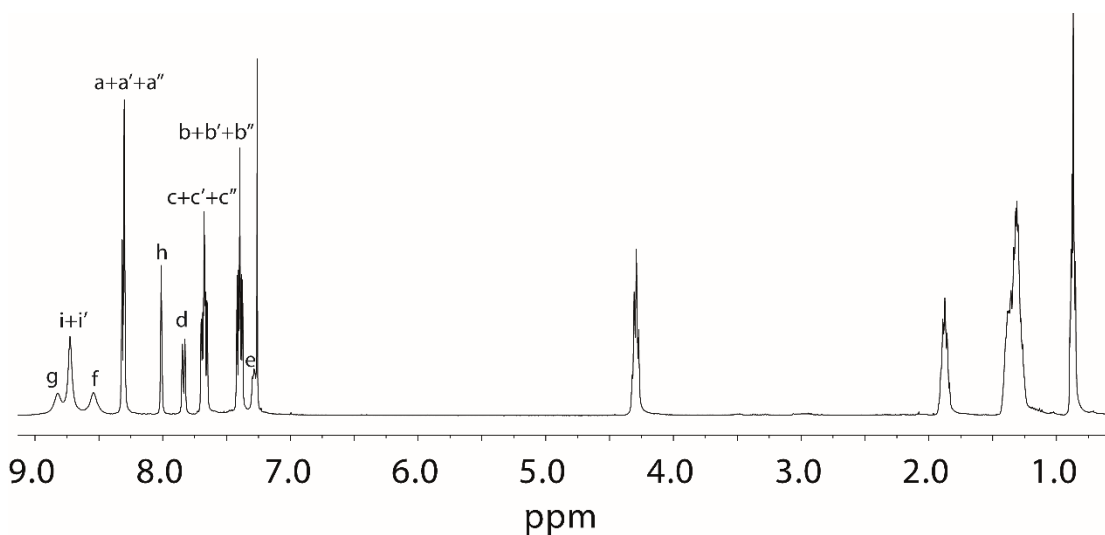

¹H NMR (400 MHz, CDCl₃) δ [ppm] = 8.82 (s, 2H), 8.73 (s, 4H), 8.54 (s, 2H), 8.34 – 8.25 (m, 6H), 8.01 (s, 2H), 7.84 (dd, *J* = 7.9, 1.6 Hz, 2H), 7.69 (dd, *J* = 4.0, 1.6 Hz, 2H), 7.68 – 7.65 (m, 4H), 7.41 (d, *J* = 5.0 Hz,

2H), 7.43 (s, 2H), 7.38 (d, J = 3.8 Hz, 2H), 7.28 (dd, J = 8.0, 4.6 Hz, 2H), 4.32 – 4.28 (m, 6H), 1.92 – 1.83 (m, 6H), 1.40 – 1.26 (m, 18H), 0.89 – 0.84 (m, 9H).
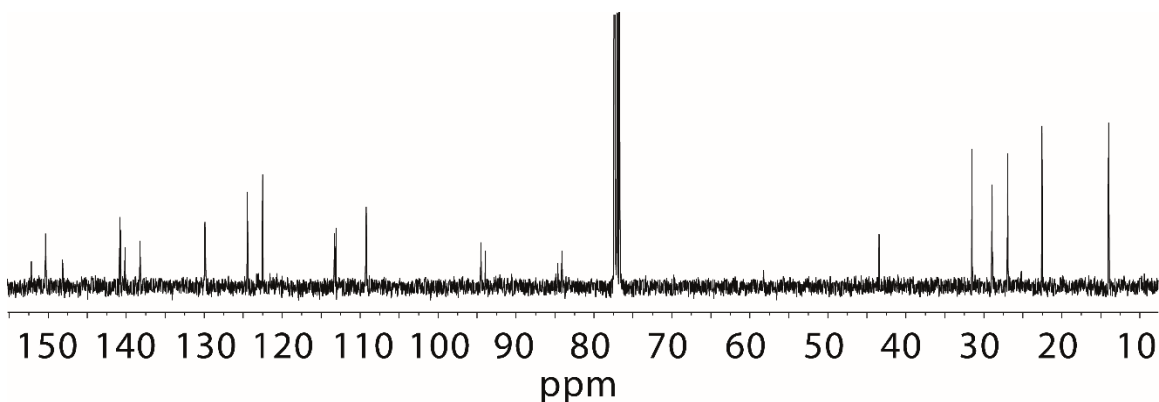
^{13}C NMR (100 MHz, CDCl$_3$) δ [ppm] = 152.18, 150.35, 148.16, 140.81, 140.79, 140.73, 140.17, 138.23, 129.96, 129.92, 129.86, 124.45, 124.39, 122.50, 122.48, 113.28, 113.12, 113.08, 109.22, 109.19, 94.51, 93.93, 84.64, 84.12, 84.10, 77.25, 43.44, 31.52, 28.94, 26.93, 22.55, 14.00.
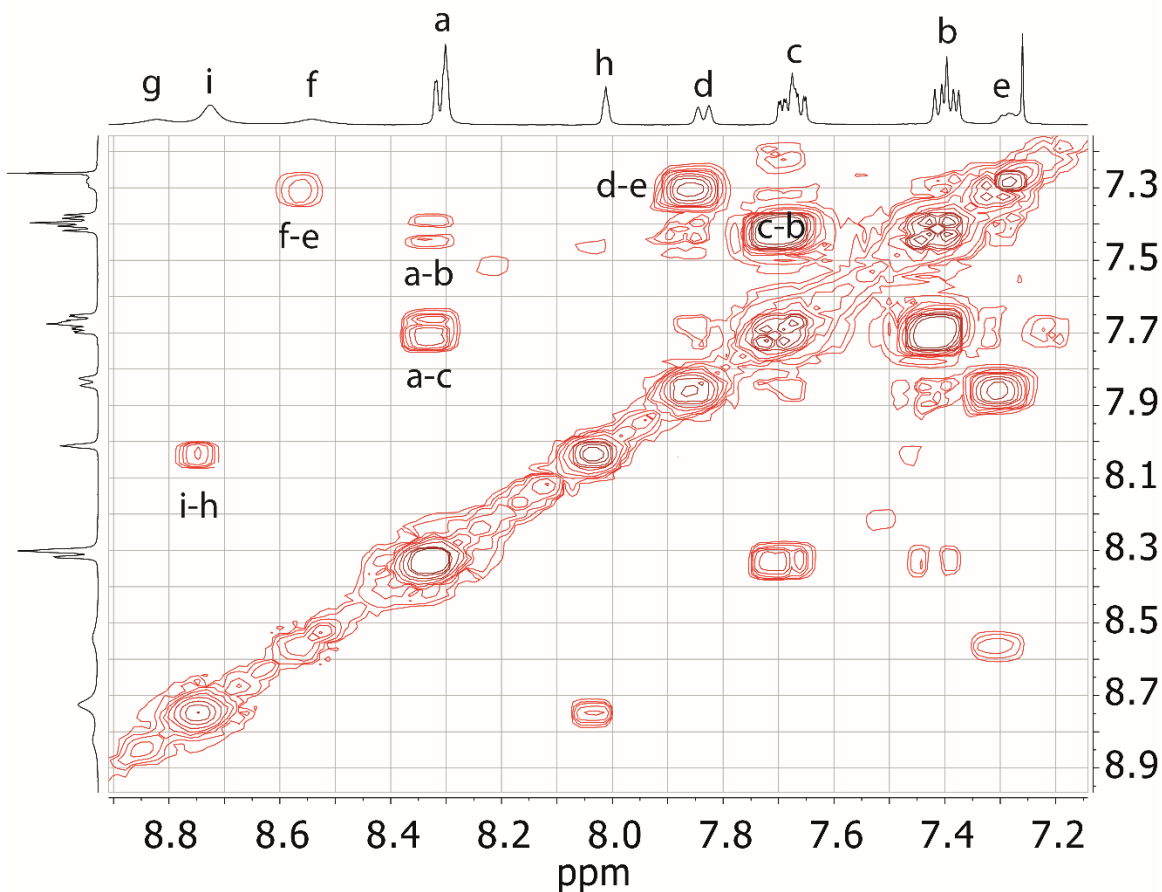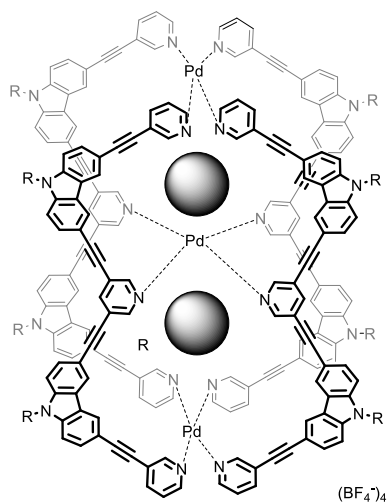

^{1}H–^{1}H COSY spectrum of **L^4** in CDCl$_3$, only showing aromatic region.

ESI-FTICR-HRMS calculated for C$_{86}$H$_{72}$N$_7$ [M+H]$^+$ m/z 1203.5849, found m/z 1203.5927.

4.4.2 Cage syntheses

Cage **1** [Pd$_3$**L^2**$_4$](BF$_4^-$)$_6$:

Cage compound **1** was formed in quantitative yield by heating a mixture of ligand **L^2** in CD$_3$CN (930 µL, 1.27 mg, 2.8 µmol) and a solution of [Pd(CH$_3$CN)$_4$](BF$_4$)$_2$ (2.1 µmol, 139 µL of a 15 mM solution in CD$_3$CN) at 70 °C for 5 h to give a 0.7 mM solution of **1**.
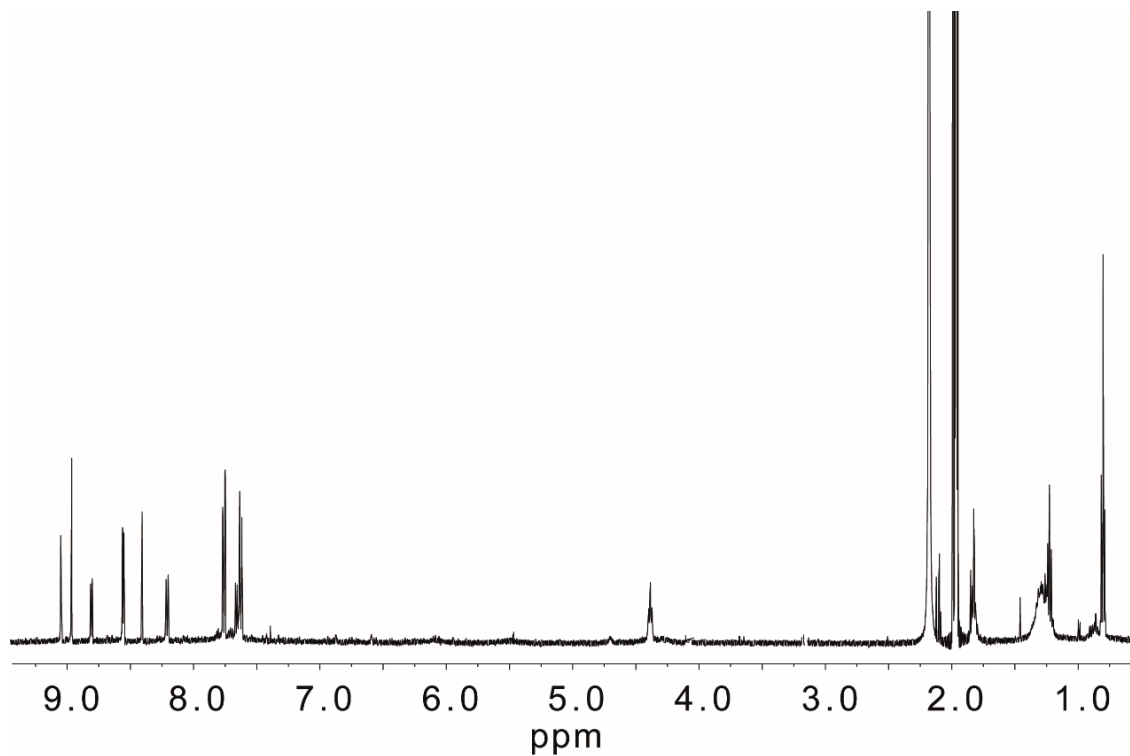
^{1}H NMR (500 MHz, CD$_3$CN): δ [ppm] = 9.03 (d, J = 1.9, 8H), 8.94 (d, J = 1.7 Hz, 8H), 8.78 (dd, J = 5.9, 1.2 Hz, 8H), 8.53 (dd, J = 4.2, 1.6 Hz, 16H), 8.38 (t, J = 1.7 Hz, 8H), 8.19 (dt, J =8.0, 1.6Hz, 4H), 7.74 (dd, J =

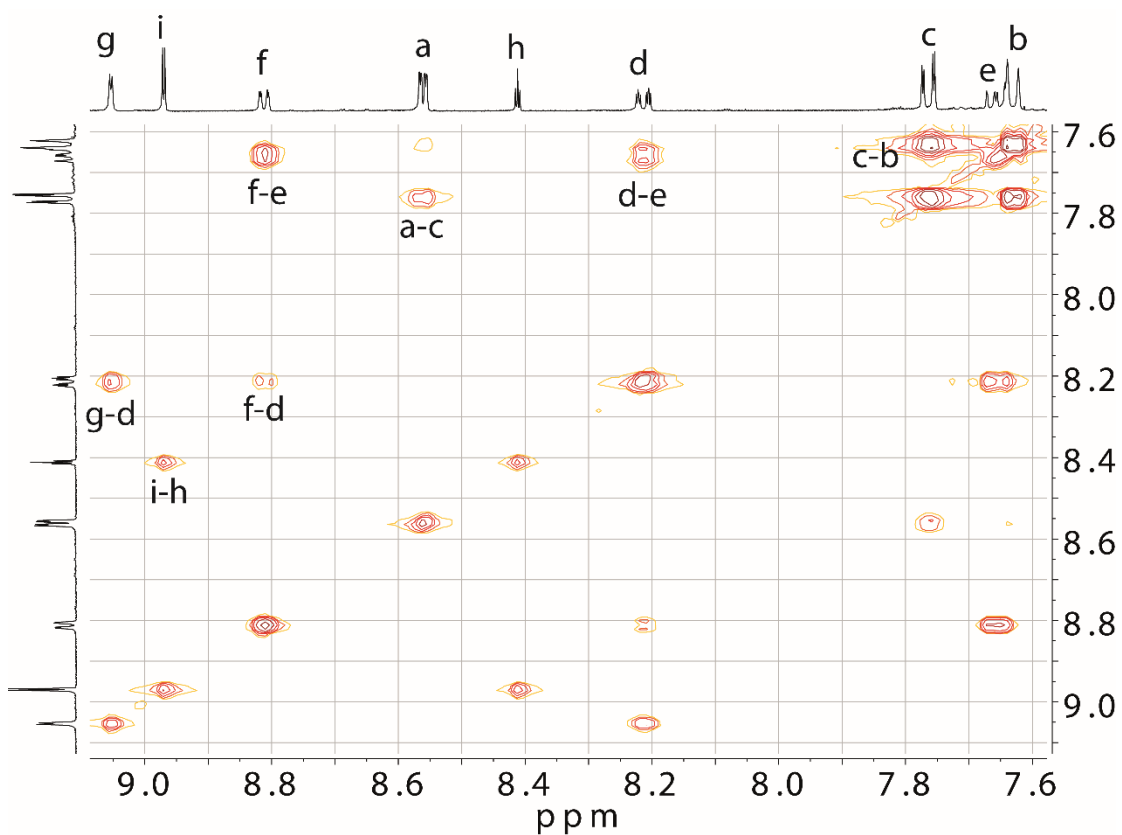8.5, 1.7 Hz, 16H), 7.63 (dd, J = 6.0, 1.8 Hz, 8H), 7.60 (d, J = 8.6 Hz, 16H), 4.36 (t, J = 7.1 Hz, 16H), 1.82 – 1.77 (m, 16H), 1.32 – 1.17 (m, 48H), 0.78 (t, J = 7.1 Hz, 24H).
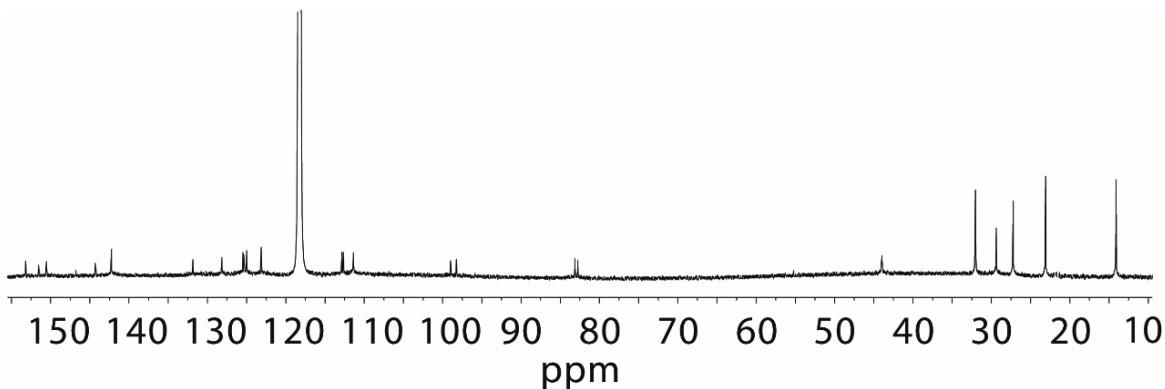
^{13}C NMR (150 MHz, CD$_3$CN): δ [ppm] = 153.18, 151.55, 150.52, 146.78, 144.30, 142.30, 142.23, 131.87, 131.84, 128.15, 125.47, 125.36, 124.99, 123.16, 123.13, 112.87, 112.68, 111.39, 111.37, 98.99, 98.24, 83.15, 82.75, 55.25, 43.97, 32.03, 29.37, 27.22, 23.09, 14.08.

^{1}H–^{1}H COSY spectrum of cage **1** in CD$_3$CN only showing the aromatic region, for ^{1}H NMR signal assignments refer to Figure 4.3b.

ESI-FTICR-HRMS calculated for [C$_{236}$H$_{196}$N$_{20}$Pd$_3$B$_2$F$_8$]$^{4+}$ m/z 951.0795, found m/z 951.0802.

Cage **2**:

Cage **2** [$Pd_6L^2_8$]$(Cl^-)_5{}^{7+}$:

Cage compound **2** was formed by heating a mixture of cage **1** (0.35µmol, 500 µL, 0.7 mM) in CD_3CN and a solution of N^nBu_4Cl (0.875 µmol, 50 µL of a 17.5 mM solution in CD_3CN) at 70 °C for 5 h to give a solution of **2**.
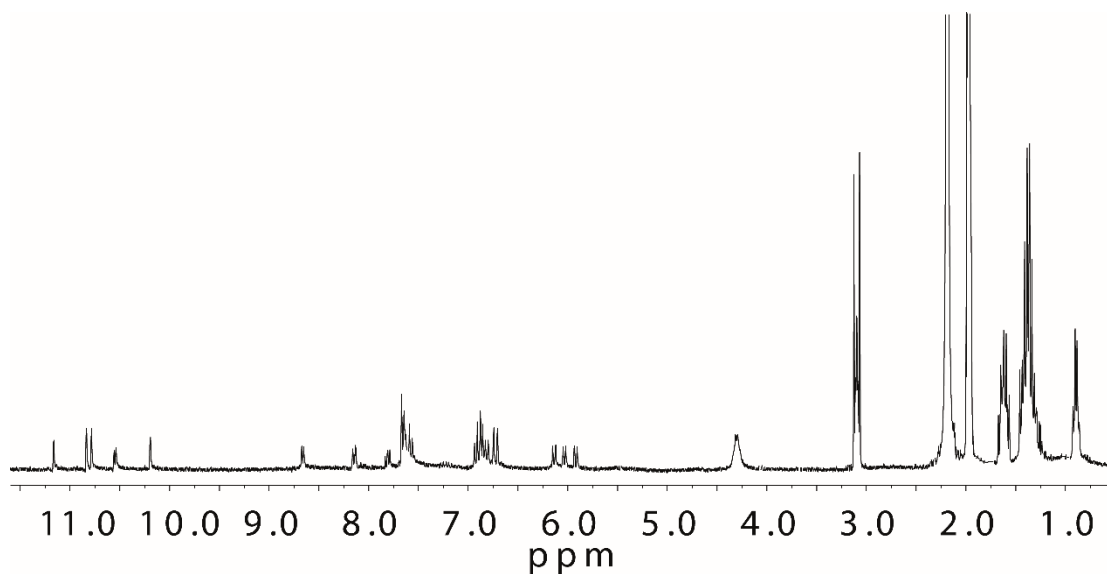
^{1}H NMR (400 MHz, CD_3CN) δ [ppm] = 11.14 (d, J = 1.9 Hz, 4H), 10.81 (d, J = 1.9 Hz, 4H), 10.76 (d, J = 1.9 Hz, 4H), 10.52 (dd, J = 6.0, 1.6 Hz, 4H), 10.17 (d, J = 2.0 Hz, 4H), 8.64 (dd, J = 6.0, 1.4 Hz, 4H), 8.12 (dt, J = 6.4, 1.7 Hz, 4H), 7.79 (d, J = 2.2 Hz, 4H), 7.65 – 7.59 (m, 16H), 7.55 (d, J = 8.7 Hz, 4H), 6.90 (d, J = 8.7 Hz, 4H), 6.87 (d, J = 8.7 Hz, 4H), 6.85 (d, J = 1.7 Hz, 4H), 6.83 (d, J = 1.5 Hz, 4H), 6.79 (d, J = 8.2 Hz, 4H), 6.72 (d, J = 1.3 Hz, 4H), 6.68 (d, J = 1.6, Hz, 4H), 6.11 (dd, J = 8.7, 1.9Hz, 4H), 6.01 (dd, J = 8.5, 1.6 Hz, 4H), 5.89 (dd, J = 8.3, 1.5 Hz, 4H), 4.31 – 4.24 (m, 16H), 1.66 – 1.53 (m, 16H), 1.43 – 1.28 (m, 96H), 0.87 (dd, J = 9.4, 4.8 Hz, 24H).
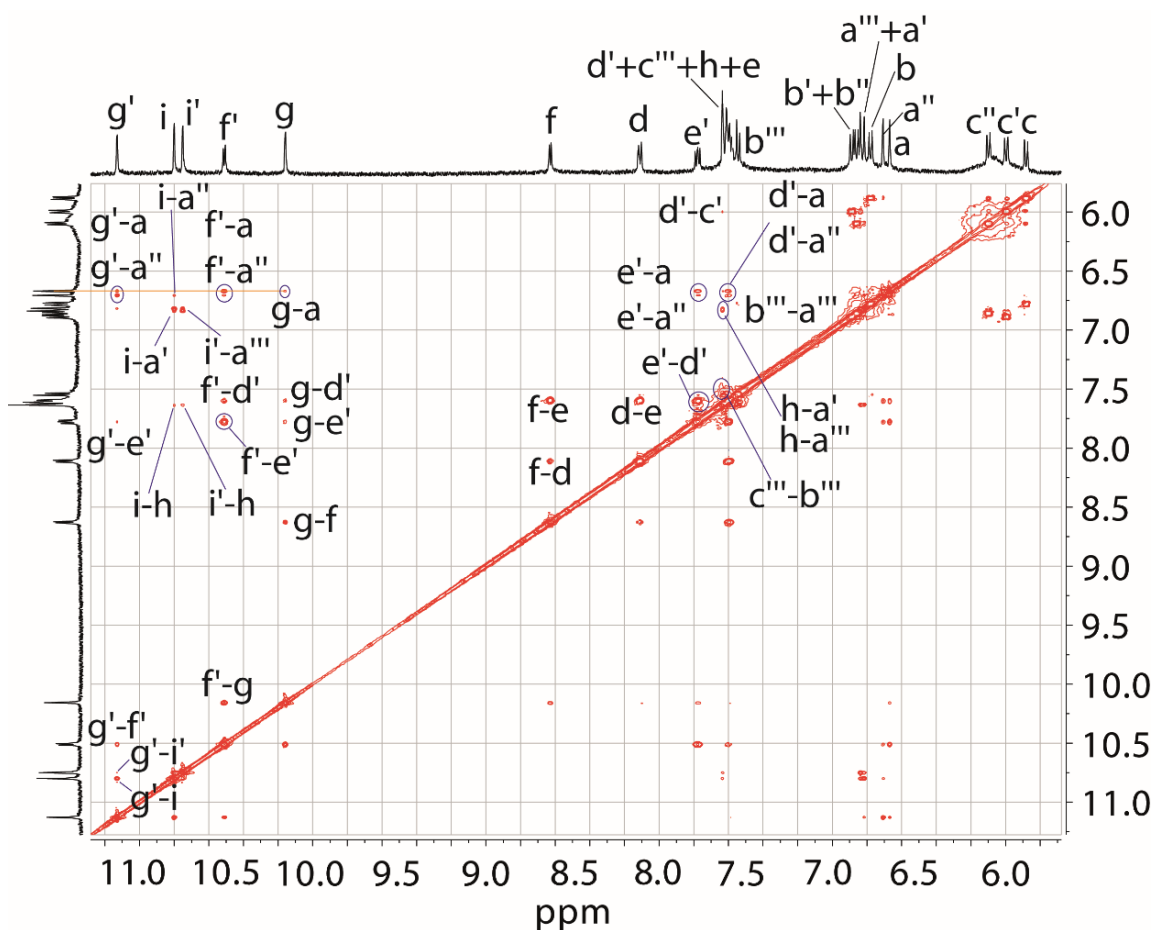
^{1}H–^{1}H NOESY spectrum of cage **2** in CD$_3$CN, only showing the aromatic region, for ^{1}H NMR signal assignments refer to Figure 4.3c.

ESI-FTICR-HRMS calculated for $[C_{476}H_{392}N_{40}Pd_6Cl_5]^{7+}$ m/z 1063.3528, found m/z 1062.7849.

Cage **3**:

Cage **3** $[Pd_6\mathbf{L^2}_8](Br^-)_5^{7+}$:

Cage compound **3** was formed by heating a mixture of cage **1** (0.35 µmol, 500 µL, 0.7 mM) in CD$_3$CN and a solution of N^{n}Bu$_4$Br (0.875 µmol, 50 µL of a 17.5 mM solution in CD$_3$CN) at 70 °C for 5 h to give a solution of **3**.

^{1}H NMR (500 MHz, CD$_3$CN) δ [ppm] = 11.16 (d, J = 1.9 Hz, 4H), 10.89 (d, J = 1.8 Hz, 4H), 10.85 (d, J = 1.9 Hz, 4H), 10.54 (d, J = 6.2 Hz, 4H), 10.30 (d, J = 1.9 Hz, 4H), 8.72 (d, J = 5.8 Hz, 4H), 8.14 (dt, J = 8.3 Hz, 4H), 7.74 (t, J = 6.7 Hz, 4H), 7.62 – 7.67 (m, 16H), 7.56 (d, J = 9.1 Hz, 4H), 6.92 – 6.90 (m, 16H), 6.81 (d, J = 8.5 Hz, 4H), 6.78 (d, J = 2.4 Hz, 8H), 6.18 (dt, J = 8.6, 1.5 Hz, 4H), 6.07 (dt, J = 8.3, 1.4 Hz, 4H), 5.95 (d, J = 8.5, 1.2 Hz, 4H), 4.33 – 4.22 (m, 16H), 1.85 – 1.79 (m, 16H), 1.40 – 1.31 (m, 96H), 0.89 – 0.84 (m, 24H).
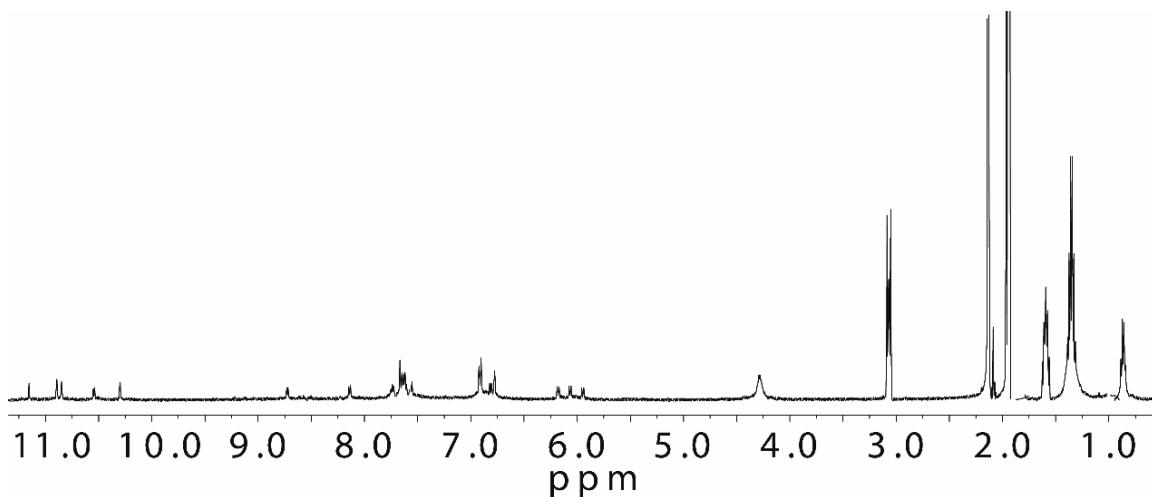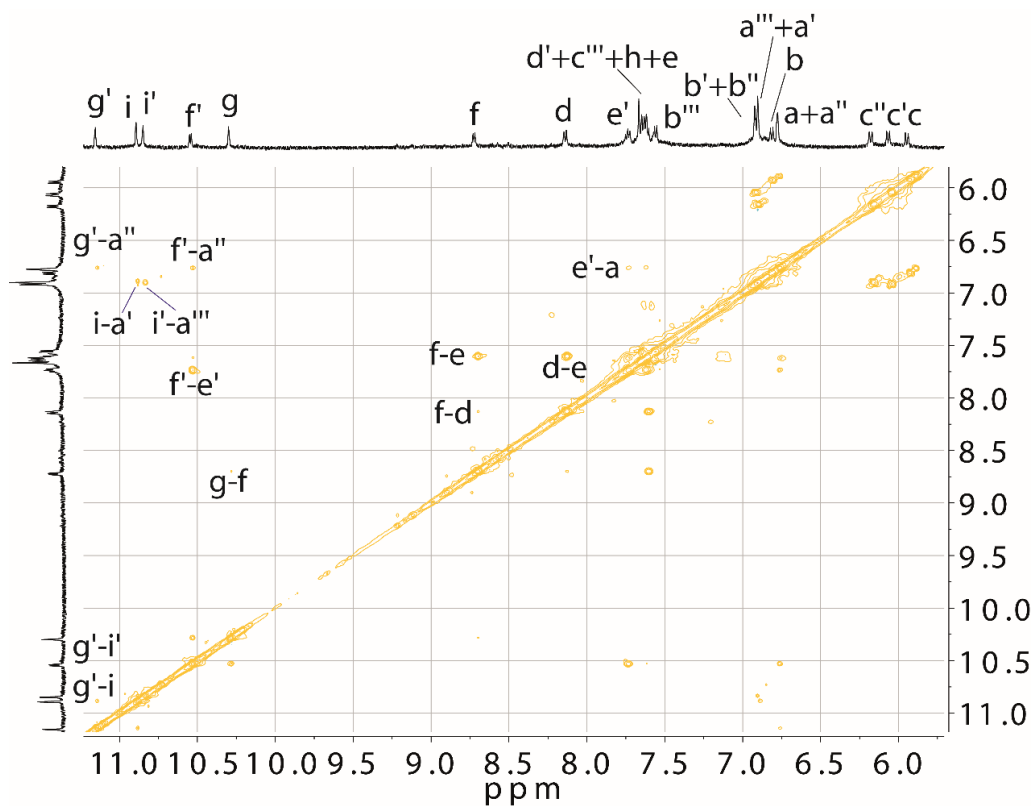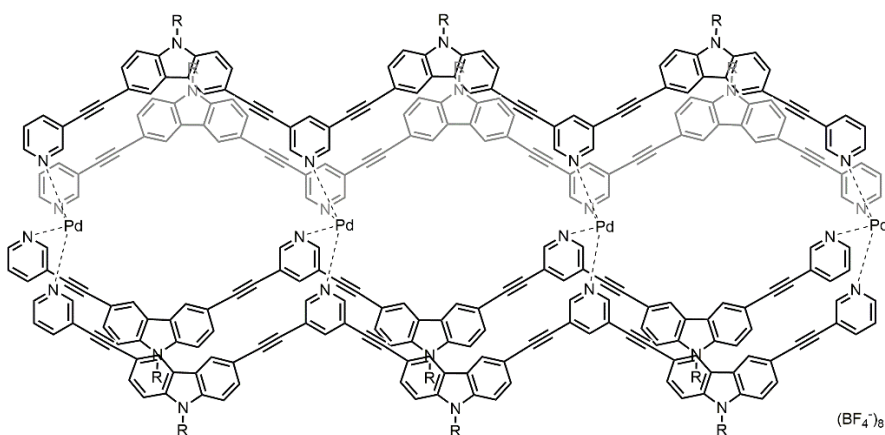

^{1}H–^{1}H NOESY spectrum of cage **3** in CD$_3$CN, only showing the aromatic region, for ^{1}H NMR signal assignments refer to Figure 4.3d.

ESI-FTICR-HRMS calculated for [C$_{476}$H$_{392}$N$_{40}$Pd$_6$Br$_5$]$^{7+}$ m/z 1094.6021, found m/z 1094.6154.

Cage **4**:

Cage **4** [Pd$_4$**L^4**$_4$]$^{8+}$:

Cage compound **4** was formed in quantitative yield by heating a mixture of ligand **L^4** in DMF-d_7 (930 µL, 3.13 mg, 2.8 µmol) and a solution of [Pd(CH$_3$CN)$_4$](BF$_4$)$_2$ (2.8 µmol, 186 µL of a 15 mM solution in DMF-d_7) at 70 °C for 20 h to give a 0.7 mM solution of **4**.
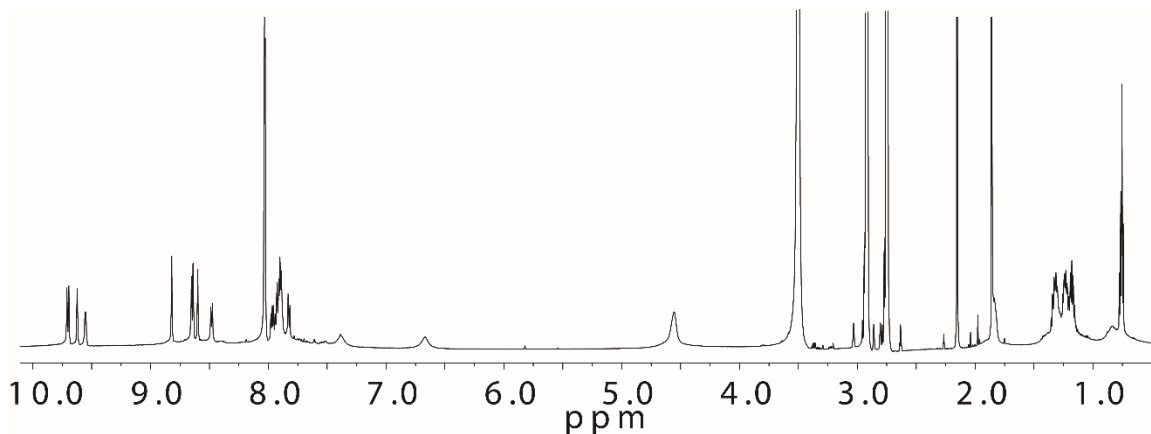
^{1}H NMR (600 MHz, DMF-d_7) δ [ppm] = 9.71 (d, J = 1.9 Hz, 8H), 9.69 (d, J = 1.9 Hz, 8H), 9.62 (d, J = 2.0 Hz, 8H), 9.55 (dd, J = 6.0, 1.4 Hz, 8H), 8.82 (t, J = 1.8 Hz, 8H), 8.65 (dd, J = 7.5, 1.5 Hz, 16H), 8.60 (d, J = 1.5 Hz, 8H), 8.48 (dt, J = 7.7, 1.6 Hz, 8H), 7.96 (dd, J = 14.6, 7.7 Hz, 12H), 7.93 – 7.87 (m, 36H), 7.82 (dd, J = 8.3, 1.5 Hz, 8H), 4.56 (s, 24H), 1.85 – 1.79 (m, 24H), 1.37 – 1.27 (m, 24H), 1.26 – 1.21 (m, 24H), 1.20 – 1.14 (m, 24H), 0.76 (td, J = 7.2, 5.5 Hz, 36H).

ESI-FTICR-HRMS calculated for [C$_{344}$H$_{284}$N$_{28}$Pd$_4$]$^{8+}$ m/z 654.3665, found m/z 654.3750.
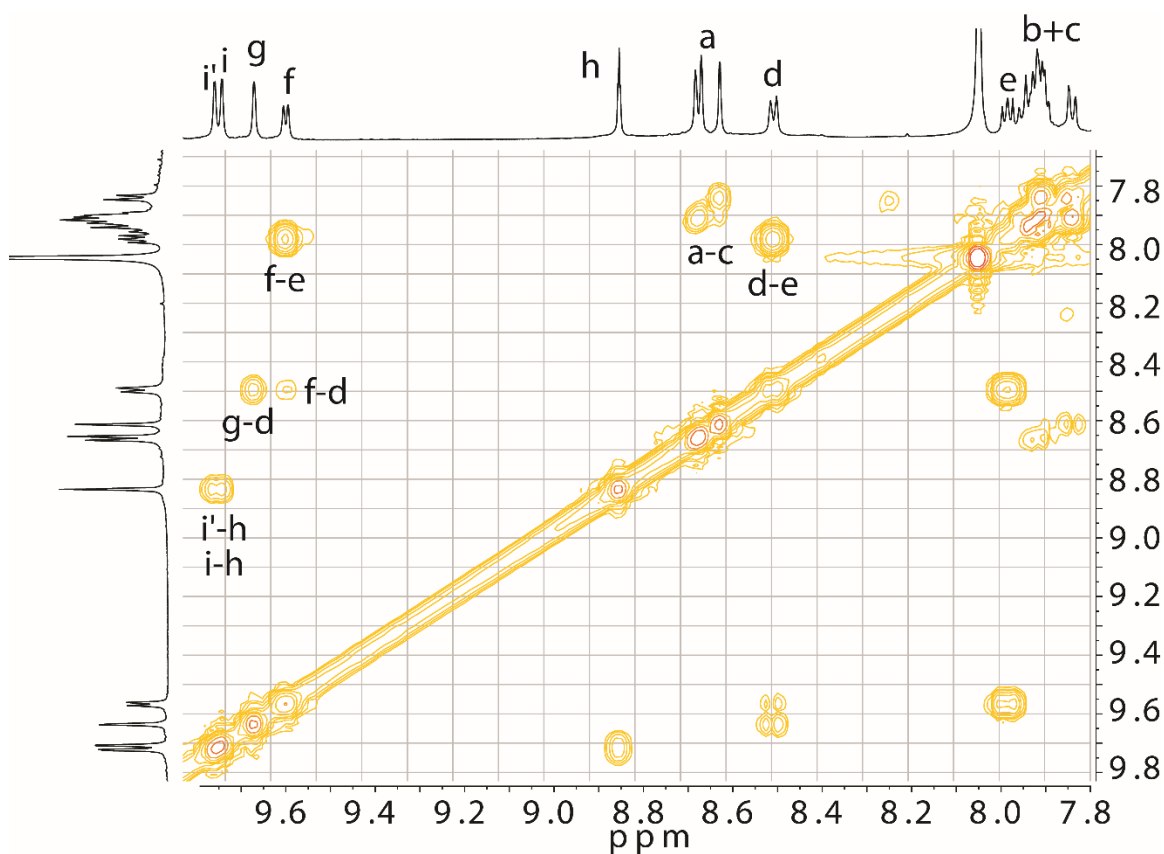
^{1}H–^{1}H COSY spectrum of cage **4** in DMF-d_7 only showing the aromatic region, for ^{1}H NMR signal assignments refer to Figure 4.11b.

4.4.3   Further NMR spectroscopy

1.5 Equivalents of bromide was added into a mixture solution containing a mixture of mono-cage [Pd$_2$**L^1**$_4$] and peanut-shaped cage [Pd$_3$**L^2**$_4$] in 2 : 1 ratio. It turned out that two interpenetrated cages formed independently without any heterogeneous assembly (Figure 4.13).
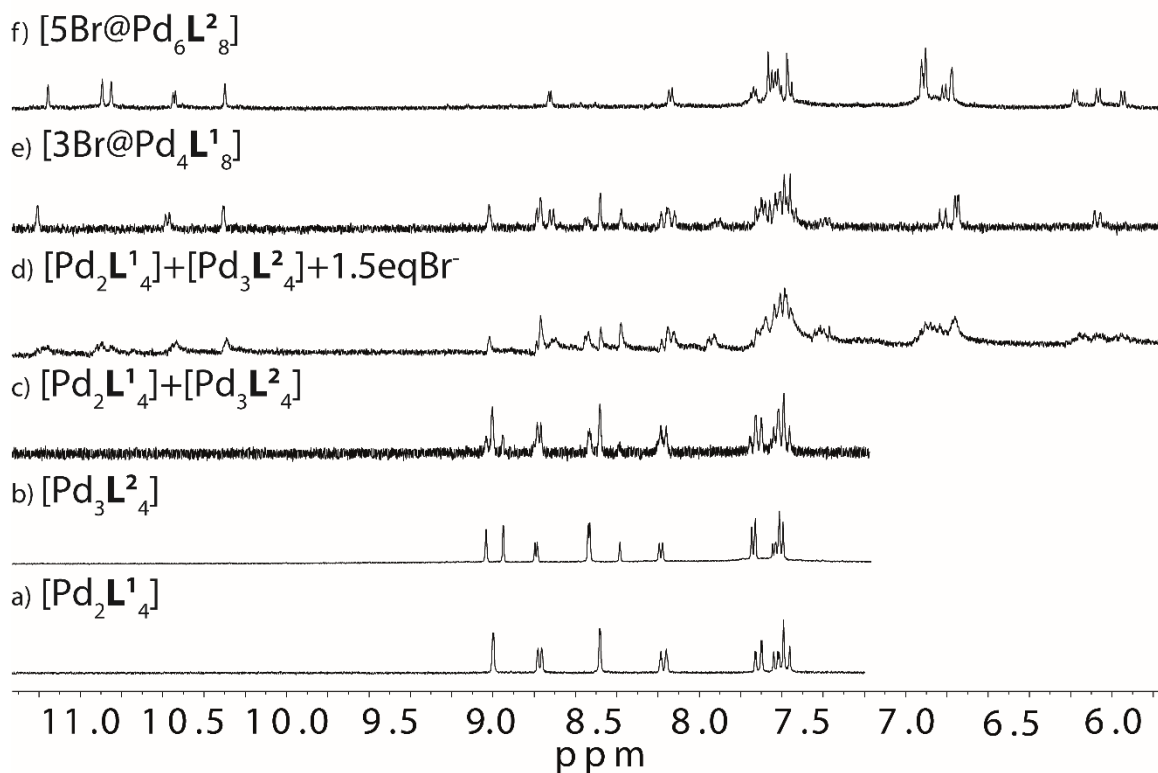
f) $[5Br@Pd_6L^2_8]$

e) $[3Br@Pd_4L^1_8]$

d) $[Pd_2L^1_4]+[Pd_3L^2_4]+1.5eqBr^-$

c) $[Pd_2L^1_4]+[Pd_3L^2_4]$

b) $[Pd_3L^2_4]$

a) $[Pd_2L^1_4]$

11.0 10.5 10.0 9.5 9.0 8.5 8.0 7.5 7.0 6.5 6.0
p p m

Figure 4.13 ^{1}H NMR (300 MHz, 298 K, CD$_3$CN) spectra of a) mono-cage $[Pd_2L^1_4]$; b) peanut-shaped cage$[Pd_3L^2_4]$; c) mixture of mono-cage $[Pd_2L^1_4]$ and peanut-shaped cage $[Pd_3L^2_4]$; d) 1.5 equivalents of bromide was added into c); e) interpenetrated cage $[3Br@Pd_4L^1_8]$ and f) interpenetrated cage $[5Br@Pd_6L^2_8]$.

4.5 References

[1] a) M. Fujita, K. Umemoto, M. Yoshizawa, N. Fujita, T. Kusukawa and K. Biradha, *Chem. Commun.* **2001**, 509; b) K. Harris, D. Fujita and M. Fujita, *Chem. Commun.* **2013**, *49*, 6703.

[2] M. Han, D. M. Engelhard, G. H. Clever, *Chem. Soc. Rev.,* **2014**, *43*, 1848.

[3] a) D. Fiedler, D. H. Leung, R. G. Bergman, K. N. Raymond, *Acc. Chem. Res.* **2005**, *38*, 349; b) D. H. Leung, R. G. Bergman, K. N. Raymond, *J. Am. Chem. Soc.* **2006**, *128*, 9781; c) M. D. Pluth, R. G. Bergman, K. N. Raymond, *Science,* **2007**, *316*, 85; d) Y. Nishinoka, T. Yamaguchi, M. Kawano, M. Fujita, *J. Am. Chem. Soc.* **2008**, *130*, 8160; e) M. Yoshizawa, J. K. Klosterman, M. Fujita, *Angew. Chem. Int. Ed.* **2009**, *48*, 3418; f) *Molecular Encapsulation: Organic Reactions in Constrained Systems* (Eds.: U. H. Brinker, J. Mieusset), Wiley, Hoboken, **2010**; g) C. J. Hastings, M. D. Pluth, R. G. Bergman, K. N. Raymond, *J. Am. Chem. Soc.* **2010**, *132*, 6938.

[4] a) D. J. Cram, *Nature,* **1992**, *356*, 29; b) L. Trembleau, J. Jr. Rebek, *Science,* **2003**, *301*, 1219; c) X. Liu, G. Chu, R. A. Moss, R. R. Sauers, R. Warmuth, *Angew. Chem. Int. Ed.* **2005**, *117*, 2030; d) V. M. Dong, D. Fiedler, B. Carl, R. G. Bergman, K. N. Raymond, *J. Am. Chem. Soc.* **2006**, *128*, 14464; e) S. J.

Dalgarno, N. P. Power, J. L. Atwood, *Coord. Chem. Rev.,* **2008**, *252*, 852; f) G. H. Clever, S. Tashiro, M. Shionoya, *Angew. Chem. Int. Ed.* **2009**, *48*, 7010.

[5] a) M. Yoshizawa, M. Tamura, M. Fujita, *Angew. Chem. Int. Ed.* **2007**, *46*, 3874; b) S. Tashiro, R. Kubota, M. Shionoya, *J. Am. Chem. Soc.* **2012**, *134*, 2461; c) Y. Inokuma, S. Yoshioka, J. Ariyoshi, T. Arai, Y. Hitora, K. Takada, S. Matsunaga, K. Rissanen, M. Fujita, *Nature,* **2013**, *495*, 461.

[6] a) B. Therrien, G. Süss-Fink, P. Govindaswamy, A. K. Renfrew, P. J. Dyson, *Angew. Chem. Int. Ed.* **2008**, *47*, 3773; b) J. E. M. Lewis, E. L. Gavey, S. A. Camerona, J. D. Crowley, *Chem. Sci.* **2012**, *3*, 778.

[7] a) Y. B. Dong, P. Wang, J. P. Ma, X. X. Zhao, H. Y. Wang, B. Tang, R. Q. Huang, *J. Am. Chem. Soc.* **2007**, *129*, 4872; b) Q. F. Sun, J. Iwasa, D. Ogawa, Y. Ishido, S. Sato, T. Ozeki, Y. Sei, K. Yamaguchi, M. Fujita, *Science,* **2010**, *328*, 1144.

[8] a) A. Stephenson, S. P. Argent, T. R. Johannessen, I. S. Tidmarsh, M. D. Ward, *J. Am. Chem. Soc.* **2011**, *133*, 858; b) N. Kishi, Z. Li, K. Yoza, M. Akita, M. Yoshizawa, *J. Am. Chem. Soc.* **2011**, *133*, 11438; c) W. J. Meng, B. Breiner, K. Rissanen, J. D. Thoburn, J. K. Clegg, J. R. Nitsche, *Angew. Chem. Int. Ed.* **2011**, *50*, 3479.

[9] S. Bandi, A. K. Pal, G. S. Hanan, D. K. Chand, *Chem. Eur. J.* **2014**, *20*, 13122.

[10] M. D. Johnstone, E. K. Schwarze, G. H. Clever, F. M. Pfeffer, *Chem. Eur. J.* **2015**, *21*, 3948.

[11] a) D. K. Chand, K. Biradha, M. Fujita, S. Sakamoto, K. Yamaguchi, *Chem. Commun.* **2002**, 2486; b) H. K. Liu, X. Tong, *Chem. Commun.* **2002**, 1316; c) D. Moon, S. Kang, J. Park, *et al*, *J. Am. Chem. Soc.* **2006**, *128*, 3530; d) S. Hiraoka, K. Harano, M. Shiro, *et al*, *Angew. Chem. Int. Ed.* **2006**, *45*, 6488.

[12] a) M. Yoneya, T. Yamaguchi, S. Sato, M. Fujita, *J. Am. Chem. Soc.* **2012**, *134*, 14404; b) X. J. Li, F. L. Jiang, M. Y. Wu, S. Q. Zhang, Y. F. Zhou, A. C. Hong, *Inorg. Chem.* **2012**, *51*, 4116; c) T. H. Noh, W. Hong, H. Lee, O. S. Jung, *Dalton Trans.,* **2015**, *44*, 787.

[13] D. Preston, J. E. M. Lewis, J. D. Crowley, *J. Am. Chem. Soc.*, DOI: 10.1021/jacs.6b11982.

[14] a) S. Freye, J. Hey, A. Torras-Galán, D. Stalke, R. Herbst-Irmer, M. John, G. H. Clever, *Angew. Chem. Int. Ed.* **2012**, *51*, 2191; b) S. Freye, R. Michel, D. Stalke, M. Pawliczek, H. Frauendorf, G. H. Clever, *J. Am. Chem. Soc.* **2013**, *135*, 8476; c) M. Frank, J. Hey, I. Balcioglu, Y. S. Chen, D. Stalke, T. Suenobu, S. Fukuzumi, H. Frauendorf, G. H. Clever, *Angew. Chem. Int. Ed.* **2013**, *52*, 10102.

[15] J. J. P. Stewart, *J. Mol. Model.* **2007**, *13*, 1173.

[16] Gaussian 09, Revision D.01, M. J. Frisch, G. W. Trucks, H. B. Schlegel, G. E. Scuseria, M. A. Robb, J. R. Cheeseman, G. Scalmani, V. Barone, B. Mennucci, G. A. Petersson, H. Nakatsuji, M. Caricato, X. Li, H. P. Hratchian, A. F. Izmaylov, J. Bloino, G. Zheng, J. L. Sonnenberg, M. Hada, M. Ehara, K. Toyota, R. Fukuda, J. Hasegawa, M. Ishida, T. Nakajima, Y. Honda, O. Kitao, H. Nakai, T. Vreven, J. A. Montgomery Jr., J. E. Peralta, F. Ogliaro, M. Bearpark, J. J. Heyd, E. Brothers, K. N. Kudin, V. N. Staroverov, R. Kobayashi, J. Normand, K. Raghavachari, A. Rendell, J. C. Burant, S. S. Iyengar, J. Tomasi, M. Cossi, N. Rega, J. M. Millam, M. Klene, J. E. Knox, J. B. Cross, V. Bakken, C. Adamo, J. Jaramillo, R. Gomperts, R. E. Stratmann, O. Yazyev, A. J. Austin, R. Cammi, C. Pomelli, J. W. Ochterski, R. L. Martin, K. Morokuma,

V. G. Zakrzewski, G. A. Voth, P. Salvador, J. J. Dannenberg, S. Dapprich, A. D. Daniels, O. Farkas, J. B. Foresman, J. V. Ortiz, J. Cioslowski, D. J. Fox, Gaussian, Inc. Wallingford CT, **2009**.

[17] R. Zhu, J. Lübben, B, Dittrich, G. H. Clever, *Angew. Chem. Int. Ed.* **2015**, *54*, 2796.

[18] a) C. Abad-Zapatero, SS. Abdel-Meguid, JE. Johnson, AG. Leslie, I. Rayment, MG. Rossmann, D. Suck, T. Tsukihara, *Nature,* **1980**, *286*, 33; b) M. G. Rossmann, E. Arnold, J. W. Erickson, E. A. Frankenberger, J. P. Griffith, H. J. Hecht, J. E. Johnson, G. Kamer, M. Luo, A. G. Mosser, R. R. Rueckert, B. Sherry, G. Vriend, *Nature,* **1985**, *317*, 145.

[19] M. Groll, L. Dizel, J. Lowe, D. Stock, M. Bochter, H. D. Bartunik, R. Huber, *Nature,* **1997**, *386*, 463.

[20] S. Löffler, J. Lübben, L. Krause, D. Stalke, B. Dittrich, G. H. Clever, *J. Am. Chem. Soc.* **2015**, *137*, 1060.

[21] H. J. Kim, E. Lee, M. G. Kim, M. C. Kim, M. Lee, E. Sim, *Chem. Eur. J.* **2008**, *14*, 3883.

[22] E. Bosch, C. L. Barnes, *Organometallics* **2000,** *19,* 5522.

Rongmei Zhu

PERSONAL INFORMATION

Date of Birth: 03.04.1988; Gender: Female

Birth Place: Jiangsu Province, China

Telephone: +0049-17682558698

Email: rongmeizhu88@gmail.com

Address: Langestrasse 135, 44137 Dortmund, Germany.

EDUCATION

PhD: Inorganic Chemistry (2013.10 – 2017.03)

Georg-August-University Göttingen

Institute of Inorganic Chemistry

Master: Science in Chemistry (2010.09 - 2013.06)

Nanjing University

School of Chemistry and Chemical Engineering

Bachelor: Applied Chemistry (2006.09 - 2010.06)

Soochow University

College of Chemistry, Chemical Engineering and Material Science

General GPA: 3.83/4.00

AWARDS

Poster Prize on IRTG Müster-Nagoya in 2014

National Encouragement Scholarship in 2009

The Second Prize of People Scholarship in 2009

The Second Prize of People Scholarship in 2008

The Second Prize of People Scholarship in 2007

Other Information

- Language skills: Chinese (native), English (fluent), German(A1)
- Proficient in Microsoft Office, Origin, Illustrate, ChemDraw, MestReNova, etc.
- Enjoy swimming, hiking, cooking, etc.